Evolution of submarine channel and lobe systems above dynamic stepped slopes

Junia Casagrande

Submitted in accordance with the requirements for the degree of

Doctor of Philosophy

The University of Leeds

Institute of Applied Geoscience, School of Earth and Environment

July 2023

The candidate confirms that the work submitted is her own, except where work which has formed part of jointly-authored publications has been included. The contribution of the candidate and the other authors to this work has been explicitly indicated below. The candidate confirms that appropriate credit has been given within the thesis where reference has been made to the work of others.

Chapter 3 – Published in Basin Research

Casagrande, J., Hodgson, D.M., Peakall, J., Benac, P.M. (2022). Fill-and-Spill, Tilt-and-Repeat (FaSTaR) cycles: Stratigraphic evolution above a dynamic submarine stepped slope. Basin Research, 34, 2162-2188. doi:10.1111/bre.12700

Casagrande, J - Main author, undertook data interpretation and manuscript preparation
Hodgson, D.M. – Discussion and manuscript review
Peakall, J. – Discussion and manuscript review
Benac, P.M. – support with seismic data analysis

Chapter 4 – Published in the Journal of the Geological Society

Casagrande, J., Hodgson, D.M., Peakall, J. (2024). A salty snapshot: extreme variations in basal erosion patterns preserved in a submarine channel. Journal of the Geological Society, https://doi.org/10.1144/jgs2023-006

Casagrande, J - Main author, undertook data interpretation and manuscript preparation
Hodgson, D.M. – Discussion and manuscript review
Peakall, J. – Discussion and manuscript review

Acknowledgements

Firstly, I would like to say how grateful I am for having the chance to complete this PhD. It was a great opportunity for me in many aspects, and I feel fortunate to be in this position.

The first thanks go to my supervisors, Dave Hodgson and Jeff Peakall, for their guidance and support throughout the process. I have learned so much from you in the past years, and I cannot thank you enough for your commitment to my development. It was an honour to work with such inspiring, high-level scientists!!!

To Petrobras, my employer, I am really grateful for the opportunity to undertake this PhD abroad. Special thanks to Carlos H.L. Bruhn, Ednilson B. Freire and Guilherme Raja-Gabaglia, for believing in my potential and making this happen inside Petrobras. I also want to thank Rita Parisi, my manager, for her unconditional support. I am grateful for the help I had from many colleagues in Petrobras, in discussions about my research, and for facilitating access and permissions to the datasets I used.

I appreciate my good friends from Brazil that kept in touch when I was distant. I am very grateful for the new friends I made during these years in the UK! You made my life happier! Victoria, Lucia, Dani, Abhi, Adriana, Ana, Tiago, Aurelia, Ru, Paola, and the rest of the "Latinas". I pretty much enjoyed the company of all of you during lunchtime at the University, and outside, at the pub, Zumba class, walks outdoors, dinners, Leeds city centre, etc..! Thank you, my colleagues, from the University, for making the office a lovely environment, Mohammed, Will, Ed, Hager, Bonita, Tim, Dan, Damjam, Bassam. Thanks to the University of Leeds staff for the institutional support during the PhD.

Finally, I would like to thank my loved ones. My parents, who always fully supported me, making all the efforts to provide the best resources they could. Thank you for valuing so much a good education, which is not the reality for many Brazilians. My sister, thank you for being my best friend, and Bruno for his love and adventurous companionship for the past years*.*

"After climbing a great hill, one only finds that there are many more hills to climb."

Nelson Mandela

Abstract

Submarine slopes with stepped profiles record sandy channel and lobe systems across depocentres and muddy bypass-prone ramps. The widely applied fill-and-spill model predicts the depositional architecture of stepped slope successions. However, this model implies a constant topographic configuration over the lifespan of a turbidite system. In contrast, the impact of dynamic slopes, with spatially variable topographic configurations, on patterns of erosion and deposition remains poorly investigated. This thesis aims to document deep-water sedimentation patterns above stepped slopes subject to active extensional salt tectonics using comprehensive subsurface datasets from the Campos Basin, offshore Brazil.

Extensive seismic mapping and well correlation of two Oligocene-Miocene deep-water successions support the interpretation of large-scale structural controls on the configuration of depocentres, and relationships between seismic geomorphology, depositional architecture, thicknesses and stacking patterns, and lithology/facies distribution above a dynamic slope topography. In the Marlim Unit area, high-resolution stratigraphic models capture the impact of subtle lateral and basinward tilting, and fluctuations in the sediment supply, which result in complex stratigraphic patterns with multiple phases, and multiple entry and exit points. Furthermore, extreme variations in the thickness of buried channel-fills are documented for the first time, which are interpreted to record a transient uplift related to salt tectonics in an otherwise subsiding depocentre. In the Albacora depocentre area, salt structures reactivated by extension and contraction formed subtle seabed topography that defined the edges of the depocentre. An elongate depression, later filled by sand-prone turbidites, developed immediately after the emplacement of a regional-scale mass transport complex. This contrasts with the role of mass wasting processes in active salt basins, which are a product of slope deformation and not a cause.

In summary, models of dynamic topographic deformation on the stratigraphic evolution of intraslope depocentres are developed, which can be applied to the extensional domains of salt basins globally.

Table of Contents

List of Tables

List of Figures

Abbreviations

ABT - Albacora turbidite unit

API - American Petroleum Institute

HARP – High-amplitude reflection package

IP – Intermediate package

LSP – Lower sand-prone package

MSC – Marlim Sul Channel

MTC – Mass transport complex

MTD – Mass transport deposit

PSDM - Pre-stack depth migration

PSTM - Pre-stack time migration

RMS - Root mean square

SEG – Society of Economic Geologists

SVS – Slope valley system

TZ – Transition zone

UMP – Upper mud-prone package

USP – Upper sand-prone package

Chapter 1 - Evolution of submarine channels and lobe systems above dynamic stepped slopes: an introduction

This chapter briefly introduces the rationale of the thesis, presents the research questions, and the aims and objectives. The thesis outline describes the content of the thesis chapters and general information about the study area and dataset are also provided.

1.1 Rationale

Submarine sediment gravity flows are volumetrically the most important flow process for moving sediment across the planet (Talling et al., 2012). Their deposits form submarine channel-levee and lobe systems, the main components of submarine fans, the largest sediment accumulations on the seafloor (Covault and Graham, 2010). Submarine fans spread across submarine slopes and basin floor (Piper and Normark, 2001; Mignard et al., 2019). The submarine slope rarely forms a smooth and uniform concave up surface; instead, an irregular topography is present across a range of scales. Stepped slope profiles are characterised by the intercalation of higher and lower gradient slope sectors, ramps and steps, respectively (Meckel et al., 2002; Prather, 2003; Smith, 2004; Prather et al., 2017; Fig. 1.1). Ramps are areas prone to sediment bypass, while steps are intraslope depocentres (e.g., Adeogba et al., 2005; Barton, 2012; Deptuck et al., 2012; Hay, 2012; Brooks et al., 2018a), which record the stratigraphic evolution of slope systems, and form important archives of palaeoenvironmental change. Intraslope depocentres above steps accumulate most of the sand in stepped profiles (59% according to Prather et al., 2017) with potential to form hydrocarbon reservoirs (e.g., Meckel et al., 2002; Booth et al., 2003; Prather, 2003; Prather et al., 2009, 2012a, 2017). Therefore, understanding the stratigraphy of these depocentres is of critical importance in driving exploration activity and in reducing uncertainties in the appraisal and development phases of existing oil and gas fields. These assets play an important role in global energy security and are potential sites for carbon capture and storage, both relevant in the energy transition scenario.
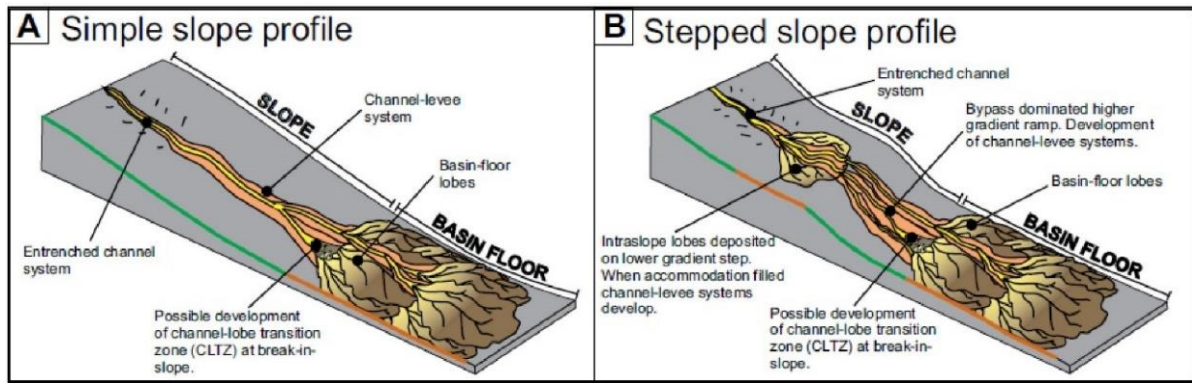
Figure 1.1: Deep-water depositional profiles. A - Idealised simple slope and B - stepped slope. In a simple slope there is no significant coarse sand deposition in the slope when compared to a stepped slope. Intraslope lobes form due to breaks in slope, depositing above steps (low gradient sections marked by orange lines in the figure). Intraslope lobes are the main target for hydrocarbon reservoirs in stepped profiles. Modified from Brooks et al., 2018a.

Stepped slope topography can result from different processes, such as salt tectonics (Prather, 2003; Stephens et al., 2003; Smith, 2004; Hay, 2012), mud diapirism (Adeogba et al., 2005, Barton, 2012; Deptuck et al., 2012), differential compaction and subsidence (e.g., Jackson et al., 2008; Spychala et al., 2015; Brooks et al., 2018a), and mass wasting processes (Spychala et al., 2015). In salt-bearing passive margins, stepped slopes are usually described as connected tortuous corridors partially confined by prominent flanking salt structures, like salt stocks and walls (e.g., Meckel et al., 2000; Prather, 2003; Smith, 2004; Hay et al., 2012; Prather et al., 2017). These structures are common in the intermediate to distal basin settings, where salt-driven contraction dominates (e.g., Cobbold and Szatmari, 1991; Demercian et al., 1993; Fort et al., 2004; Rowan et al., 2004; Brun and Fort, 2011; Davison et al., 2012; Jackson and Hudec, 2017). On mobile slopes, shallow and open steps with more subtle topography are often related to mud diapirism (e.g., Smith, 2004; Adeogba et al., 2005; Barton, 2012; Deptuck et al., 2012).

Stepped slope deposits comprise lobes, distributary channels, channel systems and mass transport deposits (Adeogba et al., 2005; Barton et al., 2012; Deptuck et al., 2012; Hay, 2012; Brooks et al., 2018). Efforts have been made to differentiate weakly confined deposition on the slope from the base of slope and basin floor settings, with the proposition of stratigraphic models for intraslope fans (e.g., Adeogba et al., 2005; Spychala et al., 2015; Jobe et al., 2017). Facies distribution, architecture and stacking

patterns reflect the depocentre geometry and accommodation patterns through time (e.g., Adeogba et al., 2005; Barton et al., 2012; Jobe et al., 2017). Step accommodation will vary due to progressive step filling but might also vary due to syn-depositional slope deformation. Vertical changes in step deformation over multiple sedimentary cycles have been reported in dynamic steps associated with mud diapirism (Deptuck et al., 2012) and differential subsidence over basement highs (Brooks et al., 2018a). The stratigraphic evolution of stepped profiles has been explained by the concepts of the fill-and-spill model, conceived from analysis of data collected in the minibasins of the Gulf of Mexico, which predicts the progressive filling and bypass of intraslope depocentres that are not deformed or are mainly mobile in their vertical axis during deposition (e.g., Winker, 1996; Prather et al., 1998; Beaubouef and Friedmann, 2000; Pirmez et al., 2000; Prather, 2000, 2003; Sinclair and Tomasso, 2002; Smith, 2004). Nevertheless, the nature of salt deformation means that a 3D dynamic slope topography needs to be considered (e.g., Madof et al., 2017; Ge et al., 2020; Jackson et al., 2020; Christie et al., 2021). Moreover, many of the present models are based on outcrop studies that are impacted by deficient palaeoenvironmental reconstructions based on 2D stratigraphic correlations, or are seismic studies without well control generally based on the amplitude and geometric character of reflections, meaning that the proposed models are speculative regarding lithological attributes.

This thesis investigates stepped slope systems in the extensional salt domain of Campos Basin, offshore Brazil. The research uses 3D high-resolution seismic reflection data calibrated by wells to investigate the stratigraphic record of shallow and open intraslope steps influenced by salt tectonics, a depocentre style not explicitly documented in the literature of salt basins. In addition, the thesis demonstrates the impact of a three-dimensionally dynamic slope during the evolution of intraslope depocentres and, in higher resolution, during the evolution of a single channel. As an outcome, this research provides new stratigraphic models that contribute to unveiling the high-resolution 3D stratigraphic signature and evolution of channel and lobe systems above dynamic stepped slopes. The models capture the interaction of slope topography and extra-basinal controls.

1.2 Research questions

1.2.1 How can the interplay of different stratigraphic controls on the record of deep-water systems deposited above mobile slopes be deciphered?

Submarine depositional architecture and facies distribution result from a complex interaction of stratigraphic controls that operate simultaneously at different intensities and scales. External factors such as tectonics, climate and eustasy control the generation, transport and nature of sedimentary particles entering the basin (e.g., Stow et al., 1984; Mutti and Normark, 1987; Rowan and Weimer, 1998; Catuneanu, 2006). Tectonics is the major agent that controls the location and height of the sediment-producing mountains, the distance of the mountains to the shoreline, the type of coastal area and the width of the shelf (Bouma, 2004). In the deep-water environment, tectonics can control the distribution of the entry points of fans and the geometry and size of transport pathways and depocentres (e.g., Reading and Richards, 1994; Jackson et al., 2008), including intraslope depocentres affected by salt tectonics (e.g., Rowan and Weimer, 1998). Climate acts in the source area influencing the freezing/thawing balance in the sediment-supplying mountains, patterns of fluvial runoff, weathering characteristics and the amount of water available for sub-aerial sediment transport (Bouma, 2004). In the basin, climatic control is reflected in the grain-size distribution and climatically driven sea-level fluctuations, such as the ones related to glaciations, which can record sea-level variations in the order of 10 m /1000 years (Stow et al., 1984). The type of feeder systems in the shelf (i.e., fluvial dominated deltas, waves and tides, fluvial incised valleys or even fan deltas) and associated processes also impact the sediment character available to be transferred to deep-water environments (Jackson et al., 2008). The sediment character also depends on the geology of the source area. Eustasy refers to global sea-level changes, including glaciations, but can also be due to other processes that induce minor fluctuations when compared to glaciations (i.e., variation in sediment input, continental collision and subduction, swelling and shrinking of midocean ridge systems; Pitman, 1979; Stow et al., 1984). The combined action of tectonics, climate and eustasy is translated into relative sea-level fluctuations.

Sequence stratigraphic models link frequency (timing), amount (volume) and type of sediment (mud vs sand) delivered to the deep sea with sea-level cycles, with preferential transfer of coarse clastic sediments to oceanic basins in periods of relative sea-level fall, and reduction in the availability of coarse and fine clastic sediment during rising sea-level and in high-stand periods (e.g., Vail, 1977; Posamentier and Vail, 1988; Reading and Richards, 1994; Galloway, 1998; Posamentier and Kolla, 2003; Bouma, 2004; Catuneanu, 2006; Jackson et al., 2008; Jobe et al., 2017). The association of sediment supply cycles and the relative sea-level curve is not always the rule (e.g., Posamentier, 1991; Burgess and Hovius, 1998). However, this link has been interpreted in most continental deep-sea depositional sites, especially along passive continental margins with broad shelves and during icehouse periods (e.g., Galloway, 1998; Covault and Graham, 2010).

In shallow water, the relationship between the rate of accommodation creation and the rate of sediment supply controls stratal stacking patterns and the key sequence stratigraphy surfaces within an inferred curve of base-level changes at the shoreline (e.g., Posamentier and Vail, 1988; Catuneanu, 2006). Accommodation refers to the space available for deposition (Jervey, 1988). In theory, this space goes from the sediment surface, at a certain position in the basin, towards the base level (roughly the sea-level in the marine environment). If this concept was applied in the deep-water setting, it would imply persistent and considerable available accommodation. However, in the submarine realm, accommodation is defined by the space between the sediment surface and the equilibrium profile (Kneller, 2003), whereas the base level refers to the deepest point in the basin that can be reached by sediment gravity flows (Carter, 1988). If the sediment surface happens to coincide with the equilibrium profile surface, an equilibrium condition is achieved, and sediment discharge is transported with minimum aggradation or degradation; however, this is likely a transitory condition (Pirmez et al., 2000).

The equilibrium profile can be altered by changes in flow properties and/or tectonic deformation that impacts seabed topography. These factors control the creation or destruction of accommodation in deep-water and, therefore, the stratigraphic patterns in deep-water systems (e.g., Pirmez et al., 2000; Kneller, 2003; Prather, 2003). The extrinsic signal in deep-water is usually interpreted in sediment supply cycles that record changes in flow properties over time (Kneller, 2003). Examples of this signature

are documented in the evolution of submarine slope channels, which ideally comprises the generation of an erosional bounding surface, created by vertical incision and lateral migration of an active channel floor, followed by aggradation of leveed-channels and final abandonment (e.g., Peakall et al., 2000; Deptuck et al., 2003; Hodgson et al., 2011, 2016; McHargue et al., 2011; Sylvester et al., 2011; Jobe et al., 2015; Covault et al., 2016). Likewise, the stacked stratigraphic succession of mass transport deposits, frontal splay turbidites and leveed-channel deposits; and thin-bedded interlobe deposits, at the lobe complex scale, are interpreted to reflect sea-level variations in the basin floor (e.g., Johnson et al., 2001; Posamentier and Kolla, 2003; Prélat et al., 2009). Physical modelling has shown the association between waxing to waning sediment supply cycles and forward and backward stepping lobe elements on the basin floor (Ferguson et al., 2020). Sequence boundaries in deep-water have been documented based on an abrupt and widespread increase in sediment supply, marked by an erosive base of a channel complex overlying distal basin plain or lobe fringes, or amalgamated sandstone sheets overlying more distal turbidite deposits (Johnson et al., 2001).

Despite the large number of studies linking sediment supply cycles with changes in flow properties, the association with allogenic forcing is often inferred, as the connection with the time-equivalent shelf/staging area is rarely preserved or observable (e.g., Flint et al., 2011; Madof et al., 2017), or the mapped deposits do not have sufficient extent to discard a possible autocyclic control (as in the case of thin-bedded interlobe deposits, which could also represent lobe fringes instead of a period of reduced sand supply; Prélat et al., 2009). Even condensed sections are not necessarily evidence for allocyclic shut-off of clastic input, as shown in hemipelagic muds in an intraslope basin in the Gulf of Mexico, where analysis of ^{18}O in foraminifera suggests both, allocyclic (i.e., eustatic high-stand) and autocyclic control (slope-system avulsion) (Prather et al., 1998). In addition, the recognition of external controls is better supported in smooth and open depositional profiles, where basin topography does not impact accommodation and the equilibrium profile (Hodgson et al., 2016). On mobile slopes, the geometric configuration of intraslope depocentres, an allogenic intra-basinal factor, can exert a first-order control on facies distribution and stratigraphic architecture and evolution of submarine systems, which have been explained by the fill-and-spill model (e.g., Winker, 1996; Prather et al., 1998; Prather,

2000, 2003; Beauboueff and Friedmann, 2000; Pirmez et al., 2000; Sinclair and Tomasso, 2002; Smith, 2004). This control is significant when the rates of slope deformation are higher than sedimentation rates, like in the initial phases of ponding in confined intraslope depocentres, which comprise sheet-like turbidites with preserved mud-caps that baselap the basin topography (e.g., Prather et al., 1998; Sinclair and Tomasso, 2000, Marini et al., 2015). In addition, variable subsidence rates, even if just in the vertical axis of a depocentre, could have a similar effect on stratigraphic architecture as fluctuations in the sediment supply (Sylvester et al., 2015). The triggering of mass transport deposits due to salt-activity at the flanks of minibasins is another example of the stratigraphic complexity on mobile slopes successions, being evidence for intra-basinal controls (Madof et al., 2017; Wu et al., 2020). However, mass-transport deposits can also be externally sourced and, depending on their characteristics regarding size, volume and composition, they might be interpreted as being allogenically controlled (e.g., Posamentier and Kolla, 2003; Wu et al., 2020). In summary, complex and dynamic topography profoundly impacts the behaviour of sediment gravity flows and associated depositional architecture, making identifying an extrinsic signal more challenging on mobile slopes than on simple slopes. Due to the highly reactive nature of salt deformation, deciphering the interplay of extra- and intra-basinal controls in intraslope salt basins is difficult, especially in shallow depocentres with rates of slope deformation that are in balance with rates of sedimentation, and where the slope is dynamic during the evolution of deep-water systems. In addition, autocyclic controls, such as avulsions (Armitage et al., 2012), levee growth, and the generation of depositional topography impacting accommodation, for instance, related to mass transport deposits (e.g., Kneller et al., 2016) or lobe-compensation (e.g., Prélat et al., 2009) are recurrent in deep water environment, and might form a similar stratigraphic signature as allocyclic controls, or partially obscure the allogenic signal (Ferguson et al., 2020, Fig. 1.2). In this thesis, the interplay of different controls on the evolution of submarine systems above salt-influenced dynamic stepped slopes ,is discussed.
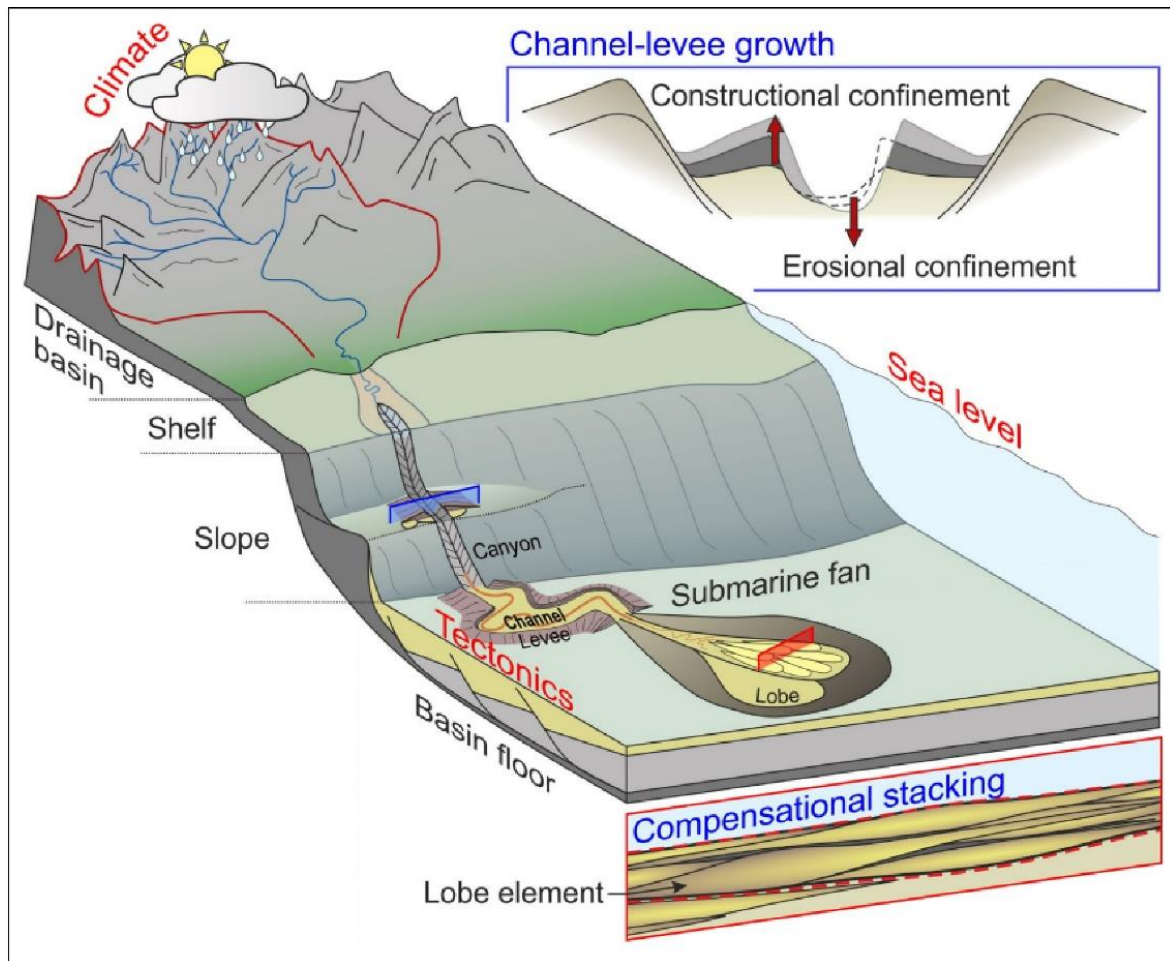
Figure 1.2: Continent to basin floor diagram showing the stratigraphic controls on deep-water systems. Climate, tectonics and eustasy (sea-level) are allogenic controls. Channel-levee growth and lobe compensational stacking are examples of autocyclic responses of submarine systems. Modified from Ferguson et al., 2020.

1.2.2 How do the stratigraphic record and configuration of topographically complex depocentres vary across different domains and under variable deformation rates in salt-bearing passive margins?

Salt-bearing passive margins are characterised by thin-skinned salt tectonics with a detachment surface at the base of the salt layer. The salt flow through gravity gliding and gravity spreading forms gravitationally-linked domains, with extension of salt and overburden in proximal settings and contraction in distal basin positions (e.g., Cobbold and Szatmari, 1991; Duval et al., 1992; Fort et al., 2004; Rowan et al., 2004; Brun and Fort, 2011; Davison et al., 2012; Jackson and Hudec, 2017). This simple mechanical

model is complicated by the interaction between extension and contraction in an intermediate position on passive margins (e.g., Fort et al., 2004; Ge et al., 2020) and by the base of salt relief that impacts local salt deformational style (e.g., Fort et al., 2004; Evans and Jackson, 2020; Ge et al., 2020). The variability in salt-related deformation creates topographically complex slopes with an abundance of complex depocentres, with configuration varying according to the salt deformational style (i.e., extensional or contractional or both), deformation rates, and position in the basin.

Minibasin-type depocentres have been widely documented in the Gulf of Mexico (Prather, 1998, 2003; Pirmez, 2000; Prather et al., 2012b; Wu et al., 2020) and in South Atlantic Basins (Oluboyo et al., 2014; Howlett et al., 2021; Rodriguez et al., 2021), reflecting highly mobile substrates that create three-dimensionally confined depressions with high rates of slope deformation compared to rates of sedimentation (Prather, 2000, 2003). Due to the importance of minibasins as slope sedimentary repositories, which might contain hydrocarbon reservoirs, these depocentres have been historically investigated regarding basin subsidence controls, internal stratal patterns and basin evolution, and stratigraphic evolution of deep-water systems (e.g., Prather et al., 1998, 2012b; Rowan and Weimer, 1998; Booth et al., 2003, Hudec et al., 2009; Kane et al., 2012; Oluboyo et al., 2014, Doughty-Jones et al., 2017; Ge et al., 2020; Jackson et al., 2020; Wu et al., 2020; Howlett et al., 2021). On the other hand, stepped slopes with weakly-confined depocentres, where subsidence is only slightly greater than sediment supply, have been less documented in salt basins. These settings have usually been described as connected tortuous corridors in between salt structures (e.g., Meckel et al., 2000; Prather, 2003; Steffens et al., 2003; Smith, 2004; Hay et al., 2012; Prather et al., 2017), with a few studies that address the stratigraphic evolution of deep-water systems in these depocentres (e.g., Smith, 2004; Hay, 2012).

Minibasins and tortuous corridors are associated with prominent flanking salt diapiric structures (i.e., stocks and walls), common in intermediate to distal basin settings, where salt-driven translation and/or contraction, and salt thickening dominate (e.g., Rowan and Weimer, 1998; Rowan et al., 2004; Brun and Fort, 2011; Howlett et al., 2021, Rodriguez et al., 2021; Fig. 1.3). In a proximal zone dominated by salt-driven extension, depocentres are described in the hanging wall of salt rollers and in troughs between rafted blocks (Anderson et al., 2000; Albertão et al., 2010), features formed

in the initial phase of passive margins evolution. Stepped profiles with shallow and open steps have been preferentially documented on mobile slopes with mud diapirism (e.g., Smith, 2004; Adeogba et al., 2005; Barton, 2012; Deptuck et al., 2012). Therefore, originally shallow depocentres, which are not associated with the healing phase of minibasins, are overlooked in salt basins. The thesis aims to document the stratigraphy of salt-controlled depocentres formed in the extensional salt domain under low to moderate deformation rates (Fig. 1.3). A comparison with other types of depocentres is provided in the synthesis (Chapter 6, section 6.2).
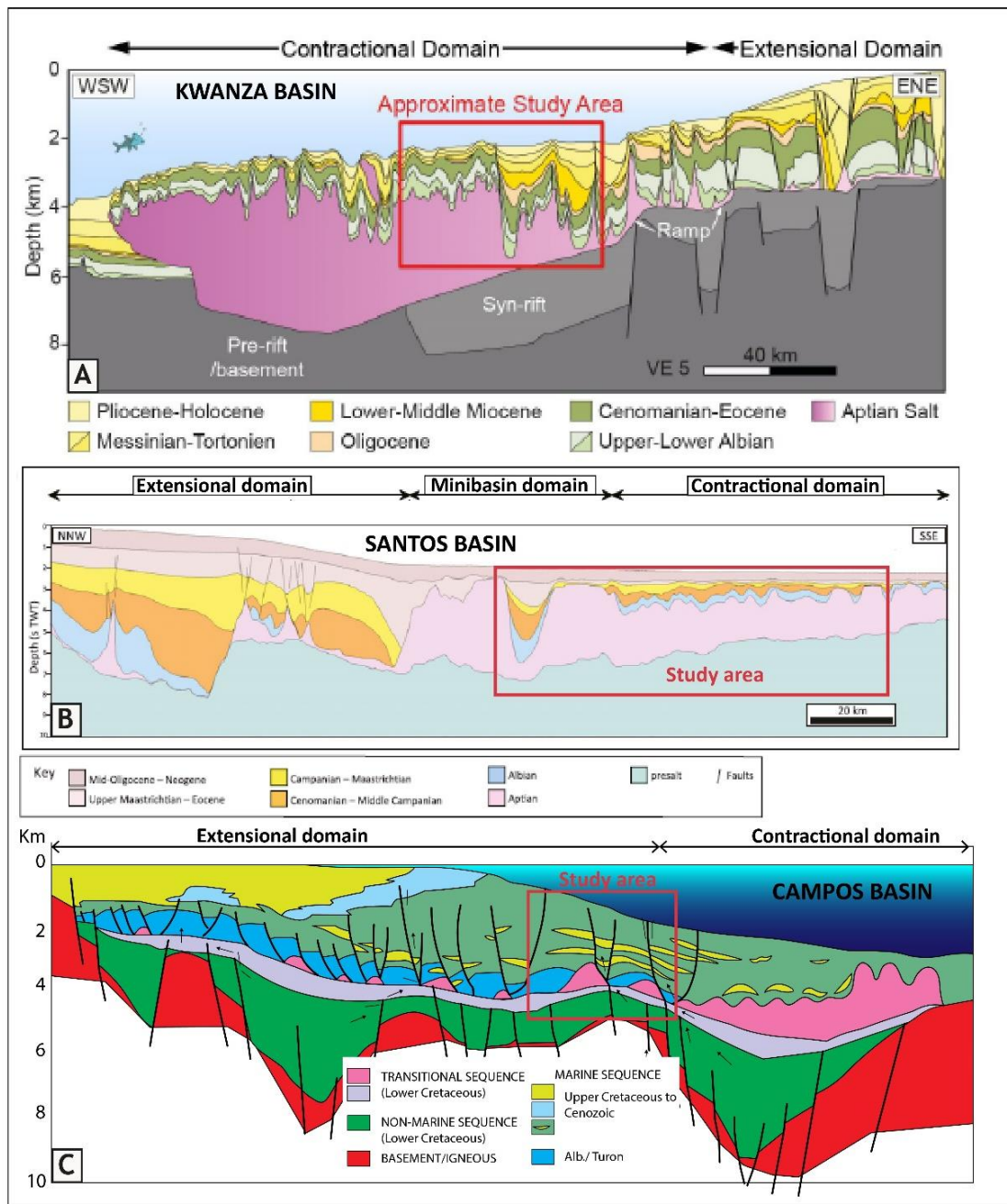
Figure 1.3: Dip geological section of South Atlantic-type passive margins. A-Kwanza basin (modified from Howlett et al., 2021). B-Santos Basin (modified from Rodriguez et al., 2021). C- Campos Basin (modified from Guardado et al., 2000; Rangel and Martins, 1998). In Kwanza and Santos basins, deep-water systems were investigated in minibasin fill in the intermediate to distal position in the basins, where contraction dominates (red square). In the Campos Basin, this thesis addresses deep-water systems deposited in intraslope depocentres in the extensional salt domain, where salt was thinned.

1.2.3 What is the impact of dynamic slopes on sedimentation, in three dimensions?

Slope topography is an important stratigraphic control on deep-water systems evolving above mobile slopes, controlling sediment dispersal pathways (Gee and Gawthorpe, 2006; Mayall et al., 2010) and depocentre formation (Prather et al., 2017). Complex but static topography has been considered in the classic fill-and-spill model, which predicts the filling to grade of accommodation space in pre-existent confined intraslope depocentres, followed by incision and bypass, as flows adjust to a lower base level established by a down dip depocentre (e.g., Prather et al., 1998; Beaubouef and Friedmann, 2000; Sinclair and Tomasso, 2002). The fill-and-spill model has also been applied in static weakly confined stepped-slopes (e.g., Adeogba et al., 2005; Barton et al., 2012; Jobe et al., 2017).

Dynamic slope topography in intraslope depocentres has been considered as vertical variation in subsidence through time in confined intraslope basins (e.g., Booth et al., 2003; Sylvester et al., 2015; Wu et al., 2020) or weakly confined steps (Deptuck et al., 2012; Brooks et al., 2018a). In these cases, the balance between slope deformation rate and sedimentation rate controls high-frequency stratigraphic cycles that stack vertically (Booth et al., 2003; Brooks et al., 2018a) or laterally compensate (Deptuck et al., 2012). The connection with down-dip depocentres is through the same exit point over time, reflecting the dominance of subsidence variation in the vertical axis.

Research undertaken in salt-withdrawal minibasins has documented variable stratal patterns in the basin fill associated with basin geometry and differential subsidence promoted by uneven salt deformation as a consequence of variations in the growth rates of salt structures, or variable deformational styles at minibasins flanks (i.e., contractional, extensional; e.g., Rowan and Weimer, 1998; Ge et al., 2019, 2020;

Jackson et al., 2020; Christie et al., 2021). These studies highlight that minibasins have a more complex evolution than pure dynamic down building. Nevertheless, minibasins generally have restricted dimensions, rarely reaching a few tens of kilometres in diameter (Hudec et al., 2009), and more frequently a few kilometres in diameter (Ge et al., 2020; Jackson et al., 2020) with thick stratigraphic successions (up to 8 km, Hudec et al., 2009), supporting a high vertical increment in subsidence as a relevant control on accommodation and basin evolution. This contrasts with dynamic shallow and open steps, where even minor longitudinal or lateral accommodation variations caused by basinward or lateral tilting, could imprint significant changes in architectural and stratigraphic patterns. In addition, minibasin studies focus on variations in stratal patterns and not on the stratigraphic architecture of deep-water systems evolving above dynamic topography. Therefore, there remains a limited knowledge base about the response of submarine channel and lobe systems to dynamic slopes that deform in three dimensions during deposition.

Depositional topography on and around mass transport deposits (MTDs) also influences slope accommodation and sediment dispersal patterns across different scales and in three dimensions (Kneller et al., 2016; Martínez-Doñate et al., 2021). Turbidites might be captured within evacuation scars (Spychala et al., 2015), within small and medium-scale top surface rugosity (Martínez-Doñate et al., 2021), or be impacted by a top MTD surface with dozens of metres of differential relief (Kneller et al., 2016). Mass transport deposits represent instantaneously deposited and, possibly, large volumes of sediments (Moscardelli and Wood, 2016; Steventon et al., 2019). This suggests the possibility of enhanced and differential compaction of underlying sediments depending on their sedimentological character or thickness variability in mass transport deposits. This could induce slope subsidence and could also influence three-dimensional variable accommodation and sediment dispersal patterns. Nevertheless, this hypothesis has not yet been discussed in mass-transport deposit literature.

1.3 Aims and objectives

The overall aim of this thesis is to improve the understanding of the stratigraphic evolution of submarine channel and lobe systems above dynamic slope settings at

different scales and under different controls within a salt-bearing passive margin. More specifically, the work aims to: i) to examine the controls on the large-scale topographic configuration of weakly confined intraslope depocentres, ii) to assess the spatial and temporal variability of lithology, architecture, and stacking patterns and interpret intra-depocentre gradient variations and 3D accommodation patterns, and propose a stratigraphic framework, iii) to investigate the influence of different stratigraphic controls during the evolution of deep-water systems, such as basin topography and sea level variations, iv) develop a new stratigraphic model for weakly confined intraslope depocentres influenced by lateral tilting (Chapter 3); v) understand submarine channels evolution above dynamic slopes (basinward tilting) and with rapid changes in accommodation (Chapter 4), and, vi) evaluate the impact of alternating salt-related extension and contraction on the configuration and evolution of a intraslope depocentre (Chapter 5).

To address these aims, the research has the following objectives:

1. to perform detailed seismic mapping and seismic attribute extraction on the target units, and regional seismic mapping on underlying stratigraphic horizons (i.e., top of the salt, top of the carbonate rafts, top Cretaceous, etc…),

2. to interpret the seismic geomorphology form attribute maps in order to make inferences about architectural elements, stacking patterns and the depositional system,

3. to produce thickness maps of the target units in order to make inferences about accommodation patterns variability, when appropriate,

4. to perform well correlation calibrated by seismic reflections' geometry in order to propose a stratigraphic framework,

5. to log cored wells in order to interpret sedimentary facies and processes,

6. to interpret well log motifs and image logs, and integrate them with core data and seismic character in order to make inferences about the depositional system,

7. to map (seismically) and interpret the structural elements (salt features and associated faults, rafts) with potential to impact deep-water accommodation in the palaeoslope during the evolution of the studied units.

1.4 Thesis outline

This thesis contains six chapters. Chapters 3 to 5 comprise the technical development chapters and are presented in this thesis in the form of manuscripts. Chapter 3 is published in Basin Research, being presented here in its final format. Chapter 4 was submitted to the Journal of the Geological Society of London, and the reviews suggest moderate revisions.

Chapter 2 – *Complex submarine slopes – a review*: this chapter summarises the main topics concerning submarine slopes with complex topography, such as types of slopes, types of depocentres in complex slopes, stratigraphic evolution of deep-water systems above complex topography, and the response of sediment gravity flows and submarine channels and lobes systems to complex topography. The chapter addresses more substantially slopes affected by salt tectonics.

Chapter 3 – *Fill-and-Spill, Tilt-and-Repeat (FaSTaR) cycles: stratigraphic evolution above a dynamic submarine stepped slope -* This chapter examines the influence of a salt-controlled dynamic slope topography on buried deep-water sedimentation above a stepped slope during the Oligocene-Miocene of Campos Basin, offshore Brazil. Extensive 3D seismic reflection mapping and well correlation were carried out to interpret thickness variations, lithology distribution and architectural patterns. Seismic geomorphology and stratigraphic truncation patterns were used to interpret a stratigraphic framework. A new model, the FaSTaR model, is proposed to explain the stratigraphic evolution of submarine channels and lobe systems in response to lateral slope tiling and sediment supply fluctuations.

Chapter 4 – *A salty snapshot: extreme variations in basal erosion patterns preserved in a submarine channel* – This chapter investigates in detail a buried submarine channel (Marlim Sul Channel) in the same area and time interval as Chapter 3, also integrating 3D high-resolution seismic reflection and well data. The basal erosional patterns, longitudinal thicknesses variations and sedimentary filling character of the channel were documented, revealing unique characteristics not commonly observed in ancient submarine channels. The chapter provides an evolutionary model for submarine channels that considers a dynamic slope with rapid readjustments caused by a transient basinward titling. This model sheds light on channel inception and long-term evolution processes that defy present paradigms.

Chapter 5 - *Intraslope accommodation controlled by salt tectonics and mass transport deposits emplacement in the extensional salt domain of Campos Basin* – This chapter assesses the impact of salt tectonics on long-term intraslope accommodation patterns within a shallow depocentre in the Oligocene-Miocene of Campos Basin, in an area approximately 50 km northwards from the area of Chapters 3 and 4. Short-term accommodation creation by the load of a large basal mass transport complex is also investigated. Extensive seismic mapping in 3D high-resolution seismic reflection, and well data were used to interpret the stratigraphic units filling the depocentre, with more detail in the large basal mass transport complex and the overlying turbidite unit. Thickness and stratigraphic patterns combined with seismic geomorphology of the stratigraphic units were used to interpret slope deformation history and subsidence. These reflect complicated patterns of salt deformation in the extensional salt domain and during a mature phase of a passive margin, a setting with poor knowledge regarding mobile intraslope depocentres.

Chapter 6 – This chapter provides an extended discussion of the research questions presented in Chapter 1. The findings presented in Chapters 3-5 and results from the literature are discussed and compared in order to provide new perspectives regarding the topics proposed in the research questions. A final section on future work recommendations provides new opportunities to deepen the research topics here presented.

1.5 Study area and dataset

This thesis investigates buried deep-water systems in two different areas in the central part of Campos Basin, more than 100 km from the coastline of Brazil (Fig. 1.4). In these areas, giant turbidite oil fields have been developed for many years. In the Barracuda and Marlim Sul oil fields (active for over 2 decades), the research focus is a contiguous deep-water system that evolved during the Oligocene-Miocene transition. The main reservoir unit of this system is here investigated (Marlim Unit). The other area refers to the Albacora Leste oil field and part of the Albacora oil field, which contain turbidite reservoirs producing for more than 15 years. The study focuses on deep-water systems that include mass transport deposits and a sand-prone turbidite unit from the Lower Miocene. In the drift phase of Campos Basin (from the

Albian to the present), all the sand-prone deep-water deposits, regardless of age, have been named the Carapebus Formation, while the siliciclastic mud-prone deep-water deposits have been named the Ubatuba Formation (Winter et al., 2007).
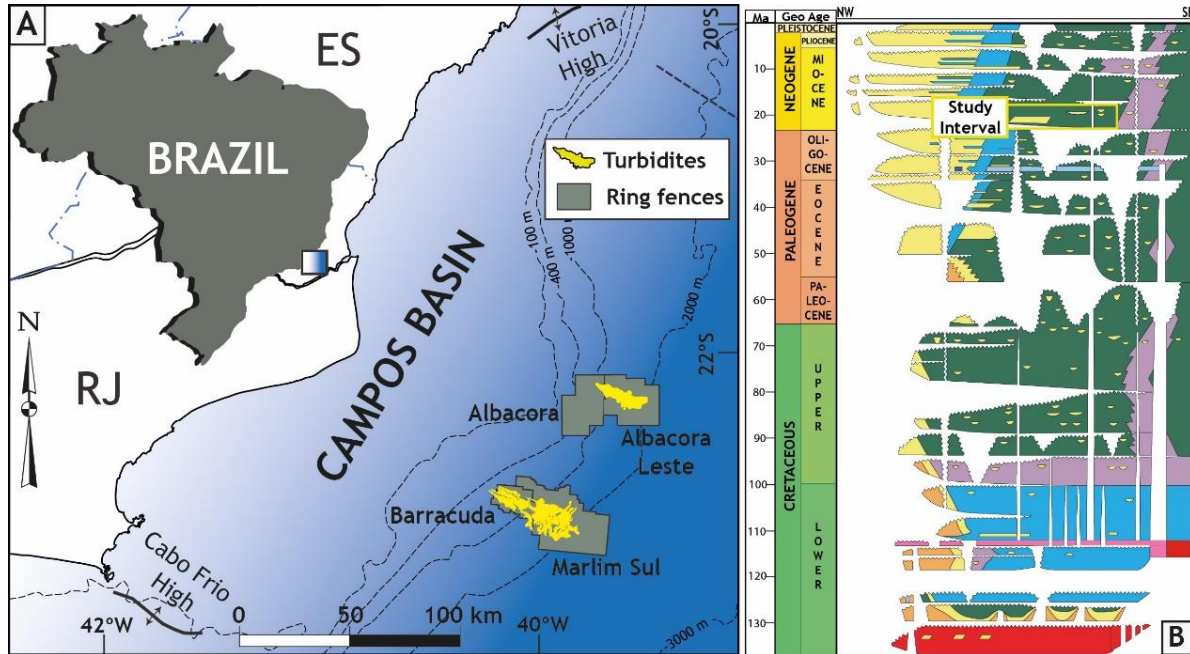
Figure 1.4: A-Location map of the two study areas in the central part of Campos Basin, offshore Brazil. B- Stratigraphic chart of Campos Basin (modified from Winter et. al., 2007). The study interval refers to deep-water deposits from the Oligocene to the Lower Miocene. Key for lithologies in the stratigraphic chart of B: red for basement, green for siliciclastic mudstones, yellow for sandstones, orange for conglomerates, blue for carbonates, pink for evaporites and pale purple for marls.

The subsurface dataset was provided by Petrobras S.A. company and by ANP, the Brazilian National Agency for Petroleum, Natural Gas and Biofuels. Three main types of data are used in this research: 3D seismic reflection volumes, well logs, including the basic wireline suite, image logs, and cores. Two seismic volumes with variable coverage and resolution were used in each of the study areas (Fig. 1.5). Seismic reflection data in the depth domain with good well calibration was available in the Albacora and Albacora Leste area. In the Barracuda and Marlim Sul area, time vs depth conversion was carried out during this research. Specifications of the seismic reflection data are provided in Table 1.1.
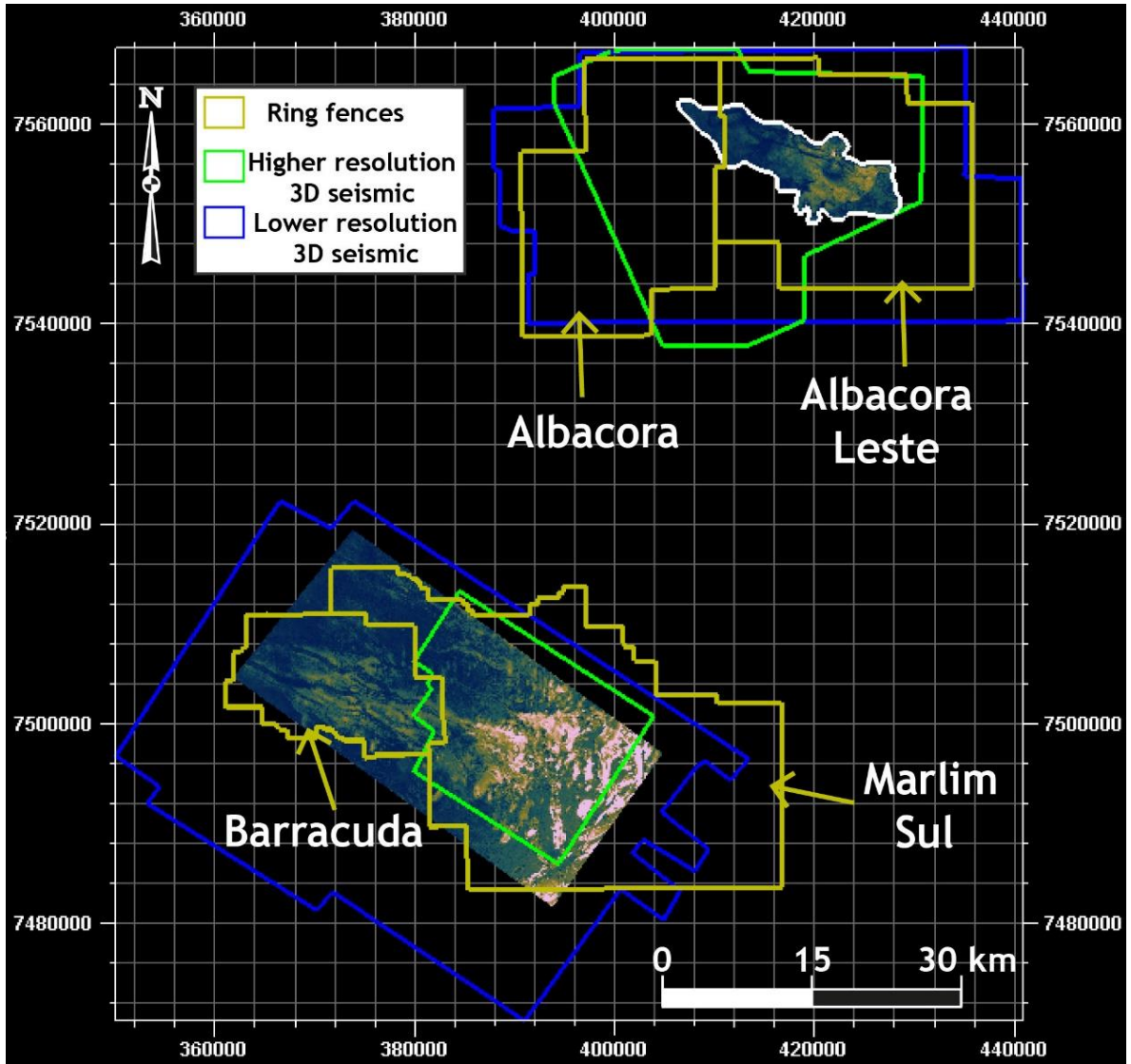
Figure 1.5: Ring fences and seismic coverage in the two study areas. Each area has two seismic volumes with different seismic resolution and coverage.

Table 1.1: Information about seismic volumes used in the thesis. Green and blue colours refer to Figure 1.5. PSTM – Pre-Stack Time Migration, PSDM – Pre-Stack Depth Migration.

Study Area	BARRACUDA / MARLIM SUL		ALBACORA/ALBACORA LESTE	
Type of Data	PSTM	PSTM	PSDM	PSDM
Domain	Time	Time	Depth	Depth
Inline interval	12.5m	12.5m	12.5m	12.5m
Crossline interval	6.25m	12.5m	6.25m	25
Vetical sampling	2ms	4ms	3m	5m
Time vs depth converted well-calibrated	NO	YES	YES	NO

There are many wells in these oil fields, which provide exceptional calibration of seismic response to lithological attributes (Fig. 1.6). All the wells contain the basic logs (gamma-ray, density, neutron and resistivity). Many contain sonic logs, and a few have image logs and cores (Figs. 1.7 and 1.8). Details on the type and quantity of data used are provided in the specific chapters.
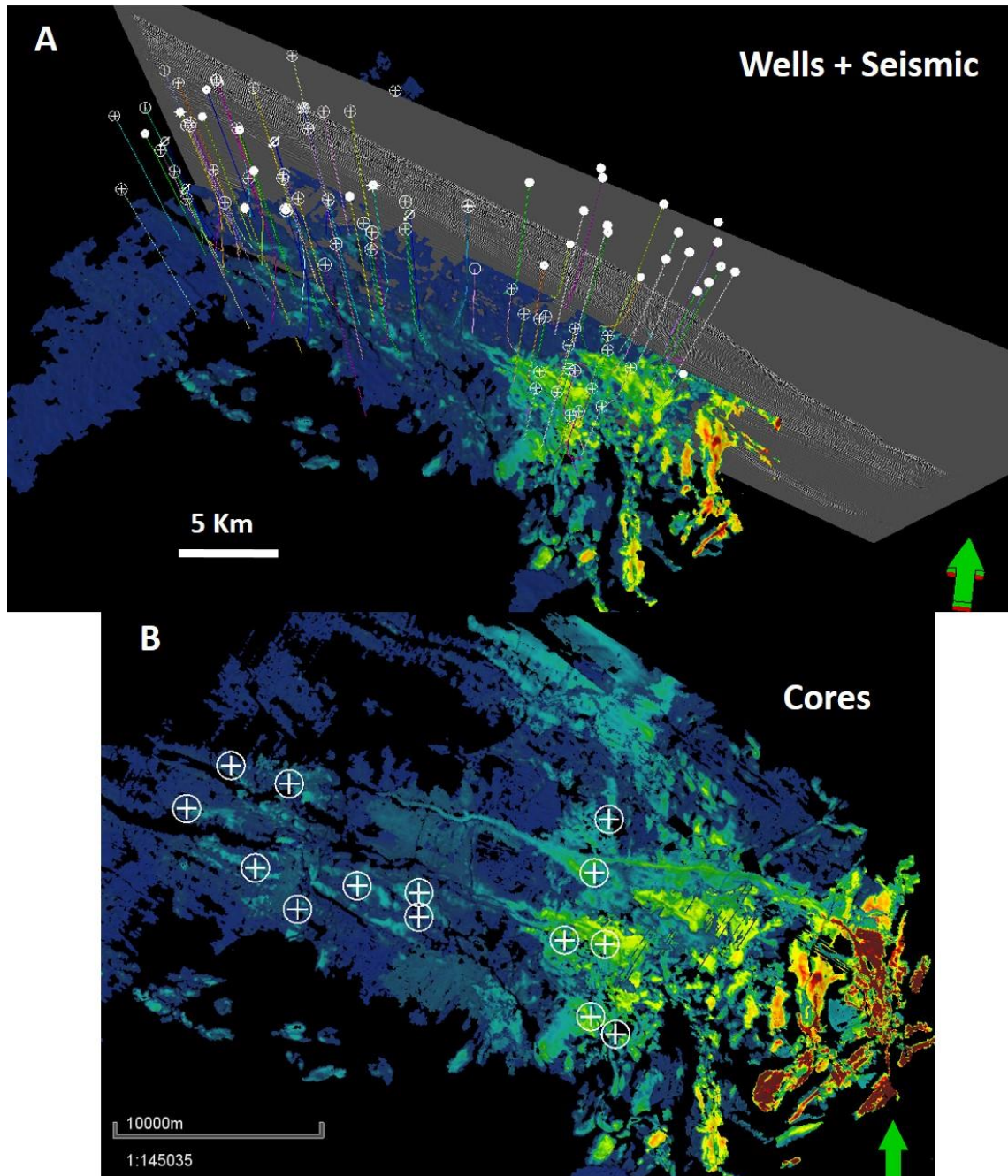
Figure 1.6: Wells in the Barracuda and Marlim Sul areas and amplitude map of turbidite reservoir (Marlim Unit, Chapter 3). A- There is a high density of wells since the study areas are in the ring fences of giant turbidite oil fields. B- There is also a significant number of cored wells.
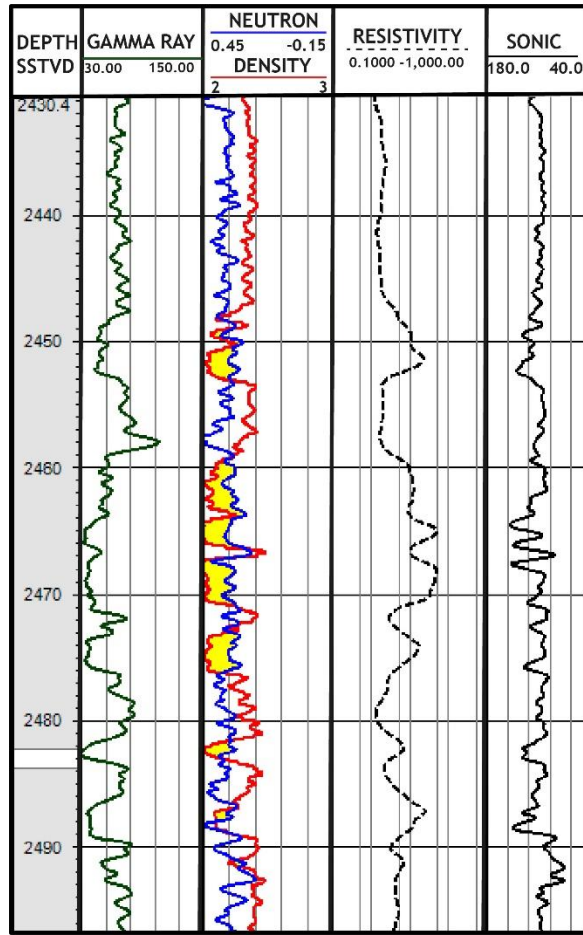
Figure 1.7: Example of a well with the complete wireline log suite (gamma-ray, neutron, density, resistivity and sonic).
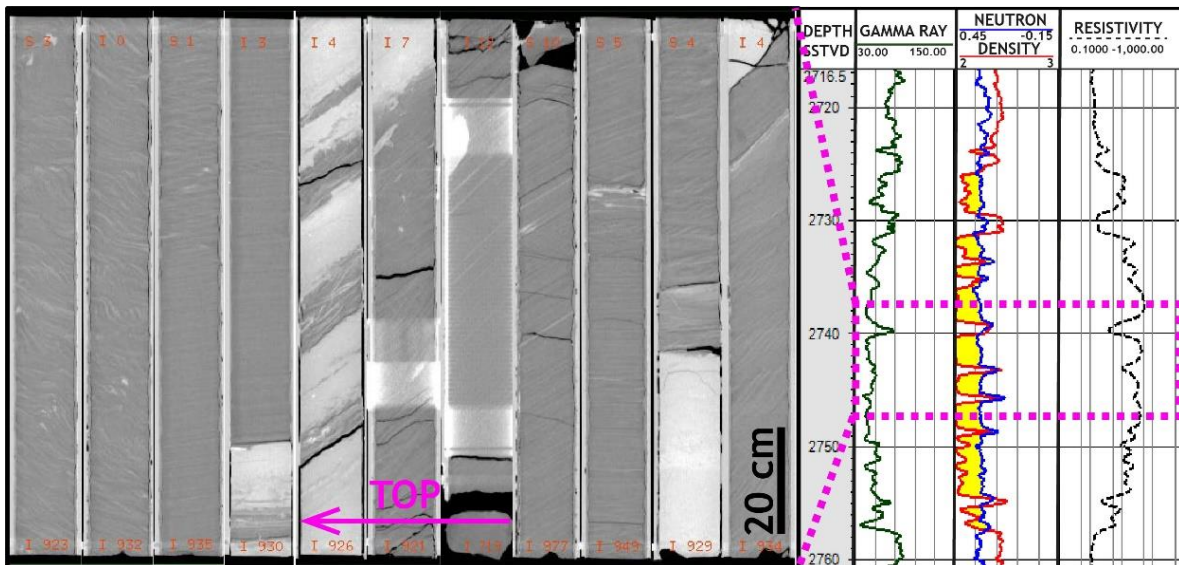
Figure 1.8: Example of a core in the Barracuda oil field (fluorescence image). Pink dotted line represents the cored interval in the logs.

Chapter 2 - Complex submarine slopes: a review

2.1 The slope

The submarine slope connects the shelf staging area to the distal basin floor region and is regarded as a site for sediment transfer to the deep-sea environment (Fig. 2.1). Although most of the sediment transported by turbidity currents bypasses the slope to be deposited in the deep basin, important sediment accumulations are concentrated in two main systems, in the submarine valley systems or in intraslope basins or aprons (e.g., Prather, 2003; Prather et al., 2017) (Fig. 2.1). Submarine valley systems comprise canyons, channels, levees, terrace deposits, and lobes (e.g., Pirmez et al., 2000; Posamentier and Kolla, 2003; Hansen et al., 2017; Prather et al., 2017). According to the distribution and character of these elements, slope valleys can vary between incised and leveed end-members (Galloway, 1998; Prather et al., 2017). Intraslope basins (Beaubouef and Friedmann, 2000), intraslope fans (Jobe et al., 2017), intraslope lobes (Brooks et al., 2018a) or submarine aprons (Prather, 2000, 2003; Barton, 2012) are sedimentary accumulations that form once flows lose their competence in transporting sediment above breaks-in-slope (Fig. 2.1). They might reflect the shape of the receiving depositional locus, which can confine the flows totally or partially.
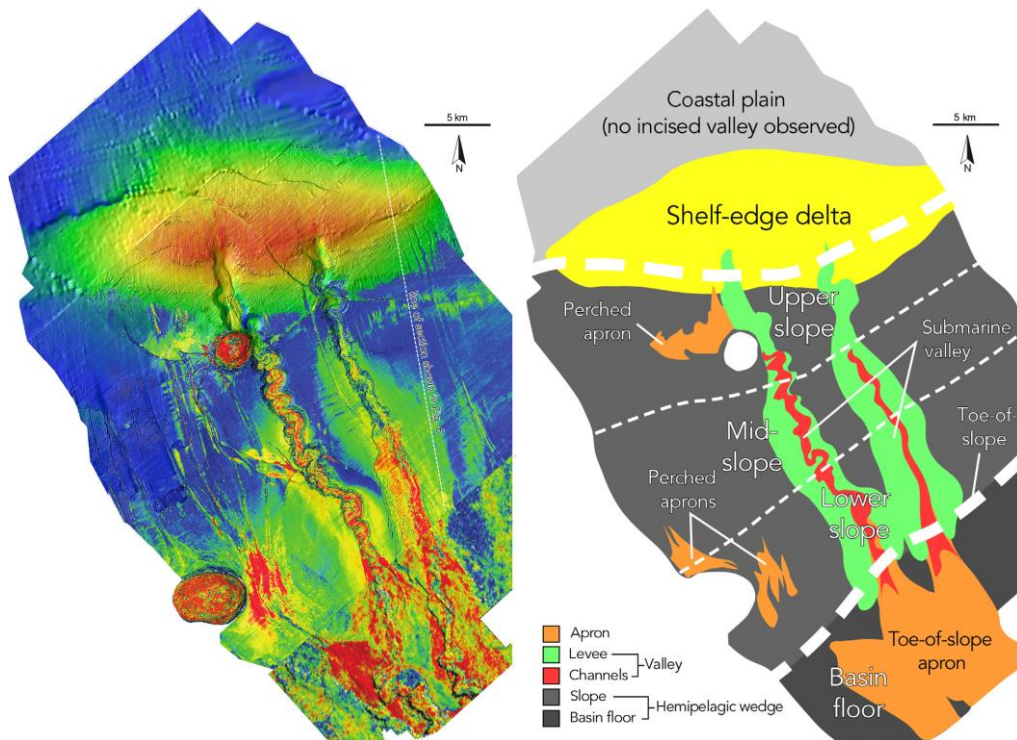
Figure 2.1: Example of shelf-to-basin floor profile with the Fuji and Einstein delta/submarine channel/apron system in the Gulf of Mexico (seismic attribute map at the left and depositional environments to the right). Extracted from Prather et al., 2017 (based on Sylvester et al., 2012). The main areas for sand accumulation in the slope are the submarine valleys and aprons.

Research undertaken worldwide has demonstrated that slope topography is a critical factor for deposition in deep-water systems, particularly important for sand-prone deposits and, therefore, turbidite hydrocarbon reservoirs. Slope topography governs submarine slope accommodation and is considered an essential element influencing submarine reservoirs' distribution, quality and architecture (Prather, 2003). Variations in slope topography deserve attention in the investigation of deep-water systems. Spatial changes in gradient cause sediment gravity flows to accelerate or decelerate, and correspondingly erode or deposit sediment (Normark and Piper, 1991). The slope accommodation and equilibrium profile concepts in the deep-water environment are essential to predict flow response to breaks in the slope and their associated deposits (e.g., Pirmez et al., 2000; Prather, 2000, 2003, 2017; Ferry et al., 2005; Adeogba et al., 2005; Barton, 2012; Deptuck et al., 2012; Hay, 2012; Wynn et al., 2012; Spychala et al., 2015; Jobe et al., 2017; Brooks et al., 2018).

2.1.1 Slope accommodation types

Slope accommodation is governed by the topography of the depositional surface and its graded or steady-state profile (Prather, 2003). The influential Prather (2000) publication classified accommodation in three main types: ponded, healed slope, and slope (Fig. 2.2). In each of these types, different processes dominate, resulting in characteristic stacking patterns, architecture and facies distribution. Ponded accommodation is formed in three-dimensional topographic lows that are able to totally capture the flows resulting in a confined style of deposition, as observed in ponded aprons (e.g., Prather, 1998, 2000, 2003) (Fig. 2.3). As a consequence, there is a tendency for high mud content from the suspended load of turbidity currents in ponded successions. In contrast, the healed-slope accommodation refers to the space above a stepped-equilibrium profile and higher angle equilibrium profiles and does not imply total confinement of the flows, resulting in sand-rich deposits (Prather, 2000). In this context, intraslope deposition is referred to by a variety of different terms, including: perched aprons (Prather et al., 2012a, 2017; Fig. 2.3), perched slope fill (Beaubouef and Friedmann, 2000), healed-slope aprons (Booth et al., 2002), transient fans (Adeogba et al., 2005), intraslope lobes (Spychala et al., 2015; Brooks et al., 2018a) and intraslope fans (Jobe et al., 2017).

According to the concepts proposed by Prather (2000, 2003), it is possible to infer that the total accommodation in the slope is the space between the depositional surface and the highest stable graded-slope angle. Moreover, Prather (2003) proposed the existence of three types of slopes, graded, below grade and above-grade, which are differentiated regarding morphological characteristics and topographic complexity (Fig. 2.2).
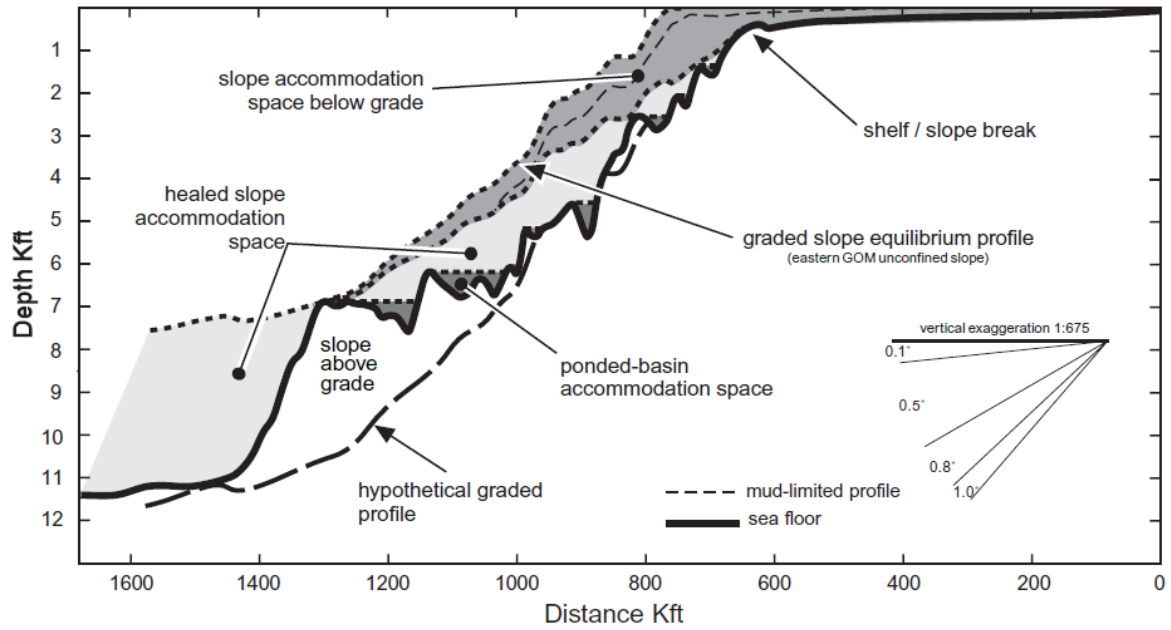
Figure 2.2: Seafloor profile from the central Gulf of Mexico that shows the kinds of slope and their related types of accommodation. From Prather, 2003 (modified from Prather, 2000).
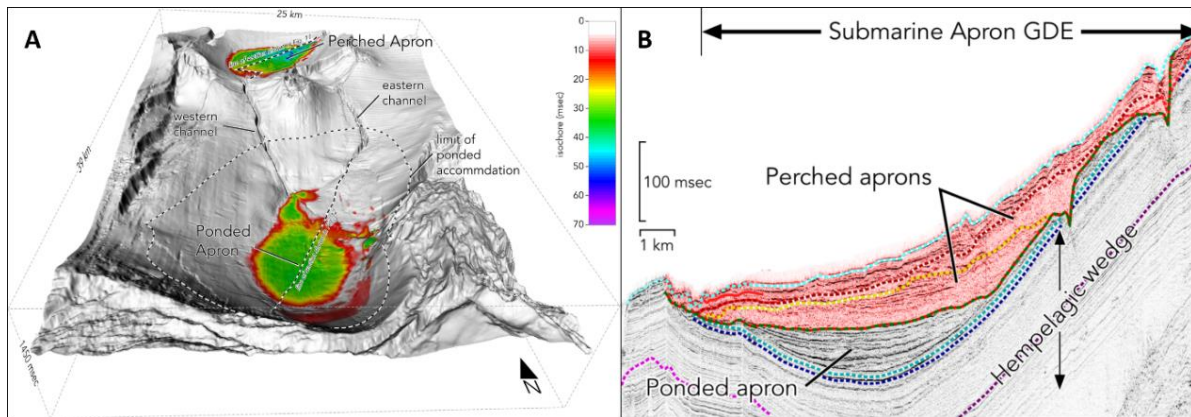
Figure 2.3: A - 3D view of the seafloor showing the two types of aprons, perched and ponded. B - Seismic section displaying the difference in confinement degree between ponded and perched aprons. GDE – gross depositional environment. From Prather et al., 2017.

Graded slopes are those characterised by stable slope angles and lack of significant topography, displaying a ramp-type morphology (Fig. 2.4). In this case, healed slope is the main type of accommodation identified, and unconfined deposition dominates the toe of the slope and basin floor regions, whereas sediment bypass characterises the upper slope.
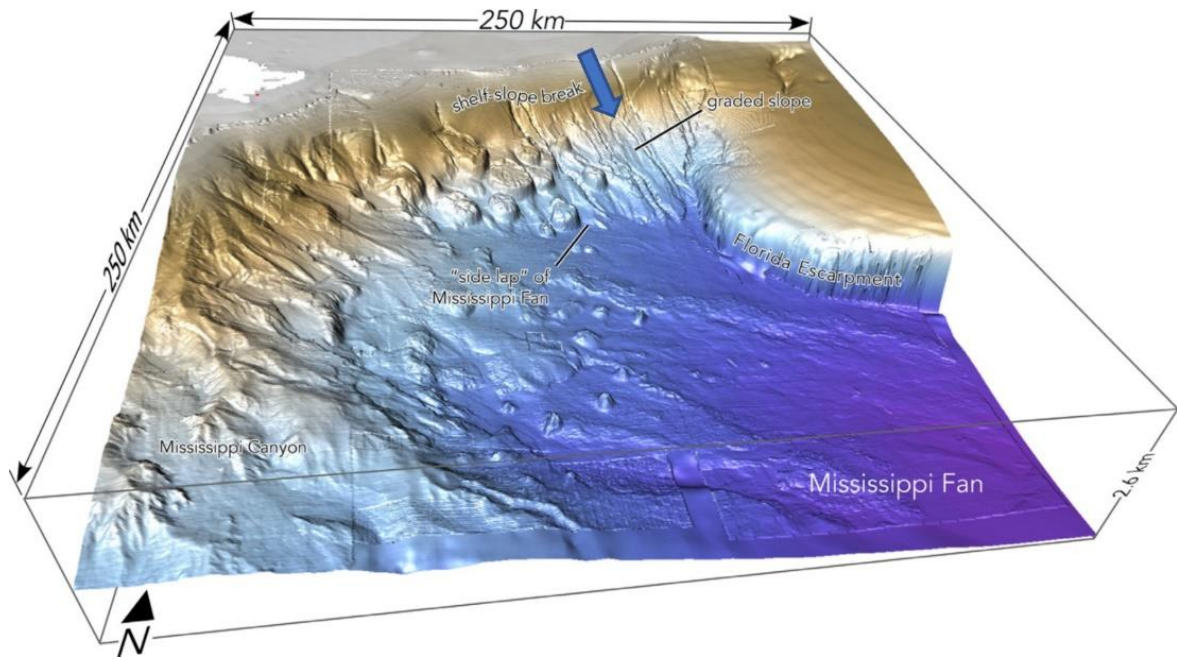
Figure 2.4: Example of a graded slope. Note the gentle slope topography (see blue arrow). Modified from Prather et al., 2017.

On the other hand, above-grade slopes are formed in areas with mobile substrates, which can generate enclosed intraslope basins with ponded accommodation (Beaubouef and Friedmann, 2000; Prather, 2000, 2003) (Fig. 2.5A) stepped profiles (e.g., Barton, 2012; Deptuck et al., 2012; Brooks et al., 2018a) (Fig. 2.5B), and even more complex configurations such as tortuous corridors (Steffens et al., 2003; Smith, 2004; Hay, 2012).

Stepped slopes are formed by the intercalation of higher and lower gradient slope sectors where sediment gravity flows are not entirely topographically confined and healed accommodation is present.
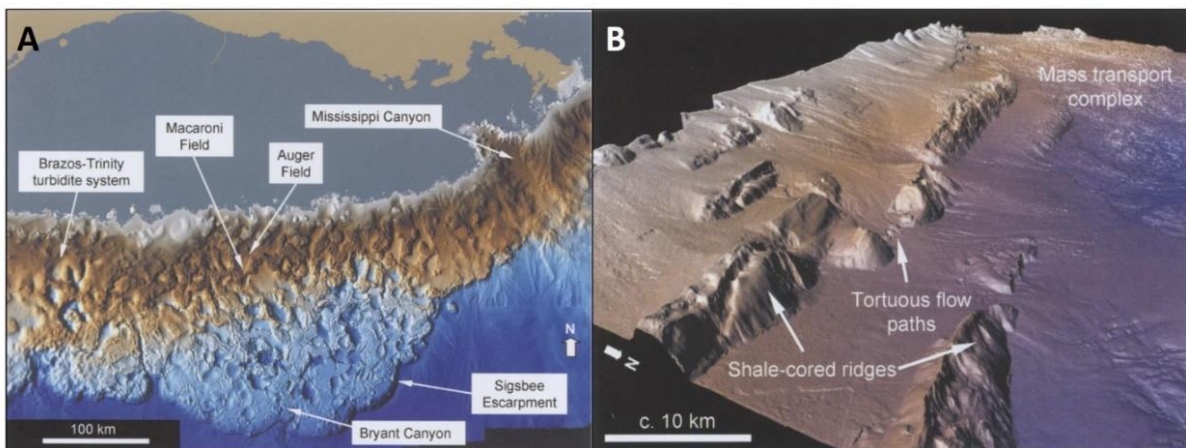
Figure 2.5: Seafloor images representing different contexts of above-grade slopes. A - Formation of ponded basins in the salt-deformed Gulf of Mexico slope. B - Stepped-slope with tortuous corridors linking the steps. Slope topography is controlled by shale ridges in northwest Borneo slope. From Smith, 2004.

Despite being widely used, the classification schemes proposed by Prather (2000, 2003) should be considered carefully since they convey a static and 2-dimensional interpretation of slope profiles and do not take into consideration the lateral and temporal variability of topography on slopes, especially in cases of active tectonic settings.

Different mechanisms can be considered to explain the creation of accommodation on the slope. The formation of above grade profiles (ponded or stepped) has been associated with halokinesis (Tomasso and Sinclair, 2000; Prather, 2003; Smith, 2004; Hay, 2012; Prather et al., 2012b; Howlett et al., 2021), mud diapirism (Adeogba et al., 2005; Deptuck et al., 2012; Prather et al., 2012a; Jobe et al., 2017), tectonics (Adeogba et al., 2005, Jobe et al., 2017) or even differential compaction (Jackson et al., 2008; Spychala et al., 2015) and slide scars (Morris et al., 2014; Spychala et al., 2015).

2.1.2 Slope equilibrium profile on mobile slopes

The erosional and depositional action of turbidity currents over periods of thousands of years leads to the development of a depth profile tending to an equilibrium condition (Pirmez et al., 2000; Fig. 2.6). This condition is reached when sediment discharge is carried through a channel with minimum aggradation or degradation. However, this situation is rare, and most systems are in a state of dynamic adjustment (Kneller, 2003). Equilibrium conditions are modified when tectonic deformation rates outpace sediment flux rates, or when there is a systematic change in the sediment flux compared to the prevailing flow conditions (Pirmez et al., 2000; Kneller, 2003). Flow density, flow thickness and the settling velocity of suspended sediment (relates to grain size) are the parameters that determine the tangent of the profile at a given point (Kneller, 2003).
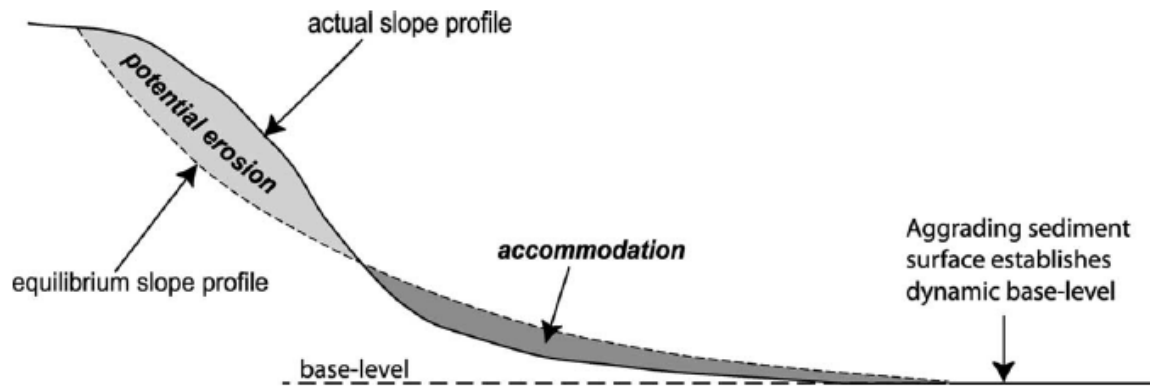
Figure 2.6: Schematic diagram of the theoretical equilibrium profile in relation to an actual slope profile. From Kneller, 2003.

On slopes with mobile substrates, the depositional profile is dynamic and frequently ungraded, and turbidite systems try to achieve a graded profile through erosional and depositional processes. The effects of seabed topography on sedimentary processes and architecture have been documented in many basins around the world. Pronounced channel incision and knickpoint formation are frequently associated with slope convexities caused by faulting and folding, common in basins affected by halokinesis (Pirmez et al., 2000), mud diapirism (Adeogba et al., 2005) and thrust and fold belts (Huyghe et al., 2004; Heiniö and Davies, 2007; Jolly et al., 2017). Higher gradient slopes also cause channels to be less sinuous and narrower, and to have less extensive levees, whereas the contrary is observed in lower gradients (e.g., Ferry et al., 2005; Deptuck et al., 2012; Fig. 2.7). Depending on the magnitude of the gradient reduction, channelised flows might lose confinement, losing their capacity to transport coarser fractions, as well as inducing flow expansion due to rapid loss of confinement (e.g., Mulder and Alexander, 2001; Spychala et al., 2020). Therefore, down dip of slope breaks are areas prone to the deposition of distributary channel and lobe complexes (e.g., Adeogba et al., 2005; Barton, 2012; Deptuck et al., 2012; Jobe et al., 2017; Brooks et al., 2018a).

Over time, regardless of the depositional environment within the deep-water spectrum, sediment gravity flows will tend to smooth out topographic irregularities by deposition and erosion in order to produce a smoothed surface that represents the equilibrium condition.
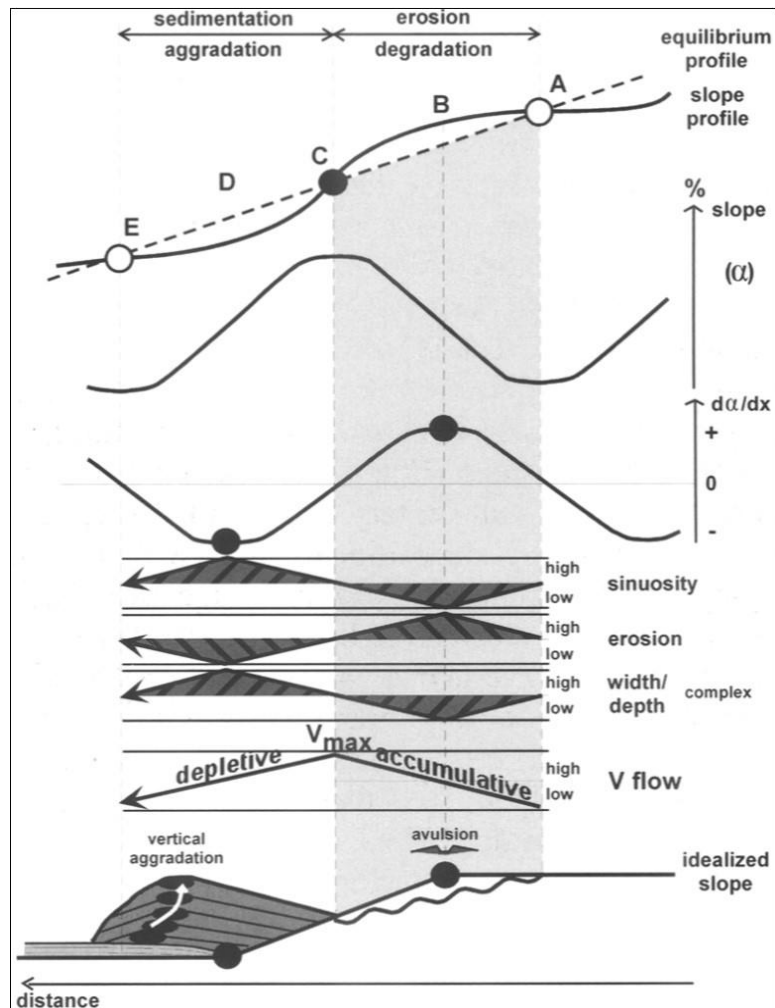
Figure 2.7: Schematic figure representing the equilibrium profile of deep-water turbidite systems, and the expected products and process related to gradient variation (see text for discussion). From Ferry et al., 2005.

The concept of the equilibrium profile has been applied to stratigraphic models that explain the evolution of depocentres in above grade slopes. The intraslope basins of the Gulf of Mexico provide a good example of the dynamics of deep-water systems in ungraded profiles. Several studies document the stratigraphic evolution of four linked Pleistocene minibasins, where slope accommodation is controlled by salt tectonics in the Gulf of Mexico (e.g., Winker et al., 1996; Beaubouef and Friedmann, 2000; Sinclair and Tomasso, 2002; Prather et al., 2012b). The stratigraphic evolutionary model proposed by Beaubouef and Friedmann (2000) proposes three phases (Fig. 2.8). The first and second phases are depositional, with the first associated with ponded filling and the second with healed accommodation filling, which the authors refer to as perched filling. At the end of this depositional stage, the basin is totally filled to its spill

point. Once this condition is established in the uppermost basin, channel incision progressively takes place, smoothing out bathymetric irregularities of the slope. This process characterises the third and last phase, which reflects the attempt of the system to achieve a graded profile through erosion and bypass. This cycle will repeat once individual basins are filled and subsequently bypassed. Over time, the topographic irregularities will be healed or smoothed, and the slope will be graded with the regional equilibrium profile. A similar model was proposed by Sinclair and Tomasso (2002), however, including a last phase of abandonment and channel backfilling (Fig. 2.9). These stratigraphic models are the foundations of the fill-and-spill model, a classic model that explain the stratigraphic evolution of static intraslope depocentres, or mobile intraslope depocentres that are dynamic only about their vertical axes.
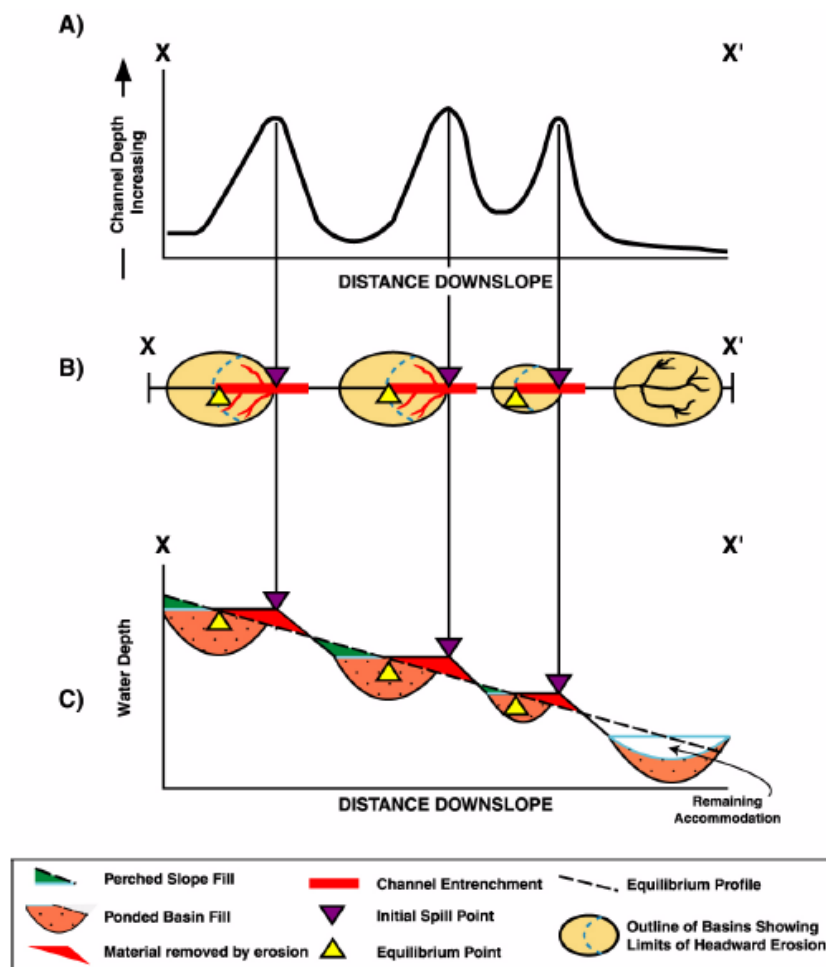
Figure 2.8: Generic fill-and-spill model to explain the evolution of intraslope basins (see text for discussion). The model was inspired by the Gulf of Mexico intraslope basins. From Beaubouef and Friedmann, 2000.
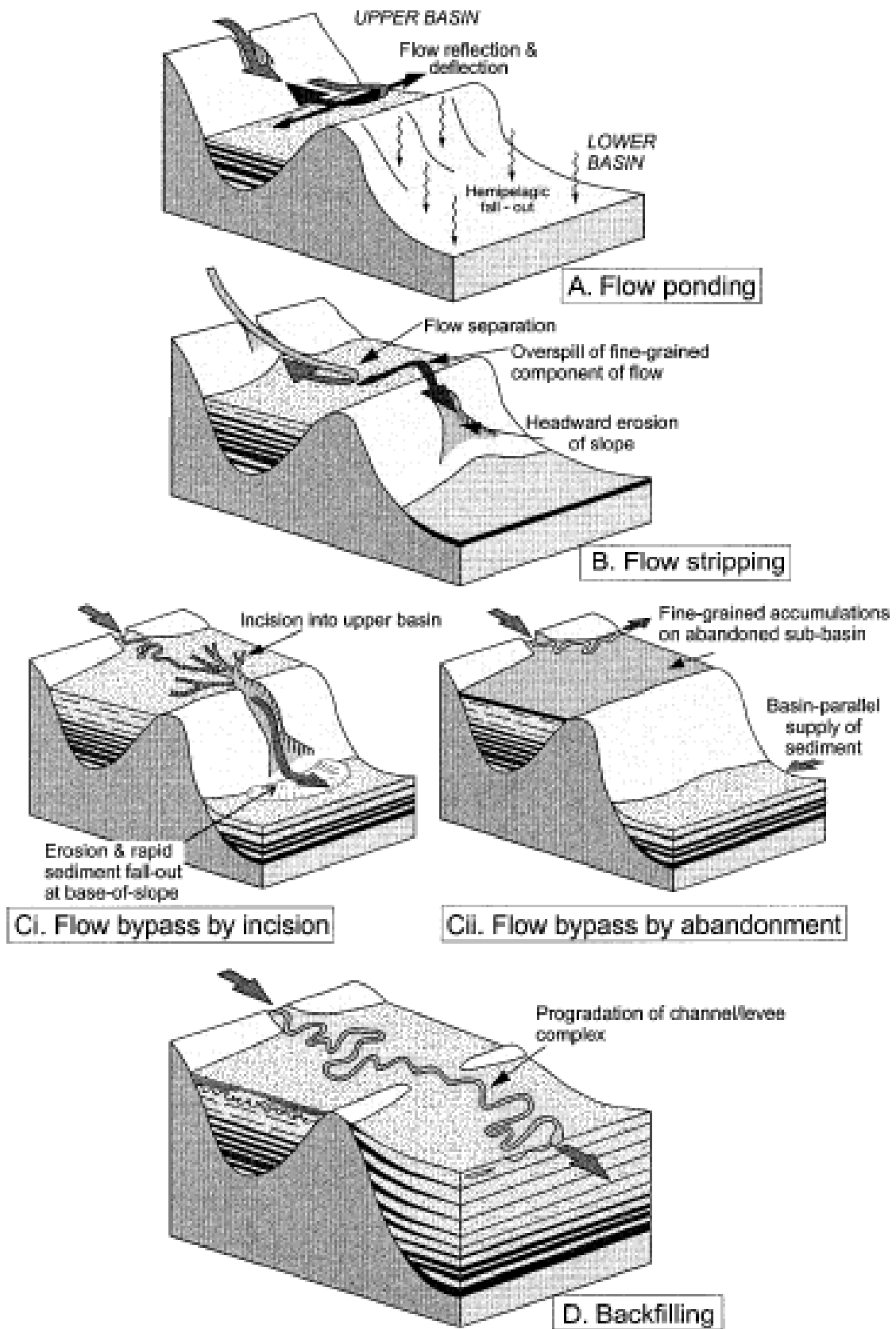
Figure 2.9: Evolutionary phases of the fill-and-spill stratigraphic model. See text for explanation. From Tomasso and Sinclair, 2002.

2.1.3 Salt-influenced slopes

Salt basins are known for having high rates of substrate mobility and, consequently complex slope topography that control sediment pathways, sand distribution and architecture of channel and lobe systems (e.g., Beaubouef and Friedman, 2000; Prather, 2003; Gee and Gawthorpe, 2006; Mayall et al., 2010; Kane et al., 2012; Oluboyo et al., 2014). Salt domes are very effective deformation agents and can affect the geology up to a radius approximately twice the diameter of the salt structure (Gee and Gawthorpe, 2006). Channels and lobes influenced by halokinesis provide good case studies to investigate the effect of inherited and growing topographic structures on turbidity current behaviour (e.g., Gee and Gawthorpe, 2006; Mayall et al., 2010; Kane et al., 2012; Oluboyo et al., 2014). Research regarding this topic suggests that the size, shape and orientation of salt structures in the slope, combined with the timing of structure growth and channel initiation and development (flow magnitude variability and periodicity), are key factors to be considered in order to understand the evolution of submarine channel and lobe systems in salt basins (e.g., Mayall et al., 2010; Kane et al., 2012; Oluboyo et al., 2014) (Fig. 2.10).

2.1.3.1 Submarine channels in a salt-controlled slope

The dynamic character of salt basins induces constant adjustments in channel profiles, possibly resulting in large-scale changes in the depositional style (e.g., Kane et al., 2012). Deflection and diversion of flows, changes in channel geometry and thinning and onlapping strata onto structural highs can be associated with inherited seabed relief that control channels (e.g., Mayall et al., 2010; Hay, 2012; Oluboyo et al., 2014). However, the resultant depositional and erosional features will depend on the balance between salt structure growth rate and channel incision rate. Channel diversion, for instance, can be a response of tectonic activity synchronous to channel development if the channel has low erosive power (e.g., Mayall et al., 2010). Additionally, evidence for coeval deformation and deposition has been recognised in other situations, such as asymmetric laterally migrating channels with offset stacking in the vicinity of salt structures (e.g. Gee and Gawthorpe, 2006; Mayall et al., 2010, Kane et al., 2012); channels that avulse (e.g. Gee and Gawthorpe, 2006; Kane et al., 2012) or thicken in the proximity of faults and domes; channels that exhibit lateral and vertical shifts and

strata that thin onto salt-cored structural highs (e.g. Gee and Gawthorpe, 2006; Mayall et al., 2010).
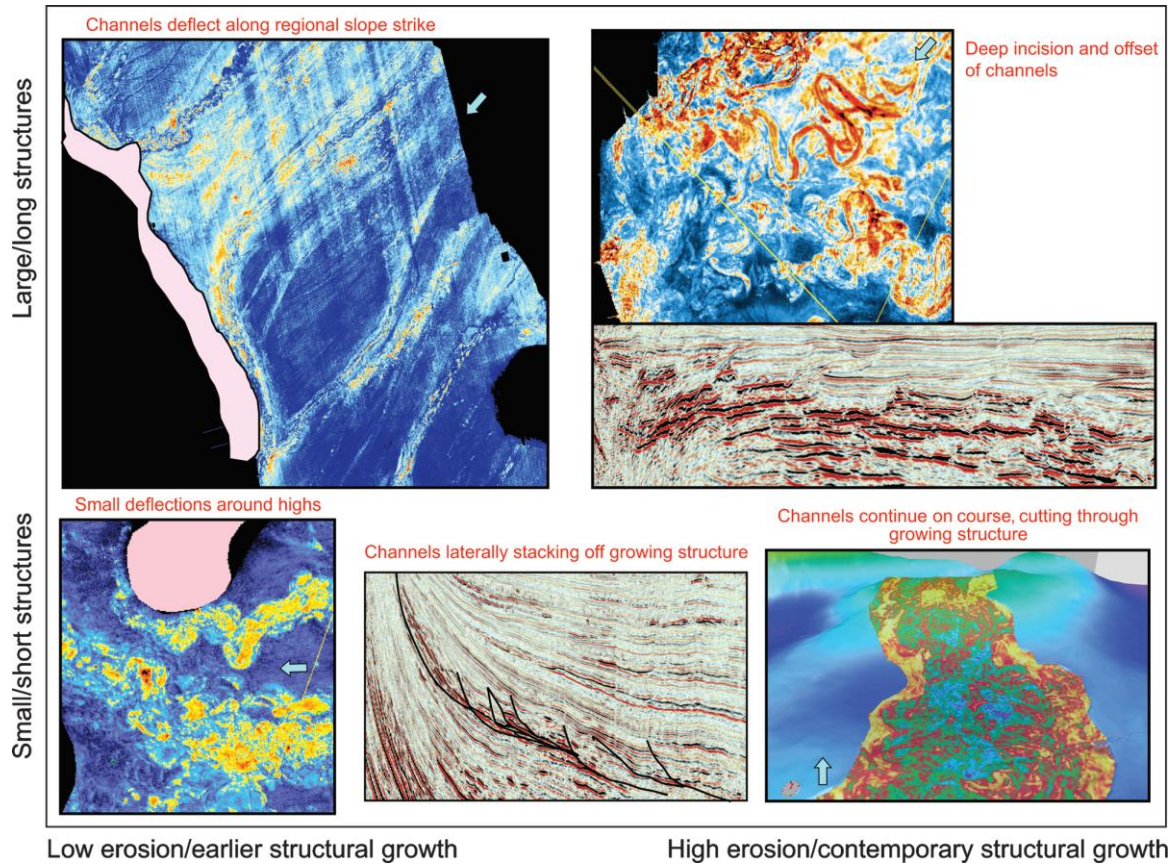
Figure 2.10: Channel responses to salt activity considering the size of the structures, the erosive power of channels, and the timing of the growth of the structures and channel development. From Mayall et al., 2010.

2.1.3.2 Salt-influenced depocentres

Salt deformation creates topographically complex slopes with preferential areas for deposition. These can be formed in the extensional/transitional/contractional domains of salt basins. Salt withdrawal basins is a generic term to designate any depocentre formed by the expulsion of underlying salt, whereas minibasin is a narrower term that refers to salt-withdrawal basins surrounded by upwelling shallow salt (Jackson and Hudec, 2017, Fig. 2.11a,b). Salt-withdrawal basins, including minibasins, sink into thick salt. Basin subsidence can be triggered by several mechanisms, including density-driven subsidence induced by sedimentary load, extension of salt structures creating accommodation above fallen diapirs or in between an extended diapir, and

due to shortening of diapirs creating a synclinal minibasin (Hudec et al., 2009; Jackson and Hudec, 2017).

Minibasins

Minibasins can be circular to elliptical in plan view, with diameters in the order of 5-25 km (Prather et al., 1998, 2012; Booth et al., 2003; Jackson et al., 2019; Wu et al., 2020), or can be elongate, being 5-10 km wide and up to 40 km long (Oluboyo et al., 2014; Ge et al., 2021; Howlett et al., 2021; Rodriguez et al., 2021). As a consequence of high subsidence rates, minibasins display thick successions that can be several kilometres thick, as reported in the Pliocene-Pleistocene in the Gulf of Mexico (up to 8 km, Hudec et al., 2009), in the Precaspian Basin in Kazakhstan (up to 5.5 km thick, Jackson et al., 2019; Duffy et al., 2021), and in many other examples where thicknesses are high but reported in seismic two-way-time (e.g., Oluboyo et al., 2014; Doughty-Jones et al., 2017; Wu et al., 2020; do Amarante et al., 2021; Rodriguez et al., 2021). These geometric characteristics support 3D confinement and high subsidence rates, reaching more than 10 km/Ma (Prather, 2000). Minibasin fill onlaps towards the flanking salt structures (Fig. 2.11b). Strata packages can be bowl-shaped (thin towards basin flanks and thicken in the basin centre), wedges (thicken in one direction) and layered (sheet-like), varying according to subsidence history (e.g., Rowan and Weimer, 1998; Jackson et al., 2020). Ponded accommodation is present, particularly in the initial stages of basin evolution (e.g., Prather, 2003; Doughty-Jones et al., 2017; Rodriguez et al., 2021).

Minibasin filling may comprise a variety of deep-water depositional systems, which will emerge from the interplay of deformation and sedimentation rates, the configuration of salt structures and variation of sediment supply trough time (e.g., Prather et al., 1998; Rowan and Weimer, 1998; Beauboueff and Friedmann, 2000; Booth et al., 2003; Howlett et al., 2021). Prather et al. (1998) propose two facies assemblages that represent the evolution of confinement within minibasins. The ponded facies assemblage is sand-rich and comprises submarine fans complexes with sand sheets and leveed channels, which can be intercalated with mass flow units and, eventually, muddy turbidites and hemipelagic drapes. This assemblage represents high confinement. The overlying bypass facies assemblage is mud-prone, comprising

leveed-channels and overbanks, muddy turbidites and hemipelagic drapes, and mass flow units, representing a low confinement stage. These facies assemblages generally represent stratigraphic phases of the fill-and-spill model (e.g., Prather et al., 1998; Beauboueff and Friedmann, 2000; Sinclair and Tomasso, 2002). The filling of minibasins might be complicated by the evolving salt structures. Mass transport complexes have been associated with remobilisation above basin flanks due to salt tectonics (e.g., Prather et al., 1998; Madof et al., 2009, 2017; Doughty-Jones et al., 2017; Howlett et al., 2021). In South Atlantic-type passive margins that display a complex array of interconnected elongate salt-walled minibasins, the routeing, geometry and stacking patterns of submarine channels and lobe systems are highly affected by the configuration and movement of the salt structures through time (e.g., Oluboyo et al., 2014; Doughty-Jones et al., 2017; Howlett et al., 2021; Rodriguez et al., 2021)

Tortuous Corridors

Tortuous corridors in salt basins are laterally confined by prominent diapiric salt structures such as stocks and walls, forming elongate depocentres connected by intervening higher gradient areas, being considered a type of stepped slope (e.g., Prather, 2003; Smith et al., 2004; Hay 2012; Fig. 2.11c,d). However, the overall configuration of tortuous corridors is considerably different from stepped slope systems formed due to other deformational agents than salt tectonics, such as mud diapirism, which tend to produce subtle gradient variations without significant lateral confinement (e.g., Adeogba et al., 2005; Deptuck et al., 2012; Prather et al., 2012a; Jobe et al., 2017, Fig. 2.5b). Regarding geometry, tortuous corridors are a few km wide but can be up to 60 kilometres long (Steffens et al., 2003). Accommodation is controlled by salt deformation, however; tortuous corridors contrast with minibasins because they are not truly silled and ponded accommodation is absent or not significant. Therefore, they are associated with lower subsidence rates when compared to minibasins. Nevertheless, as they tend to occur in areas of thick salt similar to minibasins, tortuous corridors are also associated with middle and distal basin positions of passive margins, where basinward salt flow induces salt thickening and the formation of prominent salt structures, such as walls and stocks, many of

which are associated with contractional deformation (Howlett et al., 2021; Rodriguez et al., 2021).

In 2D seismic profiles, tortuous corridors might display similar characteristics with minibasins like convergent and thinning strata that onlap towards lateral basin flanks and relatively thick stratigraphic successions (e.g., Prather, 2003; Smith, 2004; Hay, 2012, Fig. 2.11d). Nevertheless, strata are continuous and more isopachous along the corridor axis. Gradient variations along the corridor control architectural variability, with high gradient sectors promoting channelisation and erosion and lower gradient steps recording unconfined deposition like submarine distributary-lobe complexes (e.g., Smith, 2004; Hay, 2012). Hay (2012) describes a succession of stratigraphic packages, each marked by a final bypass phase and a final stage of the corridor filling marked by complete sediment bypass via large bypass channels indicating depocentre healing and that sedimentation rates repeatedly exceed deformation rates. Therefore, it is logical that tortuous corridors are interpreted to have moderate deformation rates when compared to minibasins (Meckel et al., 2002; Prather, 2003; Smith, 2004; Hay, 2012).
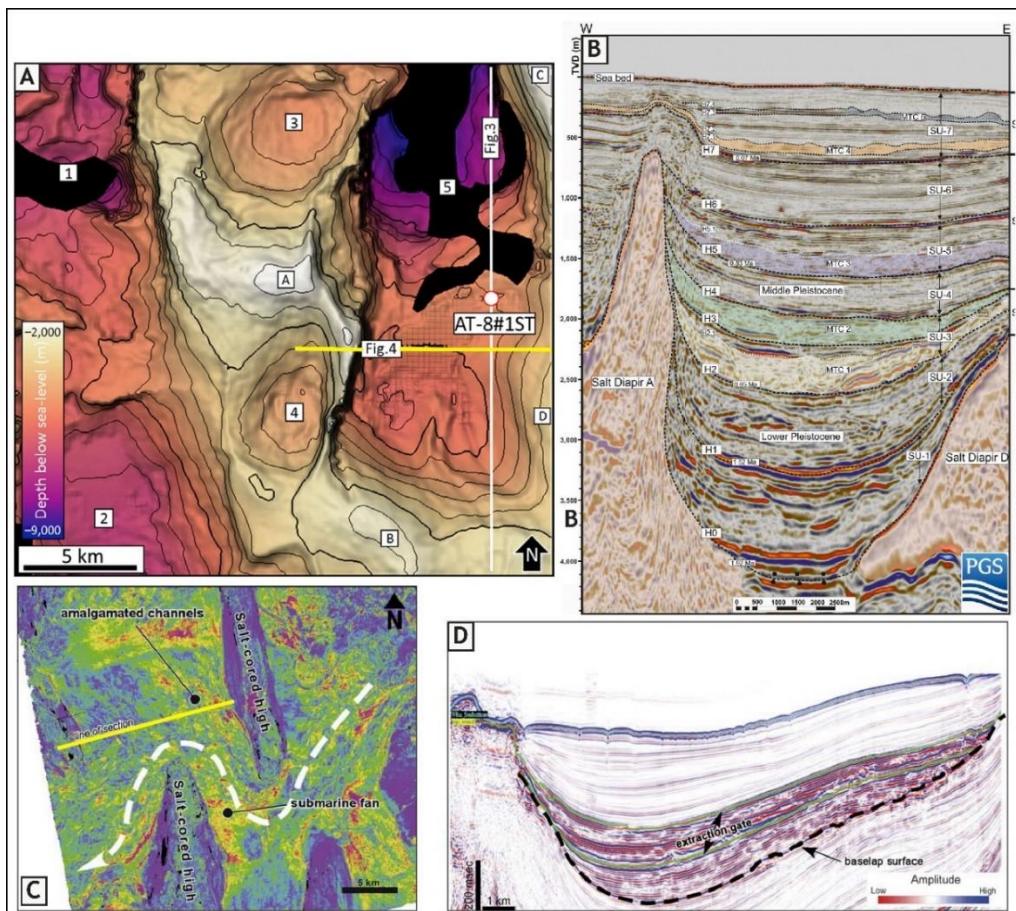
Figure 2.11: Depocentres in salt basins. A- Map view of classic minibasin with bowl-shaped geometry in the Gulf of Mexico. B- Strike seismic profile in minibasin fill (see yellow line in A for location. Note salt diapirs forming the flanks of the minibasin. A and B modified from Wu et al., 2020. C- Map view of a tortuous corridor from west Africa. D- Seismic profile of the tortuous corridor filling and salt structures. C and D modified from Prather, 2003.

Depocentres in the extensional salt domain

In areas dominated by extensional deformation, common structures are salt diapirs, salt rollers, rafts and rollovers with associated normal faults , which record high rates of thin-skinned horizontal extension (e.g., Duval et al., 1992; Demercian et al., 1993; Jackson and Hudec, 2017; do Amarante et al., 2021). During active extension and downdip salt flow, asymmetric depocentres have been documented in the hangingwall syncline of extensional faults of salt-rollers in pre-rafts and between rafts (e.g., Duval et al., 1992; Anderson et al., 2000; Broucke et al., 2004; Albertão et al., 2010; Quirk et al., 2012; do Amarante et al., 2021, Fig. 2.12). These depocentres are elongate troughs aligned with main fault trends, often strike-oriented and connected by relay ramps (Anderson et al., 2000). Their size will reflect the evolution of extensional structures. Deep widening grabens can be more than 5 km wide and dozens of km long (Duval et al., 1992, Anderson et al., 2000). In addition, extension can cause diapirs to subside, forming depressions (Jackson and Vendeville, 1992; do Amarante et al., 2021; Fig. 2.13 A). In specific cases, when the depocentre is surrounded by salt, it can be considered a type of minibasin (Fig. 2.13 B; Jackson and Hudec, 2017). Like fallen diapirs, salt walls between rafts and extensional anticlines can form depocentres once these walls are depleted during prolonged extension (Quirk et al., 2012).

Depending on the deformation rates and duration, growth (normal) faults can generate depocentres with thick successions up to 4 km thick, as documented in a Miocene graben between rafts in Kwanza Basin (Anderson et al., 2000). Divergent stratal patterns are expected towards growth faults, which might form rollovers, with thickening at the centre of the syncline and thinning at the monocline (Duval et al., 1992; Anderson et al., 2010); however, passive infill after depocentre generation is also documented in between pre-rafts (Albertão et al., 2010). Regarding deep-water deposition, the elongate depressions might capture turbidity currents. Sand-prone submarine channel and lobe complexes (Albertão et al., 2010), and erosionally

confined channel complexes that evolve into channel-levees have been documented in these depocentres (Anderson et al., 2010). Diversion and deflection of submarine channels within the hanging wall are evidence for significant seabed structural relief.
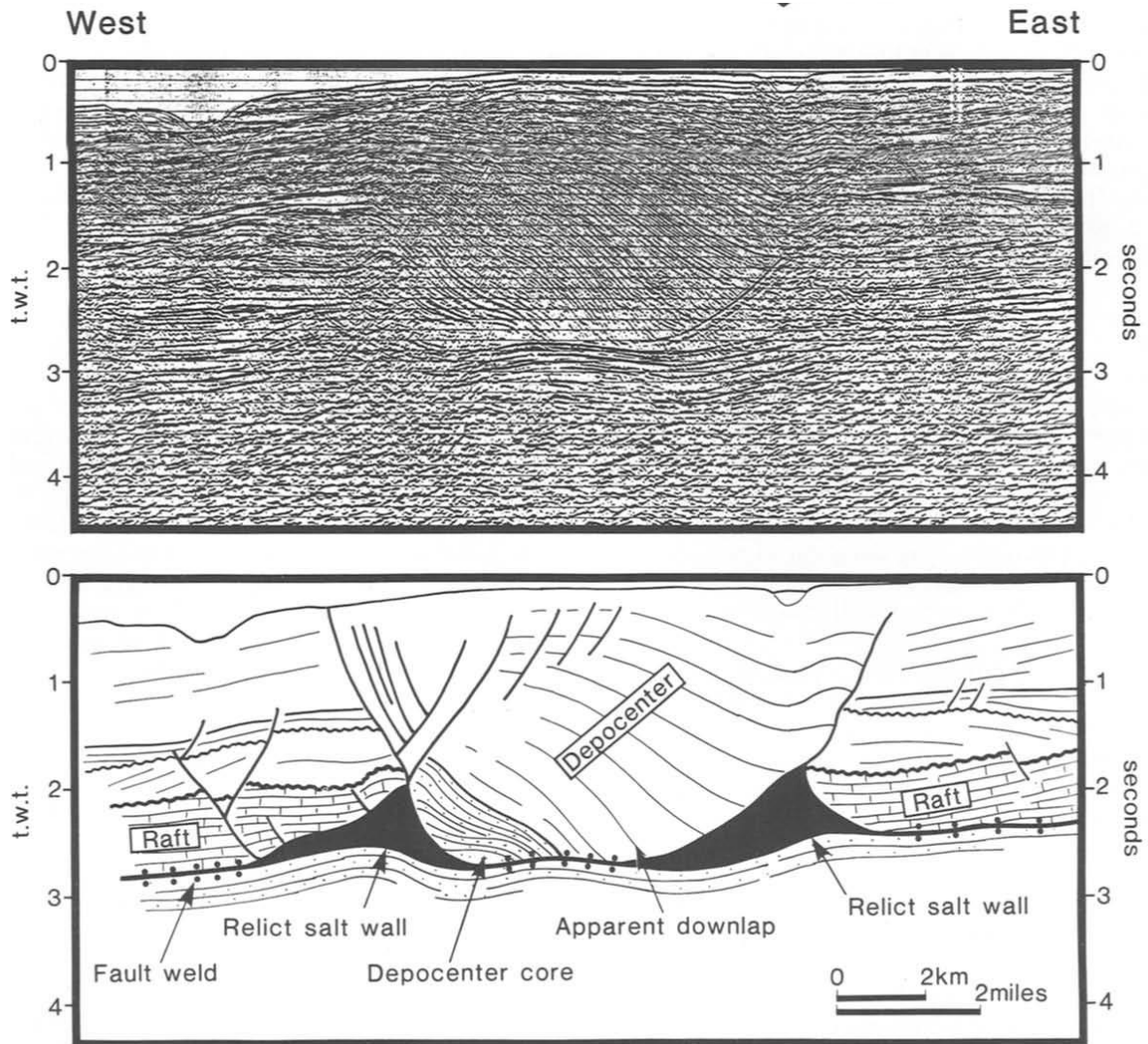
Figure 2.12: Seismic profile in the Kwanza Basin showing an example of a depocentre in the extensional domain. The depocentre opened as a half graben in between two rafts. Modified from Duval et al., 1992.
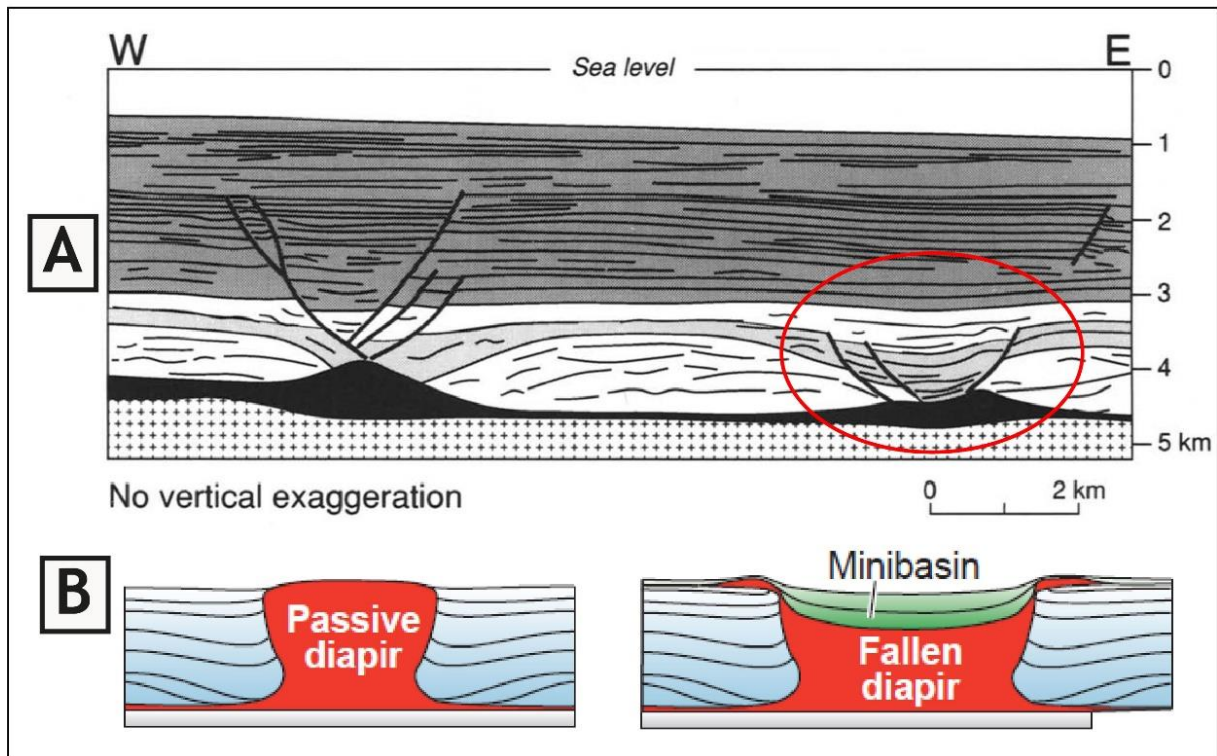
Figure 2.13: Examples of salt-related depocentres due to extension. A – Seismic profile of Campos Basin showing two diapirs formed by regional extension, firstly by reactive diapir rise and later by diapir fall. Diapir fall is particularly evident in the structure marked in the red circle, with the formation of a graben above (modified from Vendeville and Jackson, 1992). B – Diagrams showing the formation of a minibasin above a fallen diapir due to regional extension. Modified from Jackson and Hudec, 2017.

Mass transport deposits in a salt-controlled slope

Mass transport deposits are also commonly present in the stratigraphic succession of salt-controlled slope successions. Often, they are interpreted as a product of sediment remobilisation from the flanks of minibasins, being markers of salt tectonic activity (e.g., Prather et al., 1998; Madof et al., 2009, 2017; Doughty-Jones et al., 2017; Wu et al., 2020; Howlett et al., 2021). Few studies have documented externally sourced examples within minibasins. However, locally sourced mass transport deposits are commonly present (Doughty-Jones et al., 2019; Wu et al., 2020; Rodriguez et al., 2021).

2.2 Topographic control on deep-water deposition

The seafloor is not a flat or a uniformly sloping surface, instead, changes in gradient and orientation are common at various scales (Mulder and Alexander, 2001). Because gradient changes have a great impact on flow behaviour, the interaction of sediment gravity flows with topography has been a matter of discussion in the scientific community. From laboratory experiments to outcrop investigations and seismic-based studies, the investigation of this relationship has shown that topography affects deposition at a range of different scales. Evidence of this interaction has been observed in facies distribution, architecture and even in the whole basin filling, and is regarded as an essential factor in the evolution of submarine systems (e.g., Beaubouef and Friedmann, 2000; Barton, 2012; Deptuck et al., 2012; Hay, 2012; Marini et al., 2015; Brooks et al., 2018a).

2.2.1 Experimental and numerical simulation studies

Laboratory experiments, numerical studies, and direct observation of turbidity currents contribute to unveiling the physical processes and related sedimentary products that can emerge when flows are subject to changes in confinement and face gradient breaks or obstacles (e.g., Komar, 1971; Garcia and Parker, 1989; Alexander and Morris, 1994; Kneller and McCaffrey, 1999; Mulder and Alexander, 2001; Kostic and Parker, 2006; Sumner et al., 2013; Wang et al., 2017).

These studies propose explanations on how topography can induce changes in flow character and how these changes reflect processes that increase geological complexity. Turbidity currents flowing with velocities sufficient to achieve a supercritical (Froude number greater than unity) condition can have their velocity reduced by a gradient decrease and pass to a subcritical state (Froude number less than unity). This change in regime is achieved through a hydraulic jump (Komar, 1971). Understanding hydraulic jumps is important since they are implicated in major seafloor processes and are a key control governing sediment distribution in the deep sea, influencing the loci of seafloor sedimentation and, ultimately, controlling the character and distribution of modern and ancient sedimentary sequences (Sumner et al., 2013). Studies have documented that hydraulic jumps are associated with velocity decrease and flow thickness increase (e.g., Komar, 1971; Mulder and Alexander,

2001) (Fig. 2.14). As a result of the loss of competence and capacity of the flows, deposition with increased bed thickness downstream of the jump has been proposed (Garcia and Parker, 1989; Mulder and Alexander, 2001).

The monitoring of natural flows has questioned the idea that hydraulic jumps are always related to substantial changes in flow regime. Direct measurements have suggested that many submarine turbidity currents are only weakly supercritical (Sumner et al., 2013) and that Froude numbers lower than unity are usually enough to produce hydraulic jumps in stratified flows (Dorrell et al., 2016). These studies do not support the idea that the deceleration of the flow results in catastrophic deposition but propose that part of the flow can remain in suspension. Observations made by Dorrell et al. (2016) suggest that in stratified flows, their lower part may be affected by the hydraulic jump and that the internal flow expansion induces the upper part of the flow to remain in suspension and bypass rather than deposit sediments. Sumner et al. (2013) support the idea that the fluctuation between a supercritical and subcritical density current in different positions could produce a region of scattered hydraulic jumps that would favour suspension rather than deposition. This process could be the explanation for enigmatic features identified in channel-lobe transition zones on the seabed and outcrops, such as fields of scour-fills (Sumner et al., 2013; Brooks et al., 2018b; Hofstra et al., 2018).
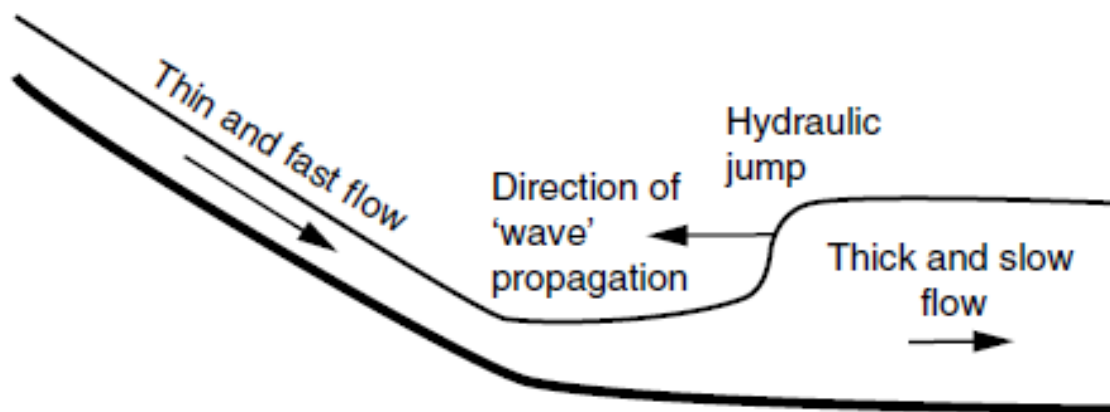
Figure 2.14: Key features of a hydraulic jump. From Sumner et al., 2013.

Regarding the deposit characteristics, experiments have demonstrated that the length and thickness of these deposits relate to the velocity of the flow on the slope and the angle of slope change (Mulder and Alexander, 2001). In addition, Garcia (1993)

documents a clear positive correlation between the grain size and thickness of post-hydraulic jump deposits. However, direct measurements of natural flows made by Dorrell et al. (2016) have shown that because the flows are stratified and maintain their capacity to transport sediments after hydraulic jumps, this simple correlation might need to be clarified. About the suspended load, different studies are also divergent. Experiments propose that a gradual response to the flow regime would result in deposits being spread out over several hundreds of metres to several kilometres (Garcia and Parker, 1989). Conversely, direct monitoring of flow parameters suggests that suspended material would become more concentrated downstream of the jump (Dorrell et al., 2016).

Hydraulic jumps are also expected when flows encounter obstacles on the seafloor. The experiments of Alexander and Morris (1994) document flow deflection and thickening as well as localised rapid deposition with increased thickness. The study of Kneller and McCaffrey (1999) was able to demonstrate the effects of topography on bed thickness variation. The authors showed that the deflection and surmounting of flows when encountering an obstacle depend on the Froude Number, and on the relationship between the flow height and the obstacle height (Fig. 2.15). Turbidity currents affected by gradient changes are non-uniform, and this characteristic controls the suspended-load fallout rate from these currents. The suspended-load fallout rate controls deposition in many ways, influencing the rate of aggradation of the bed, the formation of sedimentary structures, and sorting (Kneller and McCaffrey, 1999). Kneller and McCaffrey (1999) provide a theoretical basis for understanding how flow behaviour, interacting with obstacles, is associated with sedimentological processes that allow prediction of facies, sedimentary structures, sorting and bed thickness.
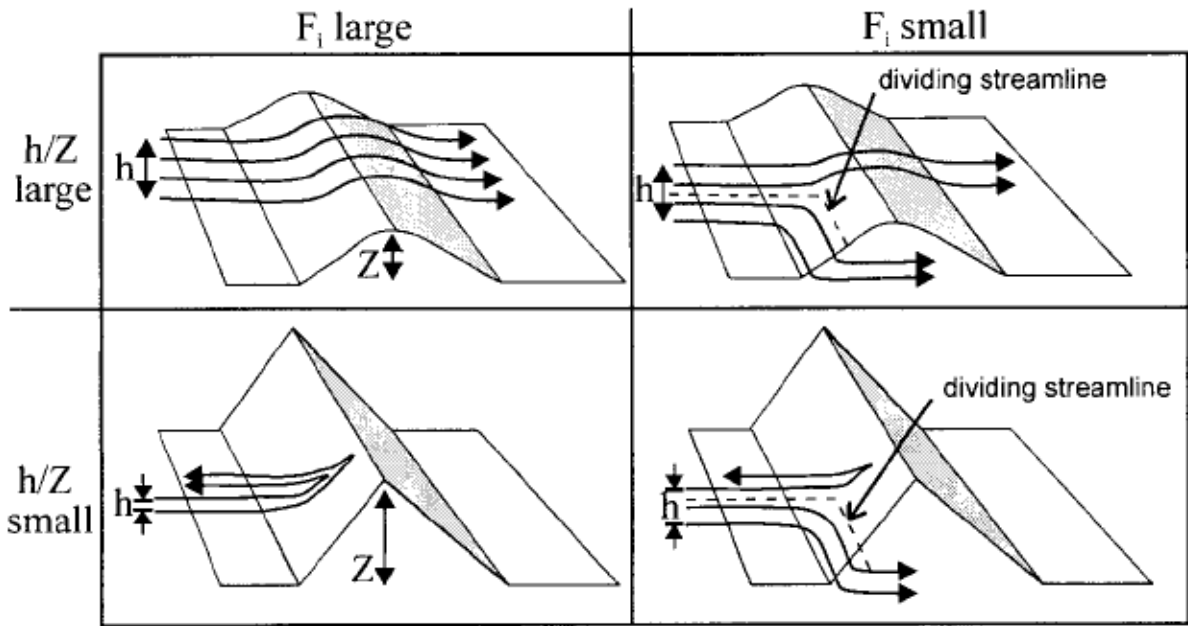
Figure 2.15: Schematic illustration showing the response of streamlines controlled by the interplay between the Froude number (F_i) and the degree of confinement. Low values of F_i result in decoupling of the flow. From Kneller and McCaffrey, 1999.

2.2.2 Rock database studies

Research carried out in outcrops and with cores in modern offshore systems has documented sedimentological and stratigraphic evidence for the topographic influence on turbidity currents. Changes in gradient are likely to cause: flow reflection and deflection shown by multiple palaeocurrent directions (Marini et al., 2015; Spychala et al., 2015); deposits that evidence flow transformation such as hybrid beds (e.g., Wynn et al., 2012; Marini et al., 2015); and facies successions indicative of unsteady flows (Spychala et al., 2015).

Stratigraphic and facies models proposed for intraslope lobes have demonstrated differences when compared to basin floor lobes. Lobes tend to be smaller in the slope and have a lower aspect ratio. The sand percentage is suggested to be considerably higher, even in the fringes, because the fine-grained component of the flows is not ponded and can bypass the slope. Moreover, a late incision phase, induced as a response to base-level adjustment, is commonly observed. All these are relevant criteria observed by studies made in outcrops in the Karoo Basin (Spychala et al.,

2015) and with cores and seismic reflection data in the Niger Delta Slope (e.g., Jobe et al., 2017) (Figs. 2.16, 2.17).
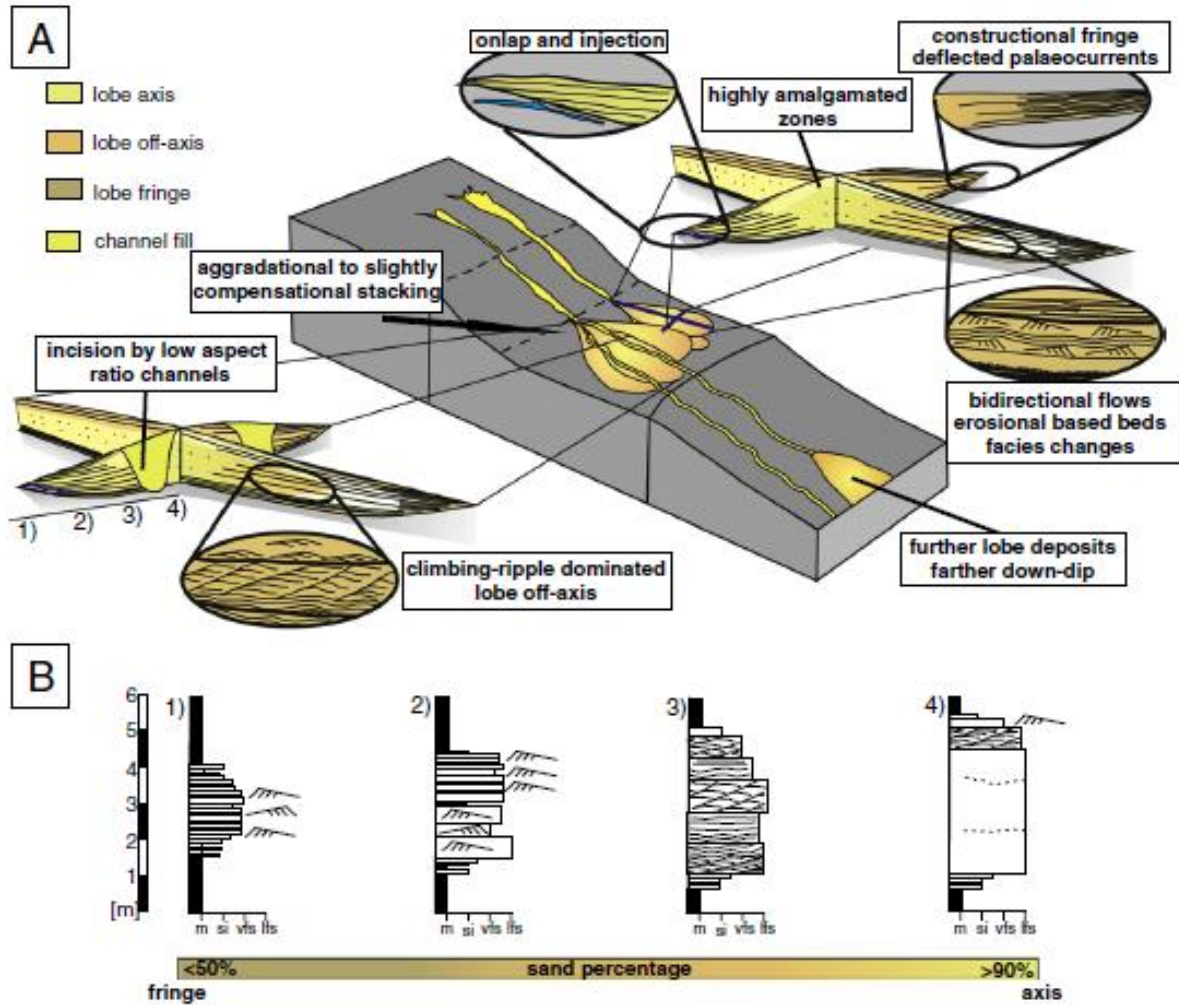
Figure 2.16: Block diagram showing the recognition criteria for intraslope lobes. Lobe axes display high-amalgamated zones while lobe fringes have structured and interbedded facies, also recording flow–slope interaction (i.e., deflected palaeocurrents, bidirectional flows). A late incision phase is also observed (see text for discussion). B – Logs representing facies and the stacking patterns for the different lobe sub-environments. From Spychala et al., 2015.
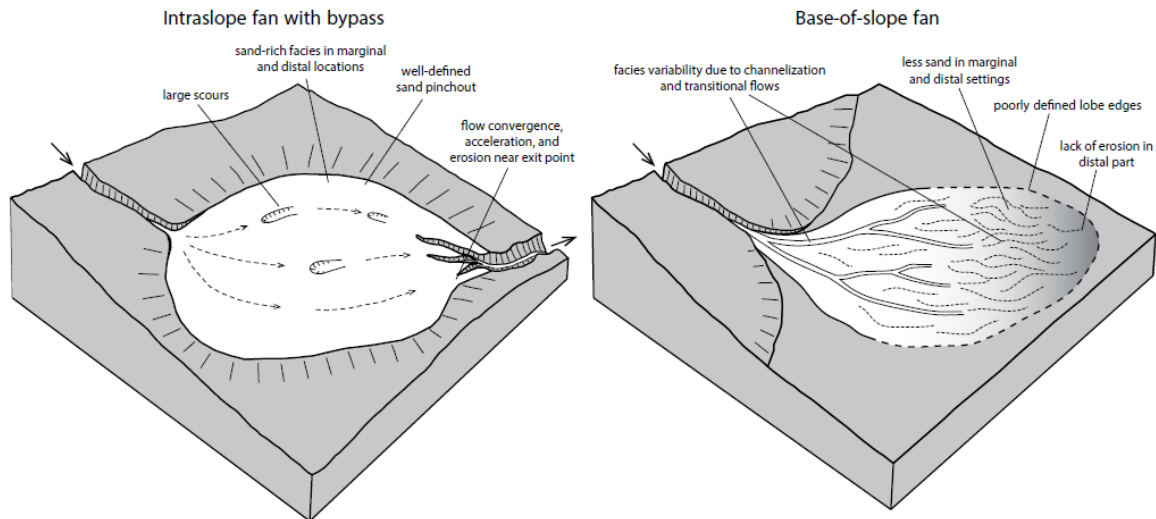
Figure 2.17: Schematic illustrations representing different facies models for intraslope lobes and base-of-slope lobes. Intraslope lobes are sandier even in marginal areas and show a late bypass phase, whereas base-of-slope fans have less sand in marginal areas and do not present a bypass phase. From Jobe et al., 2017.

The influence of topography on bed geometry was observed in abrupt bed terminations and onlapping (e.g., Wynn et al., 2012; Marini et al., 2015; Spychala et al., 2015; Jobe et al., 2017; Brooks et al., 2018a) (Fig. 2.18), whereas the degree of slope confinement has been regarded as an essential controlling factor in architecture variability and stacking patterns, with aggradational and sheet-like lobes in confined basin setting and compensational lobe stacking in semi-confined (Marini et al., 2015).
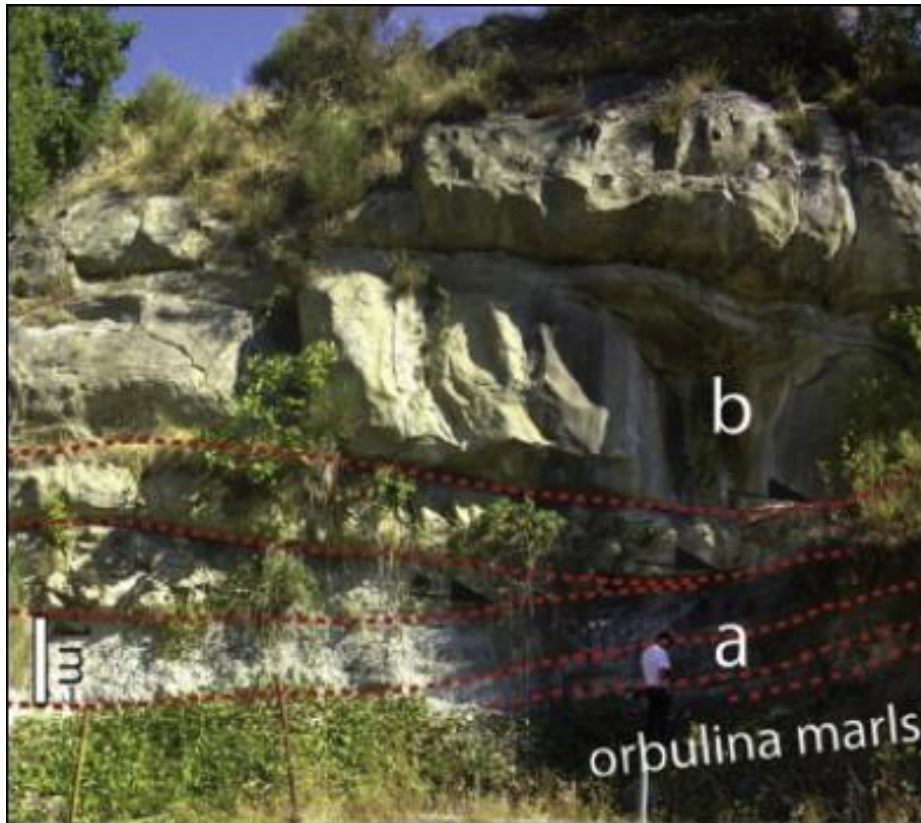
Figure 2.18: Changes in bed geometry as evidence for a confining slope setting. A – Subtle onlap of inter-lobe thin-bedded turbidites. B – Abrupt onlap of thick beds of proximal lobe environments. From Marini et al., 2015.

2.2.3 Geophysical studies

Geophysical studies based on bathymetric and seismic reflection surveys have investigated the effects of slope topography on deep-water systems offshore Africa (Prather, 2003; Adeogba et al., 2005; Gee and Gawthorpe, 2006; Barton, 2012; Deptuck et al., 2012; Hay, 2012, Wynn et al., 2012; Oluboyo et al., 2014; Picot et al., 2016; Jobe et al., 2017; Prather et al., 2017), Gulf of Mexico (Beaubouef and Friedmann, 2000; Prather, 2000, 2003) and Norway (Jackson et al., 2008). The high-quality imaging of these systems, allied to the fact that many are shallow successions, allows interpretations of topographic influence on the stratigraphic evolution of slope fans, although few have core/well control.

The occurrence of offshore intraslope fans is frequently associated with the loss of capacity of flows in transporting sediments once they pass through slope breaks (e.g., Prather, 2003; Adeogba et al., 2005; Barton, 2012; Deptuck et al., 2012). Tectonic

activity creates topography that determines the configuration of depocentres and the location of sediment transport systems (Mayall et al., 2010). Sand accumulation in the slope is more typical on slopes with complex substrates affected by halokinesis (e.g., Prather, 2003; Smith, 2004; Hay, 2012; Prather et al., 2012b; Oluboyo et al., 2014), mud diapirism (Adeogba et al., 2005; Barton, 2012; Deptuck et al., 2012; Jobe et al., 2017) and faulting or inherited topography (Jackson et al., 2008; Deptuck et al., 2012). The seismic expression of intraslope fans is usually related to moderate to high amplitude reflections, suggesting a sandy character for lithology, despite the lack of well data (e.g., Adeogba et al., 2005; Barton, 2012; Deptuck et al., 2012; Hay, 2012). Seismic attribute maps reveal unconfined planform geometries such as lobes, sheets and distributary channels, which can also be differentiated considering the continuity of reflections (Adeogba et al., 2005; Barton, 2012; Deptuck et al., 2012; Hay, 2012; Jobe et al., 2017) (Fig. 2.19).
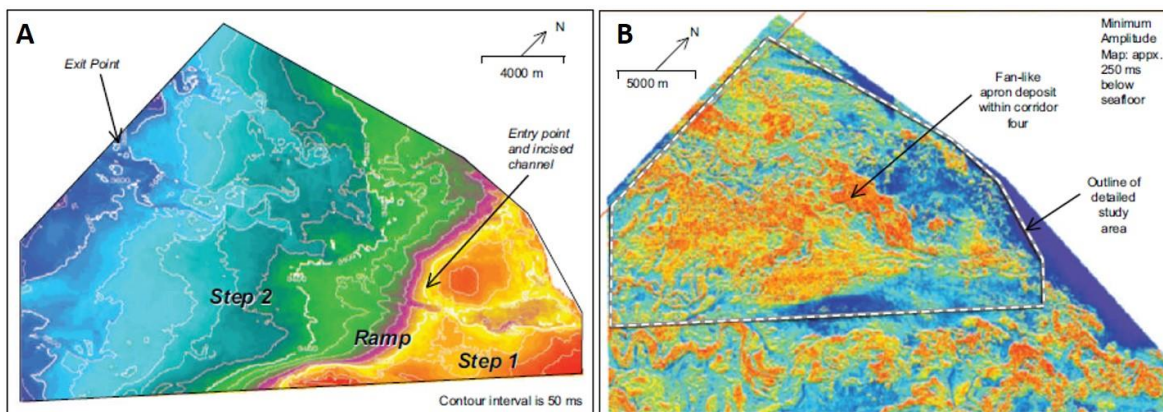
Figure 2.19: Example of intraslope fan offshore Nigeria. A – Steps and ramp in the topography map of a horizon beneath the intraslope fan. B- Amplitude map extracted at the base of the intraslope fan. Amplitudes reveal unconfined geometry above lower gradient areas of the slope. From Barton, 2012.

Slope topography variations also impact canyons and channel systems. Gentler gradients produce wider and more sinuous channels, and levees tend to be thicker, whereas the contrary is observed in steeper gradients (e.g., Adeogba et al., 2005; Ferry et al., 2005; Gee and Gawthorpe, 2006; Deptuck et al., 2012) (Fig. 2.20). Moreover, increases in gradient induce local acceleration of sediment gravity flows promoting erosion and more pronounced channel and canyon incision (e.g., Pirmez et al., 2000; Adeogba et al., 2005, Ferry et al., 2005; Jackson et al., 2008; Mayall et al.,

2010; Deptuck et al., 2012; Hay, 2012). Maximum local incisions are found at the down-slope transition from lower gradient steps to higher gradient ramps (Deptuck et al., 2012), whereas increased channelisation and dissection are also observed across intrabasinal highs in salt-dominated slopes (Hay, 2012) and in active thrust and fold belts (Huyghe et al., 2004). Knickpoints also tend to form above convexities on structurally complex slopes (e.g., Heiniö and Davies, 2004; Adeogba et al., 2005; Jolly et al., 2017; Fig. 2.21).
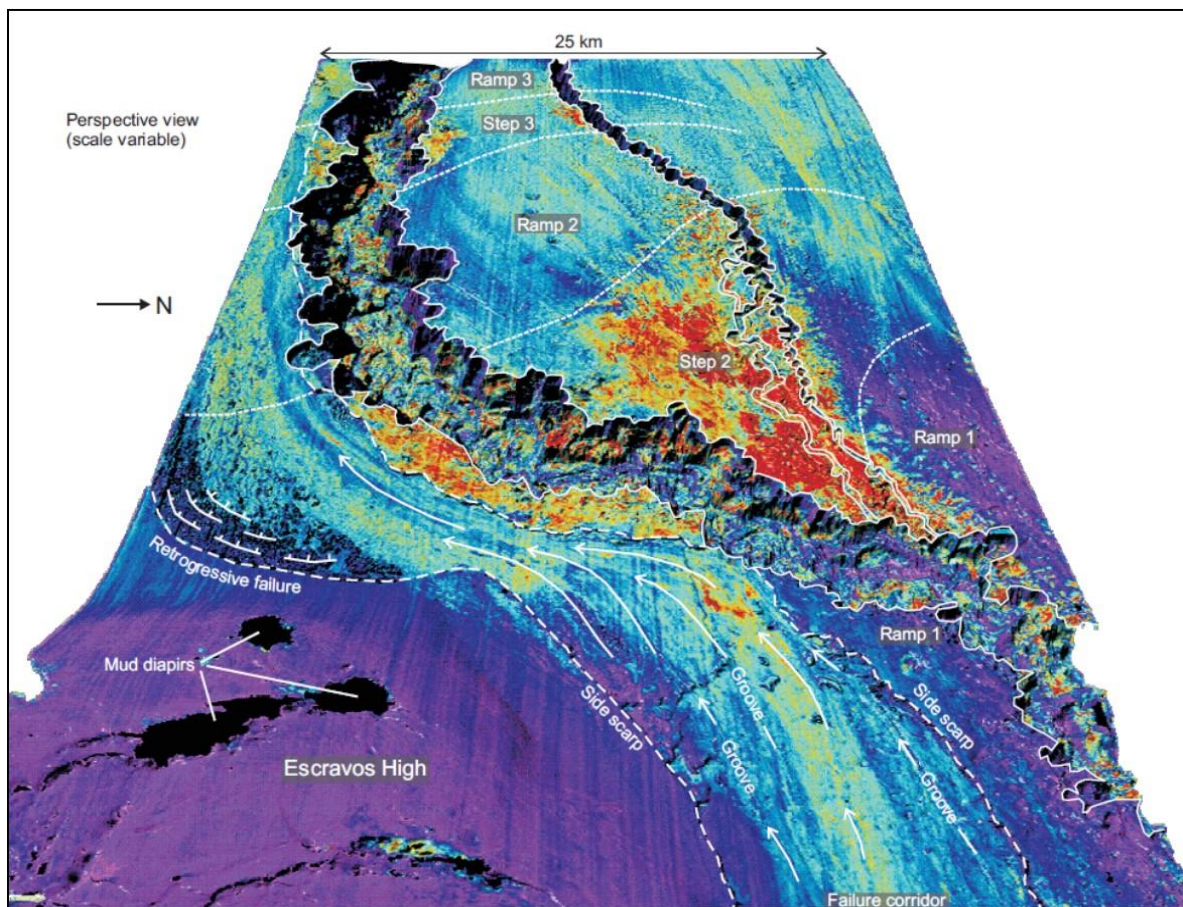
Figure 2.20: Amplitude map of Niger Delta slope with canyon incision. Notice pre-canyon unconfined deposits and their relationship with topography. Steps display amplitude anomalies (yellow and red) related to sandier deposits such as lobes or sand sheets. The canyon is deep and narrow above a ramp and wide and shallow above a step. From Deptuck et al., 2012.
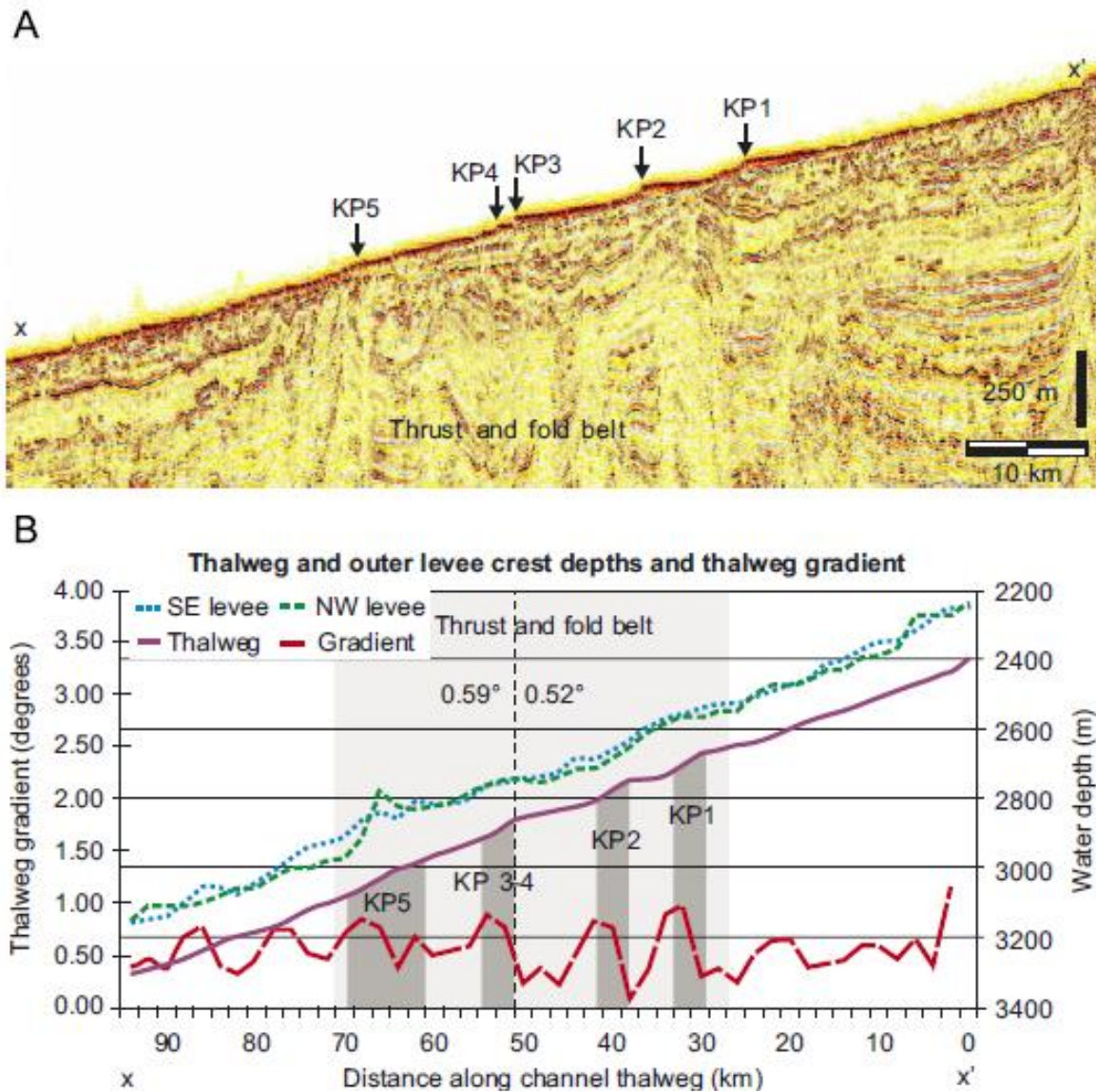
Figure 2.21: A - Association of knickpoints (KP) with structures of the thrust and fold belt. B-Knickpoints occur where there is an increase in channel gradient. From Heiniö and Davies, 2007.

2.3 Literature gaps

This thesis aims to better understand the stratigraphic evolution of deep-water systems above dynamic slopes with three-dimensionally variable accommodation patterns. The evolution of intraslope depocentres, including stepped-slopes, has been explained by the fill-and-spill model; however, this model contemplates complex but static topography, or depocentres with vertical deformation (e.g., Prather et al., 1998; Sinclair and Tomasso, 2000; Beaubouef and Friedmann, 2002). Therefore, the fill-

and-spill model is inappropriate to apply to basins with complex deformation patterns where accommodation varies laterally during the lifespan of a turbidite system.

In salt-bearing passive margins, much attention has been given to minibasin-type depocentres or tortuous corridors, which are commonly documented in intermediate to distal basin settings (e.g., Howlett et al., 2021; Rodriguez et al., 2021) where salt is usually thick due to gravitational gliding/spreading, and prone to contractional deformation (Fort et al., 2004; Rowan et al., 2004; Brun and Fort, 2011). As previously outlined, a few examples of turbidite systems in intraslope depocentres are documented in the extensional salt domain (e.g., Duval et al., 1992; Albertão et al., 2010), these being associated with initial stages of horizontal extension. Therefore, there is a lack of examples of salt-related intraslope depocentres evolving during a mature phase of salt passive margins, when most of the horizontal extensional has ceased, and low deformation rates operate across slope systems. The structural configuration (weakly confined) and the relationship between deformation and sedimentation rates in these depocentres will produce a stratigraphic signature that differs from minibasins and tortuous corridors. In minibasins, a considerable volume of small locally sourced mass transport deposits associated with sediment remobilisation from the active flanks are documented, reflecting tectono-stratigraphic cyclicity (e.g., Prather et al., 1998; Madof et al., 2009, 2017; Doughty-Jones et al., 2017; Howlett et al., 2021). In contrast, mass transport complexes in depocentres with lower deformation rates and without pronounced basin flanks might often be externally sourced large-scale deposits. Submarine accommodation at the rugose top surface of mass transport deposits has been shown to impact the routeing and architecture of turbidite systems (Kneller et al., 2016; Brooks et al., 2017; Ward et al., 2018; Martínez-Doñate et al., 2021). However, the role of large-scale MTC emplacement on the reconfiguration of the slope topography through subsidence generation has not been discussed previously.

The initiation and evolution of submarine channels occur through dynamic sedimentary processes that include erosion (Fildani et al., 2014), depositional relief (Hodgson et al., 2016), and rapid headward knickpoint migration (e.g., Heijnen et al., 2021). Headward migration of knickpoints acts to smooth the longitudinal profile of channels over time. Irregular longitudinal channel profiles in modern systems are interpreted to represent a snapshot of channel evolutions. Because these features

have only been documented in modern systems, the preservation potential of an irregular channel base in the rock record is considered to be very low. Their identification opens possibilities for new evolutionary models of submarine channels that still need to be explored.

Chapter 3 - Fill-and-Spill, Tilt-and-Repeat (FaSTaR) cycles: stratigraphic evolution above a dynamic submarine stepped slope

3.1 Abstract

The classic fill-and-spill model is widely applied to interpret topographic controls on depositional architecture and facies distributions in slope successions with complicated topography. However, this model implies a constant topographic configuration over the lifespan of a turbidite system. In contrast, the impact on patterns of erosion and deposition above dynamic slopes whose topographic configuration varies spatially over time remains poorly investigated. Here, using high-resolution 3D seismic reflection data and more than 100 wells from a 40 km long stepped slope system (Campos Basin, offshore Brazil), I document the evolution of a sand-prone turbidite system active during the Oligocene-Miocene transition. This turbidite system was influenced by vertical and lateral deformation, and I propose a new stratigraphic model to explain the resultant depositional architecture.

Two depocentres were identified as steps, with channels on the proximal step and channel-lobe complexes on the distal step, bounded by sediment bypass-dominated ramps. Lateral stepping of channels on the proximal step, and oblique stacking of the down-dip lobe complexes, each cut by through-going channels, indicate multiple fill-and-spill cycles. A persistent NE-ward stepping and thickening on the steps is interpreted to reflect lateral tilting of the seafloor driven by salt tectonics. The dynamic substrate prevented the establishment of a single long-lived conduit across the proximal step, as recorded in systems with fixed topographic configurations. The filling of through-going channels with mud at the end of each cycle suggests waxing-to-waning sediment supply cycles and periods of sand starvation, when the lateral tilting dominated and drove avulsion of the feeder channels towards topographic lows. This study demonstrates that subtle dynamic slope deformation punctuated by discrete sediment supply cycles results in complex stratigraphic patterns with multiple phases, and multiple entry and exit points, during repeated cycles of fill-and-spill, tilt-and-repeat (FaSTaR). These are likely to be present in other stepped slope systems.

3.2 Introduction

Intraslope depocentres are sites of sediment storage that record important information about the evolution of submarine slope systems, the interaction of sediment gravity flows with slope topography, and the stratigraphic connection between shallow- and deep-water environments. In addition, these areas are prone to significant sand accumulation and host economically important hydrocarbon reservoirs (e.g., Booth et al., 2003; Prather, 2003; Prather et al., 2009, 2012a). According to the topographic configuration, intraslope depocentres range from three-dimensional confined basins that record ponded accommodation (*sensu* Prather, 2003) to stepped profiles that comprise lower gradient steps with healed accommodation (*sensu* Prather, 2003), connected through higher gradient ramps.

Intraslope confined basins have been widely documented in salt-withdrawal basins that display high rates of salt mobility (e.g., Winker, 1996; Prather et al., 1998, 2012b; Pirmez et al., 2000; Prather, 2000, 2003; Beauboueff and Friedmann, 2000; Booth et al., 2003; Smith, 2004; Doughty-Jones et al., 2017) and emplacement of mass transport complexes (e.g., Wu et al., 2020; Cumberpatch et al., 2021). Stepped profiles have been associated with low rates of slope deformation and average sedimentation rates (Meckel et al., 2002; Hay, 2012), and exhibit subtle gradient changes (Brooks et al., 2018; Mignard et al., 2019), where sedimentation rates outpace deformation rates (Pirmez et al., 2000; Prather, 2003; Adeogba et al., 2005; Deptuck et al., 2012; Hay, 2012). Accommodation creation has been attributed to several factors, such as salt tectonics (Smith, 2004; Hay, 2012), mud diapirism (Adeogba et al., 2005; Barton, 2012; Deptuck et al., 2012; Jobe et al., 2017), scars of mass transport complexes (Spychala et al., 2015), and differential compaction and subsidence (Jackson et al., 2008; Spychala et al., 2015; Brooks et al., 2018). In salt basins, stepped profiles have been related to complex topographic settings such as connected tortuous corridors formed by discontinuous salt-cored structures (Prather, 2003; Smith, 2004; Hay, 2012; Oluboyo et al., 2014; Howlett et al., 2020). In these cases, salt-influenced depocentres display pronounced salt-cored structures, such as massive salt walls and stocks, typical of zones of structural shortening where salt

thickens in contractional salt domains (Demercian et al., 1993; Mayall et al., 2010; Howlett et al., 2020). In these settings, submarine channels diverge around, or converge towards, constriction points between salt structures, from where distributary systems emanate into less confined lower gradient slope sectors. However, the depositional patterns of intraslope depocentres affected by modest salt-related structural relief remain poorly investigated.

Despite the majority of documented intraslope depocentres forming on mobile slopes, the understanding of their stratigraphic evolution has relied on the classic fill-and-spill model. This model predicts a cycle of accommodation filling followed by incision and bypass in depocentres that are not deformed, or are mobile about the vertical axis, during the lifespan of a turbidite system (e.g., Winker, 1996; Prather et al., 1998; Prather, 2000, 2003; Beauboueff and Friedmann, 2000; Pirmez et al., 2000; Sinclair and Tomasso, 2002; Smith, 2004). This model has been applied in stepped-slope systems such as intraslope submarine fans (Jobe et al., 2017), transient fans (Adeogba et al., 2005) and slope aprons (Barton, 2012). In addition, the stratigraphic architecture of fill-and-spill cycles with vertical deformation has been modelled by several authors (e.g., Sylvester et al., 2015; Wang et al., 2017; Christie et al., 2021). In cases where fill-and-spill cycles are vertically stacked, the stratigraphic cyclicity is attributed to the interaction of sediment input and vertical accommodation rejuvenation created by dynamic seafloor deformation induced by fixed structural elements (e.g., Booth et al., 2003; Hay, 2012; Spychala et al., 2015; Brooks et al., 2018). However, accommodation patterns can be spatially variable during the lifespan of a turbidite system, for instance, due to basinward tilting (Jackson et al., 2021), lateral tilting (Kane et al., 2010, 2012) and the emplacement of MTCs (Wu et al., 2020). These factors that drive spatially variable topographic configurations hinder vertical stacking across sediment supply cycles and suggest that alternative stratigraphic models to the traditional fill-and-spill model need to be developed.

This work investigates the stratigraphic evolution of a sand-prone turbidite unit deposited on the Oligocene/Miocene slope of the Campos Basin, offshore Brazil. This turbidite unit evolved above a stepped slope, with low relief, that exhibited complex topography influenced by extensional salt-tectonics and differential compaction. Extensive seismic stratigraphic mapping and well data analysis were carried out in order to: i) characterise the depositional systems and link the spatial variability in

architecture, thickness and sand distribution with seafloor topography; ii) define a high-resolution stratigraphic framework across the stepped profile; iii) interpret how slope topography influenced the stratigraphic evolution of the study unit; and iv) propose a high-resolution stratigraphic model for turbidite system evolution above dynamic stepped profiles.

3.3 Regional geological setting

The study area is located in the central part of Campos Basin, offshore Brazil, more than 120 km from the coastline, in water depths ranging from 600-2000 m (Fig. 3.1A). The Campos Basin is located on the eastern Brazilian continental margin, covering an area of 115,000 km^2, mostly offshore of Rio de Janeiro (RJ) and Espírito Santo (ES) states (Fig. 3.1A). The Cabo Frio High defines the southern margin, and the Vitoria High defines the northern margin (Mohriak et al., 1998; Winter et al., 2007), with a small onshore portion to the west (Bruhn et al., 2003) (Fig. 3.1A). The Campos Basin, presently a passive margin, originated from the break-up of the Gondwana supercontinent during the Upper Jurassic/Lower Cretaceous (Chang et al., 1992; Fetter et al., 2009) and is infilled with a 9000 m thick sedimentary succession (Guardado et al., 2000). Three main megasequences form the stratigraphy of Campos Basin: Non-marine Rift Megasequence, Transitional Megasequence and Marine Megasequence (Guardado et al., 2000) (Fig. 3.1B, C). Winter et al. (2007) named these sequences Rift, Post-Rift and Drift, respectively. The rift megasequence (Upper Neocomian to Lower Aptian) relates to the Mesozoic break-up process, with rift depocentres infilled by volcanics and continental sediments (Guardado et al., 2000; Winter et al., 2007). Coarse siliciclastic sediments and microbial carbonates overlain by evaporites deposited from the Middle to Upper Aptian record the transition from continental to marine environments during a tectonically mild post-rift stage, forming the Transitional or Post-Rift Megasequence (Guardado et al., 2000; Winter et al., 2007). The Marine or Drift Megasequence (Albian to present) evolved in a context of thermal subsidence and salt tectonics and presents a transgressive-regressive trend of marine sedimentation (Guardado et al., 2000; Winter et al., 2007). This megasequence records at its base a shallow-water carbonate platform that was progressively drowned due to thermal subsidence and eustatic sea level rise (Bruhn et al., 1998), leading to the deposition of widespread siliciclastic and hemipelagic

deep-water sedimentation up to the Upper Cretaceous/Paleocene (Chang et al., 1992; Guardado et al., 2000; Winter et al., 2007) (Fig. 3.1B). The regressive phase (Paleocene to present) was driven by increased sediment supply and eustatic sea-level fall, characterised by the progradation of synchronous depositional systems composed of shallow-water carbonates, siliciclastic paralic and deep-water systems (Winter et al., 2007; Bruhn et al., 1998) (Fig. 3.1B). This study focuses on a deep-water sand-prone interval, informally named here the Marlim Unit. This unit forms part of the regressive phase of the Marine/Drift Megasequence and was deposited during the Oligocene-Miocene transition (~23 Ma), which coincides with a transient global cooling event associated with ice sheet expansion on Antarctica (Beddow et al., 2016) (Fig. 3.1B, C).

The Campos Basin basement is characterised by NE-SW and NW-SE oriented horst and graben structures bounded by normal antithetic and synthetic faults developed during the rift phase (Guardado et al., 2000; Castro and Piccolini, 2015; Fig. 3.1C). Post-rift thermal subsidence tilted the passive margin, inducing early-stage seaward flow of the Aptian salt (Cobbold and Szatmari, 1991; Quirk et al., 2012; De Gasperi and Catuneanu, 2014). As marine sedimentation progressed, gravity spreading of the overburden enhanced salt mobility (Mohriak et al., 2008). Post-Albian time is characterised by widespread salt tectonics (Mohriak et al., 2008), associated with the formation of a detachment surface at the base of the Aptian Salt (Fetter, 2009). However, post-rift reactivation of the basement fabric is documented, and coupling between basement reactivation structures and salt tectonics can be observed in structural highs (Fetter, 2009).

Two salt tectonic domains are recognised down the basin margin: i) an up-dip extensional salt-thinned domain characterised by salt rollers, rafts, extensional anticlines, salt pillows and associated normal faults, and ii) a down-dip compressional salt-thickened domain where salt stocks, salt walls/ridges and compressional salt tongues are documented (e.g., Cobbold and Szatmari, 1991; Demercian et al., 1993; Mohriak et al., 2008; Fetter, 2009). An intermediate domain between the extensional and compressional domains is described as the transitional domain (Mohriak et al., 2012) or multiphase domain (do Amarante et al., 2021) and shows variable deformation styles. The Marlim Unit sits in the extensional domain, where salt-cored listric normal faults record large amounts of downslope extension related to the

stretching and fragmentation of the Albian-Cenomanian carbonate interval (raft tectonics phase, e.g., Demercian et al., 1993; Quirk et al., 2012) (Fig. 3.1C). The bulk of the extension had occurred by the end of the Albian (Quirk et al., 2012). However, salt-tectonics continued to be active during the Upper Cretaceous and Cenozoic (Cobbold and Szatmari, 1991; Demercian et al., 2003; Fetter, 2009).

Salt tectonics plays a key role in deep-water sedimentation patterns in the Campos Basin. Salt-related seafloor deformation controlled accommodation patterns on the slope, leading to the accumulation of large volumes of sand-prone turbidites from the Upper Cretaceous to the Neogene (e.g., Cainelli and Mohriak, 1999; Guardado et al., 2000; Winter et al., 2007; Albertão et al., 2010). These slope turbidite systems, such as the Marlim Unit, form prolific hydrocarbon reservoirs. Therefore, there is an abundance of seismic reflection and core/well data. These data permit more in-depth study of mobile substrates and deep-water sediment transport and deposition patterns.
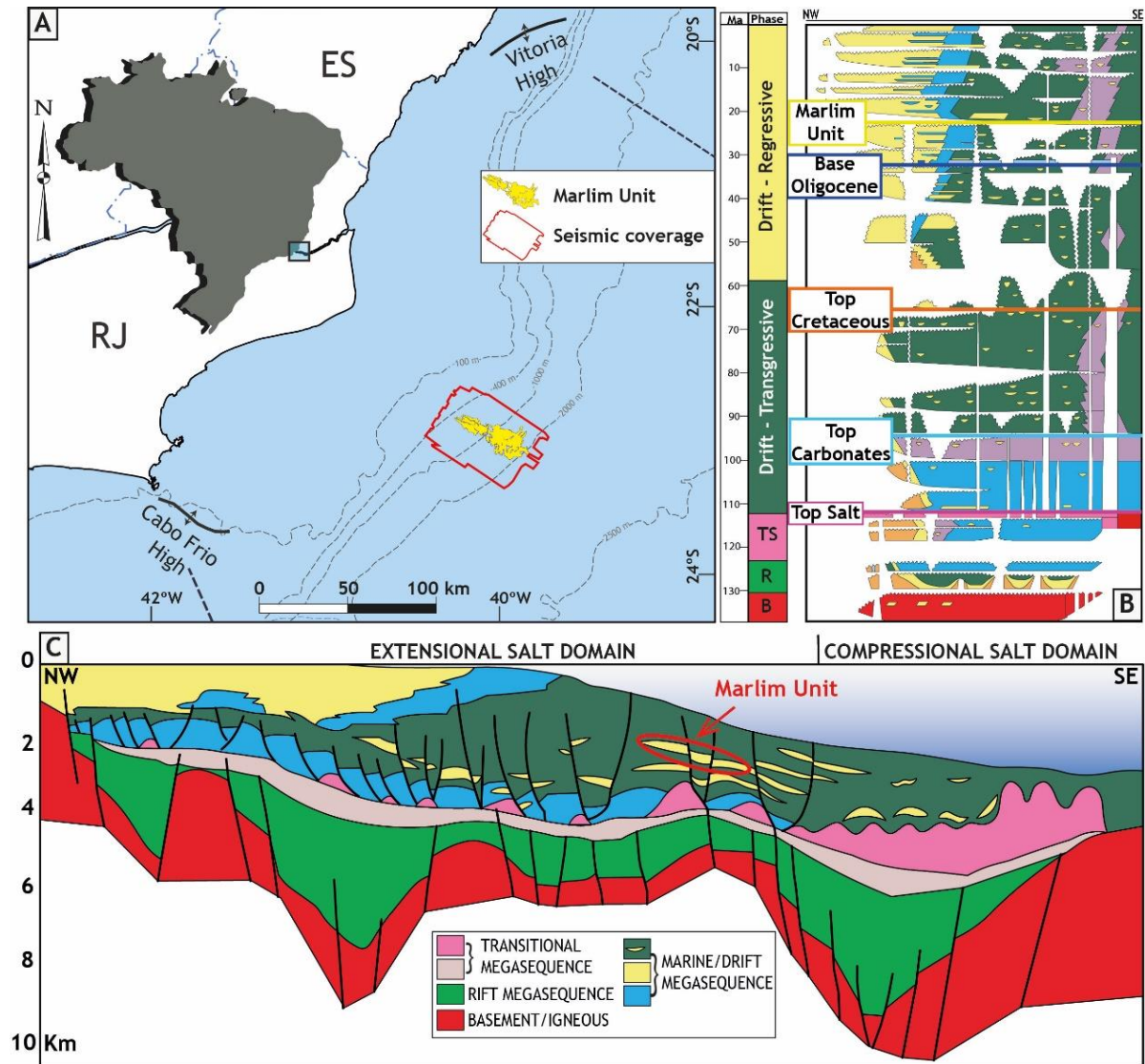
Figure 3.1: A - Location map of Campos Basin and the Marlim Unit study area in the central area of the Basin (modified after Bruhn et al., 2017). Inset map of Brazil at the top left with a blue box showing the location of the rest of the figure. ES = Espirito Santo state, RJ = Rio de Janiero state. B – Stratigraphic chart of Campos Basin with the main stratigraphic phases (megasequences; modified after Winter et al., 2007). The seismic horizons used in this study are named at the left. The top carbonates include the Cenomanian marl interval. Key for lithologies in the stratigraphic chart of B: red for basement, green for mudstones, yellow for sandstones, orange for conglomerates, blue for carbonates, pink for evaporites and pale purple for marls. In the column phases of the chart, B refers to basement, R to rift and TS to transitional (see text for explanation). C - Schematic geological dip section representing the stratigraphic framework and the structural style of Campos Basin (modified after Guardado et

al., 2000 and Rangel and Martins, 1998). The Marlim Unit position in the geological section is
marked in the red ellipse and sits above the extensional salt domain.

3.4 Data set and methods

This study uses a comprehensive subsurface data set comprising multiple 3D high-resolution seismic reflection volumes, 110 wells with basic wireline logs, and 231.3 m of core from 12 wells. The full-stack seismic volume is a merge of two different volumes, acquired in 1999 and 2010. The merged volume was processed as a PSTM (Pre-Stack Time Migration) in 2014 to generate a single volume that covers the whole study area. The bin size spacing is 12.5 m for inlines and crosslines, and the vertical sampling is 4 ms. The average seismic frequency in the Oligocene-Miocene interval is around 30 Hz, resulting in a vertical resolution of approximately 22 m (using an interval velocity of 2650 ms from an average obtained with sonic logs), although thinner events can be detected. A higher resolution 3D PSTM volume processed in 2006 (bin size 12.5 m for inlines and 6.25 m for crossline, and 2 ms vertical sampling), which covers part of the study area, was used to check interpretations in areas of structural complexity.

Both seismic reflection datasets were processed to zero-phase wavelet and are shown with SEG normal polarity. A negative reflection coefficient is linked to a trough and indicates a decrease in acoustic impedance (check Marlim Unit Top, Fig. 3.2). The Marlim Unit contains oil-saturated high porosity sandstones and typically corresponds to a pair of reflections, where the top is mapped in a trough and the base in a peak. Horizon interpretation from the larger amplitude volume covered around 740 km² and was performed using automatic and manual reflection tracking. The RMS (root mean square) amplitude map, extracted between the top and base horizons, was assessed to be the best option for the analysis of seismic geomorphology since it represents the seismic response of the Marlim Unit as a whole. A time versus depth conversion was performed in the larger seismic volume using a 3D velocity model calibrated by the velocity function of 38 wells (Fig. 3.2). This process allows for the proper assessment of the thickness variations and improved seismic and well data integration. A thickness map of the Marlim Unit, calibrated by wells, was calculated and filtered for areas where the seismic horizons were mapped with high confidence, mainly in areas of moderate to high RMS amplitude values. Therefore, the map excludes areas with very low-

amplitudes, where the seismic mapping is uncertain and produces anomalous thickness patterns.

Several wells with standard wireline logs (gamma-ray, resistivity, density, neutron and sonic) were used to calibrate seismic response. The top and base markers of the Marlim Unit consist of lithological breaks seen in cores and changes in well logs patterns. The breaks are identified between low porosity (and higher density), low resistivity and high radioactivity mudstones; and high porosity (and lower density), high resistivity and low radioactivity sandstones or interbedded lithologies (intercalation of mudstones and sandstones) (Fig. 3.2). Within the Marlim Unit, a simple electrofacies classification created using the density and neutron logs was used to assess lithological variability and sand percentage. Although gamma-ray logs have good correspondence with the neutron and density logs, they were not used due to the arkosic composition of the sandstones. Core descriptions at cm-scale provided sedimentological information regarding facies and grain size (Fig. 3.2). The integrated data analysis allowed the definition of architectural elements.

Strike stratigraphic sections were hung from a stratigraphic datum to: i) provide insights into thickness and architectural changes, ii) constrain the position of key stratigraphic surfaces, and iii) support the development of an evolutionary stratigraphic model. The stratigraphic datum was identified by a change in well log patterns within a fine-grained interval above the Marlim Unit. This change is observed in all the wells and is marked by an increase in gamma-ray, neutron and transit time values and a slight decrease in the density and resistivity values (Fig. 3.2), and possibly represents a lithological contact between a unit with higher carbonate content and a predominantly siliciclastic interval. The carbonate interval might be related to a higher amount of pelagic sediment, marking a condensed section.
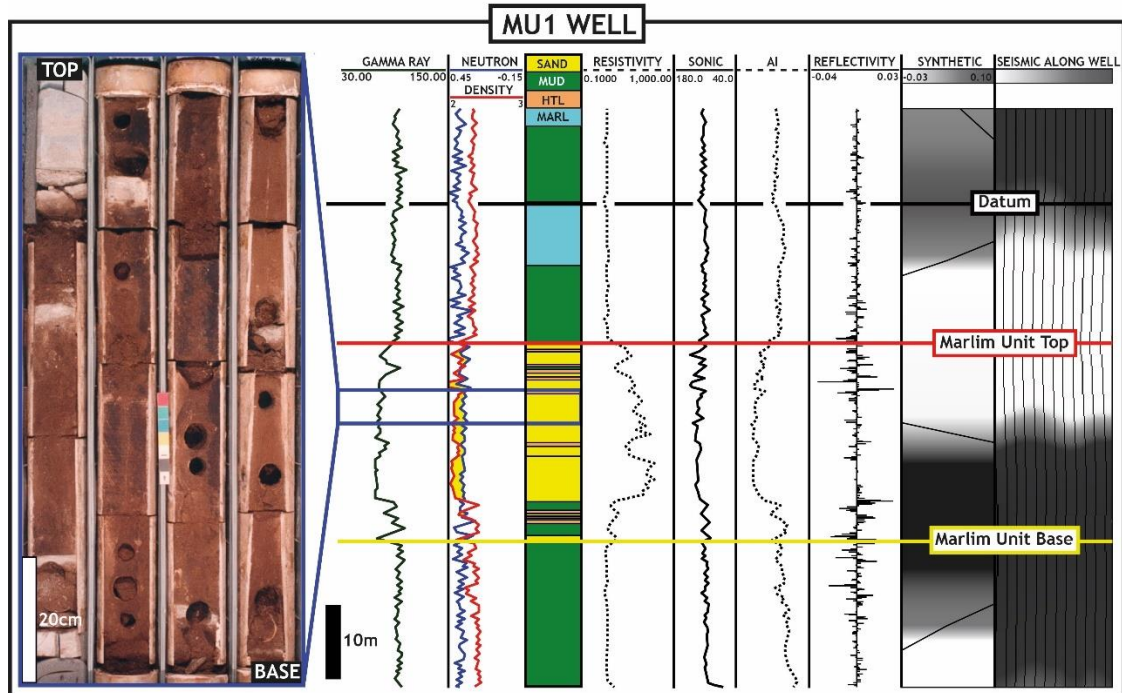
Figure 3.2: Example of well logs characteristics of the Marlim Unit and the datum used (see text for explanation). The lithology log shows three electrofacies (sandstone in yellow, mudstone in green, and heterolithics in pale orange). The light blue package marks the higher carbonate content interval used as a stratigraphic datum. The dark blue box represents an example of a cored interval (fine-grained structured sandstones). The Marlim Unit's seismic expression is mostly a single seismic loop (trough + peak). It can be seen in the synthetic seismogram (top marked in a trough and base in a peak) that fits with the seismic log extracted in the well trajectory showing the adjustment made by the time versus depth conversion. Units: API (American Petroleum Institute) for gamma-ray, g/cm^3 for density, porosity units for neutron, ohm/m resistivity, ms/ft for sonic, kPa.s/m for AI (acoustic impedance). Other wells will be presented in the same units.

3.5 Results

3.5.1 Marlim Unit geological setting

The Marlim Unit is a buried sand-prone submarine slope system, 14 km wide and 40 km long, which deepens southeastward below the modern Campos Basin slope, forming the most prominent sand-prone package in the study area (Fig. 3.3). At the time of the Marlim Unit deposition, the Campos Basin had evolved to a passive margin physiography, with a well-defined continental shelf, slope and basin floor (De Gasperi

and Catuneanu, 2014). Like other Oligocene and Miocene deep-water sandstones of the Campos Basin, the Marlim Unit is arkosic and fine-grained, reflecting a sediment source area landward of wide coastal plains (Fetter et al., 2009). The relatively young age and high impedance contrast between the sand-prone Marlim Unit and the bounding fine-grained deposits favour the extraction of high-quality seismic images. Amplitude maps reveal distinctive geomorphological patterns in two depositional domains. The up-dip domain is characterised by moderate to high-amplitude patchy to lobate anomalies, truncated by low-amplitude elongate anomalies, and high-amplitude elongate anomalies. These elongate anomalies are interpreted here as mud-filled channels and sand-filled channel complexes, respectively (Fig. 3.3; see section 3.4.2 for detail). In contrast, the down-dip domain comprises moderate- to high-amplitude lobate features truncated by high-amplitude elongate anomalies, interpreted as channel-forms (Fig. 3.3; see section 3.4.3). These two domains are linked by a reduced amplitude transition zone (TZ, Fig. 3.3).
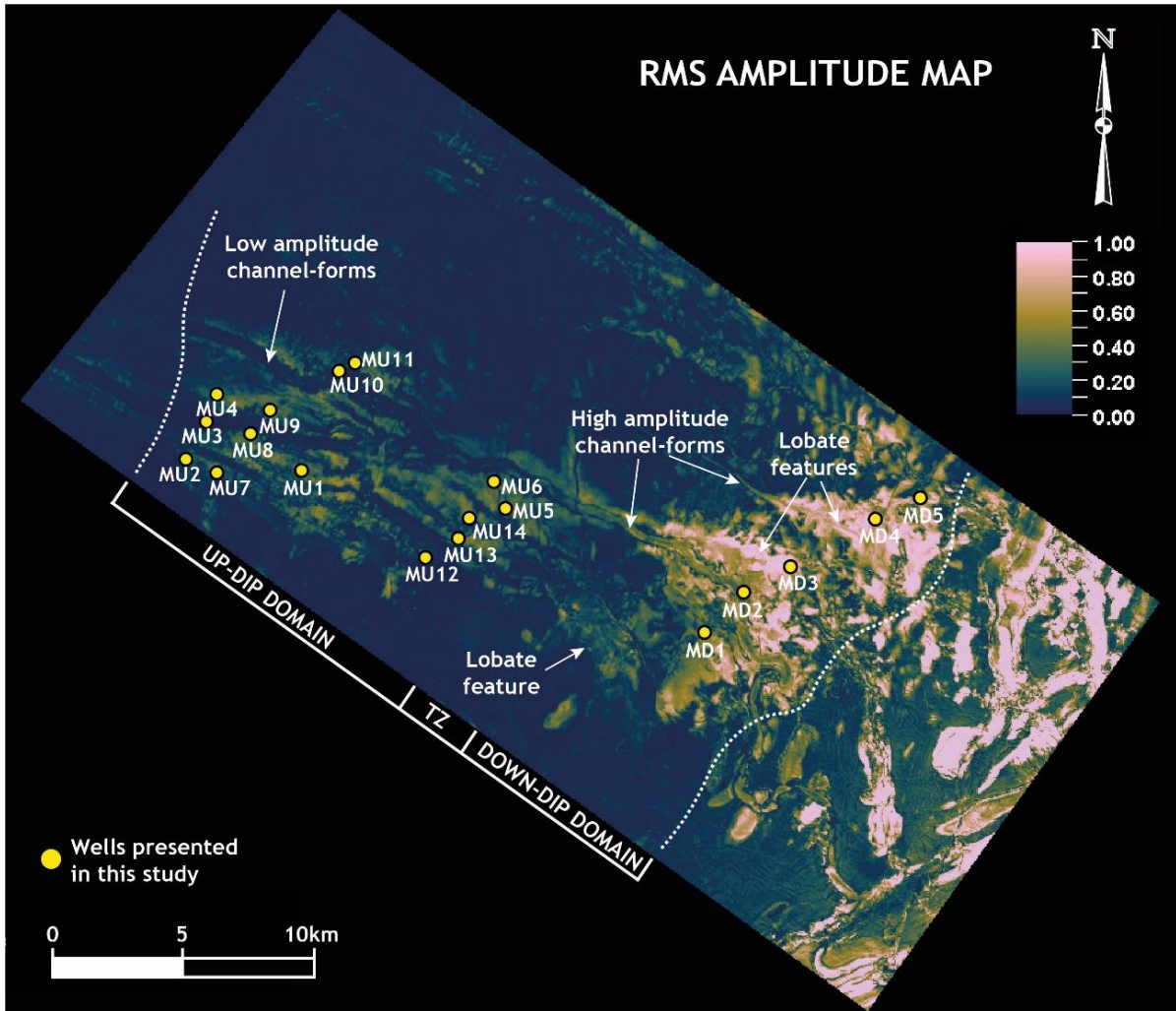
Figure 3.3: RMS amplitude map extracted between the top and base of the Marlim Unit. Up-dip and down-dip domains show distinct seismic geomorphological responses and are connected by a transition zone (TZ). Up-dip, the seismic geomorphology suggests elongate high- to moderate-amplitude anomalies truncated by linear low-amplitude channel-forms, whereas the down-dip domain comprises moderate to high-amplitude lobate features truncated by high-amplitude channel-forms.

Salt tectonics has played a key role on the regional stratigraphic architecture across the Campos Basin palaeoslope (e.g., Cainelli and Mohriak, 1999; Guardado et al., 2000; Winter et al., 2007; Albertão et al., 2010). The long-term impact of halokinesis in the basin supports the investigation of its effects on sedimentary processes during the evolution of the Marlim Unit. Normal faults, which can be listric and/or have an associated lateral component, are common in the study area. Divergent reflection patterns indicate stratal thickness increases towards fault planes active during post-salt sedimentation, including the Marlim Unit (Fig. 3.4C). Many of these faults bound

the Albian-Cenomanian carbonate blocks, or rafts, fragmented during the raft tectonics, a process described as an extreme thin-skinned extension of overburden over a detachment surface above salt (e.g., Duval et al., 1992; Jackson and Hudec, 2017) (Fig. 3.4A, C). Raft tectonics generated syn-tectonic lows and eventually troughs that were healed by siliciclastic Upper Cretaceous sediments, a process commonly described in the Campos Basin (e.g., Moraes et al., 2007; Jackson and Hudec, 2017). The areas where carbonate rafts occur are subject to less compaction than areas where the post-salt stratigraphic succession predominantly comprises marine mudstones. Therefore, the more rigid carbonate rafts are interpreted to induce subtle gradient variations on the slope due to differential compaction (e.g., Collier, 1991; Jackson et al., 2008; Privat et al., 2021). This effect is supported by bounding stratal thickness patterns and subtle convexity of the reflections (Fig. 3.4C).

The raft tectonics and subsequent fault reactivations resulted in a complex structural configuration of rafts (highs) separated by lows (graben-like areas and troughs) and salt structures (Fig. 3.4C). In the up-dip domain, the Marlim Unit was deposited partially above carbonate rafts and partially above an area where these rafts were markedly displaced, leading to the formation of a graben-like structure bounded by curvilinear faults orientated NW-SE and NE-SW (Fig. 3.4). The transition zone coincides with an area between two carbonate rafts, where a thick salt wall formed, and with a structural high formed by faulting in a raft (bounded by antithetic and synthetic NE-SW oriented faults). In the down-dip domain, the Marlim Unit was deposited in part above the flanks of carbonate rafts and above a zone where no major carbonate rafts are observed. Intense faulting is observed in this area and basinward, and a series of N-S to NE-SW oriented normal faults (mainly synthetic) follow the orientation of salt structures, forming high displacement faulted rafts and/or prominent rollover features (Fig. 3.4).

The isopach map shows that thicknesses are highly variable, ranging from a few metres to more than 90 m (Fig. 3.4B). Average thicknesses are 22 m in the up-dip domain and 26 m in the down-dip domain, indicating that large areas of the Marlim Unit are close to the vertical seismic resolution. Consequently, the seismic reflections' character shows limited variability in amplitude profiles.

A

Top Salt

Top Carbonates

Structural Top
+
−

UP-DIP DOMAIN
TZ
DOWN-DIP DOMAIN

N

0   5   10km

B

Thickness (m)
80
60
40
20
0

Marlim Unit
Thickness

UP-DIP DOMAIN
TZ
DOWN-DIP DOMAIN

N

0   5   10km

KEY

- - - Top Marlim Unit
- - - Top Carbonates

- - - Base Oligocene
- - - Top Salt

- - - Top Cretaceous
- - - Top Rift

○ Areas with fault control on deposition in the interval that includes the Marlim Unit

↓ Areas with increased thickness in grabens

● Major faults in seismic profile and map view

★—★ Area of interest - Marlim Unit

C

Salt
Raft
Raft
Salt

TZ

500ms

0 2 4 6 8 10km

1:122070

X   X'

Figure 3.4: Structural configuration in the study area (fault traces at the Marlim Unit level on the maps). A – Focus on the structural tops of the salt layer and the carbonate rafts with a transparent surface of the Marlim Unit displayed above; warm colours indicate higher structures and, therefore, lower depths (see text for explanation). B – Focus on the Marlim Unit thickness map displayed above grey structural tops of the salt layer and carbonate rafts. C - Dip seismic section X-X' (see A, time domain, 5x vertical exaggeration). The orange arrows indicate areas with increased thicknesses in grabens, supporting syn-sedimentary fault activity. The black circles indicate clear fault control on deposition from the base of the Oligocene to the top of the Marlim Unit in the vicinities of the area of interest marked between the two yellow stars. The carbonate rafts were displaced above the salt and control overlying thickness patterns due to differential compaction (see how the interval between the Top Cretaceous and the Marlim Unit thins above the rafts). The TZ (transition zone) partially coincides with a relative structural high formed due to faulting in a raft. The Marlim Unit is very thin in the seismic profile, and the base is interpreted in the black peak just below the top, shown as a red seismic horizon.

3.5.2 Up-dip domain architectural elements

The up-dip domain of the Marlim Unit is characterised by NW-SE oriented low and high-amplitude elongate seismic anomalies, which cut seismic anomalies with patchy to lobate morphologies. Outside and up-dip of this domain is an area of overall dim amplitude anomalies without clear geomorphology, which, through calibration by well data, is marked by high mud content (Fig. 3.5A, 3.5B).

A

RMS
1.00
0.80
0.60
0.40
0.20
0.00

0 km   1.5 km   3 km

B

Area of
high mud
content

V'

⊕ MU 11

Y'

MU4

C2b

Lobe

C4

MU3

C2a

Z'   C2

MU2

C0b

C0c

C1b   MU6

C1a   MU5

C0a

Z

RMS
1.00
0.80
0.60
0.40
0.20
0.00

V

C1

Lobes

C0

0 km   1.5 km   3 km

C

V'

C2b

Y'

MU4

MU3

C2a

Z'   C2

MU2

C0a

C0c

C4

C0b

C1a

C1b   MU6

MU5

Z

Thickness (m)
80.00
60.00
40.00
20.00
0.00

V

C1

C0

0 km   1.5 km   3 km

Main faults   Convergence points   Flow path   Exit points   Thick features
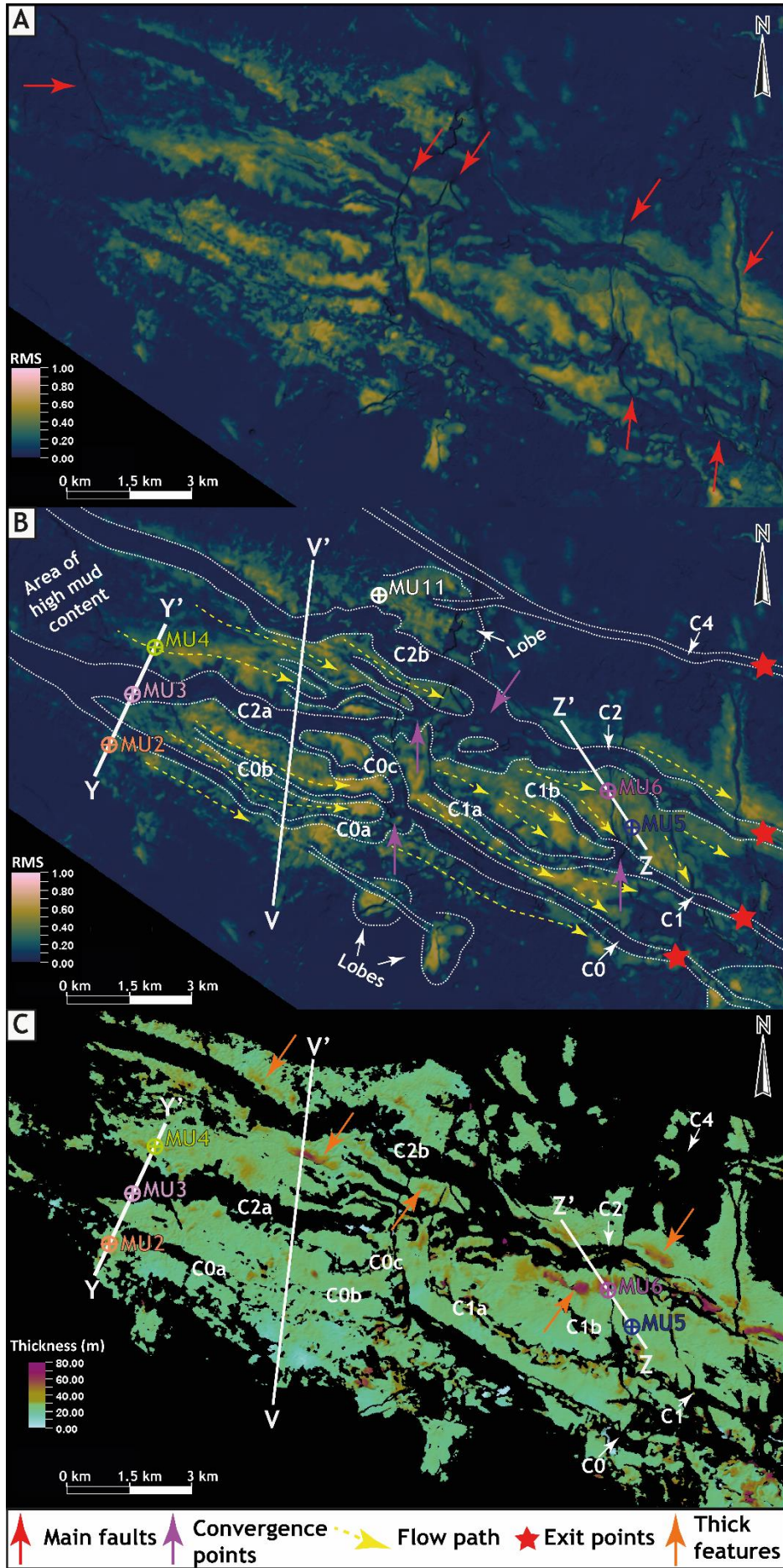
Figure 3.5: A and B – Uninterpreted and interpreted RMS amplitude map focused on the up-dip domain. A- Red arrows indicate the main faults in the area. B- Yellow arrows mark the path of high-amplitude anomalies. Dashed white lines mark geomorphological patterns of the mud-prone channel-fills, which show convergence points (purple arrows) when crossing faults (red arrows). The red stars mark the exit points of the mud-prone channel-fills towards the Transition Zone. Mud-filled channels are named C0, C1, C2 and C4 (C3 is only down-dip) and their branches with letters a, b and c. Seismic profiles marked in B are shown in figures 3.6 and 3.7. C – Up-dip domain thickness map. Orange arrows indicate thicker elongate features interpreted as channel-fills.

3.5.2.1 Low-amplitude elongate anomalies

Observations: The most distinctive architectural features in the up-dip domain are parallel to sub-parallel low-amplitude elongate features with low planform sinuosity and channel-form (Fig. 3.5A, 3.5B), which truncate underlying reflections (Fig. 3.6). The low-amplitude features are named C0, C1, C2 and C4 (C3 is only down-dip) and range from narrow and shallow, like C0, C1 and C4 (up to 300 m wide, 30 m estimated incision depth), to wide and deep, like C2 (up to 600 m wide, 60 m estimated incision depth) (Figs. 3.5 and 3.6). These channel-forms display channel branches that crosscut and locally converge when crossing faults (Fig. 3.5). Well log motifs that intersect the low-amplitude elongate channel-forms are similar to the overlying stratified mudstone successions. Well intersections also support a thin (a few metres) coarser-grained basal unit (Fig 3.7A).

Interpretation: The geometry and basal erosion of the low-amplitude elongate anomalies, and the similarity to well log motifs from overlying mudstone successions, support interpretation as mud-filled submarine channel-fills. The coarse basal unit represents a sediment bypass-dominated phase of channel development. The mud-filled channels C0, C1, C2 and C4 exit the up-dip domain and pass across the TZ in four different locations (Fig. 3.5B). The lengthening of the mud-filled channels across the TZ suggests a connection with the down-dip domain.
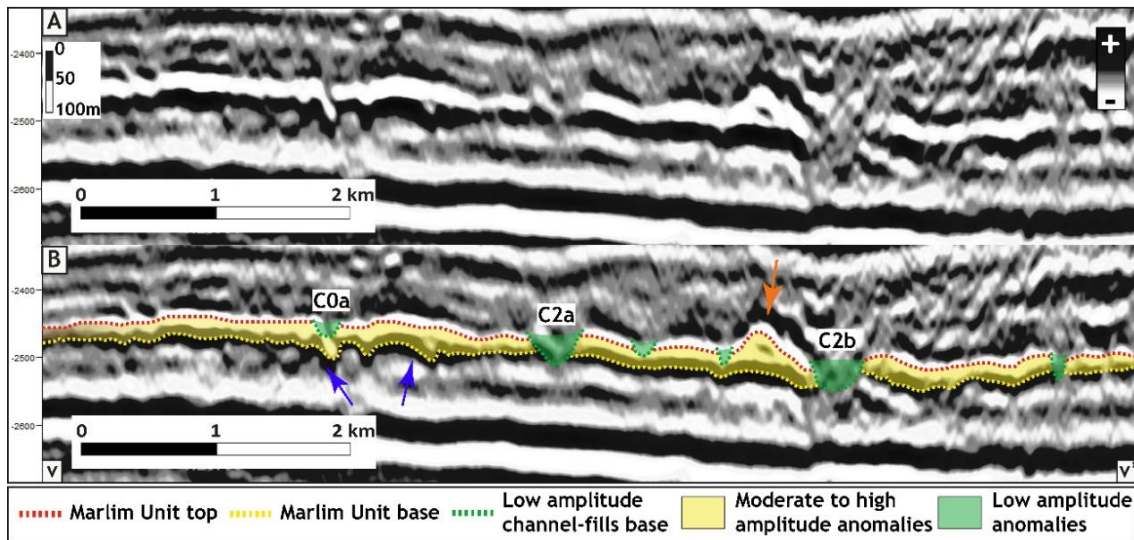
Figure 3.6: A and B – uninterpreted and interpreted V-V' strike seismic amplitude profile (depth, 5X vertical exaggeration) showing the seismic expression of the Marlim Unit in the up-dip domain. Note high-amplitude reflections cut by low-amplitude channel-fills and the irregular character of the base reflection suggesting basal erosion notches (blue arrows). The orange arrow indicates a feature interpreted as a transverse cut of a channel-fill with positive relief due to more compaction of the finer-grained sediments that flank the channel-fill axis. This feature corresponds to an elongate thicker body on the thickness map. See Figure 3.5 for the location of the seismic line.

3.5.2.2 High-amplitude elongate anomalies

Observations: The RMS map shows moderate to high-amplitude elongate anomalies that form flat- to irregular-based and continuous to semi-continuous reflections in seismic profiles, which truncate underlying reflections, and which are themselves cut by the mud-filled channels (Figs. 3.5, 3.6 and 3.7). Locally, these reflections thicken in seismic profiles and correspond to thicker elongate (>50 m thick) features in the thickness map (Figs. 3.5C, 3.6 and 3.7B). Well log motifs (gamma-ray, density and neutron) are variable. Well calibration indicates moderate to high sandstone percentage (average 58%) for these moderate to high-amplitude reflections. Cores display limited grain size variation, and fine-grained structured sandstones dominate the sandier packages (Fig. 3.7B).

Interpretation: Observations of the planform morphology of individual thicker moderate to high-amplitude seismic anomalies with basal truncation support the interpretation of the moderate to high-amplitude elongate anomalies as

submarine channel complexes. Flat to irregular-based high-amplitude reflections are attributed to laterally stacked sand-prone channel-fills. Similar seismic responses have been associated with amalgamated channel complexes (e.g., Jackson et al., 2008; Kane et al., 2010; Li et al., 2021). External levees are not identified in seismic profiles or well data. Therefore, the channel complexes are interpreted to be confined through erosion and degradation of the slope profile. The channel complex interpretation is further supported by the well log motifs and sedimentary facies that indicate sand-and intercalated sand and mud fills. Local amplitude decreases correlate to the intercalation of sandstone and mudstone packages, which support the interpretation of channel margin deposits (e.g., Hodgson et al., 2011) of laterally stacked channel-fills (Fig. 3.7A).

3.5.2.3 Moderate to high-amplitude patchy to lobate anomalies

Observations: Moderate to high-amplitude anomalies form indistinct patchy morphologies due to truncation by the mud- and sand-filled submarine channels. Moderate to high anomalies form lobate features at the SW and NE edges of the up-dip domain (Fig. 3.5B). A cored well (MU11) that intersects a small lobate seismic anomaly at the NE edge of the up-dip domain (Fig. 3.5A, 3.5B) records interbedded intervals composed of clean and laminated sandstone and bioturbated sandy mudstone facies, suggesting hybrid beds.

Interpretation: The patchy moderate to high-amplitude anomalies truncated by the submarine channels are likely sand-prone. However, it is not possible to distinguish whether these are remnant channel-fills or lobes, or a combination. The cored well (MU11) that records hybrid beds suggest the presence of intraslope lobes (e.g., Haughton et al., 2009; Hodgson, 2009; Kane et al., 2017; Southern et al., 2017), which were better preserved at the SW and NE edges of the up-dip domain. It is important to note, however, that parts of the up-dip domain are close to the limits of seismic resolution and were eroded by flows that carved the channels, subsequently filled with mud. Therefore, some of the elongate seismic patterns might be misleading and remnant lobe deposits might be more widely preserved across the up-dip domain.
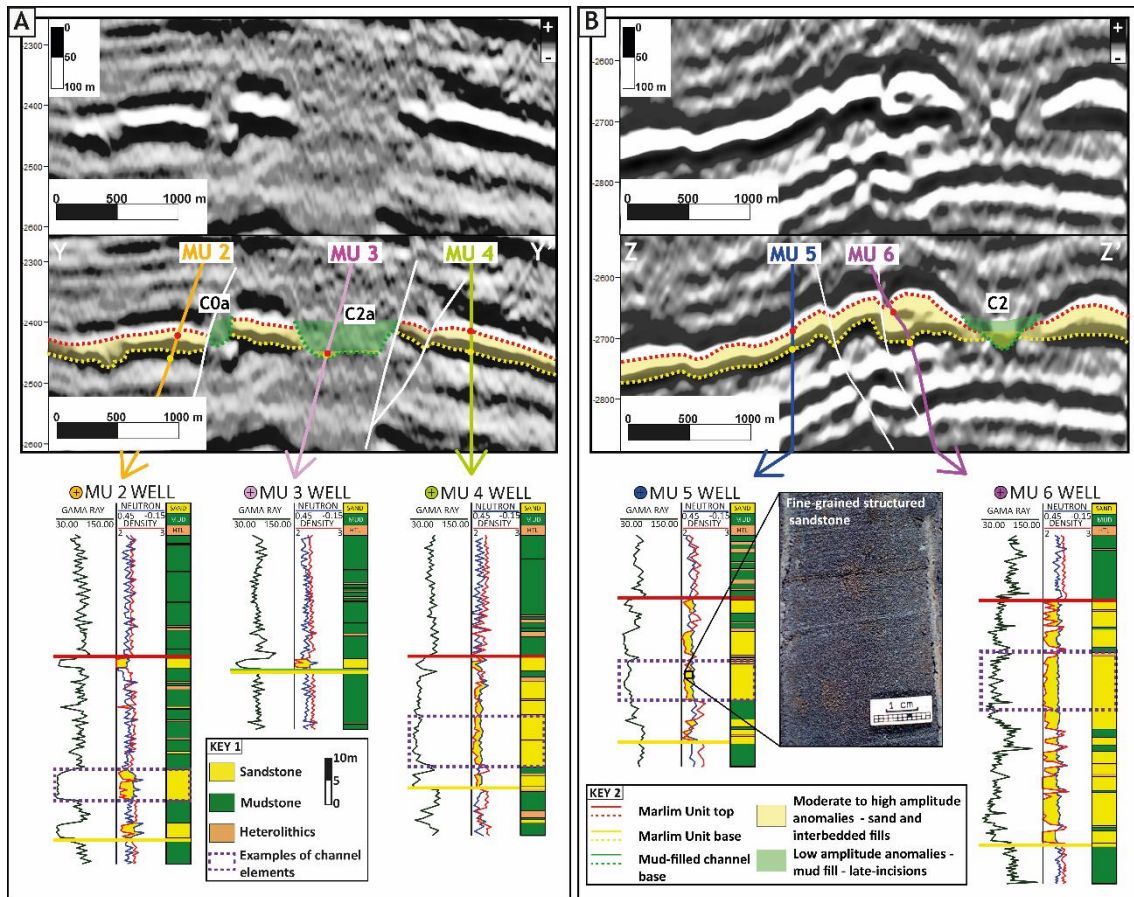
Figure 3.7: A- Y-Y' detailed strike seismic amplitude profile (depth, 5x vertical exaggeration) with three well intersections. MU2 – example of heterogeneous and laterally stacked channel-fills. MU3 - well intersecting mud-prone channel-fill. MU4 - example of sand-prone channel-fill. B- Z-Z' detailed strike seismic profile (depth, 5x vertical exaggeration) with two well intersections. MU5 – cored well with fine-grained structured sandstones. MU6 - example of a sand-prone channel-fill intersecting a high thickness feature in the seismic profile (with scale compatible with a perpendicular section of a submarine channel) seen on the thickness map as an elongate thicker body. Basal truncation is suggested by the reflections' patterns. See Figure 3.5 for location of the seismic lines.

3.5.3 Down-dip domain architectural elements

3.5.3.1 Moderate to high-amplitude lobate anomalies

Observations: Four lobate features characterised by moderate to high-amplitudes are identified in the down-dip domain (named LA, LB, LC and LD) (Fig. 3.8). The features range in area from 10 km² to 20 km². Seismic profiles and attribute maps

reveal that they are connected to, and are cut by, high-amplitude elongate anomalies that connect to channel-fills C0, C1, C2 and C4 from the up-dip domain. Well data and seismic amplitudes indicate that these channels, in the down-dip domain, have a sand-prone infill (Figs. 3.3, 3.8 and 3.9), except for channel C0, which remains mud-filled above feature LA. The sand-prone channel-fill C1 cuts feature LB, C2 cuts features LC and LD, C3 emerges between features LC and LD, and C4 cuts feature LD (Fig. 3.8). Logs from wells that intersect channels C2 and C4 reveal a blocky pattern, suggesting highly amalgamated sandstone beds (Fig. 3.9). A continuous cored interval from two wells that intersect C2 confirms amalgamated moderately sorted, fine- to medium-grained structureless sandstones, with coarse sand (<5%). A fine-grained interval <10 m thick, composed of bioturbated siltstone with well-preserved trace fossils (*Zoophycus*), is observed with sharp contacts within the sand-prone packages towards the top of the fill of channel C2 (Fig. 3.9). Calibration with well logs suggests that this siltstone interval is present in the eight wells that intersect channel C2.
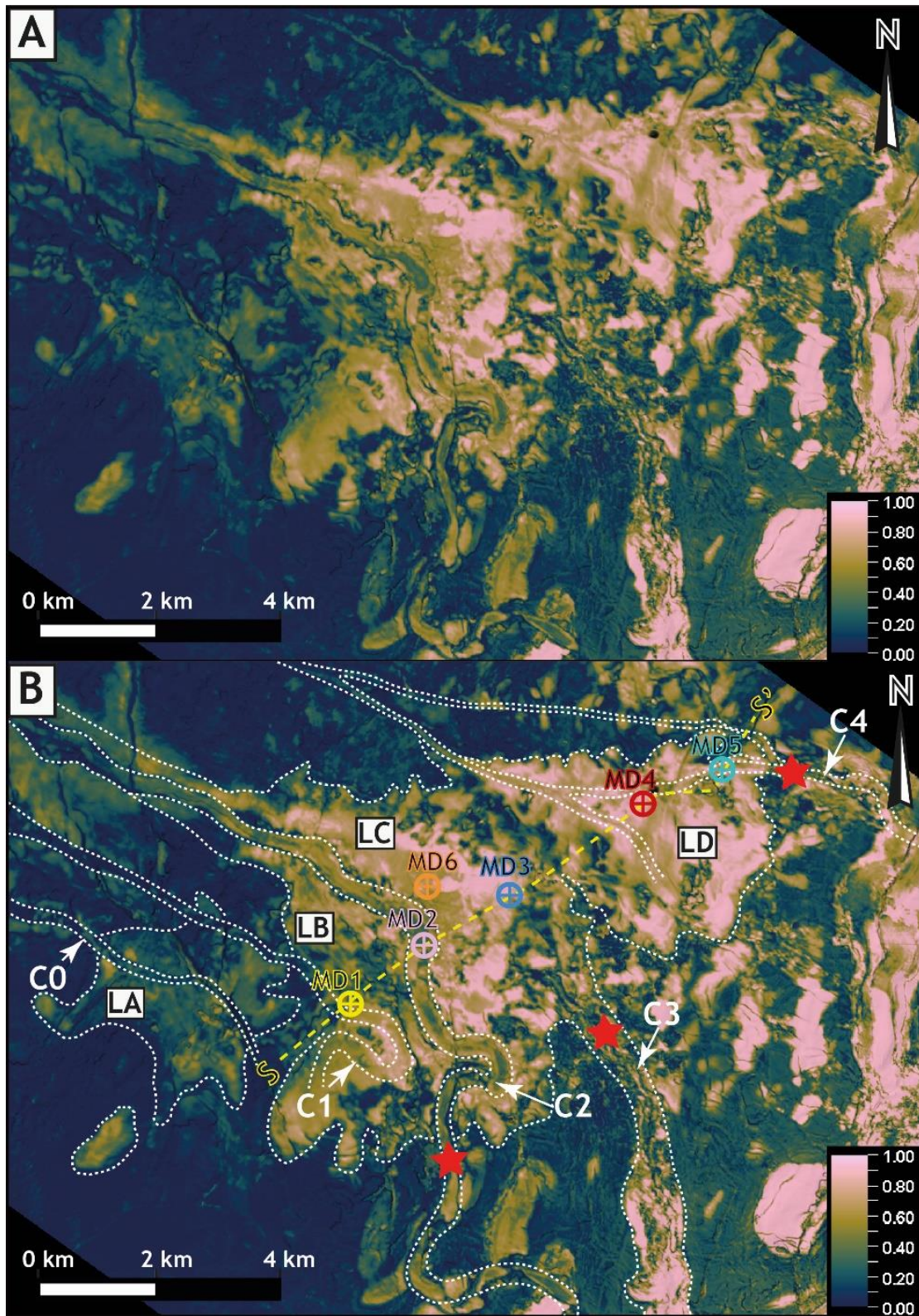
Figure 3.8: Marlim Unit RMS amplitude map focusing on the down-dip domain. A - Uninterpreted. B – Interpreted, with white dashed lines marking the lobate features (LA to LD) and the channel incisions, which are also indicated by the white arrows (C0 to C4). The red stars mark points where the channels extend beyond the down-dip domain. S-S' section and wells are shown in Figure 3.9.

Compared to the mud-filled channels, the sand-prone counterparts are wider with higher sinuosity (see channels C1 and C2; Fig. 3.8). Channel C4 also widens and branches (Fig. 3.8). Channel C3 forms a partially preserved high-amplitude feature that converges down-dip of LC and LD towards channel C2 (Fig. 3.8). Channels C2, C3, and C4 are mapped to exit the down-dip domain in different locations, and to extend basinward (Fig. 3.8).

Well data indicate that a high sandstone percentage characterises lobate features LB, LC, and LD (75% on average). Many wells that intersect different seismic facies display blocky gamma-ray and density-neutron log signatures, interpreted as amalgamation of porous sandstone packages (higher porosity as the separation between density and neutron logs increases) (Fig. 3.9). Therefore, the architectural interpretation is based on reflections' characteristics combined with log patterns. High-amplitude, continuous to semi-continuous and tabular to mounded reflections are recognised in features LC and LD. In contrast, moderate to high-amplitude, discontinuous and irregular-based reflections are present in LA and LB. The edges of features LB, LC and LD present moderate sandstone percentage (~50%) with the intercalation of sandstone and mudstone beds (well MD-3 in feature LC, Fig. 3.9). Lithology data are not available in feature LA. In general, there is a thickness reduction from the feeder point towards the distal parts of features LC and LD, although wells show moderate thicknesses (around 20 m thick) in these distal areas (Fig. 3.9), and amplitude continuity suggests a well-defined sand pinch-out (features LB, LC and LD, Fig. 3.8). A cored well intersecting the central part of feature LC displays well-sorted fine-grained structureless and structured sandstones (well MD-6, Fig. 3.8B).

Interpretation: Continuous to semi-continuous bright amplitude reflections with fan-shape morphology have been frequently associated with stacked lobes in intraslope settings (e.g., Adeogba et al., 2005; Jackson et al., 2008; Deptuck et al., 2012; Jobe et al., 2017; Howlett et al., 2020; Li et al., 2021). On the other hand, discontinuous high to moderate amplitude reflections have been related to distributary channel networks (e.g., Hay, 2012) and channel complexes (e.g., Barton, 2012; Kane et al., 2012). Blocky wireline log responses (low gamma-ray values, low-density values and low neutron reading) that reflect amalgamated sandstone beds have been associated with channels (e.g., Kane et al., 2012; De

Gasperi and Catuneanu, 2014; Chima et al., 2019) and lobes axes (e.g., Prather et al., 1998; Steventon et al., 2021). Intraslope lobes or fans are described as having relatively high sand content towards the fringes and well-defined sand pinch-outs, differing from the fringes of basin floor lobes that can be quite mud-prone, thin and with poorly defined pinch-outs (e.g., Spychala et al., 2015; Jobe et al., 2017). Therefore, the seismic facies and geomorphology of features LC and LD are consistent with an interpretation of intraslope lobe complexes. In contrast, the external planform morphology of features LA and LB suggests relatively unconfined deposits, but the seismic reflections' characteristics suggest channelised elements. The arrangement of these elements in planform amplitude patterns is inconclusive as the amplitude response is affected by faulting and reservoir fluids (oil versus water contact). However, due to the lobate external shape, features LA and LB are interpreted as distributary channel complexes. The high sandstone percentage observed in feature LB suggests amalgamated channels, whereas the seismic character suggests higher lithological variability in LA.
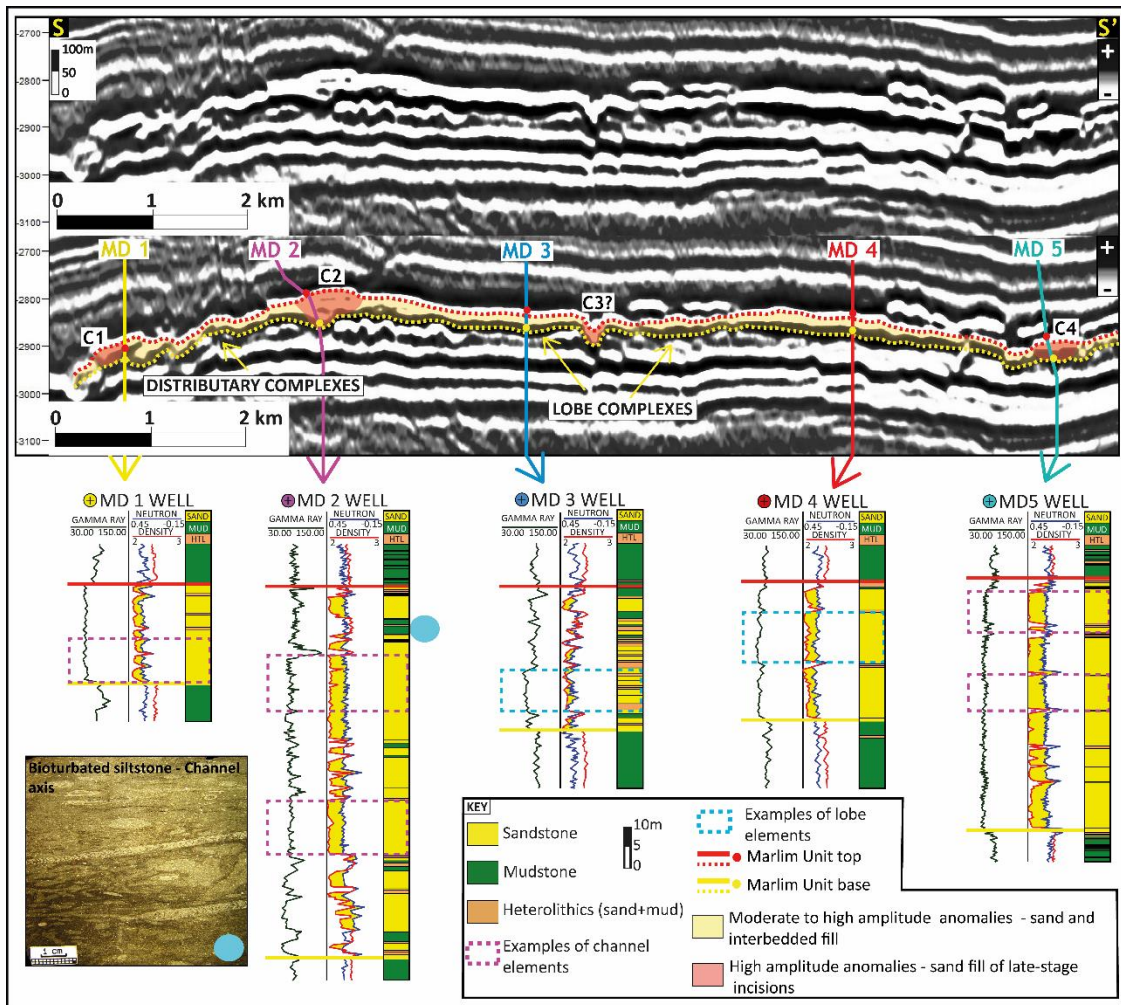
Figure 3.9: S-S' strike seismic amplitude profile (depth, 5X vertical exaggeration) crossing LB, LC and LD features with five well intersections. Reflections' continuity and truncation differentiate distributary channel complexes from lobe complexes (see text for explanation). Blocky well log motifs are common and highlight the high sandstone percentage in the area. Examples of architectural elements' log response are marked on the wells. The MD1 well intersects distributary channel complexes deposits. The MD2 and MD5 wells intersect the axes of thick late incision channel-fills (C2 and C4, respectively). The MD3 well shows a moderate sandstone percentage in interbedded successions found at the marginal positions of lobes, whereas high sandstone percentage shown by the MD4 well relates to central positions. Core of the bioturbated siltstone interval was recorded within the sand-prone axis deposits of channel C2 (see text for explanation). See Figure 3.8 for location of the seismic profile.

3.5.4 Topographic configuration and control of the Marlim Unit

The large-scale topographic configuration of the slope during the evolution of the Marlim Unit is interpreted from the seismic architecture and lithological attributes described above (Figs. 3.10 and 3.11). In addition, some control is invoked through correlation with the spatial distribution of underlying salt structures, carbonate rafts and associated faults (Fig. 3.11). The seismic reflection data show no evidence for down-dip sills or three-dimensional closure, and the cores show no sign for flow ponding, such as turbidites with thicker normally graded mud caps.
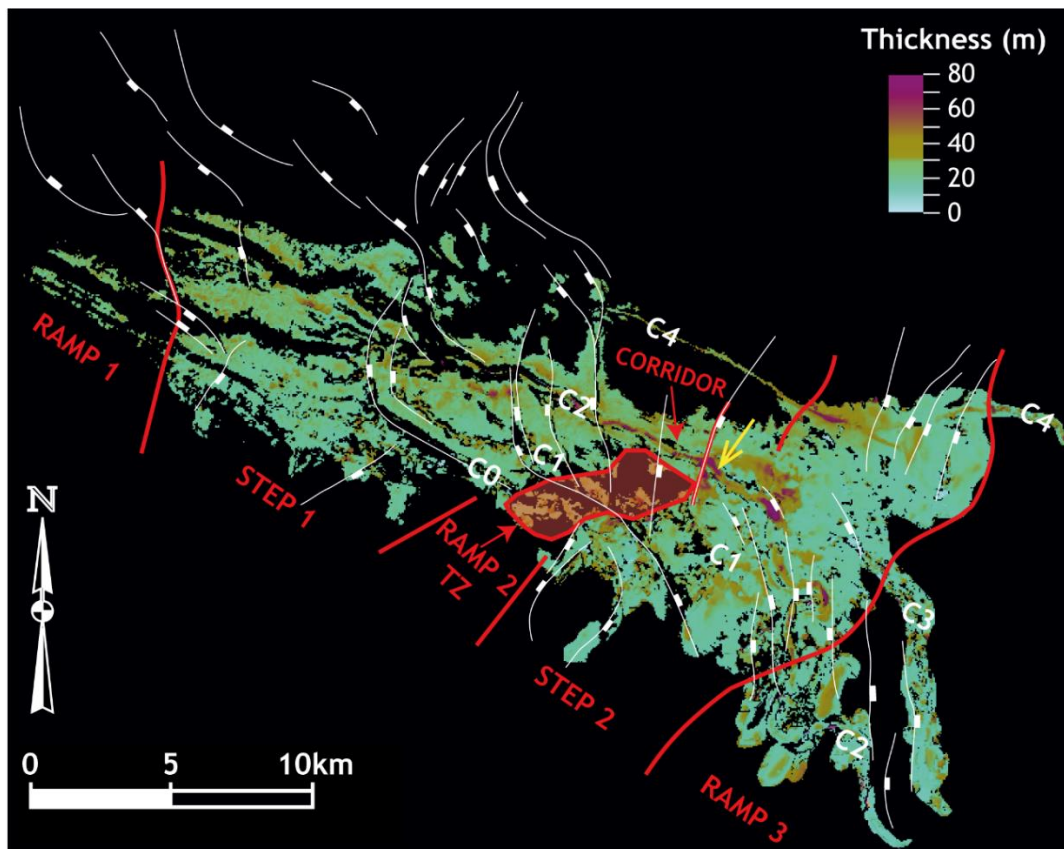
Figure 3.10: Marlim Unit structural and thickness map with the location of the slope breaks (marked by red lines) and slope sectors. The up-dip and down-dip domains are interpreted as steps edged by high gradient ramps (the TZ includes a ramp and a corridor). Note that some slope breaks coincide with faults. Channels C0 to C4 are marked. See the increased thickness recorded at the slope break of step 2 (yellow arrow, features LB, LC and C2) and the general trend of thickness increase from the SW towards the NE.

The up-dip and down-dip domains are depocentres with multiple channels that cut lobes, separated and bounded by low-amplitude but channelised areas (Fig. 3.3), which support the presence of a stepped slope profile. The two depocentres represent up-dip (step 1) and down-dip (step 2) steps (Figs. 3.10 and 3.11). Up-dip of step 1, irregular and low-amplitude anomalies and the dominantly mud-prone character of the deposits indicate a propensity for sediment bypass and lower preservation potential for sand, suggesting deposition in a higher gradient sector of the slope (ramp 1 – a bypass-dominated zone *sensu* Stevenson et al., 2015). The slope break from ramp 1 to step 1 partially coincides with a synthetic NW-SE salt-rooted normal fault that edges a carbonate raft (Fig. 3.10).

The transition zone between steps 1 and 2 comprises two distinct elements: an area of weak to moderate amplitudes, which is laterally associated with a high-amplitude and sand-prone narrow elongate feature (Figs. 3.3, 3.10 and 3.11). The low-amplitude area supports high mud content and low preservation for sand. Therefore, this area is interpreted as a high-gradient ramp that allowed flows to bypass and connect the steps. The channels that feed and cut the lobate features LA and LB down-dip support this configuration (Figs. 3.10 and 3.11). In contrast, the high-amplitude narrow zone is interpreted as a corridor above the lateral flank of a carbonate raft where flows converged and directly connected steps 1 and 2. This corridor formed between the higher gradient ramp and a positive topographic feature that possibly originated from differential compaction above the apex of the same raft (Fig. 3.11), as supported by thinner strata towards the centre of the structure.

The lobate features of step 2 formed above the down-dip flanks of carbonate rafts towards an area without major underlying rafts. Feature LC and parts of LB form at the exit of the corridor, down-dip of a slope break that coincides with a SW-NE synthetic fault that forms a structural high that was orientated transverse to flows (Fig. 3.10). Increased thickness of the lobes and channel-fill (C2) adjacent to the fault plane support that this structure was an active feature during deposition (Fig. 3.10, yellow arrow). The slope break of feature LD is not associated with any resolvable structure, although differential compaction at the flanks of the carbonate raft underlying LD could have impacted the palaeoslope configuration. Down-dip of step 2, channels C2, C3 and C4 extend basinward as isolated

features, and there is no significant sand deposition associated with the Marlim Unit outside of these channels. I interpret that these channels evolved in a steeper slope sector compared to steps 1 and 2. Thinning of Cenozoic strata above rollover anticlines and above faulted blocks associated with salt-rooted listric normal faults suggest the presence of irregular bathymetric features down-dip of step 2. Despite the observed lateral variability in expression, this area is referred to as ramp 3.

The contrasting depositional characteristics observed on steps 1 and 2 (architecture, thickness patterns and sandstone percentage) suggest differences in the geometry of the associated slope breaks and accommodation on the steps. The sand-prone lobe complexes documented in features LC and LD above step 2 support an abrupt slope break, which led flows to lose their capacity to transport coarser fractions, as well as inducing flow expansion due to rapid loss of confinement (e.g., Mulder and Alexander, 2001; Spychala et al., 2020). The thickness increase recorded downstream of the slope break in the proximal parts of step 2 also suggests substantial gradient variations. This interpretation is supported by experimental studies that show thicker slope break deposits associated with abrupt gradient changes (e.g., Mulder and Alexander, 2001; Kubo, 2004). Conversely, a milder slope break, between ramp 1 and step 1 and in features LA and LB, would permit flows to remain channelised. Channel stability across mild slope breaks has been documented in channels in intraslope basins described by Booth et al. (2003) and Barton (2012).

In summary, the geomorphological patterns of the Marlim Unit point to a complex palaeoslope topography comprising alternating depositional (steps) and bypass-prone areas (ramps), with breaks-in-slope of variable magnitudes and physiography that are related to underlying salt-related tectonic features (Fig. 3.11). The presence of multiple mud- and sand-filled channels that connect the steps across the ramps (Figs. 3.5, 3.8 and 3.11) suggests multiple non-synchronous sediment conduits. Gradient variations imposed by slope breaks along channel profiles were probably readjusted via up-dip migrating knickpoints based on observations from modern and ancient systems (Deptuck et al., 2012; Heijnen et al., 2020; Guiastrennec-Faugas et al., 2021; Tek et al., 2021; Allen et al., 2022). The age relationship between the late-stage channels and the step

deposits requires a high-resolution stratigraphic framework, which is discussed in the next section.
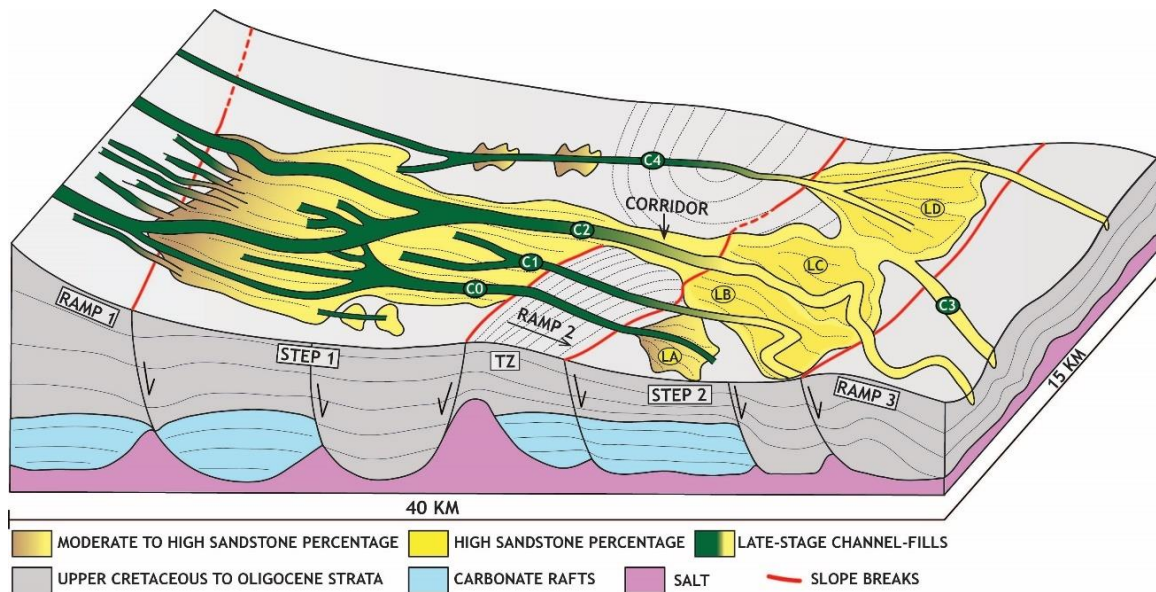
Figure 3.11: Large-scale topographic configuration of the stepped slope representing a static view of the seafloor at the end of the Marlim Unit deposition. Steps 1 and 2 form two stratigraphic linked depocentres that record channel and lobe complexes (see text for explanation).

3.5.5 Stratigraphic framework

Stratigraphic relationships observed in seismic reflection data support interpretations of key surfaces and the relative age of deposits. The up-dip submarine channel complexes in step 1 form an 8-10 km wide zone composed mainly of laterally stacked channel-fills that are cut by the mud-filled channels C0, C1, C2 and C4 (Figs. 3.5, 3.6 and 3.7). The same configuration is documented in step 2, where these channel-fills are sand-prone (except C0) and cut the lobate features (Figs. 3.8 and 3.9). These observations support late-stage channel lengthening and incision of sand-prone deposits.

More detailed stratigraphic age relationships were observed on step 2, where the nature of the depositional system (i.e., unconfined deposition) implies an overall higher preservation potential compared to the channel complexes of step 1. The irregular and sharp external shape of feature LA suggests it was partially eroded. It is interpreted that the erosion, at least in part, is due to truncation by channel

C1, the late-stage channel interpreted to have fed feature LB. In addition, LA is surrounded by LB, which formed in a space not occupied by LA (Fig. 3.8). These observations support LA being older than LB. The age relationship between LB and LC is not clear, and their relative position does not favour any interpretation in this sense. However, these features present distinct internal architecture and apparently have different feeder channels, supporting two depositional phases (Figs. 3.8 and 3.9). C2 cuts between the two features, supporting that it is younger than LB and LC. A more compelling age relationship is observed between LC and LD. LD shows a classical lobate geometry, meaning that the feature is well preserved. On the contrary, the NE edge of LC suggests truncation by a channel (Fig. 3.8). This could be C3; however, there is not sufficient seismic resolution to map C3 in this area. Also, the relative position between both features supports progradation of the system since C4, the LD feeder channel, lengthened further basinward before losing confinement (when compared to LB and LC). In summary, the geomorphological patterns suggest an overall oblique progradational stepping/compensational trend towards the NE, where LA is the oldest feature and LD the youngest (Figs. 3.3 and 3.8).

The stratigraphic framework of step 1 is summarised in two correlation panels orientated SW-NE, orthogonal to the channels, hung from the carbonate-prone stratigraphic datum and calibrated with nine wells (Fig. 3.12). The correlation panels highlight the pervasive mud-filled channels, with varying widths and depths, which incise into sand-prone channel-fills and lobes. Truncation surfaces within the sand-prone channel complexes are identified: i) where abrupt reduction in amplitudes related to the edges of the elongate seismic anomalies occur, and/or ii) in areas with abrupt and substantial thickness increase (Fig. 3.12). We assume that lower amplitude values at the edges of high-amplitude seismic bodies can be associated with channel margin deposits that onlap onto erosion surfaces (e.g., Hodgson et al., 2011), and that abrupt differences in thicknesses in the strike direction are related to channel truncation.

Well calibration supports interpretations of lithology distribution, architectural elements and stacking patterns. Preservation of laterally stepping channel-fills that comprise intercalated mud- and sand-prone packages related to channel margin deposits are common at the proximal part of step 1 (Fig. 3.12, panel 1

wells MU8 and MU9). Homogeneous sand-prone amalgamated channel-fills associated with axial deposits prevail at the distal part (Fig. 3.12 panel 2, wells MU13 and MU6). At the SW end of the panels, wells that intersect dim seismic amplitudes suggest thin, and moderate to low sand content, high aspect ratio geometries (Fig. 3.12, both panels). At the NE end of panel 1, high aspect ratio geometries intersected by two wells are depicted (wells MU10 and MU11, Fig. 3.12). The wells show a moderate sandstone percentage (MU11 facies include hybrid beds) and were drilled in a moderate to high-amplitude anomaly without clear elongate shape. Considering the seismic amplitude character, well data and relative position in the system, the high aspect ratio deposits are interpreted as remnant deposits of (frontal) lobes that were truncated by the channels.

Both panels reveal an overall NE-ward thickness increase, culminating in thick channel deposits of more than 40 m (41 m in well MU9, 51 m in well MU6, Fig. 3.12). This pattern is corroborated by the thickness map (Fig. 3.10) and suggests that accommodation progressively increased in the same direction. The panels also illustrate truncation surfaces that represent composite erosion surfaces that consistently step to the NE. The interpreted trend in lateral channel migration is supported by the depositional patterns of step 2. The physical continuity of the late-stage channels between both steps strongly suggests that these areas were stratigraphically linked during the evolution of the Marlim Unit. Therefore, I interpret that the stratigraphic evolution above steps 1 and 2 shared a NE-ward migration history.

STRIKE STRATIGRAPHIC SECTIONS - STEP 1
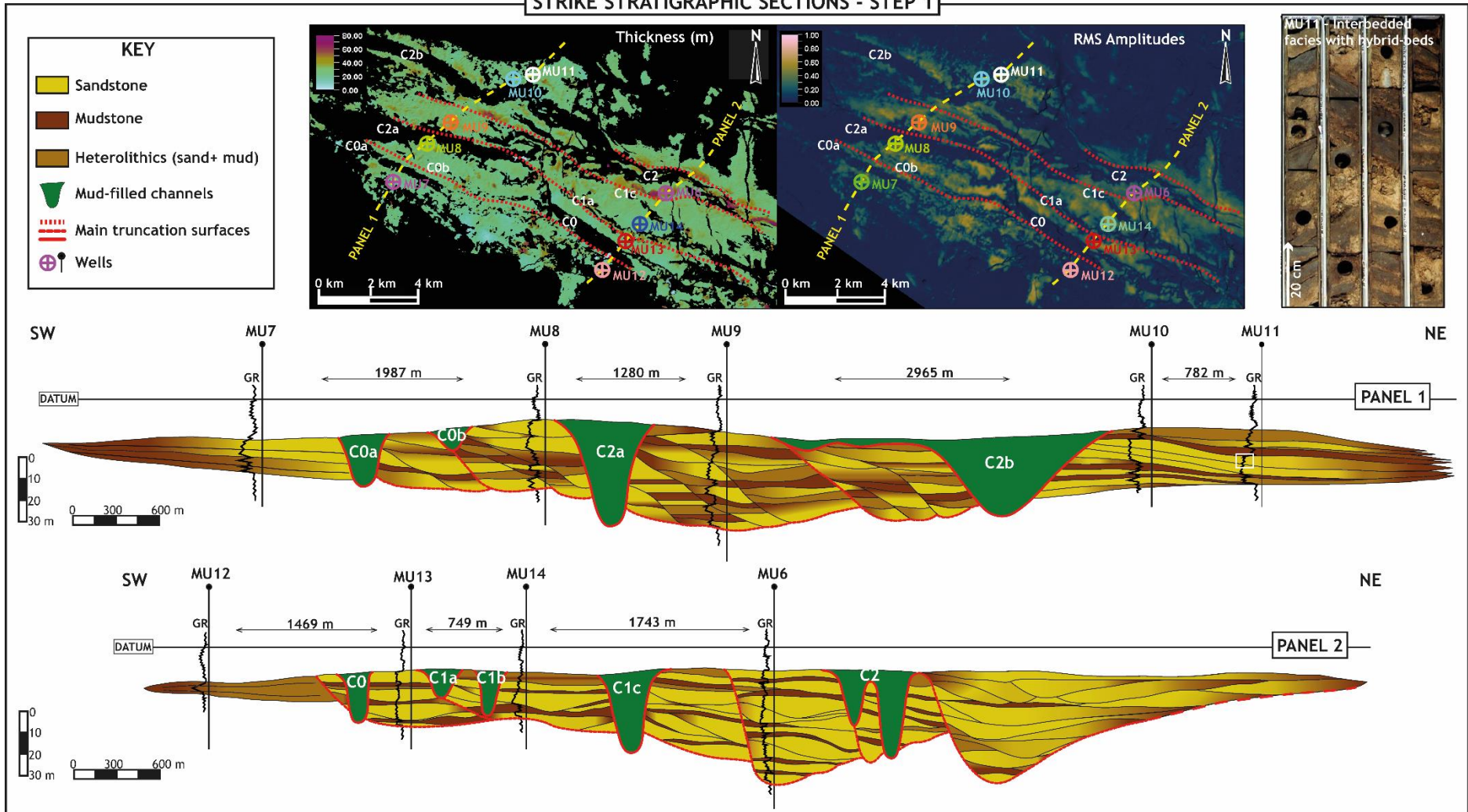
Figure 3.12: *Interpreted strike panels that summarize the stratigraphic framework of step 1. Note the thickness increase trend towards NE calibrated by wells. C0 (a, b), C1 (a, b, c) and C2 (a, b) represent the mud-filled channels that cut the sand-prone channel complexes and, eventually, older lobes. The red lines depict truncation surfaces. The red truncation surfaces related to the sand-prone channel-fills are depicted in the thickness and amplitude maps and are interpreted in areas with abrupt thicknesses variations and/or amplitudes reduction. The black lines that limit internal architectural elements follow well logs breaks, however, their geometry is not resolved by seismic and, therefore, is speculative. Lobes are interpreted on both edges of panel 1 and at the SW edge of panel 2.*

I interpret that a sediment bypass-dominated period following incision occurred in the late-stage channels before they were filled with mud and/or sand (channels C0 to C4). Similar channels commonly link intraslope depocentres at the final stages of a fill-and-spill cycle, once accommodation is healed and a new down-dip base level is established (e.g., Adeogba et al., 2005; Prather et al., 2012b; Spychala et al. 2015; Jobe et al., 2017). Several studies have documented bypass-dominated channels that exit intraslope basins at a single point, in accordance with the classic fill-and-spill model (e.g., Winker, 1996; Prather et al., 1998; Beaubouef and Friedmann, 2000; Pirmez et al., 2000; Sinclair and Tomasso, 2002; Smith, 2004; Adeogba et al., 2005; Barton, 2012). In contrast, a number of studies figuratively show 2 or 3 exits, but these are inferred, as channels are either not identified through these putative exits (Meckel et al., 2002), or evidence for these has been removed by subsequent erosion (Deptuck et al., 2012). In contrast, in the Marlim Unit, the bypass-dominated channels exit step 1 in four different locations and feed the lobate features of step 2. The bypass-dominated channels also exit step 2 at distinct locations (Figs. 3.5, 3.8 and 3.11). This suggests multiple laterally associated stratigraphic cycles, each representing an episode of accommodation creation, healing, and bypass in both steps (fill-and-spill cycles), and abandonment of the final channel.

3.6 Discussion

3.6.1 The Marlim Unit: stratigraphic evolution above a dynamic stepped slope

The Marlim Unit evolved above a stepped slope in an extensional salt domain, where downslope extension and salt-thinning prevailed. However, most of the extension had finished at the time of deposition, and much of the salt had flowed basinward (Quirk et al., 2012). The negative relief created by the salt-controlled raft tectonics was largely healed, implying only minor effects of salt-related deformation on the slope. Nevertheless, salt tectonics remained active and amplified by the reactivation of basement structures (Fetter, 2009). Therefore, due to the long-term trend of waning salt-related deformation, I propose a scenario where low deformation rates and subtle seafloor topography, disturbed by local fault reactivation, controlled accommodation creation in the Marlin Unit slope.

The deformation style is interpreted from architectural patterns and stratigraphic relationships. The thickening direction of multiple fill-and-spill cycles to the NE, together with the persistent migration of the submarine channels and lobes in the same direction, orientated transverse to the stepped slope profile, supports syn-sedimentary lateral tilting. This contrasts with basinward tilting, where submarine conduits tend to have fixed positions (e.g., Jackson et al., 2021). Without invoking a lateral tilt, the documented thickening direction and stacking pattern would need to be explained by the turbidite system initiating on the higher part of the steps (SW) and working their way progressively to lower elevations to the NE. However, turbidity currents are ground-hugging and have a strong tendency to preferentially fill topographic lows through deposition (e.g., Straub et al., 2009), and, therefore, this alternative scenario is considered highly unlikely.

Submarine channel systems that evolve above slopes that undergo lateral tilting can be controlled by growth faulting in extensional settings (e.g., Kane et al., 2010) or by salt dome uplift in halokinetic basins (e.g., Gee and Gawthorpe, 2006; Kane et al., 2012). On step 1, the prevalence of intercalated deposits supports the presence of laterally stepping channels with channel margin deposits

preferentially preserved (e.g., Hodgson et al., 2011; Fig. 3.12, panel 1). These channel-fills are similar to channel systems that laterally migrate in response to tilting caused by halokinesis (e.g., Gee and Gawthorpe, 2006; Kane et al., 2012). However, despite the evidence for tectonic activity related to salt-cored structures in the Oligocene/Miocene interval (Fig. 3.4), the exact cause of the lateral tilting, either uplift to the SW and/or subsidence to the NE, is challenging to determine as no specific structural element influencing the large-scale patterns of deposition is identified. Moreover, the effects of the syn-sedimentary deformation are interpreted here at a very high-resolution scale. Although I interpret the effects, the primary cause is difficult to demonstrate in seismic reflection data, especially in a setting of low deformation rates and complex interaction between halokinesis, differential compaction and, possibly, reactivation of basement faults.

The seismic geomorphological patterns suggest four fill-and-spill cycles in both steps. The geomorphological patterns in each cycle, and the stratigraphic evolution of the lateral tilting slope of step 1, are reconstructed in Figure 3.13. Here, accommodation is interpreted to be spatially more limited when compared to step 2, which records distributary channel and lobe complexes suggestive of an area prone to sediment dispersion. Above step 1, the high propensity for erosion and bypass resulted in an incomplete stratigraphic record. The cycles are defined by the mud-filled channels and their incisional relationship with the sand-prone channel complexes. Step 2 has higher preservation, and each cycle refers to one of the lobate features and associated incision (Fig. 3.8). Less clear is the relationship of the lobate features and C3, which could have been formed during cycle 3 or 4. The "fill phase" of each cycle relates to the sand-prone deposition before the late incisions, and the "spill phase" is associated with the bypass-dominated phase of these incisions (C0 to C4) prior to filling with mud and/or sand. After the spill phase, I interpret that the lateral tilting prevailed and drove a NE-ward shift in the location of each cycle, therefore, the cycles are here referred to as FaSTaR cycles (Fill-and-Spill, Tilt-and-Repeat). The following section will discuss the interplay between sedimentation and slope deformation within the evolutionary history of the Marlim Unit.
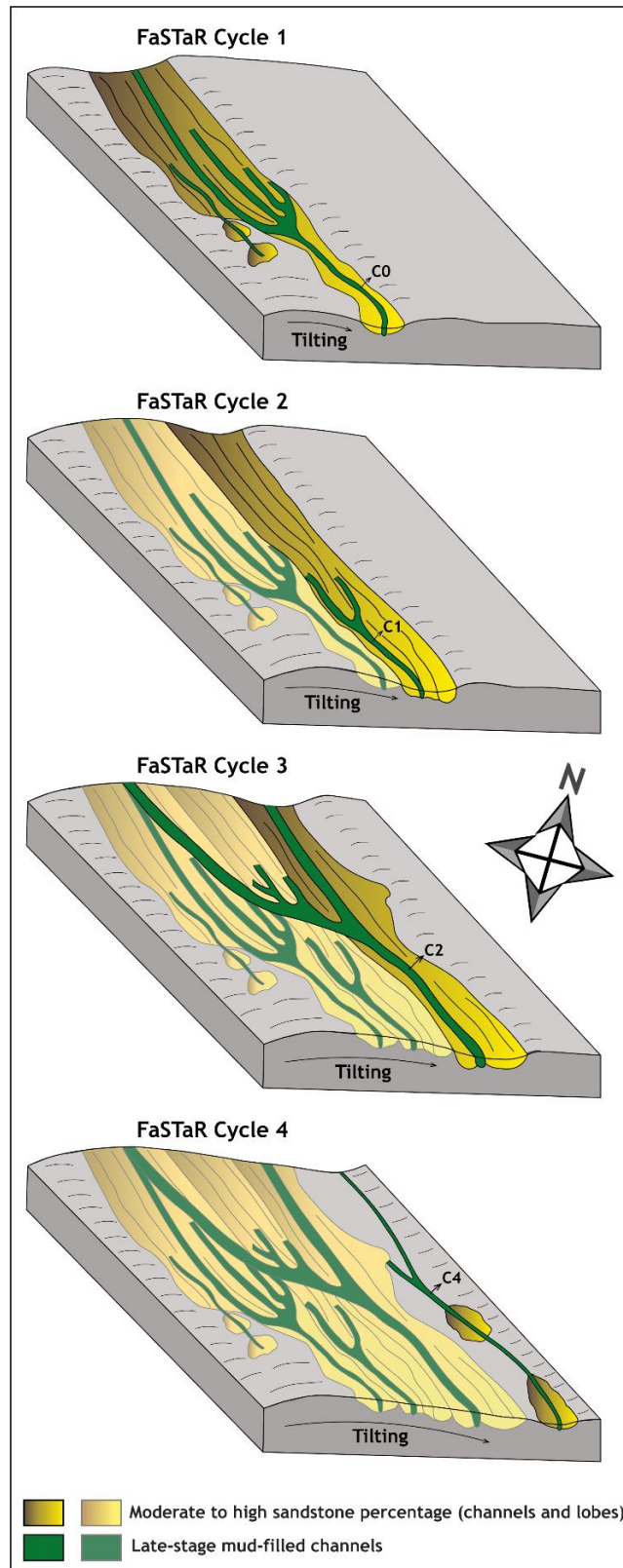
Figure 3.13: Three-dimensional diagrams that show the evolution of the Fill-and-Spill, Tilt-and-Repeat (FaSTaR) cycles on step 1 (see text for explanation). Note the thickness increase towards the NE attributed to higher accommodation controlled by the lateral tilting (peaking at cycle 3).

3.6.2 Intra- and extra-basinal stratigraphic controls on the Marlim Unit

Slopes evolve depending on the interplay of substrate mobility and sediment flux (Prather, 2003), which are controlled by intra- and extra-basinal factors, respectively. The incisions identified in the FaSTaR cycles (through-going in three of the four cycles) indicate that effective basinward sediment bypass beyond ramp 3 was repeatedly established, which suggests that a local graded profile was reached in each cycle (e.g., Adeogba et al., 2005; Deptuck et al., 2012). Therefore, it is interpreted that the sedimentation rate outpaced the rate of lateral tilting prior to, and during, these incisional periods. As outlined previously, the general structural context points to comparatively low rates of slope deformation (primarily lateral deformation in this case) relative to the duration of the sediment supply cycles, as commonly documented in stepped slope systems (e.g., Prather, 2003; Deptuck et al., 2012). Moreover, low rates of lateral tilt are also supported by the lack of flow ponding and by the stratigraphic connection between the steps, which suggests that the axial slope dip (regional slope gradient) was more critical for sediment dispersal patterns than the lateral structural dip caused by tilting.

The record of complete cycles (i.e., healing and bypass phases) indicates that enough sediment was available to infill accommodation and bypass basinward. However, it does not necessarily indicate that the sediment supply was constant during the Marlim Unit deposition. The partial filling of the late-stage channels with sandstones suggests that these channels had sand-prone flows during their lifespan. However, up-dip, the same channels are filled with stratified mudstones (analogous to the laminated and bioturbated siltstones cored in channel C2, Fig. 3.9), here related to the settling of low-density turbidity currents and hemipelagic sediment fallout. This spatial difference in infill character of the conduits suggests an initial phase of backfilling with sands, followed by sand starvation and, ultimately, channel abandonment (e.g., Prather et al., 1998; Peakall et al., 2000a, b). This occurs repeatedly and reflects an external control on the sediment supply that resulted in discrete waxing-and-waning fill-and-spill cycles, and periods of sand starvation, when coarse clastic sedimentation was negligible but lateral tilting was active (Fig. 3.14).

Above step 1, the sand-prone channel complexes form a composite body with overall high connectivity locally incised by the mud-filled channels. Lateral stratigraphic continuity of channel deposits above tilting surfaces results from gradual migration (combing) and has been associated with relatively low rates of tilting and/or short periods between flows, whereas pronounced stepping (avulsion) and/or isolated channel ribbons are associated with rapid tilting and/or long return periods (e.g., Peakall et al., 2000c; Kane et al., 2010, 2012). The infill by mud in the through-going incisions suggests a long return period of the flows between the cycles. However, the overall stratigraphic signature supports low rates of tilting and, likely, a short return period of the flows during the fill and spill phases of each FaSTaR cycle.

The organised and predictable stratigraphic record of the sediment supply cycles suggests that accommodation was created by a continuous slow-moving tilting slope at a quasi-constant deformation rate (Fig. 3.14) that acted as a background control rather than being controlled by short-lived random tectonic perturbations, which would result in a less ordered record. The end of a FaSTaR cycle and the start of a new one at the end of a sand starvation period are marked by the re-routeing of the feeder channels, which is here attributed to up-dip avulsions to areas with accommodation (Fig. 3.14). The mechanism for channel avulsions can be explained by the interplay between the deformation style operating in the Marlim Unit slope (intra-basinal control) and the cyclic fluctuations in the sediment supply (extra-basinal control). The turning point for triggering avulsions could be reached once the cumulative deformation caused by the continuous lateral tilting provoked structural changes capable of altering accommodation patterns on the slope (creating a new topographic low). At the onset of a new cycle, when enough coarse sediment was again available in the system, the returning flows would interact with a substantially modified slope with a higher potential for forming a new conduit, as also proposed by Kane et al. (2012).
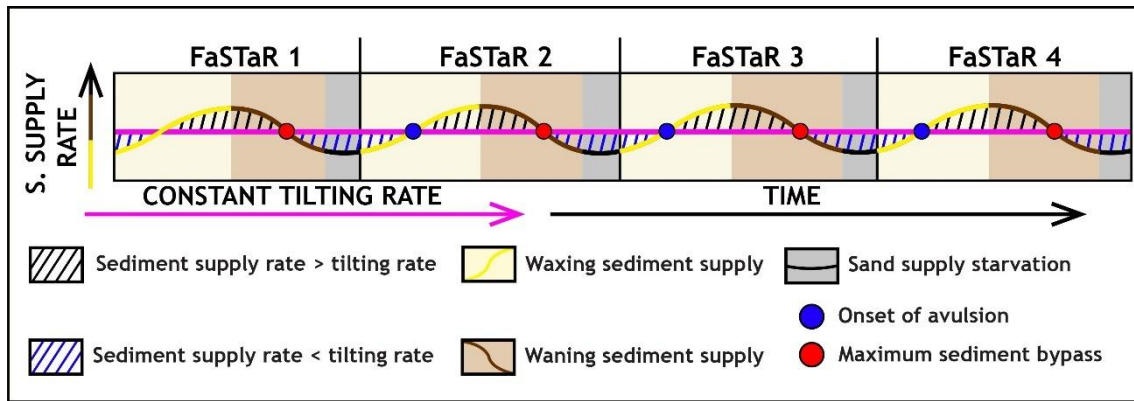
Figure 3.14: Sediment supply rate versus tilting rate in each FaSTaR cycle. The cycles comprise phases of waxing and waning sediment supply, and periods of sand starvation. The rate of tilting outpaces the rate of sediment supply during the end of the waning phase and the start of the waxing phase (including the sand starvation period). Conceptually, the maximum cumulative sediment bypass is positioned at the inflection point of the waning curve and the onset of avulsions at the inflection point of the waxing curve, when substantial coarse sediment is again available.

3.6.3 The impact of the slope configuration on the FaSTaR cycles

Pre-existing structural elements controlled the basinward stepped profile (Fig. 3.11). Underlying structural features such as rafts, salt rollers, and associated faulting played a crucial role in the position and character of slope breaks between ramps and steps. Turbidity currents are sensitive to gradient changes and respond differently according to the magnitude and type of topographic variations (e.g., Alexander and Morris, 1994; Garcia and Parker, 1989; Kneller and McCaffrey, 1999; Mulder and Alexander, 2001; Kubo, 2004; Morris and Alexander, 2003; Deptuck et al., 2012; Stevenson et al., 2013). Therefore, the style of filling and spilling varies between cycles according to the evolving slope configuration.

The large-scale topographic template interpreted for the Marlim Unit slope (Fig. 3.11) suggests three different slope configurations during the stratigraphic evolution (Fig. 3.15). Cycles 1 and 2 are interpreted to have evolved in a similar topographic template comprising two steps (steps 1 and 2) and three ramps (ramps 1 to 3) (Fig. 3.15A). In part, sedimentation in the steps evolved synchronously as there was no confining counter slope to pond sediment up-dip

(Fig. 3.15-A1 and A2). Ramp 1 was prone to bypass, which fed sediment through the laterally migrating channels above step 1. The channels of step 1 sourced sediments to lobate features LA and LB on step 2. Seismic geomorphology and amplitude strength indicate that lobate feature LA is smaller and less sand-prone when compared to other lobate features (Fig. 3.8), suggesting that either the flow magnitude and sand content were lower in an initial phase of the Marlim Unit evolution or more sediment was bypassed basinward during this cycle. I infer that incision at the slope breaks at the downdip edges of the steps, where a knickpoint likely formed and eroded headward to smooth the channel profile, occurred once the steps were filled to the spill point, starting from the down-dip edge of step 1, the first step to heal (Fig. 3.15-A1, A2, A3). However, the exit point of step 2 is not clearly observed in seismic reflection data. At a final stage, a through-going channel incised cycle 1 deposits (C0) and cut through part of step 1 in cycle 2 (C1) (Figs. 3.11 and 3.15A4). Later, the conduits were filled with mud (C0) and partially with mud and sand (C1).

The slope configuration during cycle 3 differs from cycles 1 and 2 since a corridor acted to connect steps 1 and 2 in the early evolution of the cycle (Fig. 3.15-B0 and B1). The topographic difference formed by the fault-controlled slope break at the corridor's exit was progressively healed (Fig. 3.15-B2). Total filling of steps 1 and 2 meant channels were able to transfer sediment across step 2 and ramp 3 (Fig. 3.15-B2) and form a through-going incision on the stepped profile (channel C2), which evolved from the down-dip edge of step 2 upwards (Fig. 3.15- B3 and B4). C2 was later partially filled by sand from ramp 3 up to the distal part of step 1, and mud from step 1 towards ramp 1 (Fig. 3.11).

During cycle 4, step 1 recorded thin, moderate to low seismic amplitude deposits in a restricted area, incised by a mud-filled channel (C4), implying limited accommodation. Therefore, the site represents a bypass-dominated zone (*sensu* Stevenson et al., 2015) that extends from ramp 1 to step 2 (Fig. 3.15-C0). The deposition started on step 2 by building lobate feature LD (Fig. 3.15-C1). As step 2 was filled, a deep incision occurred at the edges of step 2 towards ramp 3, and deposition took place up-dip in areas with available accommodation on the bypass-dominated zone (Fig. 3.15-C2). Once accommodation was healed, headward incision formed a through-going incision across the slope profile (C4)

(Fig. 3.15-C3 and C4). Channel C4 was filled with sand up to the intermediate portion of the bypass-dominated zone, and then mud up-dip (Fig. 3.11).

The different topographic profiles and the history of the FaSTaR cycles reflect the spatial and temporal evolution of the Marlim Unit stepped slope. The slope profile during cycle 4 (a single step between two bypass-prone ramps, Fig. 3.15C) suggests that the tilting, responsible for accommodation patterns and lateral stepping, was less active in step 1 at the end of the Marlim Unit deposition, at least compared to the duration of the sediment supply cycle. The size of the lobate features, and their thickness and lithology suggest a substantial increase in the volume of sand bypassed and deposited from cycle 2 onwards.
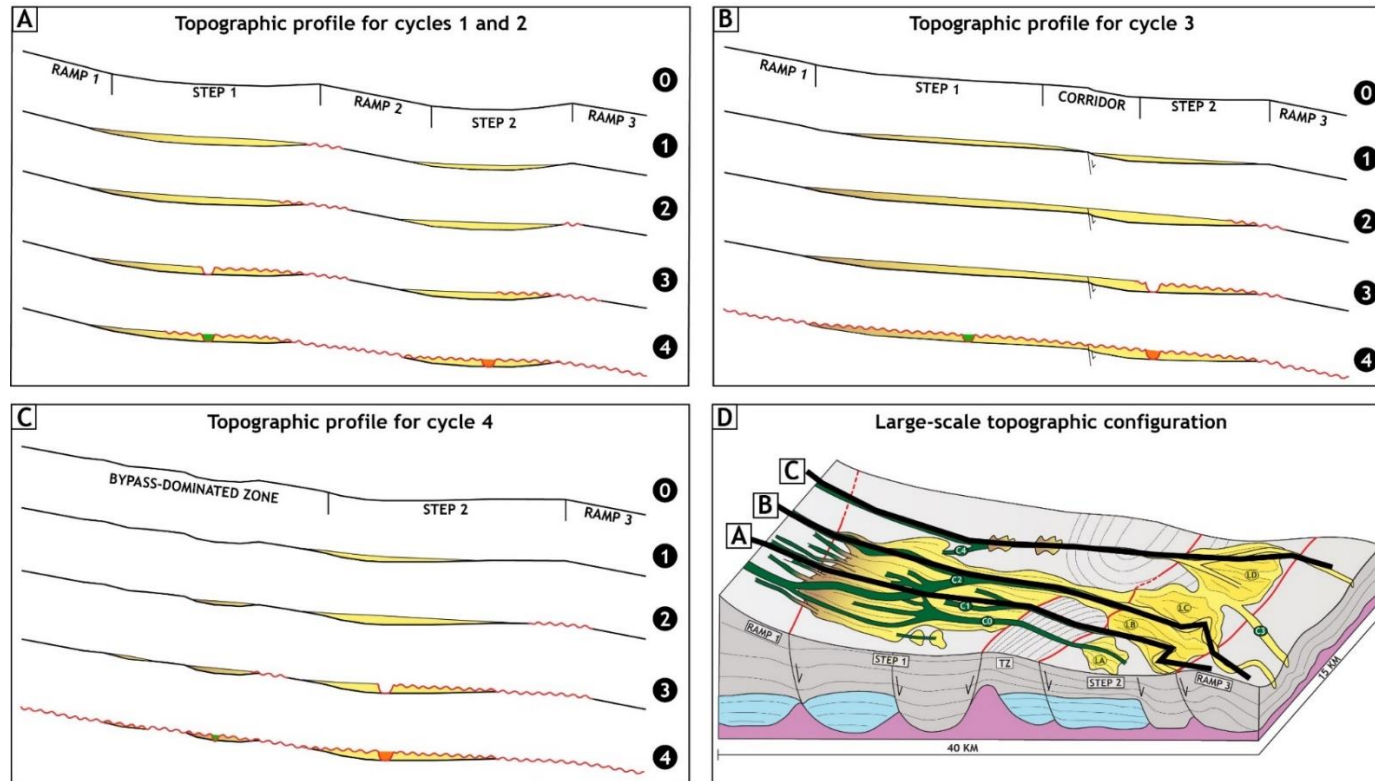
Figure 3.15: Stratigraphic evolution of each FaSTaR cycle according to the palaeotopographic configuration. Time "0" represents the initial slope configuration. A- Cycle 1 and 2 (stage 4 represents cycle 2 since in cycle 1 the incision is through-going and totally mud-filled). B- Cycle 3. C- Cycle 4. See text for detailed explanations on each cycle. D- Location of the profiles on the topographic configuration. The profiles show the evolution of late incisions C1, C2 and C4 (red curly lines). Therefore, they are dip sections representative of where these incisions occurred. Green represents the mud filling of the late incisions and orange represents the sand filling.

3.6.4 The FaSTaR model: a new stratigraphic model for dynamic stepped slope systems

The Marlim Unit comprises several laterally associated FaSTaR cycles and multiple exit points that progressively offset to the NE. From this stratigraphic signature, I propose the FaSTaR model (Fig. 3.16A), a new stratigraphic model that captures the high-resolution temporal and spatial evolution of connected slope depocentres in stepped slopes, in response to sediment supply fluctuations and lateral slope tilting. The sediment supply fluctuations are interpreted to respond to extra-basinal factors (i.e., sea level changes/climate) that control the timing and duration of the waxing-to-waning sediment supply cycles and periods of sand starvation, whereas the lateral slope tilting is an intra-basinal factor that controls accommodation patterns during these cycles.

The FaSTaR model is different from the classic fill-and-spill model, which proposes a single fill-and-spill cycle or vertically stacked cycles to explain the stratigraphic evolution of intraslope basins with fixed topographic configurations and, therefore, with a fixed entry and exit point where sediment is bypassed towards the next downslope depocentre (e.g., Winker, 1996; Prather et al., 1998; Prather, 2000; Beaubouef and Friedmann, 2000; Pirmez et al., 2000; Sinclair and Tomasso, 2002; Smith, 2004) (Fig. 3.16B). Another difference to the traditional fill-and-spill model is the number of incised channel complexes above step 1. The combination of a mild slope break from ramp 1 to step 1 and spatially limited accommodation in response to lateral tilting, prevented flows from forming more unconfined deposits such as distributary channels and lobes. These are more typical of static, undeforming stepped slope systems, or stepped slopes with vertical variation in accommodation patterns (e.g., Adeogba et al., 2005; Deptuck et al., 2012; Hay et al., 2012; Spychala et al., 2015; Brooks et al., 2018) (Fig. 3.16).
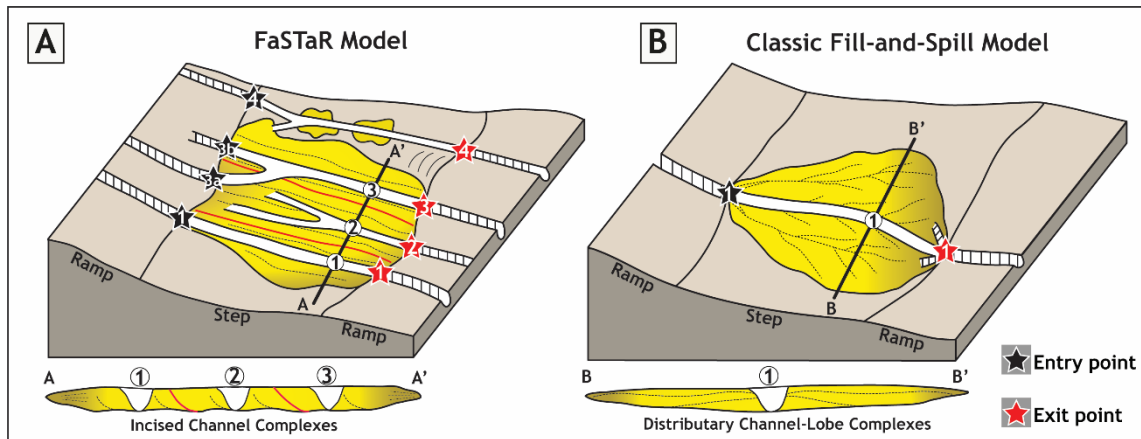
Figure 3.16: Schematic summary of the FaSTaR model (A) and the classic fill-and-spill model (B). The FaSTaR model is composed by several laterally associated cycles and multiple entry and exit points (red lines represent main truncations and limits between cycles). It contrasts with the classic model that predicts a single, or vertically stacked, cycle(s) and a single entry and exit point. The depositional architecture is also distinct. The FaSTaR cycles record incised channel complexes, whereas in the classic fill-and-spill models turbidity currents produce more unconfined deposits, such as distributary channels and lobes (see text for detailed explanation).

Few studies document the impacts of lateral slope tilting on the evolution of deep-water deposition, and these focus on submarine channels affected by growing salt structures (e.g., Gee and Gawthorpe, 2006 and Kane et al., 2012) and extensional faulting (e.g., Kane et al., 2010). However, lateral slope tilting may occur above any dynamic slope, which can be affected by a variety of structures, including fold-and-thrust belts, mud diapirs, salt tectonics and generic faulting. Therefore, given the prevalence of basins affected by mobile slopes around the world, I predict that the FaSTaR model is widely applicable to a range of settings where a component of lateral tilt is present. The relationship between tilting rate and sediment supply rate will ultimately dictate the emerging stratigraphic patterns. The model presented here shows an ordered record with complete fill-and-spill cycles intercalated with sand starvation periods. However, different rates and timing between controls could result in different signatures, for instance, incomplete cycles, lack of starvation periods or premature avulsions.

3.7 Conclusions

This study uses 3D seismic reflection data calibrated to numerous wells and core to document the stratigraphic evolution of the Marlim Unit; a passive margin sand-prone stepped slope system active during the Oligocene-Miocene transition, which was deposited above a slow-moving tilting substrate affected by extensional salt-tectonics. The model here proposed brings a new perspective on how stepped slope systems evolve. The main conclusions of this study are:

- Salt-related faulting and differential compaction originated from underlying carbonate rafts controlled the large-scale stepped slope configuration and, consequently, the location of depocentres and bypass-prone areas, and sand distribution. The slope profile is formed by two steps connected by a transition zone (ramp and corridor) and is bounded by two high gradient ramps. Step 1 (up-dip) records low sinuosity incised channel complexes and remnant deposits of lobes, and step 2 (down-dip) records four lobate features formed by distributary channel and lobe complexes. The stratigraphic connection between the steps is supported by several bypass-dominated channels, later filled by mud and sand, which truncate deposits on the steps across the slope profile.

- Differences in architectural patterns, thickness and sandstone percentage in the steps suggest lateral variability in the magnitude of the slope breaks. The deposition of high sandstone percentage distributary channels and lobe complexes, locally thicker down-dip of the slope break, suggests abrupt slope breaks, whereas channelised deposits with moderate to high sandstone percentage support mild slope breaks.

- Seismic geomorphology and truncation patterns between the lobate features of step 2 support the unidirectional migration trend for the whole system. The shape, relative position and incisional relationships between the lobate features and the bypass-dominated channels that incise them support a unidirectional migration trend towards the NE on step 2. The stratigraphic link between the steps suggests the same trend for the laterally stepping channels interpreted on step 1.

- Several through-going bypass-dominated channels that enter and exit the steps in multiple locations indicate laterally associated fill-and-spill cycles (4 cycles in

the case of the Marlim Unit). These fill-and-spill cycles thicken to the NE. Moreover, these channels suggest that a local graded profile was achieved and the sediment supply rate outpaced deformation rate in each cycle. However, the mudstone filling of these incisions suggests a period of sediment supply reduction and sand starvation, reflecting fluctuations in the sediment supply cycles (waxing-waning) and channel abandonment.

- Lateral slope tilting is invoked as the mechanism to explain the thickness patterns, the accommodation creation for each cycle, and the unidirectional migration trend of channel and lobe systems. As the lateral tilting component plays an essential role in the stratigraphic evolution, the cycles are here named FaSTaR (fill and spill, tilt and repeat) cycles.

- The repeated ordered pattern of accommodation filling and bypass in all the FaSTaR cycles is compatible with a constant rate of lateral tilting combined with sediment supply fluctuations. During periods of sand starvation and, therefore, long return periods between flows, lateral tilt rate outpaced sediment supply rate and the cumulative slope deformation induced channel avulsion at the start of a new FaSTaR cycle. Within each FaSTaR cycle, lateral connectivity and moderate to high sandstone percentage support short return periods between flows and relatively low rates of lateral tilting.

- Three-dimensional variability in the location and character of the slope breaks controlled the patterns of erosion and deposition and the evolution of each FaSTaR cycle. Three different slope configurations are proposed. FaSTaR cycles 1 and 2 evolved above two steps and three ramps, with step 1 being healed before step 2. During the FaSTaR cycle 3, deposition in the steps co-evolved since they were connected by a corridor and, during FaSTaR cycle 4, the slope profile comprised a single step edged by ramps.

This study demonstrates that fluctuations in sediment supply combined with comparatively low rates of syn-sedimentary lateral slope tilting produce distinctive depositional architecture that can help to inform the interplay of external and internal controls on a high-resolution scale. This study provides a new model that predicts the stratigraphic signature of stepped slopes with vertical and lateral variation of accommodation patterns over time.

Chapter 4 - A salty snapshot: extreme variations in basal erosion patterns preserved in a submarine channel

4.1 Abstract

Active submarine channel bases are marked by large erosional features, such as knickpoints and plunge pools. Their presence in ancient channel-fills has rarely been documented, meaning their importance in submarine channel morphodynamics requires investigation. Using seismic reflection data calibrated by wells from a buried submarine channel-fill I document erosional features 100s m long and 10s m deep, here interpreted as knickpoints and a plunge pool, and provide a mechanistic process for their transfer into the stratigraphic record for the first time. Channel incision patterns are interpreted to record a transient uplift in an otherwise subsiding depocentre. Local structural complexities in the channel slope formed zones of preferential scouring. A switch to a depositional regime preserved the irregular channel base inhibiting their upstream migration and smoothing of the channel base. Their formation and preservation record responses to salt tectonics, and provides a unique snapshot of the formative processes of an ancient submarine channel. The presence of these exceptional basal scours indicates that headward erosion processes did not operate rapidly, challenging the paradigm that knickpoint migration controls channel evolution. Our results of this study show that the primary erosion of the main channel surface, and long-term channel evolution, are dominated by far more gradual processes.

4.2 Introduction

Submarine channels are primary long-term conduits for the delivery of terrigenous and anthropogenic particulates across continental slopes to the deep ocean floor (Carter, 1988; Hubbard et al., 2014; Kane and Clare, 2019). Their longitudinal profile and stratigraphic record are interpreted to reflect variations in slope gradient and flow properties (Pirmez et al., 2000; Kneller, 2003; Ferry et al., 2005; Covault et al., 2011).

Intrabasinal factors, such as tectonics (e.g., Gamberi and Marani, 2007; Heiniö and Davies, 2007; Georgiopoulou and Cartwright, 2013; Micaleff et al., 2014; Stright et al.,

2017; Mitchell et al., 2021), mass transport deposits (Tek et al., 2021; Allen et al., 2022) or autogenic channel processes (Sylvester and Covault, 2016; Heijnen et al., 2020; Guiastrennec-Faugas et al., 2021), can perturb profiles and induce knickpoint development. The abrupt changes in channel floor gradient associated with knickpoints (Gardner, 1983; Heijnen et al., 2020) can increase flow velocity and turbulence, leading to hydraulic jumps (Komar, 1971), enhanced channel base scouring (Sumner et al., 2013; Dorrell et al., 2016), and eventually the formation of plunge pools (Gardner et al., 2020; Guiastrennec-Faugas et al., 2020, 2021). These erosional features produce uneven channel floor topography in modern deep-water environments (e.g., Bourget et al., 2011; Dalla Valle and Gamberi, 2011; Guiastrennec-Faugas et al., 2020, 2021; Gardner et al., 2020; Mitchell et al., 2021), providing a snapshot of the formative processes of submarine channels (e.g., Heijnen et al., 2020).

Geomorphic features associated with abrupt variations in channel gradient (i.e., knickpoints, plunge pools, crescentic bedforms) are considered highly dynamic and ephemeral (e.g., Heiniö and Davies, 2007; Hage et al., 2018; Guiastrennec-Faugas et al., 2020, 2021; Heijnen et al., 2020; Chen et al., 2021; Tek et al., 2021). Time-lapse seabed mapping of active modern systems with sandy surficial sediments has documented headward erosion rates >100s metres per year (Guiastrennec-Faugas et al., 2020, 2021; Heijnen et al., 2020). Consequently, knickpoints migration have been argued to be the key driver of channel evolution in many submarine channel systems (Heijnen et al., 2020), rather than sediment redistribution by three-dimensional flow fields related to channel curvature (e.g., Peakall et al., 2007; Peakall and Sumner, 2015; Morris et al., 2022).

Through time, submarine channel profiles tend towards a smooth graded profile, which balances flow capacity and sedimentary load (Pirmez et al., 2000; Kneller, 2003; Gerber et al., 2009; Covault et al., 2011; Pettinga and Jobe, 2020). Consequently, preserved submarine channel deposit thicknesses are constant longitudinally over 1-10s km (Di Celma et al., 2011; Macauley and Hubbard, 2013; Jobe et al., 2020), and relatively smooth profiles are assumed in numerical models (e.g., McHargue et al., 2011; Sylvester et al., 2011). A rare example of preserved scours has been documented in a buried Quaternary submarine channel-fill; these are <10 m deep and

300 m to 1 km in length (Snedden, 2013). However, the detailed processes and implications of such remnant scours have not been examined.

Here, I present a unique example of a buried submarine channel-fill that evolved above a dynamic stepped-slope during the Oligocene-Miocene transition in the Campos Basin, offshore Brazil. The channel-fill preserves extreme longitudinal variations in basal erosion patterns (10s m deep, 100s m long) formed above a cohesive substrate. Seismic mapping and well data analysis were carried out in order to: (i) assess channel incision and thickness patterns and their relationship with underlying deposits; (ii) examine the channel-fill sedimentology, architecture and stratigraphy; (iii) propose mechanisms for the generation of local increased channel accommodation, ultimately recorded in exceptionally large and spatially variable channel thicknesses; and (iv) explain the generation and preservation of the incisional basal channel surface from an evolutionary perspective. I propose that the interaction of sediment gravity flows with a seafloor topography deformed by salt, controlled the development and preservation of channel incision patterns.

4.3 Study area, data and methods

The Campos Basin, offshore Brazil (Fig. 4.1), evolved from a rift during the Gondwana break-up (Jurassic/Lower Cretaceous) to a marine passive margin from the Albian to the present day (Chang et al., 1992; Fetter, 2009). I focus on a submarine channel-fill, informally named the Marlim Sul Channel (MSC; Fig. 4.1) (channel C2 of Chapter 3 and Casagrande et al., 2022), which incised sand-prone channel- and lobe-complexes deposited on a 40 km long stepped slope during the Oligocene-Miocene transition (Marlim Unit of Chapter 3 and Casagrande et al., 2022). The stepped slope configuration was controlled by extensional salt-tectonics and the associated fragmentation of the Albian-Cenomanian carbonate-prone interval (raft tectonics) that overlies Aptian evaporites (Casagrande et al., 2022; Fig. 4.1A).
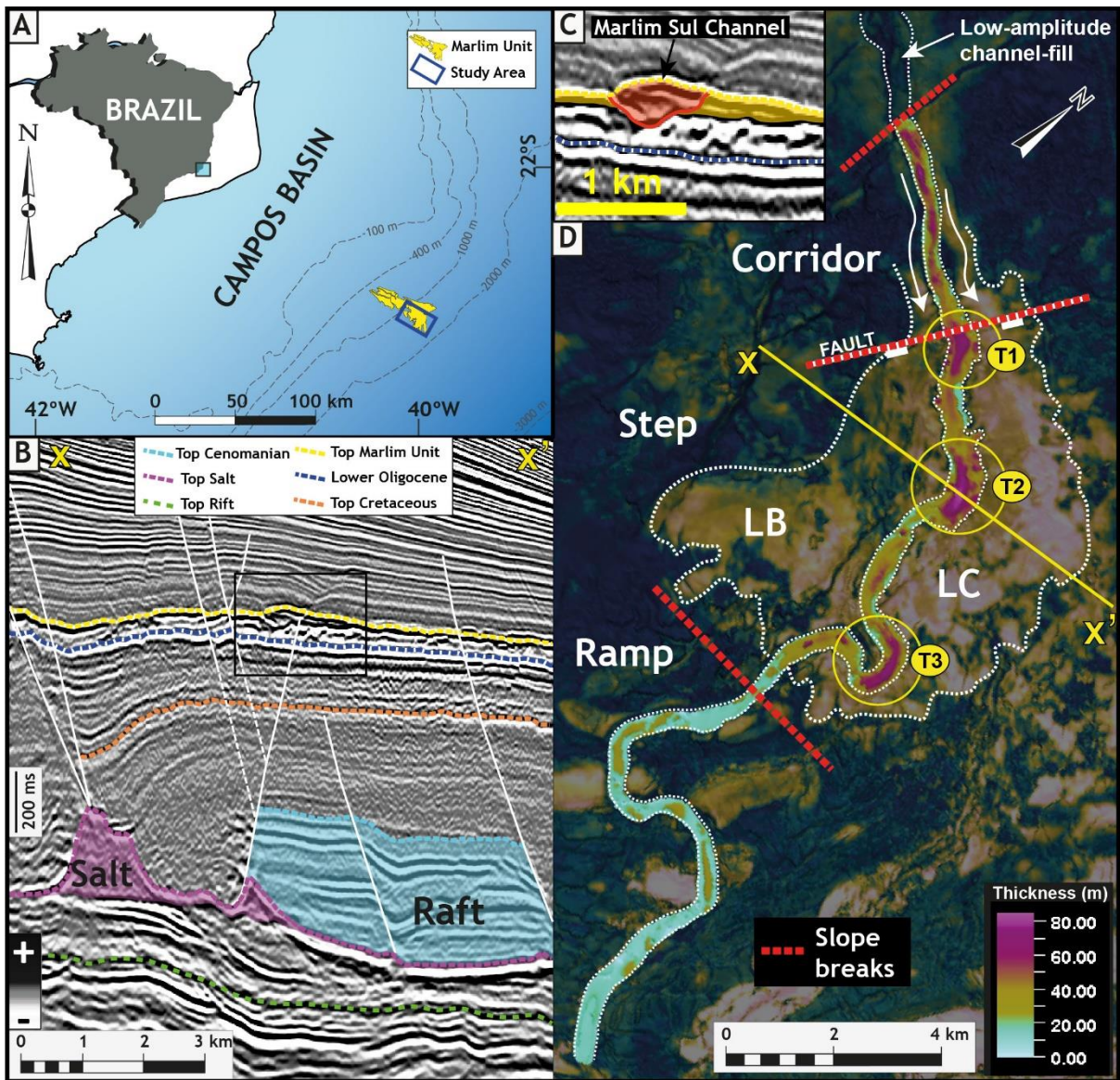
Figure 4.1: A- Location map of Campos Basin and the study area within the Marlim Unit (blue polygon). B- Strike seismic profile of the study area (time, 5x vertical exaggeration, see D) showing the structural configuration associated with salt rollers and rafts. Several faults (white lines) crosscut the top Marlim Unit. The Lower Oligocene refers to the regional stratigraphic event Blue Marker (Winter et al., 2007). (C) Inset of seismic section in B, showing the MSC (in orange) cutting below the lobate features LB and LC (in yellow). D- RMS amplitude map overlain by the thickness map of the Marlim Sul Channel (MSC). The slope sectors are marked in between red dotted lines (slope breaks). The slope break at the entrance of the step coincides with a fault. The high thickness areas (T1, T2, and T3) are marked in yellow circles above the step, where the channel cuts the lobate features LB and LC.

Through calibration with well data, the MSC-fill passes down dip from mud-prone deposits with low root mean square (RMS) amplitude values to sand-prone deposits with moderate to high RMS amplitude values (Casagrande et al., 2022). Here, the sand-prone channel-fill sector is investigated.

To document the basal surface and fill of the channel, two 3D high-resolution PSTM (pre-stack time migration) seismic reflection datasets were used. Acquisition parameters are: i) bin size 6.25 m for crossline and 12.5 m for inlines with 2 ms vertical sampling (approximate vertical resolution of 18 m), and ii) bin size 12.5 m for inlines and crosslines with 4 ms vertical sampling (approximate vertical resolution of 22 m). Both volumes are converted to the depth domain. Seismic reflection data were processed to zero-phase wavelet and are shown with SEG normal polarity. The Marlim Unit top is a trough with a negative reflection coefficient that indicates a decrease in acoustic impedance, whereas the base is a peak. Seismic interpretation was carried out using high-resolution automatic and manual reflection tracking and was calibrated by 24 wells with basic wireline logs (gamma-ray, density neutron, sonic and resistivity). Eight wells (two cored) intersect the MSC-fill. Seismic geomorphology was interpreted in an RMS amplitude map. Real thicknesses were obtained from a map of the top and base seismic horizons using the higher resolution depth converted seismic volume.

Longitudinal thickness variations of the channel-fill and the lobate features (LB and LC) were assessed by several measurements extracted from the thickness map and plotted graphically (Fig. 4.2). Within the channel-fill, the measurements are spaced every 400 m and were extracted at the thickest points of the channel cross-section. A total of 26 measurements were taken above the step; the same number was obtained in the lobate features. The 400 m distance was also used to plot the graph for LB and LC to match with channel measurements and facilitate comparison between thicknesses. Thickness values in the lobes were extracted between 500 m and 1000 m lateral to the MSC. Channel-fill stratigraphy was interpreted in a correlation panel along the MSC-fill based on well data and 3D seismic reflection. The panel is hung from a laminated mudstone package observed in all the wells (see more in the channel-fill section).

4.4 Results

4.4.1 The Marlim Sul Channel (MSC)

The MSC is readily observed in maps and profiles from seismic reflection data. Based on thickness patterns extracted between the mapped top and basal surfaces (reported by average, minimum, and maximum depths, and the standard deviation (SD)), morphology and topographic configuration, the sand-prone channel sector is divided into three segments: corridor, step and ramp (Fig. 4.1D) (see Fig. 3.11, Chapter 3). Abrupt longitudinal changes in channel-fill thicknesses are observed at three sites above the step (T1, T2 and T3), where the channel incises two sand-prone lobate features, LB and LC (Fig. 4.1C).

Corridor segment: The channel has very low sinuosity and constant width (300-350 m) (Fig. 4.1D). Average thickness is 56 m (41-75 m; 8 m SD). The channel cuts partially preserved linear high amplitude anomalies, which well calibration shows to be sand-prone and 30 m thick.

Step segment: A salt-rooted synthetic normal fault, which cuts a carbonate raft, trends perpendicular to the channel course. The increased thickness and architectural changes across the fault support the interpretation of a break-in-slope between the corridor and step at the seafloor during the evolution of the Marlim Unit (Casagrande et al., 2022, fault marked in Fig. 4.1C and shown in map view and seismic profile in Fig. 4.3A and B). Above the step, the average channel-fill thickness is 52 m (26-86 m, 14 m SD). There are marked channel-fill thickness changes documented at bends T1, T2 and T3 (Figs. 4.1D and 4.2), which share similar thickness maxima and downstream lengths, but different characteristics and relationships to adjacent structural and stratigraphic elements. Channel width varies from 250 to 670 m and is wider at bends T1 and T2 (Fig. 4.1D). The channel is weakly sinuous across the step, apart from one pronounced bend at T3 (Fig. 4.1D).

Ramp segment: The distal part of the MSC is on the ramp, where the channel has a constant width (350 m wide) and is thinner than on the step and corridor (average 18 m, 11-36 m, 7.3 SD) (Figs. 4.1D and 4.2). The well-seismic calibration in the study area indicates that moderate to high seismic amplitudes relate to a sand-prone fill (Casagrande et al., 2022).

In summary, the average channel thickness data indicate that the channel-fill is thicker above the corridor and lower gradient step, relative to the higher gradient ramp (Fig. 4.2). There are three prominent areas of anomalously thick channel-fills, T1, T2 and T3, which are examined in more detail below.
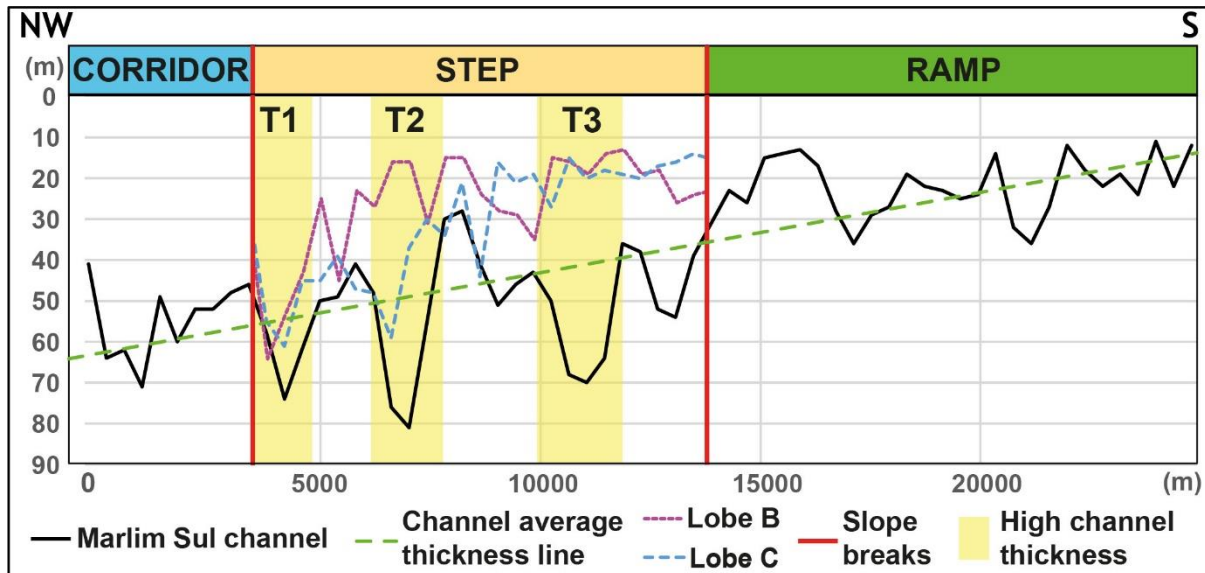
Figure 4.2: Graph showing longitudinal thickness variations along and parallel to the channel thalweg (across the corridor, step and ramp, up-dip to down-dip) and the lobate features LB and LC (across the step). Note the relationship between the areas of high channel thickness and lobes. The areas of locally increased thickness (T1-3) are marked in pale yellow. Note the overall downstream decrease in thickness, and the limited incision at the step-to-ramp slope break. The average decrease in channel thickness values along the transect (green) from 63-to-13 m are used to calculate a gradient of 0.17°.

4.4.2 Relationship between the Marlim Sul Channel and older deposits

The break-in-slope at the step favoured the formation of LB and LC distributary channel and lobe complexes (Chapter 3 and Casagrande et al., 2022). Low sinuosity high-amplitude seismic features in the corridor connect with LB and LC at the entrance of the step, which are interpreted as feeder channels (see white arrows in Fig. 4.1D). The MSC incised the corridor and step deposits between the feeder channels and the lobes complexes (Fig. 4.1C). Seismic mapping indicates truncation of reflections below the Marlim Unit, which is supported by thinner lobe thicknesses on average of LB (~20 m) and LC (~60 m) when compared with T2 thicknesses (Figs. 4.2 and 4.4).

These observations support the complete removal of LB and LC beneath the MSC (Fig. 4.1C) and deep incision below the lobes.

A few metres of cores in some wells indicate that the rocks underlying the lobes and the channel-fill are laminated and bioturbated mudstones (Fig. 4.5E). Calibration with well logs in the cored wells and the well log patterns in several other wells show that the stratigraphy underlying the channel-fill and the lobes has higher gamma ray and density than the sand-prone deposits of LB and LC and the channel-fill itself (Fig. 4.6B), and a density and neutron logs cross over pattern (density log to the right and neutron to the left) suggesting non-reservoir facies. These mudstones form most of the deposits that were eroded by channel incision. There is a broad trend of decreasing channel thickness along the channel from the corridor to the ramp (Fig. 4.2). The magnitude of this decrease is 0.11° along the channel path (25 km), or 0.17° considering a straight measured distance of 17 km (Fig. 4.2). T1-3 punctuate this trend (Fig. 4.2). Notably, there is no significant change in channel thickness across the step-to-ramp transition.

4.4.3 Anomalously thick areas (T1-3)

The three anomalously thick channel-fill sites (T1-3; Figs. 4.1, 4.2 and 4.4) are all located on 'clockwise' orientated meanders on the step, and they have differing relationships to faults and adjacent deposits (LB and LC).

T1 is 1 km long and 350 m wide, and initially thickens downstream from 45 to 75 m in 350 m (average basal slope gradient: ~5°; Fig. 4.4B1), and then thins from 75 to 45 m in 650 m (average basal slope gradient: 2.6°). Thickness patterns support T1 as a longitudinally asymmetric feature (Fig. 4.4B1). At T1, the channel around the bend is on average 150 m wider (maximum width of 550 m) than the corridor up-dip and also the next bend down-dip. T1 also coincides with the break-in-slope at the up-dip edge of the step (Figs. 4.3, 4.4A and 4.4B1). The synthetic normal fault associated with the slope break is interpreted to have influenced T1 formation, and minor outboard faults do not show evidence of movement during the Marlim unit (Fig. 4.4B2). Similar thickness increases are observed down dip of the break-in-slope in the adjacent lobate features LB and LC (Fig. 4.4A), suggesting that the lobes and channel thicknesses record the same local accommodation control.

T2 is in the central part of the step, where the MSC thickens from 40 to 86 m over a downstream distance of 1 km (~2.6° average gradient), then abruptly thins downstream to 32 m in 400 m (Figs. 4.2 and 4.4C1) forming an average counter slope of ~8°. T2 also coincides with a wider (~650 m) and more sinuous channel segment compared to the immediately downstream channel bend that turns anticlockwise (~250 m) (Fig. 4.4A). The zone of thickest deposits is 1.4 km long and a maximum of 350 m wide (Fig. 4.4C1). Highly irregular channel edges are observed at the contact with LC (Fig. 4.4A, see black arrow). On the outer bend, T2 is partially bounded by a NW-SE normal fault (Figs. 4.3C, 4.4A and 4.4C2). At depth, the outer bend fault is salt-rooted and coincides with the edges of an underlying carbonate raft (Fig. 4.3C), and is mappable to the base of T2. The MSC reflections within T2 are rotated and thicken towards this fault (Fig. 4.4C2). The rotation and thickening of the reflections towards the salt-rooted fault suggests that it was active during the evolution of the MSC, and induced a local depression during channel incision. The geometry of the outer bend supports that the fault formed a synthetic listric fault segment as it propagated and widened towards the contemporaneous seafloor, as has been documented in exhumed systems (e.g., Hodgson and Haughton, 2004; Baudouy et al., 2021).

T3 is located on a tight bend in the MSC, 1.5 kilometres up-dip from the step-ramp slope break and thickens downstream in 1 km from 45-to-75 m (average gradient of ~1.5°, Figs. 4.4A and 4.4D1), then thins from 75-to-40 m in 530 m (average gradient of ~4°). The maximum width and length are 280 m and 1.6 km, respectively. The area of thickening is located at the centreline of the channel, not towards the outer bend. Overall, the bend displays similar upstream and downstream widths (~400 m). T3 is intersected by the same fault system present at T2 (Fig. 4.4A). The faults are parallel to the main channel orientation with a complex configuration that forms a graben, with T3 parallel to one of the bounding faults of the graben (Fig. 4.4D2). Thickening of the reflections above the Marlim Unit in the central low block of the graben (Fig. 4.4D2, see pink arrows), and the lack of morphological changes in the bend across the faults suggest post-MSC fault movements. However, the reflections within T3 are rotated and thicken towards the outer bend, with onlapping reflections above T3 (Fig. 4.4D2). I interpret that the rotation and thickening of the reflections are due to a listric fault segment that parallels the outer bend of T3 (Fig. 4.4D2).
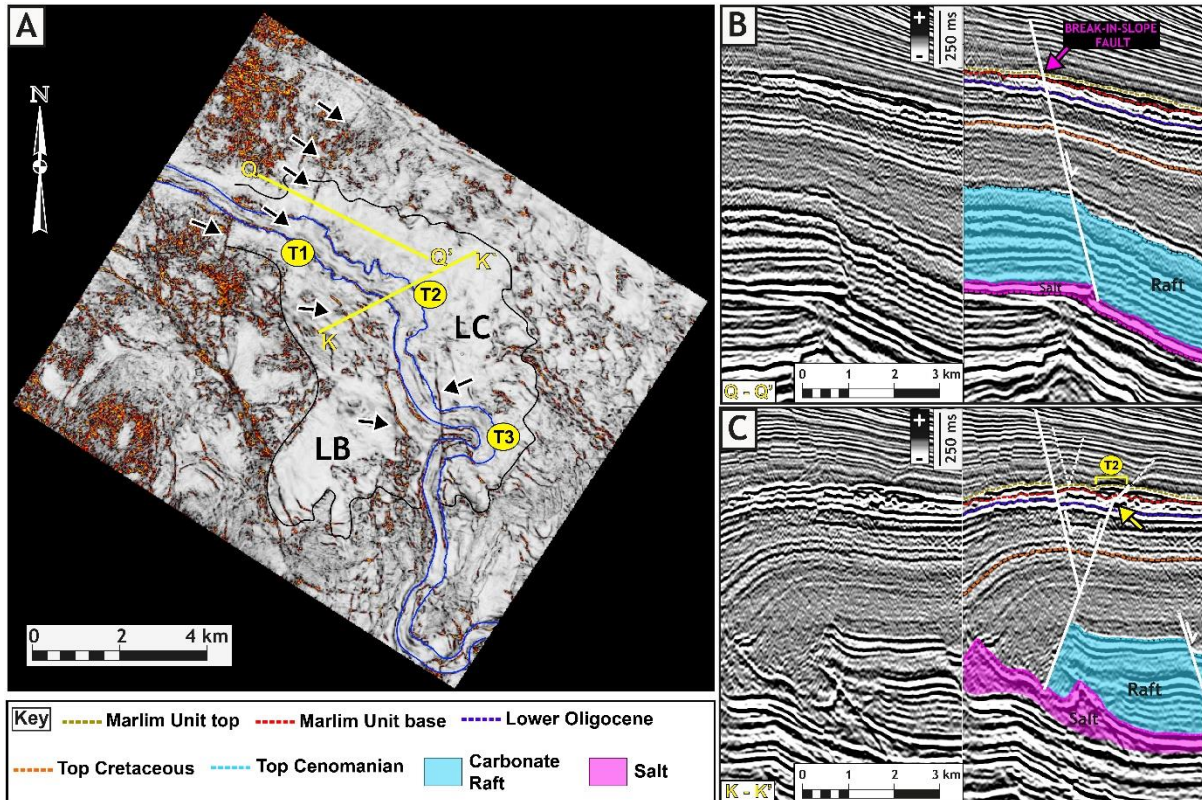
Figure 4.3: Large-scale structural control on the MSC (marked in blue lines). (A) Seismic variance attribute map extracted from the top MSC horizon. Some of the faults in the area are indicated by black arrows, including the fault that controls the break-in-slope from the corridor to the step. T1-3 are marked on the map (for thicknesses see Fig. 4.4A). (B) Dip seismic profile, uninterpreted and interpreted, (higher resolution seismic volume, time domain, 5x vertical exaggeration, location in A), crossing the fault associated with the slope break between the corridor and the step. (C) Strike seismic profile, uninterpreted and interpreted, (higher resolution seismic volume, time domain, 5x vertical exaggeration, location in A) crossing T2. Note the structural configuration in the area with the fault at the edge of the carbonate raft affecting T2. This fault bifurcates (yellow arrow), forming a secondary fault at the outer bend of T2 (see text for explanation).
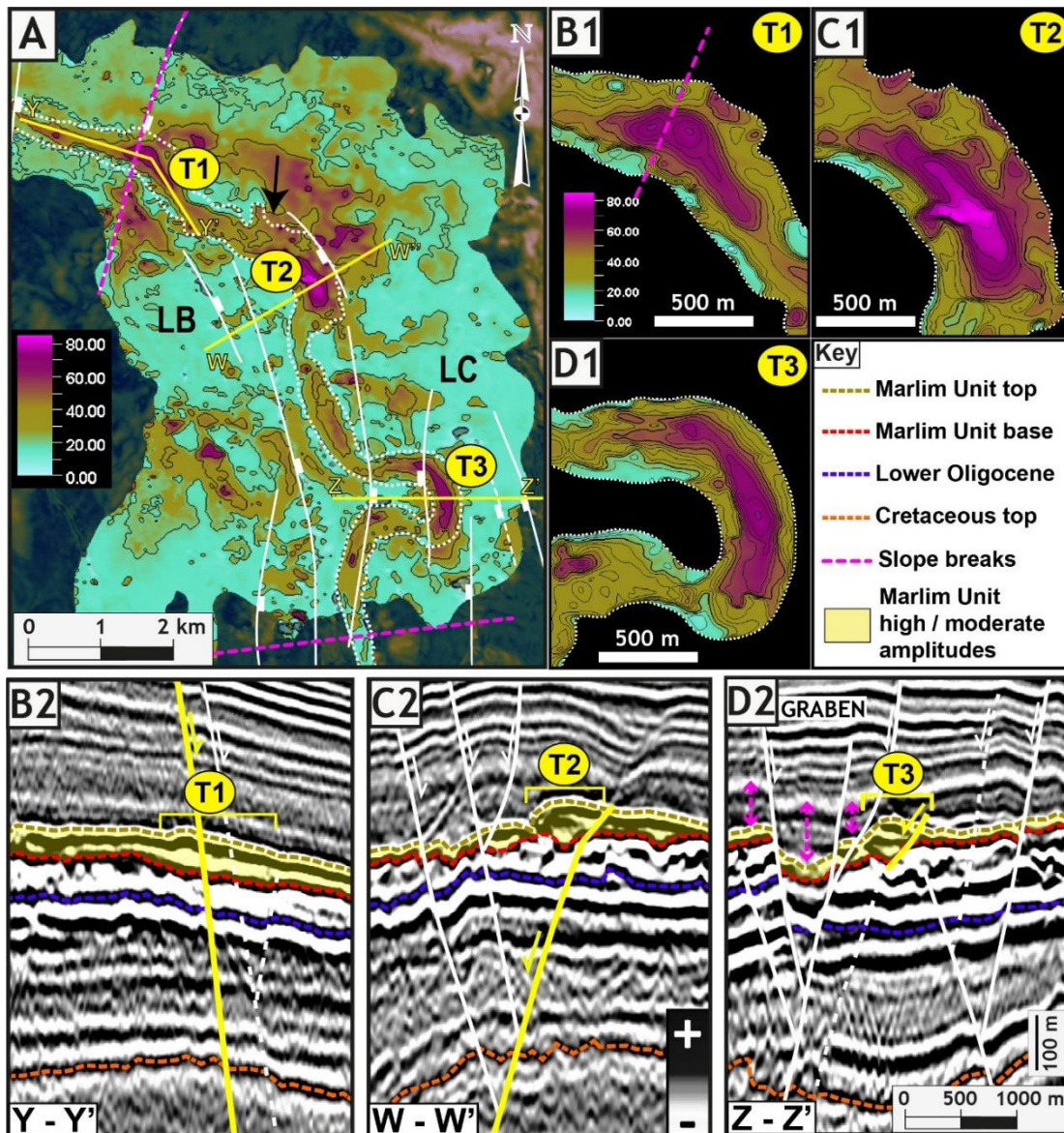
Figure 4.4: A - Thickness map (m) of the lobate features (LB and LC) and the MSC-fill with main faults. Slope breaks in dotted pink lines (the slope break at the entrance of the step coincides with a fault). Channel geomorphology is marked by white dotted lines. Note the irregular channel edges marked with a black arrow.B1 - Detailed thickness map from T1. B2 - Dip seismic section crossing the slope break and longitudinally orientated in the T1 area. Note, a main fault is associated with the slope break (yellow line) and other less important faults (dashed lines). All these faults are related to T1 formation. C1 - Detailed thickness map from T2. C2 - Strike seismic section crossing the T2 area. Note the close association of the yellow fault with T2 and how the base of the channel cuts underlying reflections at a deeper level than the lobes. D1 - Detailed thickness map of T3. D2 - Strike seismic section crossing the T3 area. Several faults form a graben. Pink arrows indicate variable thicknesses within this structure. The yellow fault is inferred as a structural control on T3. All the seismic profiles are shown in depth with 5x vertical exaggeration.

4.4.4 Channel fill sedimentology and stratigraphy

The sedimentology of the MSC-fill is constrained by cores from two wells (W2 and W8), which indicate a predominant fill of moderately sorted amalgamated structureless, fine-grained sandstones (Fig. 4.5), with subordinate medium- and rare coarse-grained sandstones. Well-sorted fine-grained sandstones with plane-parallel lamination are secondary (Fig. 4.5). No coarse-grained or mud clast-rich layers are observed within the channel-fill. Well logs motifs from gamma-ray and density/neutron are mainly blocky, which is compatible with the homogeneous character of the sandstones (Figs. 4.5 and 4.6). Structureless sandstones record rapid deposition from turbulent high-density flows (Lowe, 1982). Traction in less dense flows interpreted from plane-parallel laminated sandstones is a subordinate process. The paucity of coarse-grained residual lags in the cores suggests depletive flows during channel filling.

In the upper part of the channel-fill, a unit characterised by the abrupt intercalation of sandstone beds with bioturbated laminated mudstones (Figs. 4.5 and 4.6), named the upper mud-prone package (UMP), is identified in all the wells above the step, suggesting longitudinal continuity (Fig. 4.6). The UMP culminates with a 3-5 m thick mudstone package (Figs. 4.5 and 4.6). Due to its fine-grained siliciclastic composition, and crude lamination, the mudstones are interpreted as dilute turbidity current deposits (Talling et al., 2012), possibly with a minor contribution of background sedimentation. The UMP is interpreted as a period of sand starvation. Abrupt changes from sandstone to mudstone facies in a channel-fill have been related to channel deactivation (Mutti and Normark, 1987). The impedance contrast between oil-saturated sandstones and the UMP permits seismic detection of the fine-grained package. Seismically, the top of the UMP coincides with a change in seismic polarity (a black peak indicates an increase in acoustic impedance due to a relatively higher density), which can be tracked in the thickest parts of the channel-fill in the step and corridor (Fig. 4.6A, see white arrows).
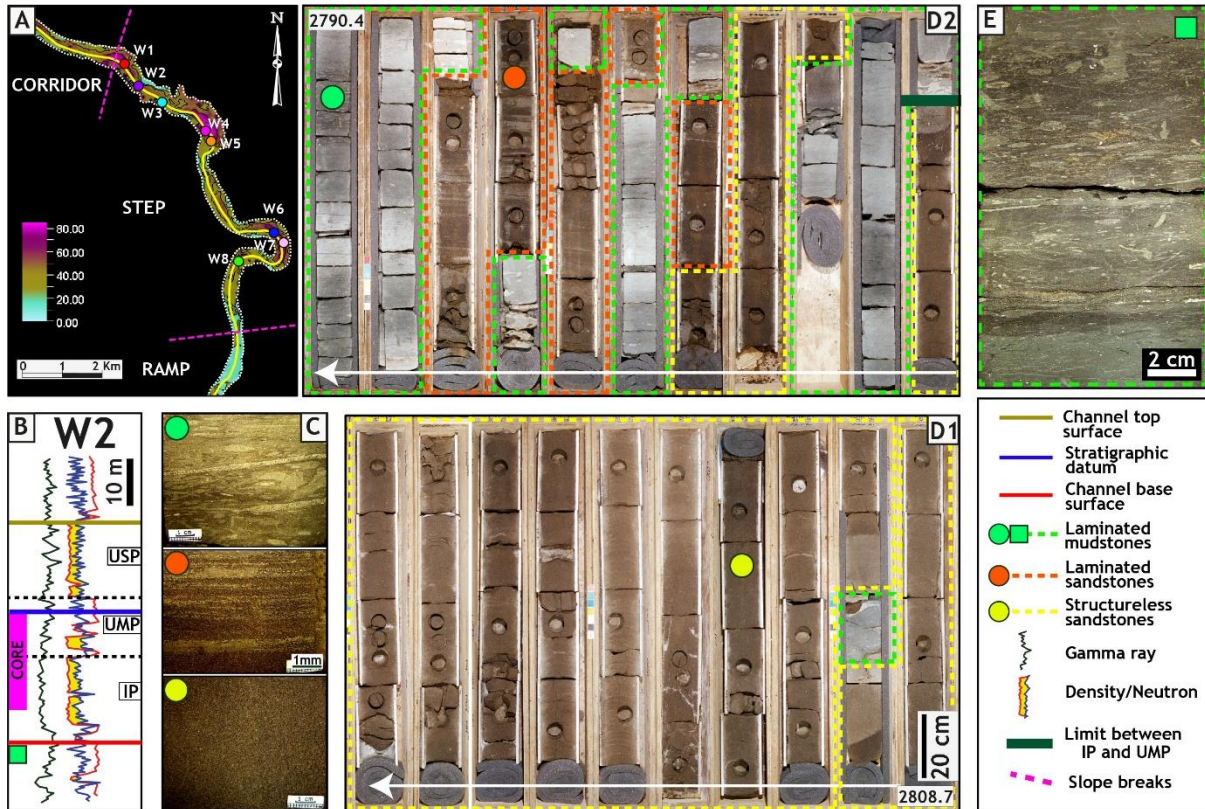
Figure 4.5: A - MSC thickness map with well locations (W1-8), W2 and W8 have cores. The yellow line in the middle of the channel in the map refers to the seismic profile and stratigraphic panel of Figure 4.6. B - Well logs for W2; note the cored interval marked i in pink. Stratigraphic packages marked in the well logs (intermediate package (IP), upper mudstone package (UMP), upper sandstone package (USP)). (C) Main sedimentary facies observed in the cores within the channel-fill, coloured circles indicate the position in the core boxes. (D1,2) Representative photographs of sedimentary facies in cores of W2 (sampled the IP and UMP). (E) Photograph of the bioturbated and laminated mudstones below the MSC. The green box shows the position in the log in B.

The seismic profile along the channel-fill shows high-amplitude semi-parallel seismic reflections. In T2 and T3, well correlations support that the basal reflections likely pinch out against the channel base , suggesting that deposition was contained by the incisional surface (Fig. 4.6A). Towards the top of the channel-fill, greater reflection continuity is supported by well log correlations.

The longitudinal continuity permits the MSC-fill to be sub-divided into a lower sand-prone package (LSP), overlain by a fine-grained unit, the lower mud-prone package (LMP, up to 4 m thick; Fig. 4.6B). The LSP and LMP are interpreted to be the oldest

preserved MSC-fill, with the LMP recording a regional reduction of sand supply. An overlying intermediate package (IP) comprises two sand-prone units intercalated with an interbedded (mudstones and sandstones) unit (Fig. 4.6B). Above the UMP is the upper sand-prone package (USP). Based on the correlation of the LSP and IP, I interpret that the USP is the only package recorded in the MSC-fill above the ramp (Fig. 4.6B).

The recognition of mud-prone and sand-prone stratigraphic packages supports waxing-to-waning sediment supply cycles during the fill of the MSC. The increased continuity of the stratigraphic packages suggests an aggradational pattern to the infill. Together, the evidence from the sedimentology and stratigraphy of the MSC supports passive filling without modification of the topographic irregularities at the base of the channel after infilling commenced.
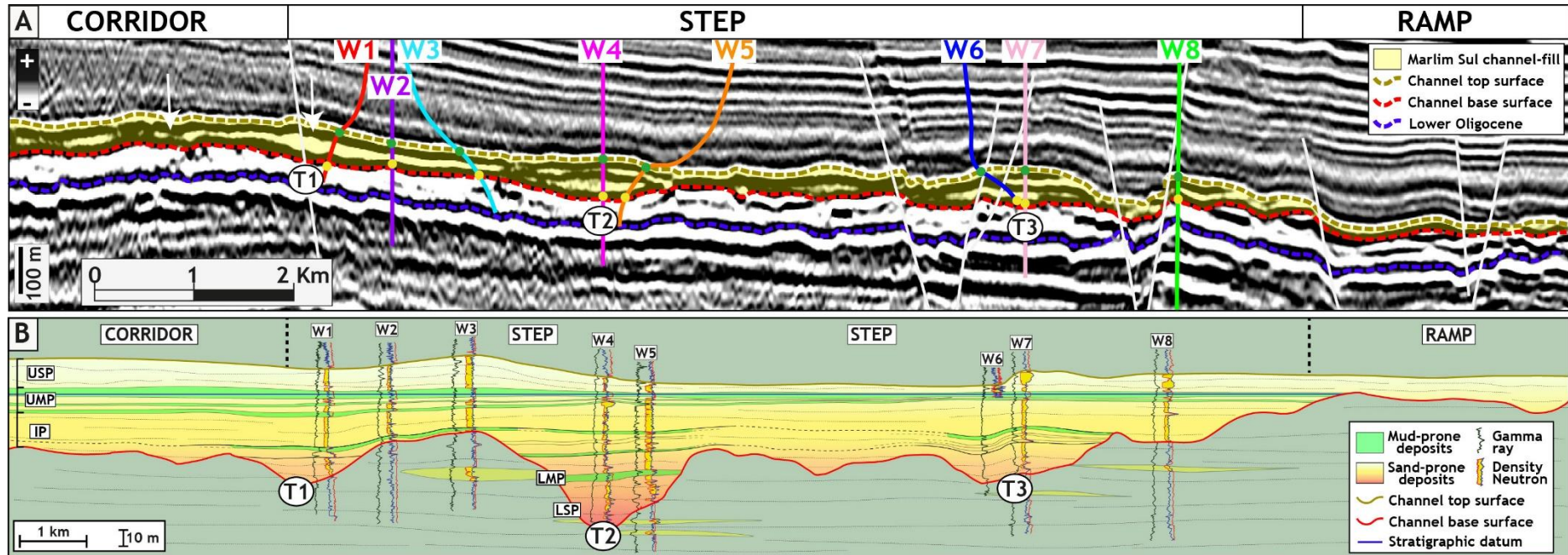
Figure 4.6: A - Longitudinal seismic profile (depth domain, 5 x vertical exaggeration) along the MSC-fill (location in figure 4.5A). Well calibration indicates that internal seismic reflections are related to the intercalation of sand- and mud-prone packages, although not all are resolved. Seismic reflections are in general semi-parallel and increase continuity stratigraphically. The upper mudstone package (UMP) top reflection is a peak, see white arrows. Note how this reflection is continuous along most of the channel-fill. B - Stratigraphic panel calibrated by the wells and by the seismic profile shown in A (with more vertical exaggeration). The channel-fill stratigraphy comprises sand-prone packages intercalated with mud-prone packages (lower sand-prone package (LSP), lower mudstone package (LMP), intermediate package (IP), UMP, upper sandstone package (USP)). These packages are depicted with an overall tabular geometry and are related to multiple sedimentary phases. The thickest mudstone unit of the UMP is used as the stratigraphic datum. The channel-fill stratigraphy and sedimentology are interpreted to reflect a passive style of deposition, with progressive healing of the channel base topography. The geometry of the beds within the packages is speculative since the beds are not observed in seismic data.

4.5 Discussion

4.5.1 Marlim Sul Channel (MSC) evolution

4.5.1.1 The incisional phase

The MSC architecture reveals a progressive increase in incision depth with distance up-dip, and three anomalously deep areas of incision that punctuate this trend. This pattern is contrary to that predicted by equilibrium slope concepts in above grade slopes, where deeper incision is expected across slope convexities such as the step-to-ramp break, and shallower incision or aggradation (e.g., channel-levee systems) above low gradient areas such as a step (e.g., Pirmez et al., 2000; Ferry et al., 2005; Deptuck et al., 2012; Shumaker et al., 2018). Here, I assess why this channel does not fit the standard model and examine the mechanics that caused the observed channel evolution.

There is a progressive longitudinal decrease in channel thickness, and thus incision, across the corridor, step, and ramp. Channel thickness and, consequently depth of incision, is greatest up-dip in the corridor (56 m) and step (52 m), and progressively decreases by $0.17°$ in a downslope direction towards the ramp (18 m). This suggests a primarily longitudinal deformation of the seafloor, and that the forcing mechanism operated on a considerably longer length scale than the scale of the observed ramps and steps. Furthermore, the channel is observed to incise below the adjacent lobes, and reach 50-60 m depth outside of T1-3. Given that channel widths are ~300-670 m, then width:depth ratios are around 5-11, which represent low aspect ratios for primary submarine channels (e.g., Konsoer et al., 2013; Jobe et al., 2016; Shumaker et al., 2018), although they are similar to other heavily incised systems (e.g., Allen et al., 2022).

The combination of progressive longitudinal change in incision, its continuity across ramps and steps, incision to well below the adjacent lobes, and the very narrow nature of the filled conduit, implies that there was pronounced uplift to drive channel incision. Furthermore, this uplift was greatest in the up-dip parts, diminishing down-dip to primarily record a basinward tilt (Fig. 4.7). The uplift led to an increase in channel gradient (Fig. 4.2), resulting in enhanced incision. This relationship has been

documented from morphometric analysis of submarine channels (e.g., Shumaker et al., 2018). However, here the incision is also linked to the total uplift, and because this increases up-dip, the maximum incision is higher in proximal locations. Despite the pronounced uplift, the 'stream power' (erosive power) of the submarine channel flows was sufficient to keep up with deformation in the case of an antecedent channel, or to regrade the slope in the case of channel propagation. Slope regrading by channel-forming processes, such as knickpoints and deep incision, has been demonstrated in other channel systems evolving above mobile slopes (e.g., Mayall et al., 2010; Kane et al., 2012; Jolly et al., 2017; Pizzi et al., 2023).

The exact cause of this deformation is challenging to determine in seismic reflection data. However, the study area is affected by salt tectonics, and associated syn-sedimentary slope deformation and tilting have been proposed to control the evolution of the Marlim Unit (Casagrande et al., 2022). Locally, the MSC is affected by salt-related faults, but the progressive nature of this tilting across the corridor, step and ramp indicates that the uplift is related to movement on underlying structures at a greater wavelength and, therefore, likely from outside the study area.

The channel shows greater sinuosity on the step than in the corridor or ramp, suggesting that despite the overall longitudinal tilting, the subtle slope differences between these domains were sufficient to drive morphological change in the channel. The channel may have initiated and propagated through the area during or after the period of uplift, or it may have already formed prior to the uplift as an antecedent system. The lack of obvious bend amplitude growth during this incisional phase in bends T1-T3, which are characterised by near vertical channel thickness accumulation, suggests that the channel was present prior to uplift.
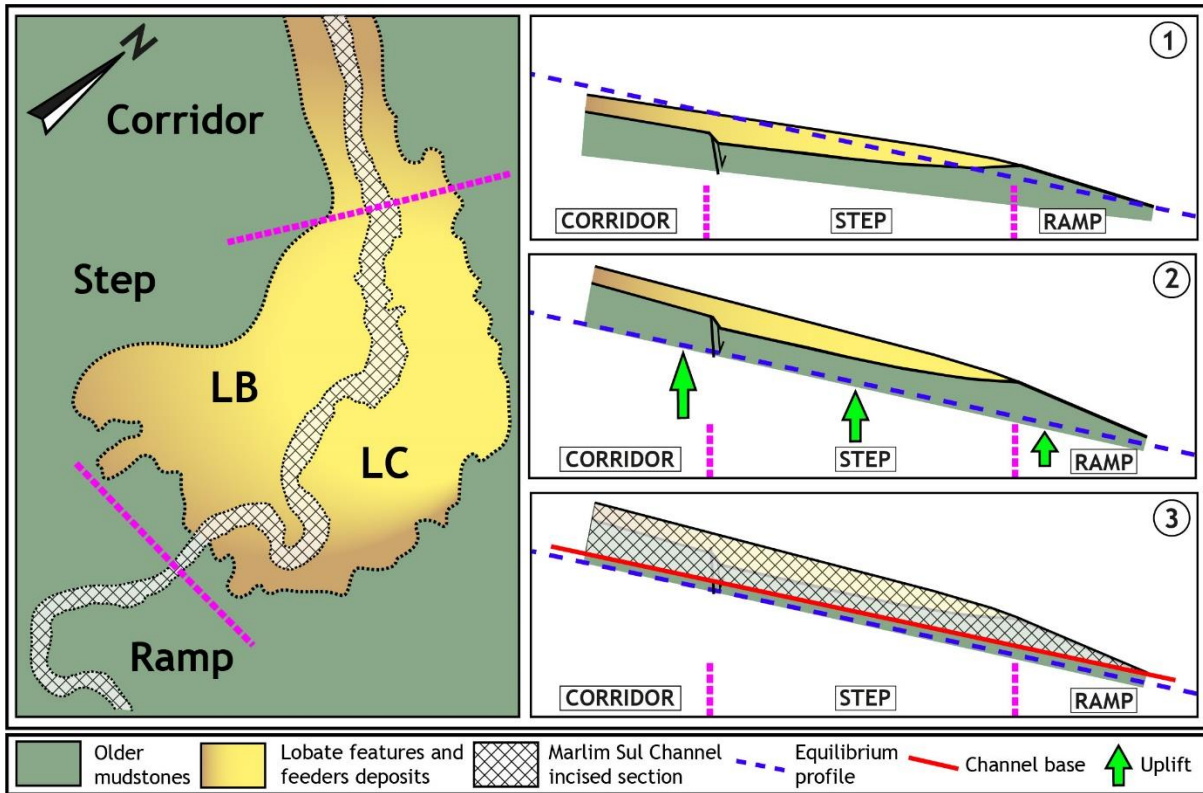
Figure 4.7: Marlim Sul Channel (MSC) incision across the stepped-profile and above the lobate features and older mudstones. Pre-incision stage shown in 1. Channels are expected to incise deeper across slope convexities, such as step-to-ramp slope breaks and incise less across low gradient areas, such as steps. However, the incision patterns in the MSC are explained by an uplift stage (2), which increased the gradient and led to the whole area being above the equilibrium profile. The uplift magnitude decreases down dip (green arrows with different sizes). Consequently, differential vertical incision is produced as flows erode deeper across the corridor and step than above the ramp (3). By the end of the incisional phase, the sand-prone deposits related to the lobate features were removed as flows incised deep into the older mudstones, however, a graded profile was not achieved. For clarity, the rugosity of the channel base surface is not represented (for which see Figure 4.2, and note that the y-axis in that figure is reversed relative to this figure, to highlight the channel rugosity, and the back-tilting).

4.5.2 A scoured channel base surface

The channel base is characterised by three exceptionally deep erosional areas (T1-T3), each ~1 km long, that have >20 m relief, and up to ~40 m, with 1.5-5° average gradients on the up-dip scour surface, and 2.6-8° average gradients on the down-dip scour surface. These gradients are 1 to 2 orders of magnitude greater than the

gradient calculated from the average longitudinal variation in channel thickness (0.17°). Whilst the original seafloor slope is hard to ascertain, the present seafloor slope in the study area of 1.5° may provide a broad guide, and this suggests that these up-dip scour gradients likely represent major increases in the original seafloor slope.

4.5.2.1 Controls on basal scour development

Here, I concentrate on T1-3, kilometre-scale scours; however, the rugosity along this erosional surface is very high.

T1: The spatial association of T1 and high thickness patterns in the lobes (LB and LC) immediately downstream of the fault-controlled slope break (Fig. 4.3B) suggests a structural control in accommodation. Therefore, the fault controlling the slope break is interpreted to have been active during the deposition of the lobes and the evolution of the channel. The incisional feature is up to~30 m deep, with a clear concavity, and extends downdip from the slope break for ~700 m, and up-dip for ~300 m (Fig. 4.4B1). The concave morphology of the scour, and its position close to the fault at the slope break, suggest that this is a channelised plunge pool (cf. Mitchell, 2006; Gardner et al., 2020; Guiastrennec-Faugas et al., 2020, 2021). Such plunge pools are observed to be quite short longitudinally (~50 m) as a function of channel width, W, (~0.33 W) in recently deposited sandy substrates (Guiastrennec-Faugas et al., 2021). However, these can be longer (500-2000 m) and cover a wide range with respect to width (~0.16-2 W) in more consolidated substrates, as might be expected in the example herein, given the magnitude of basal erosion (Mitchell, 2006; Gardner et al., 2020). T1 width is ~350 m, so a plunge pool of ~1 km length fits within the observed trends, albeit one of the most elongated relative to channel width (maximum 400 m) documented to date. Plunge pool depths in these stronger substrates can be up to 200 m for slope gradients of ~3° (Mitchell, 2006) or 100 m at slopes of ~10° (Gardner et al., 2020), with the former gradients more like the present-day seafloor gradient in the study area (1.5°). Such channelised plunge pools have been linked to the formation of hydraulic jumps (Mitchell, 2006; Sumner et al., 2013; Dorrell et al., 2016; Gardner et al., 2020; Guiastrennec-Faugas et al., 2020, 2021). The fact that the scour is observed to extend up dip beyond the slope break is consistent with observations at unconfined slope breaks where plunge pools extend into the slope (e.g., Lee et al., 2002; Hodgson et al., 2022).

T2: The deepest area of incision, up to 40 m greater than the average depths of incision, is around the bend apex across the central part of the channel, extending up dip on the inner channel bend (Fig. 4.4C1). I interpret the fault system at the outer bend of T2 (i.e., salt-rooted fault that bifurcates) led to the formation of a depression in the channel (Fig. 4.3C). The magnitude of the depression, ultimately reflected in the anomalous thickness patterns of T2 and the rotation of the reflections (Fig. 4.4), suggests that the fault system was active during channel development, with rates of syn-sedimentary faulting in balance with channel-forming processes. The steep gradient at the upstream end of T2 records a knickpoint. This knickpoint may have undergone headward erosion around the bend, forming the present-day scoured surface. Channelised flows traversing knickpoints experience increased flow velocities driving substrate entrainment (Sumner et al., 2013; Dorrell et al., 2016), which explains deep scouring at T2. The channel widens to ~650 m here, partly reflecting that bend apices are wider than inflections (Palm et al., 2021), but also suggesting that the presence of the listric fault, and the associated scouring, broadened the channel.

T3: The erosional feature starts from the up-dip bend inflection point, and extends around the bend and past the apex. The maximum incision is >30 m above the average channel incision depths and is typically along the channel centreline, with the deepest area extending across at least half of the width of the channel (Fig. 4.4D1). The rotation and thickening of the MSC reflections towards the outer bend is evidence for syn-sedimentary activity of the listric fault segment during channel incision, forming a localised depression at the seafloor. As with T2, the up-dip part of the depression formed a knickpoint that may have undergone headward erosion up to the bend inflection.

T1, T2 and T3 represent local increases in channel depths during the incisional phase of the MSC. They are explained by the interaction of the flows with a complicated slope affected by salt-related faults, perpendicular (T1) or parallel (T2, T3) to the main flow direction. The formation of fault-related knickpoints and associated scours (T2, T3) and plunge pool (T1) are interpreted to have been preserved prior to large-scale knickpoint migration and smoothing of the channel base. These are rare examples of filled geomorphic features, which have been mostly documented in modern channels (Bourget et al., 2011; Dalla Valle and Gamberi, 2011; Guiastrennec-Faugas et al., 2020, 2021; Heijnen et al., 2020; Gardner et al., 2020), with only a few examples of

knickpoints preserved in buried channel systems (Adeogba et al., 2005; Heiniö and Davies, 2009; Stright et al., 2017). The scale of these reported knickpoints is similar to the features presented here. Nevertheless, the basal scours in the MSC are much larger than scours previously documented for submarine channels (maximum depth of 9 m for scour bends; Snedden, 2013). This study provides a comprehensive three-dimensional understanding of these features and explains their preservation.

The deformation associated with the development of large scours in the two bends, and the plunge pool at T1, was sufficiently rapid to lead to large-scale erosion, but slow enough to allow channel-forming processes to not be so disturbed that channel avulsion or crevasse splay development occurred (e.g., Casagrande et al., 2022). This suggests that the timescales of deformation and channel development are comparable. It is unknown whether fault-induced deformation in extensional salt-driven domains is typically in the same range as channel-forming processes, or whether this is an exceptional example.

4.5.3 A snapshot in time: the exceptional preservation of a scoured channel base surface

Given that the basal surfaces of submarine channels record long-term erosion and/or sediment bypass (e.g., Mutti and Normark, 1987; Deptuck et al., 2007; Hubbard et al., 2014; Hodgson et al., 2016) as channels tend to reach equilibrium, the formation of a smooth basal surface is expected (Sylvester et al., 2012; Hubbard et al., 2014). However, the preservation of kilometre-scale scours and a highly rugose basal surface suggests that the process of channel base smoothing was interrupted relatively soon after the formation of these features (Fig. 4.8). Up-dip knickpoint migration of scours in T2 and T3 was limited, suggesting that the cessation of erosion was relatively rapid, or that the erosion rate declined sufficiently that further migration of knickpoints was reduced, prior to full cessation of erosion. As the preserved geomorphic features scale with the basal channel surface, I interpret that the incision surface is the product of a single channel element (*sensu* Sprague et al., 2005; McHargue et al., 2011) and not a composite surface (i.e., not a channel complex). However, the channel-fill, with sand and mud-prone packages that reflect variations in the sediment supply, represents multiple waxing-and-waning cycles in sediment supply pointing to the fill being a composite body comprising several channel storeys (*sensu* Sprague et al., 2005).
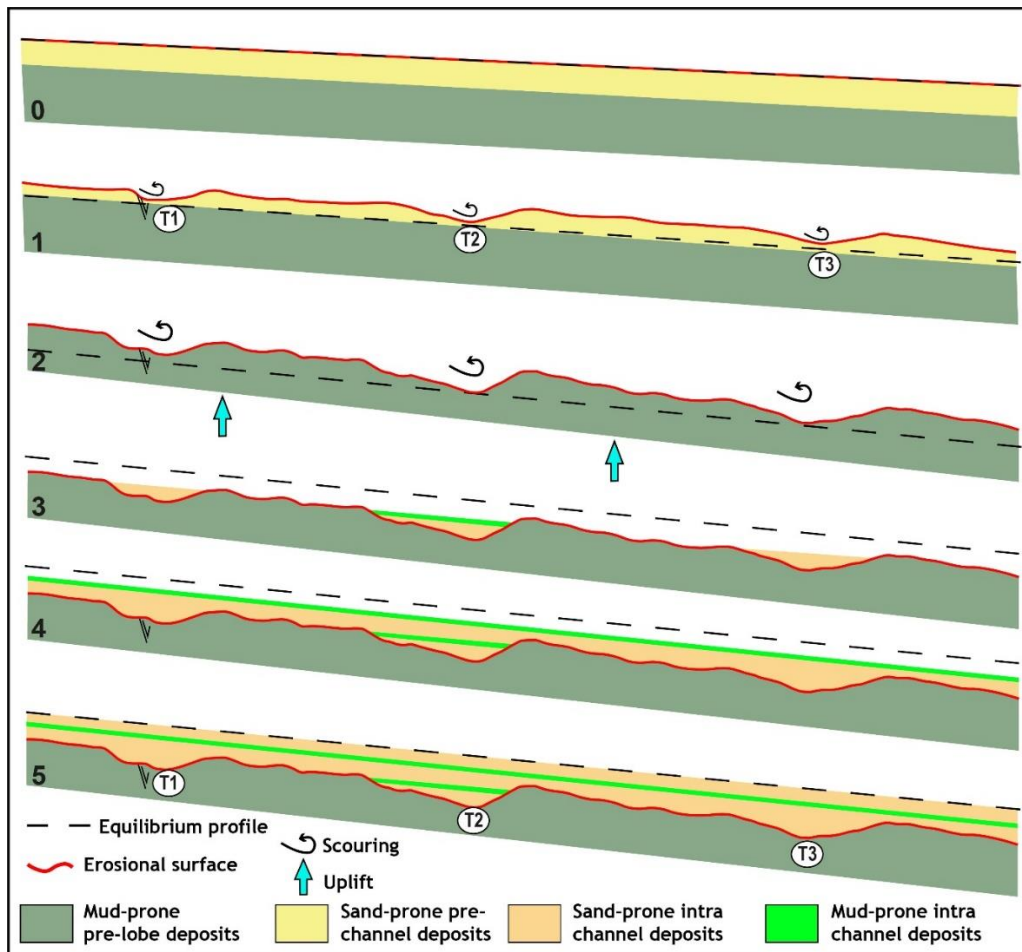
Figure 4.8: Evolutive model for the formation and preservation of the basal erosional surface. 0 – Time before channel incision when accommodation was healed by sand-prone deposits. 1- Channel Incision starts (antecedent channel). 2- Basinward tilting causes uplift, positioning the slope surface above the equilibrium profile, and basal scouring is enhanced forming the deep areas of T1, T2 and T3. 3 - Abrupt shift from the incisional mode to the depositional mode. The depositional surface is now below the equilibrium profile. The deeper parts of T1-T3 are filled first. 4 – Channel filling progress by vertical aggradation towards shallower areas of the channel. 5 – The channel is totally filled.

So, what caused the preservation of this snapshot of a basal surface prior to later smoothing? The cessation of erosion in this channel could have been related to several processes, including a rapid switch from uplift to subsidence, a change in flow properties leading to a change from erosion to deposition, or avulsion and complete or gradual channel abandonment. Avulsion can be dismissed here as the architecture of the MSC fill records a passive style of deposition, much of it characterised by thick structureless sands indicative of the passage of high-density turbidity currents.

Consequently, there is clear evidence that the channel stayed open and active long after the burial of the basal surface.

A return to subsidence after transient uplift would lead to the channel base moving towards a different longitudinal slope equilibrium marked by deposition to reduce the thalweg gradient. The incoming flows would have less erosive power and capacity to transport their load, thereby "fossilising" the thalweg morphology and producing the facies and stacking patterns interpreted in the MSC-fill. The interpreted transient and rapid salt-related uplift phase, with a basinward tilt, could have occurred during a longer period of overall subsidence, for example, due to a change in the mode of diapir growth (e.g., Jackson and Hudec, 2017) and/or a change in tilt direction due to the application of a non-uniform load (e.g., Duffy et al., 2021).

The length-scale of the basinward tilting is much longer than the length of the corridor-step-ramp. Therefore, the transient uplift is a far-field effect of salt tectonics beyond the study area and formed in the context of overall lateral tilting observed across a broader area (Casagrande et al., 2022) in this extensional salt domain. Furthermore, the formation of several deep scours at the channel base are interpreted to be a function of syn-sedimentary faulting driven by underlying salt movement. Thus, a transient switch to uplift and reactivation of faults as a near-field response to far-field salt tectonics would be consistent with the dominance of salt tectonics on the evolution of this system. In the Campos Basin, extensional reactivation of salt-rooted salt structures has been observed during the Oligocene and Miocene in the study area (e.g., Casagrande et al., 2022), and regional studies document salt tectonics activity during the Paleogene and Neogene as a response of transpression and transtension in basement structures (e.g., Fetter, 2009) and during the Paleogene due to the continuation of the regional thin-skinned extension (do Amarante et al., 2021).

Alternatively, a change in flow character could lead to the preservation of the channel base morphology. Reduction in flow magnitude, sediment concentration, or a change in sediment calibre to one with less fines (less efficient), or some combination of these, would result in flows that will be more depositional, raising the theoretical equilibrium profile (e.g., Kneller, 2003). Thus, at a given point in the system, there may be a change from flows being dominantly erosional to depositional. This change might have occurred through a relatively gradual change in boundary conditions linked to extra-basinal allocyclic controls such as sea-level variations (e.g., Deptuck et al., 2003), but

is enough to pass a threshold from dominantly erosional to dominantly depositional (or non-erosional) flow behaviour. This scenario is likely supported by the channel cutting down to a harder, less erodible substrate, as already discussed, and the mantling of the channel base by harder to entrain material, like gravels or mud clasts. Initial changes in flow conditions may have acted to reduce erosion of the plunge pool and knickpoints, for instance, by a change from supercritical to subcritical flow regimes. Further changes in flow conditions would then progressively decrease the erosion rate, before passing the threshold for deposition.

In summary, the preservation of the undulating channel base morphology, and lack of channel smoothing, could be linked to a return to subsidence after transient uplift, or a change in flow properties, or a combination of both factors (Fig. 4.9).
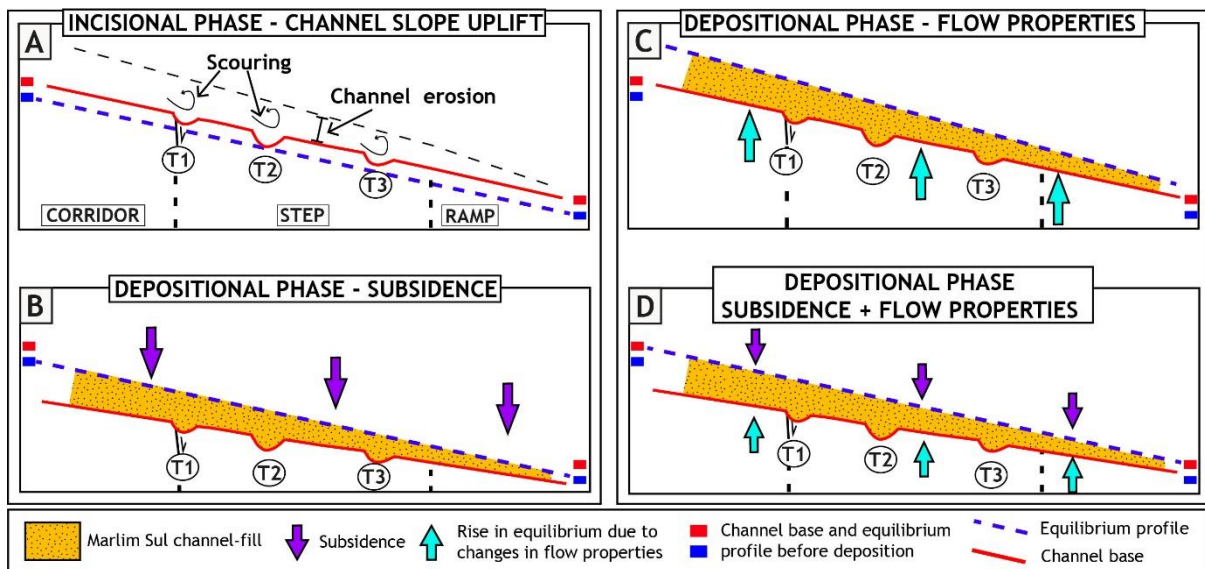
Figure 4.9: Diagrams illustrating how subsidence and/or changes in flow properties can induce a shift in the channel operating mode, from erosional to depositional. A- Incisional phase when the channel base is above the equilibrium profile. B – Depositional phase induce by subsidence. The channel base is lowered below the equilibrium profile. C - Depositional phase induce by changes in flow properties. Channel base remains in the same position after the incisional phase and the equilibrium profile is raised. D – Depositional phase induced by subsidence and changes in flow properties. The channel base is lowered below the level of the incisional phase and the equilibrium profile is raised.

4.5.4 Implications for knickpoint erosion and its influence on channel evolution

Observations of knickpoints and associated scours on the order of metres to >10 m in modern submarine channel systems and canyons have revealed that they can migrate upstream at rates of up to hundreds of metres per year (Guiastrennec-Faugas et al., 2020, 2021; Heijnen et al., 2020). This dynamism, and their impact on vertical and lateral erosion, have been used to argue that knickpoints control channel evolution (Heijnen et al., 2020). However, these observations of rapid knickpoint migration are in sandy, largely cohesionless sediments, within active channels.

Here, I show an example of a channel cut into consolidated and cohesive mud-prone substrates. Whilst true timescales for erosion of this channel example are unknown, the fault-induced deformation occurs on timescales sufficiently slow that they do not induce channel avulsion, or other major channel planform changes (e.g., Holbrook and Schumm, 1999; Peakall et al., 2000). Furthermore, the knickpoints generated at T1-T3 have not had time to dissipate, whilst simultaneously smoothing the basal surface, something that takes place on decadal timescales in modern examples with cohesionless substrates (Guiastrennec-Faugas et al., 2020; Heijnen et al., 2020). Consequently, knickpoint migration in consolidated, cohesive, mud-prone substrates is likely associated with much slower migration rates than in modern sandy examples (see also Allen et al., 2022).This suggests that rapid knickpoint migration in weak substrates may not be representative of erosion during channel inception, or long-term controls on channel evolution, but rather mark periodic overprint whose long-term stratigraphic record may be limited, and primarily recorded in the channel fill.

The limited retreat of basal knickpoints observed herein suggests, in the generic case of submarine channels in consolidated mud-prone substrates (or equivalent high-strength substrates), that the long-term evolution of the basal geomorphic surface of a channel element is not primarily controlled by knickpoint erosion. Instead, channel evolution and bend development are likely controlled by the three-dimensional flow fields of traversing currents (e.g., Giorgio Serchi et al., 2011; Dorrell et al., 2013; Sumner et al., 2014), which in turn are related to channel curvature (e.g., Peakall and Sumner, 2015; Morris et al., 2022). However, knickpoint migration likely play a key

role in basinward reworking of sediment during aggradation of the conduit (Heijnen et al., 2020; Guiastrennec-Faugas et al., 2021).

4.6 Conclusions

The Marlim Sul channel comprises a rare example of a highly rugose submarine channel base preserved in an ancient system influenced by salt tectonics. The channel base contains geomorphic features considered ephemeral in modern systems, and dominated by three areas with anomalous (10s m) channel thicknesses. Channel incision patterns across the stepped profile are interpreted to reflect a salt-controlled transient uplift and basinward tilting of the slope. This scenario is controlled by a combination of far-field salt tectonics (a change to basinward tilt) and near-field salt tectonics (activation of listric faults), which is a scenario likely applicable to other evaporite-dominated basins worldwide. The singular preservation of these erosional features results from a combination of factors (salt tectonics, substrate strength, and/or flow and sediment supply) that induced changes in flow behaviour from erosional to depositional and inhibited channel base smoothing. The exceptional nature of this salt-generated basal scouring preserved in this 'salty snapshot' challenges the present paradigm that knickpoint migration dominates channel processes and evolution. Our results show that the primary erosion of the main channel surface, and long-term channel evolution, are controlled by far more gradual processes.

Chapter 5 - Intraslope accommodation controlled by salt tectonics and mass transport deposits emplacement in the extensional salt domain of Campos Basin

5.1 Abstract

The study of the stratigraphic evolution of deep-water systems in intraslope depocentres of salt basins has focussed on highly confined minibasins dominated by contractional salt tectonics. In contrast, few studies document the changing accommodation and evolution of deep-water systems in intraslope depocentres in areas dominated by extensional salt tectonics, or in areas with both extensional and contractional salt tectonics. Here, using high-resolution 3D seismic reflection data calibrated by wells, I demonstrate the impact of alternating salt tectonics, and the emplacement of mass transport complexes, in accommodation patterns within an intraslope depocentre formed in a mature passive margin phase of the Campos Basin, offshore Brazil.

The large-scale configuration of the depocentre is controlled by salt structures at the edge of an underlying carbonate raft. These structures formed during extension but were reactivated by extension and contraction, creating subtle seabed topography that defined the edges of the depocentre. The partial fragmentation of the raft induced the formation of a salt structure, which also accommodated contraction through inversion and uplift, and extension through subsidence. This alternating deformational style impacted accommodation patterns during the emplacement of a large mass transport complex and created a trough within the larger depocentre, which was filled by sand-prone submarine channels and intraslope lobes. In addition, the instantaneous weight of the large mass transport complex is interpreted to have enhanced subsidence by compaction and amplification of the ongoing slope deformation, also impacting accommodation patterns during the evolution of the intraslope lobes. This contrasts with the genetic interpretation for mass wasting processes in active salt basins, which are a product of slope deformation and not a cause.

5.2 Introduction

Intraslope depocentre fills are stratigraphic repositories that record the complicated process interactions of sediment gravity flows and seabed topography in submarine slope settings. These depocentres contain most of the sand deposited in submarine slopes (aprons of Prather et al., 2017), provide an enigmatic archive of environmental change (Jobe et al., 2017), and can contain hydrocarbon reservoirs that hold significant economic resources (e.g., Booth et al., 2003; Prather, 2003; Prather et al., 2009, 2012).

Intraslope depocentres are frequently documented in salt basins, where halokinesis deforms the substrate and plays a key role in the topographic configuration of submarine slope (e.g., Prather et al., 1998, 2012; Rowan and Weimer, 1998; Beaubouef and Friedmann, 2000; Prather, 2003; Oluboyo et al., 2014). Salt basins in passive margins present thin-skinned salt tectonics. Gravity gliding and spreading induce the seaward flow of salt above a detachment surface, leading to the formation of kinematically-linked deformational domains, where salt-related extension and thinning predominates up-dip, and salt contraction and thickening down-dip (e.g., Cobbold and Szatmari, 1991; Demercian et al., 1993; Fort et al., 2004; Rowan et al., 2004; Brun and Fort, 2011; Davison et al., 2012; Jackson and Hudec, 2017).

Despite extensional domains being an inherent component of salt-bearing passive margins, the evolution of deep-water systems deposited in intraslope depocentres in these settings has been poorly documented in comparison to contractional domains. For example, the stratigraphic evolution of minibasins and tortuous corridors in areas of thick salt structures in contractional domains has been extensively studied, in Atlantic passive margins (Hay, 2012; Oluboyo et al., 2014; Doughty-Jones et al., 2017, 2019; Ge et al., 2020; Howlett et al., 2021; Rodriguez et al., 2021), and in the Gulf of Mexico (Prather et al., 1998, 2012; Booth et al., 2003; Prather, 2003; Smith, 2004). In extensional domains, sediment gravity flow deposits (i.e., turbidites and debrites) have been described to preferentially accumulate in the hanging wall of salt rollers and in troughs between rafted blocks (Anderson et al., 2000; Albertão et al., 2010). Furthermore, submarine channel and lobe systems have been documented on stepped slopes influenced by differential compaction above rafts and dynamic salt-related topography (e.g., Casagrande et al., 2022).

Contrasting structural styles of different salt domains are expected on passive margins (Fort et al., 2004). Nevertheless, salt is highly dynamic, and the domains interact through upslope migration of the contraction front and downslope migration of extension (Fort et al., 2004; Ge et al., 2020). In addition, translation above a complex relief at the salt base forms locally variable stress fields that can cause extension and contraction of the salt and its overburden (Fort et al., 2004; Ge et al., 2020). The interaction between extension and contraction has been described preferentially in the mid-slope of passive margins, where ramp syncline basins (Evans and Jackson, 2020; do Amarante et al., 2021) and minibasins are documented (Ge et al., 2021). Therefore, these interactions should be recorded in depocentres in translation areas. Minibasins, in particular, record high rates of slope subsidence that generate ponded accommodation and thick successions (e.g., Prather, 2000, 2003). Accommodation creation can reflect different mechanisms (i.e., density-driven, salt-related contraction and extension; Hudec et al., 2009; Ge et al., 2020). Their stratigraphy has been shown to record salt-sediment interactions, with particular emphasis on locally sourced mass transport deposits, which are volumetrically important in the basin-fill and mark periods of uplift of the minibasin flanks (Omosanya and Alves, 2013; Doughty-Jones et al., 2019; Madof et al., 2009, 2017; Wu et al., 2020; Cumberpatch et al., 2021; Rodriguez et al., 2021). In the extensional domain, however, the interaction of different deformational styles impacting the evolution of intraslope depocentres has not been documented. In addition, the geometry, accommodation type, stratal patterns and stratigraphic record of depocentres in these settings differ from minibasins, especially considering successions deposited in a mature stage of basin evolution, which are stratigraphically distant from the source salt layer. In this context, depocentres are shallower and lack ponded accommodation, characterising stepped slopes (e.g., Casagrande et al., 2022).

This study investigates the stratigraphic evolution of an intraslope depocentre flanked by salt-cored structures that evolved during the Oligocene-Miocene in the distal extensional salt domain of Campos Basin. Alternating salt-related contractional and extensional salt tectonics controlled accommodation patterns during the evolution of the depocentre, which was filled and modified by mass-transport complexes sourced from outside the depocentre, which are intercalated with turbidite systems. Extensive seismic mapping and well data analysis were carried out to: (i) understand the large-scale controls on depocentre configuration; (ii) characterise the depositional systems

and associate thickness patterns, seismic facies and depositional architecture with topographic control; (iii) compare intraslope depocentres in different salt domains, (iv) understand the controls on 3D patterns of accommodation, and (v) propose the stratigraphic evolution of the turbidite unit above the basal mass transport complex.

5.3 Geological setting

The study area is in the central part of the Campos Basin, 100 km offshore Brazil in water depths between 100-2000 m and coincides with the Albacora and Albacora Leste oil fields (Fig. 5.1). The Campos Basin is one of several eastern Brazilian continental margin basins that originated from the break-up of the Gondwana supercontinent during the Upper Jurassic/Lower Cretaceous and evolved into a passive margin up to the present day (e.g., Chang et al., 1992; Fetter et al., 2009; Contreras et al., 2010). The basin-fill is divided into three megasequences that record different tectono-stratigraphic settings (e.g., Guardado et al., 2000; Winter et al., 2007; Fig. 5.1). The first is the Rift Megasequence (Winter et al., 2007) or Non-marine Rift Megasequence (Guardado et al., 2000), which is characterised by volcanics and continental sediments that infill rift depocentres from the Upper Neocomian to Lower Aptian. This is followed by the Post-rift Megasequence (Winter et al., 2007) or Transitional Megasequence (Guardado et al., 2000), which comprises coarse siliciclastic sediments and microbial carbonates overlain by evaporites deposited in a relatively tectonically quiescent period from the Middle to Upper Aptian. The early post-rift marks the transition from basement-involved faulting and rapid subsidence to a period of limited faulting and low subsidence driven by the cooling of the lithosphere (do Amarante et al., 2021). This period records the transition from continental to marine sedimentation. The last phase is the Drift Megasequence (Winter et al., 2007) or Marine Megasequence (Guardado et al., 2000), which evolved during thermal subsidence. It is characterised by a transgressive (from Albian to Eocene) to regressive sedimentation trend (Paleocene to present), which is controlled by basin subsidence, sediment supply and eustatic variations (e.g., Chang et al., 1992; Bruhn, 1998; Guardado et al., 2000; Winter et al., 2007; Contreras et al., 2010).

At the base of the transgressive phase, the basin-fill records a high-energy carbonate platform setting, which was progressively drowned due to thermal subsidence and

eustatic sea level rise (e.g., Chang et al., 1992; Bruhn, 1998; Contreras et al., 2010; Fig. 5.1). The regressive phase is marked by the progradation of synchronous depositional systems (shallow-water carbonates, siliciclastic paralic and deep-water systems; Bruhn, 1998; Winter et al., 2007). From the late Albian to the present, the progressive opening of the South Atlantic gradually established bathyal conditions and widespread hemipelagic and siliciclastic deep-water sedimentation (e.g., Chang et al., 1992; Guardado et al., 2000; Winter et al., 2007).

The study interval is part of a Lower Miocene deep-water succession characterised by intercalated mass transport complexes (MTC) and sand-prone turbidites, here informally named the Albacora Interval (Fig. 5.1). The focus of this work is mainly the basal mass transport complex (MTC1) and the overlying sand-rich turbidite unit (Albacora turbidites 1 – ABT1). The second MTC (MTC2) and turbidite unit (ABT2) are documented for context (see Fig. 5.2 for the subdivisions of the Albacora Interval). The Albacora Interval (detailed in the next section) forms part of the regressive phase of the Marine or Drift Megasequence (Fig. 5.1). During its deposition, the basin had a well-established passive margin physiography comprising a continental shelf, slope and basin floor (De Gasperi and Catuneanu, 2014). The arkosic composition and fine-grained character of the Cenozoic turbidites in the Campos basin, including the turbidites of the Albacora Interval, are related to a sediment source area landward of wide coastal plains (Fetter et al., 2009).
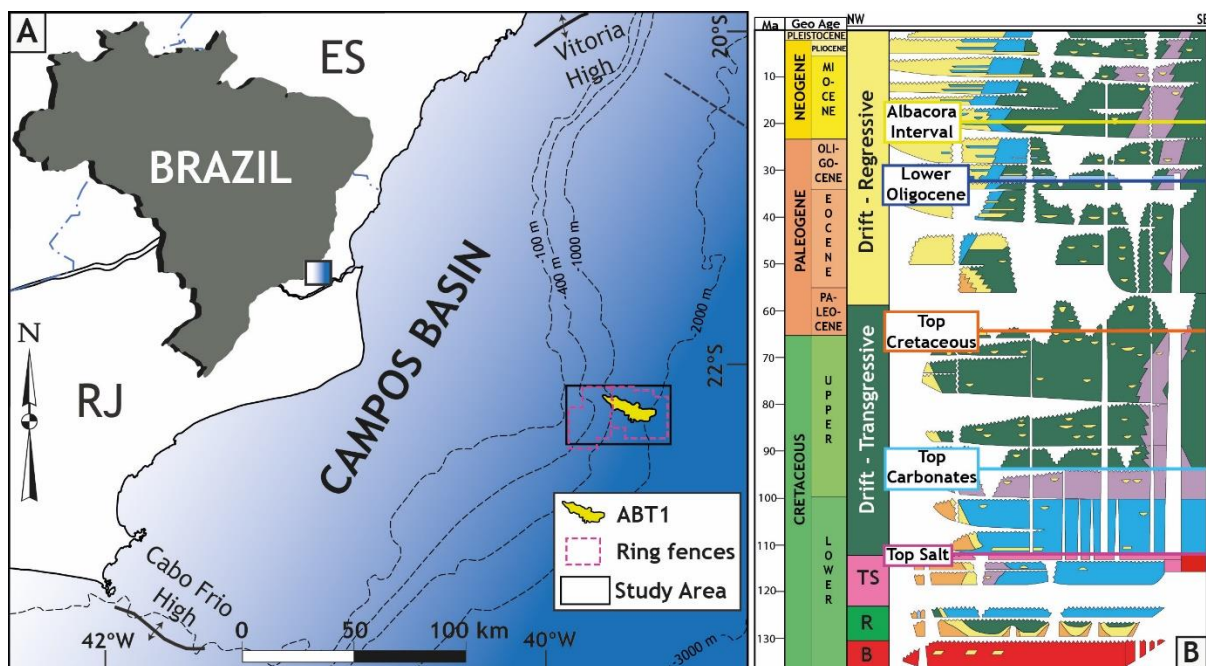
Figure 5.1: A- Location map of the study area corresponding approximately to the boundary of Albacora (pink polygon to the West) and Albacora Leste (pink polygon to the East) offshore Brazil. B- Campos Basin stratigraphic chart (modified from Winter et al., 2007). The main regional stratigraphic surfaces used in this work are marked on the chart. The Albacora Interval is Lower Miocene and is part of the regressive phase of the Marine/Drift Megasequence of the basin. Key for lithologies in the stratigraphic chart of B: red for basement, green for mudstones, yellow for sandstones, orange for conglomerates, blue for carbonates, pink for evaporites and pale purple for marls. In the chart, B refers to basement, R to rift and TS to transitional (see text for explanation).

The structural configuration of the Campos Basin reflects much of the position of rift basement structures (NE-SW and NW-SE orientated horst and graben; Guardado et al., 2000; Castro and Piccolini, 2015), and salt tectonic structures related to the Aptian evaporites of the Transitional or Post-Rift Megasequence (Chang et al., 1992; Guardado et al., 2000; Winter et al., 2007). Salt tectonics started during an early post-rift stage with seaward salt flow due to thermal subsidence and related basinward tilting of the passive margin (i.e., gravity gliding; Cobbold and Szatmari, 1991; Davison et al., 2012; Quirk et al., 2012), and progressed with gravity spreading of the overburden (Mohriak et al., 2008). The formation of a detachment surface at the base of the Aptian salt characterises thin-skinned salt-tectonics, a widespread process in Campos Basin, leading to contrasting deformational domains, with extension dominating up-dip and contraction down-dip (e.g., Cobbold and Szatmari, 1991; Demercian et al., 1993; Mohriak et al., 2008; Fetter, 2009; Quirk et al., 2012; do Amarante et al., 2021), with a control of basement structures on salt flux and, consequently, on the spatial distribution of the domains (Fetter, 2009; do Amarante et al., 2021).

Characteristic extensional structures include listric normal growth faults and associated salt rollers, rafts, salt welds, periclinal ("turtle") anticlines, and collapsed diapirs (e.g., Cobbold and Szatmari, 1991; Demercian et al., 1993; Mohriak et al., 2008; Do Amarante et al., 2021, see some of these on Figs. 2.13 and 5.2). Raft tectonics, characterised by the fragmentation and displacement of the Albian-Cenomanian carbonate platform, in particular, is a common process in Campos Basin, representing the most extreme form of thin-skinned extension (e.g., Duval et al., 1992; Demercian et al., 1993; Rouby et al., 2002; Quirk et al., 2012, Fig. 3.4).

The elements that characterise the distal contractional domain are salt anticlines underlying buckle folds, salt walls and stocks that flank minibasins (Fig. 2.11), asymmetric salt walls emplaced above reverse faults, deep basins wedged between conjugate reverse faults, salt tongues above thrusts, and reverse fault propagation folding (e.g., Demercian et al., 1993; Mohriak et al., 2008; Fetter, 2009; do Amarante et al., 2021). An intervening domain between the extensional and contractional tectonics is documented as the transitional (Mohriak et al., 2012), intermediate (Cobbold and Szatmari, 1991) or multiphase domain, where evidence for extension and contraction coexist in response to multiple, kinematically variable phases of deformation (do Amarante et al., 2021).

5.4 Dataset and methodology

This study uses a comprehensive dataset comprising two 3D seismic reflection volumes calibrated by 43 wells. The volumes differ in coverage and resolution, and both were processed as PSDMs (pre-stack depth migration) and to zero-phase wavelet, here shown with SEG normal polarity (a negative reflection coefficient is linked to a trough and indicates a decrease in acoustic impedance). The seismic reflection volumes are used in the depth domain. The higher resolution volume was calibrated by well data for better depth control. It does not cover the whole study area but has enough coverage to be the main seismic volume used here to interpret the Albacora Interval. The bin size spacing is 12.5 m for inlines and crosslines, and the vertical sampling is 3 m. The average seismic frequency in the Lower Miocene section is around 30 Hz, resulting in a vertical resolution of approximately 23 m (2700 ms is the velocity used). The lower resolution seismic reflection data covers the whole study area and is used to assess the large-scale geological context. The bin size spacing is 12.5 m for inlines and 25 m for crosslines, and the vertical sampling is 5 m. The average seismic frequency in the Lower Miocene is around 19 Hz, resulting in a vertical resolution of approximately 35 m (2700 ms is the velocity used).

Seismic reflection interpretation was carried out through combined manual and automatic reflection mapping across an area of approximately 675 km^2 in the smaller volume and 1190 km^2 in the larger volume. Seismic attribute maps (amplitude and seismic variance – edge method) were extracted from the bounding surfaces of MTC1 and ABT1 using the higher resolution seismic volume. The seismic variance attribute

is used for the detection of stratigraphic and structural discontinuities (Brown, 2011), therefore, aiming to identify basal features of the MTC1. The root mean square (RMS) amplitude attribute computes the square root of the sum of squared amplitude values divided by the number of samples within a specified window. The squaring of amplitude values within a window causes the high amplitudes to stand out above the background. Therefore, the RMS attribute is recommended to image hydrocarbon reservoirs, as the ABT1, where the RMS was extracted between the top and base surfaces for seismic geomorphology analysis. Seismic amplitudes are locally affected by poor imaging below marine infrastructure (i.e., production rig), and by fluid contacts. In addition, as the study area sits below the modern Campos Basin slope, there are down-dip changes in the overburden thickness causing variations in the amplitude values. An overall increase of the amplitudes is observed as the overburden thins down-dip, and the seismic signal is less affected by absorption. In addition, the stepped morphology of the modern Campos Basin slope produces seismic multiples. Therefore, several factors alter amplitude values in the study area, and these are considered when interpreting the seismic reflection data, especially the attribute maps correlating amplitude strength to lithology.

Well data include basic wireline logs (gamma ray, density, neutron, sonic and resistivity), two image logs (one resistivity log and one density/neutron log) and 52 m of core distributed in 6 wells. The sand-rich unit ABT1 is almost totally cored in one well (AB6 well), half cored in a second well (AB3 well), and there are a few metres of cored section in four other wells. The mass transport complex at the base of the Albacora Interval (MTC1) has a few metres (maximum 5 m in well AB3) of its top cored in four wells. Lithology can be inferred using the image logs. High resistivity in the image logs of hydrocarbon-saturated intervals indicates high-porosity reservoirs and, therefore, sand-prone facies. Lower resistivity, and therefore conductive layers, indicates a lack of effective porosity, supporting mud-prone facies. For density image logs, low-density values are indicative of high-porosity rocks, being enhanced by hydrocarbon saturation when compared to water reservoirs (oil is less dense than water), whereas higher density values indicate increase in mud content and reduced porous space with free fluids.

5.5 Results

5.5.1 Salt tectonics in the study area

Several salt structures with different orientations and forms are observed in the study area. The major features are salt walls, inverted salt rollers and inverted salt-cored grabens located at the northern, eastern, and southern flanks of a large Albian-Cenomanian carbonate raft, respectively (Fig. 5.2). Internally, the raft is partially fragmented by N-S oriented normal faults that formed salt-cored grabens of the same orientation, some of these were also inverted (Fig. 5.2).

The growth of the salt structures is primarily related to extension as the salt flowed in between the fragmented blocks of the Albian-Cenomanian carbonate platform (rafts and pre-rafts) during the Lower Cretaceous, when these structures were likely close to, or at, the surface (Fig. 5.2). The evolution of the extension generated elongate troughs above the salt structures, which were healed by deposition during the Upper Cretaceous, marking the end of the raft tectonics (Fig. 5.2). In addition, there is evidence for contractional deformation superimposed on the extensional structures, with tectonic inversion marked by thrusts and folding above the salt rollers at the eastern flanks of the raft, and the uplift of salt-cored grabens (Fig. 5.2). Structural onlaps, stratal thinning above salt-cored structures, and the formation of basin synclines, support shortening from the Cenozoic until the present day (Fig. 5.2).

The major salt wall at the North of the study area (Fig. 5.2C) is bounded by normal faults in the southern flank, suggesting extension or transtension. However, the truncation of reflections near the seabed above the structure suggests recent uplift (Fig. 5.2C). Therefore, this feature is a product of multi-phase deformational events. The thinning of the Oligocene to Lower Miocene strata (including the Albacora Interval) above this structure, and thickening above the hangingwall suggest syn-depositional activity. This thickened section above the hangingwall thins towards the south, away from the fault, where the raft is flanked by a present-day inverted graben (Fig. 5.2C). Therefore, the Oligocene to Lower Miocene strata present a subtle wedge-shape geometry that suggests increased subsidence towards the normal fault system that bounds the salt wall at the North. Below MTC1 in this area, a high-amplitude reflections package (HARP) with lens-shaped reflections is interpreted as multiple slope valley-

fill systems (SVS) (Figs. 5.2C, 5.3; more details in the next section). The sand-rich Albacora Interval (ABT1, ABT2) are also part of the stratigraphic record in this thicker section. This suggests that sediment gravity flows were preferentially routed towards this area through time. The change from slope valley systems to the lobate shape of ABT1 and ABT2, and the thinning of MTC1 and underlying Oligocene strata above the salt-cored structures at the edges of the raft, support the formation of an intraslope depocentre immediately before and during the evolution of the Albacora Interval, which is here informally named the Albacora depocentre (Fig. 5.2A). The position of the Albacora depocentre in the basin (100 km from the coastline) and the occurrence of extensional salt structures within the raft tectonics context suggest that the study area sits at the basinward edge of the extensional salt domain of the Campos Basin. The depocentre has a semi-elliptical shape, being 35 km long and 20 km wide (700 km^2). The sand-prone ABT1 and ABT2 units are concentrated in the northern part of the depocentre and align with the salt wall.

Legend:

- - - - - Basement top
- - - - - Salt base
- - - - - Salt top
- - - - - Raft top
- - - - - Cretaceous top
- - - - - Lower Oligocene
- - - - - Base Albacora unit
- - - - - Top Albacora unit
★ Thrust fault
⬆ Uplifted salt-cored graben
⇒ Structural onlaps
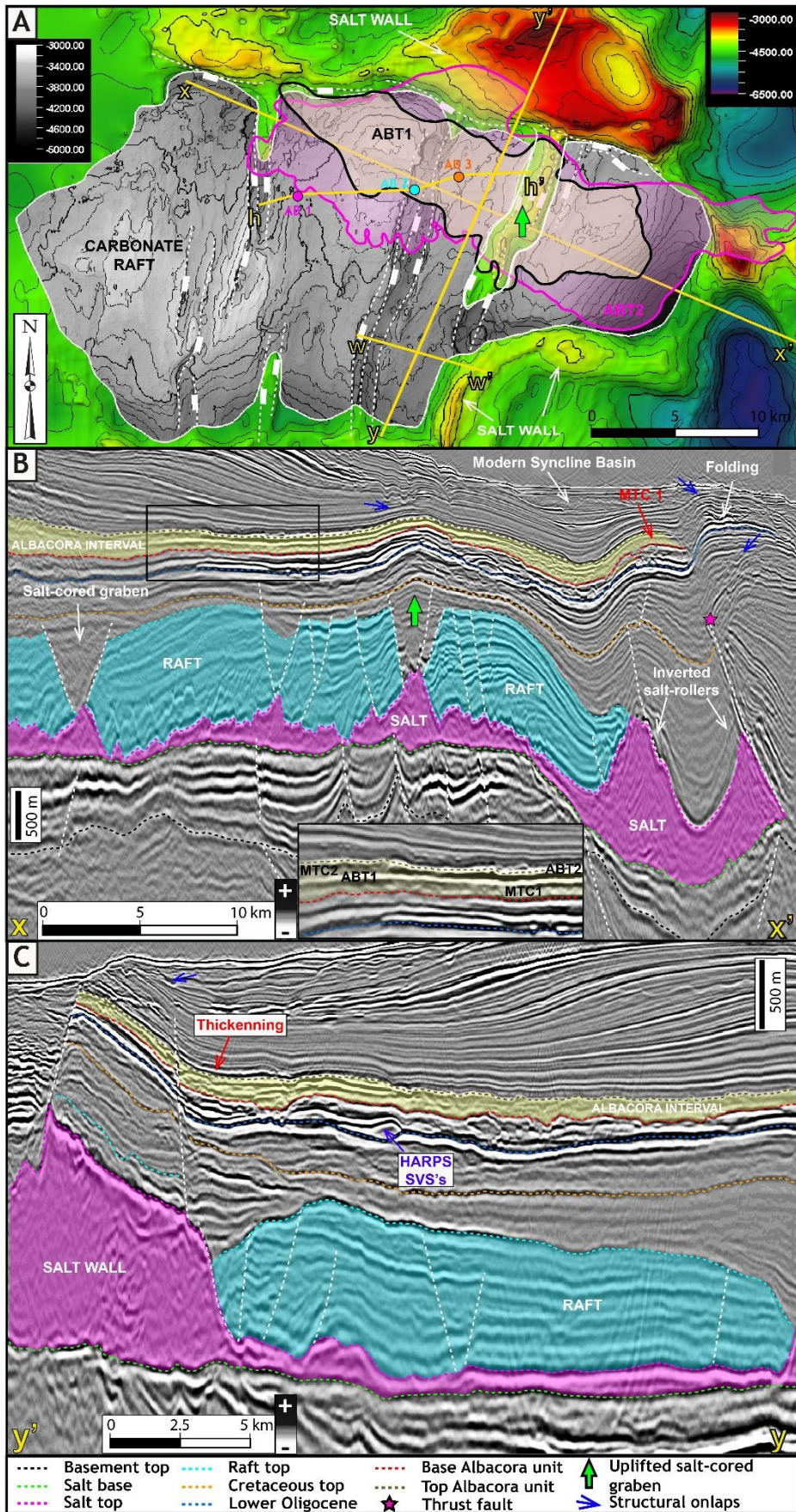
Figure 5.2: General geological context of the study area. A- Salt structural top map with the carbonate raft in grey and external limits of ABT1 and ABT2. The area of the map refers to the black rectangle on the map of Figure 5.1. The salt structures that flank the raft define the Albacora depocentre, sand-prone turbidites concentrate towards the North, close to the flank of the salt wall. N-S salt-rooted faults (white dashed lines) partially fragment the raft. B- Dip seismic profile (depth domain, 5x vertical exaggeration, lower resolution seismic volume). A series of normal N-S oriented faults derived from the fragmentation of the carbonate raft occur underneath the Albacora Interval (coloured in yellow), forming elongated troughs (grabens) and the salt structures at the edges of the raft. Some of the extensional faults were inverted under a contractional strain field, producing fault propagation folding related to salt rollers and buckling of the graben fill (green arrow). Seismic inset in the black rectangle shows the subdivisions within the Albacora Interval (MTC1, ABT1, MTC2 and ABT2). C- Dip seismic profile (depth domain, 5x vertical exaggeration, lower resolution seismic volume). Extensional fault flanking the salt wall at the northern edge of the depocentre controlled sediment dispersal patterns and accommodation, inducing thickening of the Oligocene-Miocene section and concentration of sand-prone deep-water deposition (SVS's- slope valley systems, Albacora interval turbidites). The timing of the contractional deformation is constrained by structural onlaps (see blue arrows and text for explanation) and thickness patterns, which are evidence for syn-depositional deformation of the Albacora Interval and throughout the stratigraphic column.

5.5.2 Albacora Interval

The Albacora Interval comprises MTCs (MTC1 and MTC2) intercalated with sand-prone units (ABT1 and ABT2, Fig. 5.3). The entire interval has an average thickness of 150 m and overlies low to-high- amplitude reflections (Fig. 5.3). These are interpreted to be related to older turbidite slope valley systems (SVS's, further explanation in the MTC1 section). The basal MTC1 is thick (average thickness of 75 m) and covers a larger area (see next section) than MTC2, which is thinner (average thickness of 45 m) and can be at the limit of the seismic resolution, so its total extent is misleading. Based on seismic geomorphological patterns that reveal lobate and channellised features (Fig. 5.3 D, E), calibrated by wells, the sand-prone ABT1 and ABT2 are interpreted as turbiditic units, which form important oil reservoirs that stand out in seismic reflection data. ABT1 covers a smaller area (see section ABT1 below) than ABT2 (Fig. 5.3 D,E). Both have similar average thicknesses, around 25 m. A borehole-calibrated seismic facies framework summarises the seismic character of the

Albacora interval and the underlying slope valley system (Fig. 5.4). The MTC1 and the ABT1 unit are the focus of this study and are described in the following sections.
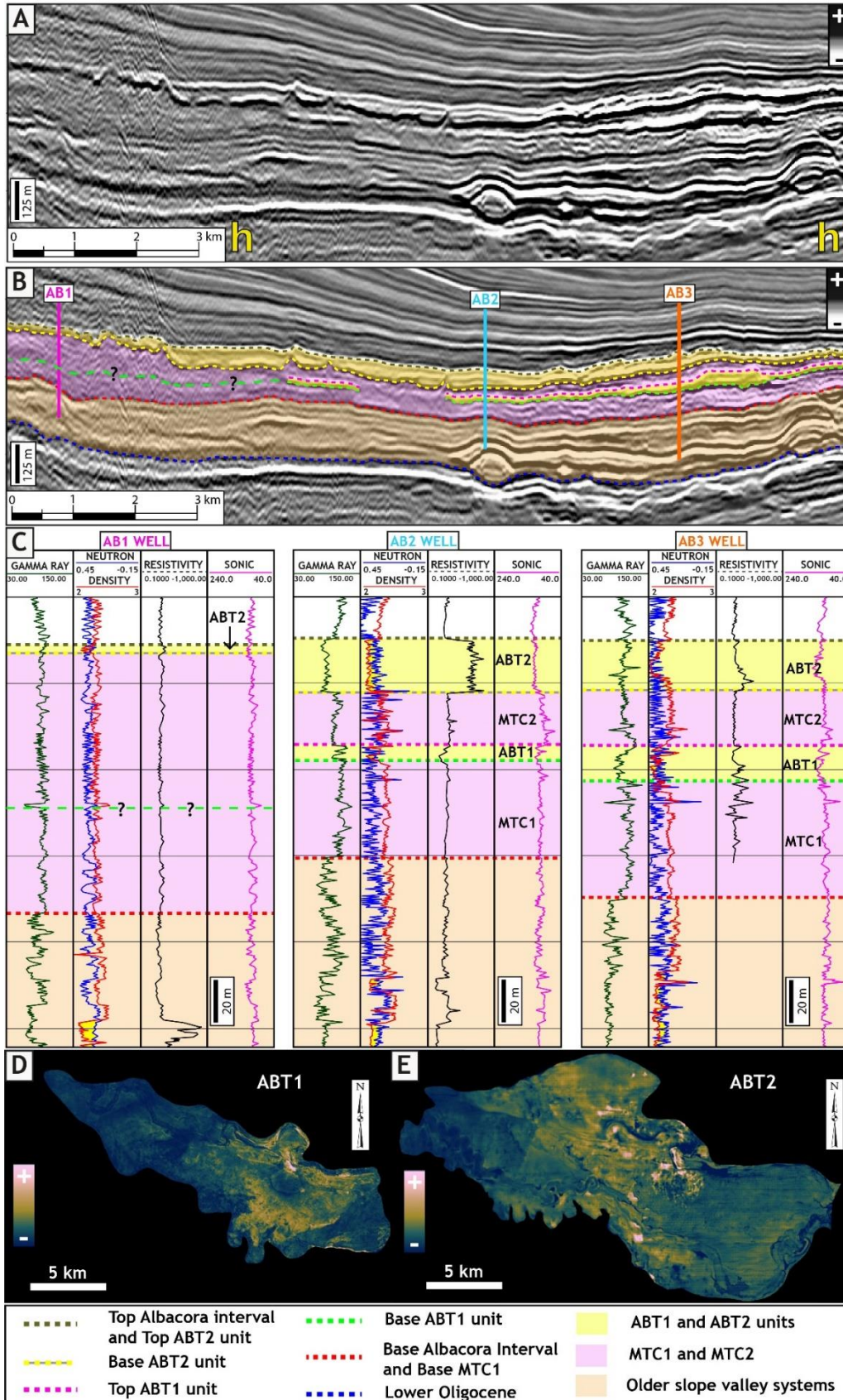
Figure 5.3: General overview of the Albacora Interval. A and B are uninterpreted and interpreted dip seismic profiles, respectively (depth domain, 5x vertical exaggeration, higher resolution seismic volume, see location in Figure 5.2A), showing the intercalation of mass transport complexes (MTC1 and MTC2) with turbidites (ABT1 and ABT2). Note seismic facies for the MTCs. To the left, transparent to chaotic reflections and towards the right, contorted and partially continuous reflections with variable amplitude strength. C- Well log calibration in the Albacora Interval and underlying slope valley systems. The average thickness of the Albacora Interval is 150 m, well AB1 records around 120 m. Where the ABT1 unit pinches out, the well log breaks suggest the limit of the MTCs. D and E – Amplitude map showing the seismic geomorphology of the ABT1 and ABT2 turbidite units. Note the lobate and channel features, typical of submarine fans.
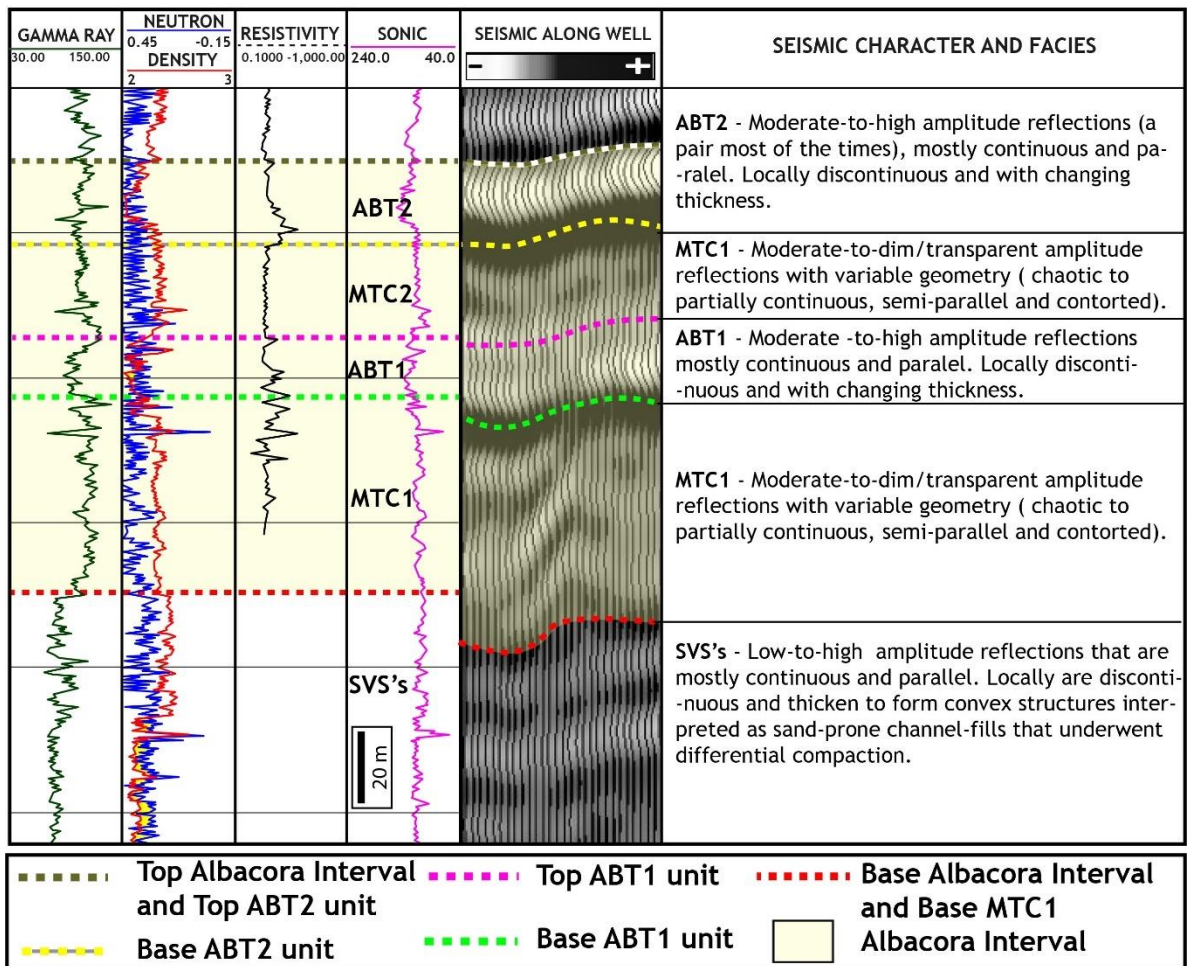
Figure 5.4: Seismic character/facies of the main units in the study area, calibrated by a borehole (AB-3 well, see location on Fig. 5.2A). Note seismic reflections character along the well with variable amplitude strength and reflection geometry.

5.5.3 Mass Transport Complex 1 – MTC1

MTC1 is described here according to geometry and thickness patterns, seismic character (facies and bounding surfaces) and well calibration.

5.5.3.1 Geometry and thickness patterns

Description: MTC1 covers a minimum area of 985 km^2, has an average seismic thickness of 75 m (below ABT1 turbidites), and has a well-calibrated thickness of 67 m. Therefore, an estimated minimum volume for MTC1 is ~73 km^3. In areas where the ABT1 unit is absent, MTC1 and MTC2 form an amalgamated package up to 200 m (Fig. 5.3). Overall, the geometry is tabular in areas of low structural complexity. A headwall scarp and lateral margins to MTC1 and features such as ramps and flats (e.g., Bull et al., 2009) are not identified within the dataset. It extends beyond the flanks of the raft, but thinning is observed above the salt-cored structures at the edges of the raft (Fig. 5.2B, C). The MTC1 also thins above internal salt-cored structural highs and thickens into structural lows. Abrupt thinning of MTC1 above the N-S oriented high (positively inverted graben, green arrow in Fig. 5.2B) in the middle of the Albacora depocentre is suggested by seismic mapping and confirmed by two wells, which show a thickness reduction from more than 60 m to approximately 20 m in a 2.5 km strike distance (Fig. 5.5). This high coincides with the uplifted graben, interpreted to record contractional tectonics (Fig. 5.2B). In map view, an extension of the thinned area above the inverted graben can be observed (Fig. 5.6A). A depth map of the Lower Oligocene horizon shows a structural high related to the inverted graben on stratigraphic surfaces at the present day (Fig. 5.6B). The geometry of the uplifted area in the Lower Oligocene map is similar to the area with lower thicknesses on the MTC1 thickness map, above and at the flanks of the inverted graben (Fig. 5.6A).

Local thickness variations of MTC1 within the depocentre are related to the previous depositional system and/or topography and differential compaction. Seismic variance extraction from the basal surface of MTC1 reveals that MTC1 deposits overlie at least three NW-SE oriented slope valley systems (Fig. 5.7). The seismic profile of Figure 5.5 shows that MTC1 thickens into one of the conduits (see blue arrow). Well calibration reveals that these channel systems consist of sand- and mud-prone deposits associated with high-to-moderate amplitude reflections that can be lens-

shaped (i.e., channel-fills) or plane-parallel (i.e., channel margins or overbanks) (Figs. 5.3 and 5.5).

Interpretation: The thinning of MTC1 above the salt structures at the edges of the raft and above the inverted graben, where the raft is partially fragmented, suggest that these structural features imposed a topographic control during emplacement of MTC1. In particular, the abrupt thinning of MTC1 above the inverted graben indicates that this structure had a seabed expression during emplacement. Thickening of the MTC1 within the conduits of older slope valley systems suggests that MTC1 either exploited partially-filled channelised topography and/or more easily entrained less cohesive and sand-rich substrate of the channel-fill (Ortiz-Karpf et al., 2018). The interaction of MTC1 with an unconsolidated sand-prone or soft mud-prone substrate (high and low-density turbidites) might be the reason for the lack of evidence for kinematic indicators at the seismic scale at the MTC1 base, such as grooves (e.g., Bull et al., 2009). Subtle thinning of MTC1 deposits above a convex lens-shape channel-fill feature suggests positive depositional topography created by differential compaction as a further control on MTC1 thicknesses (see AB2 well location in Fig. 5.2A). In summary, the MTC1 interacted with sand-and-mud-prone deposits related to older slope valley systems, as well as structural features expressed in the palaeosurface, during emplacement. The depositional topography related to these systems, negative or positive, affects MTC1 thickness patterns.
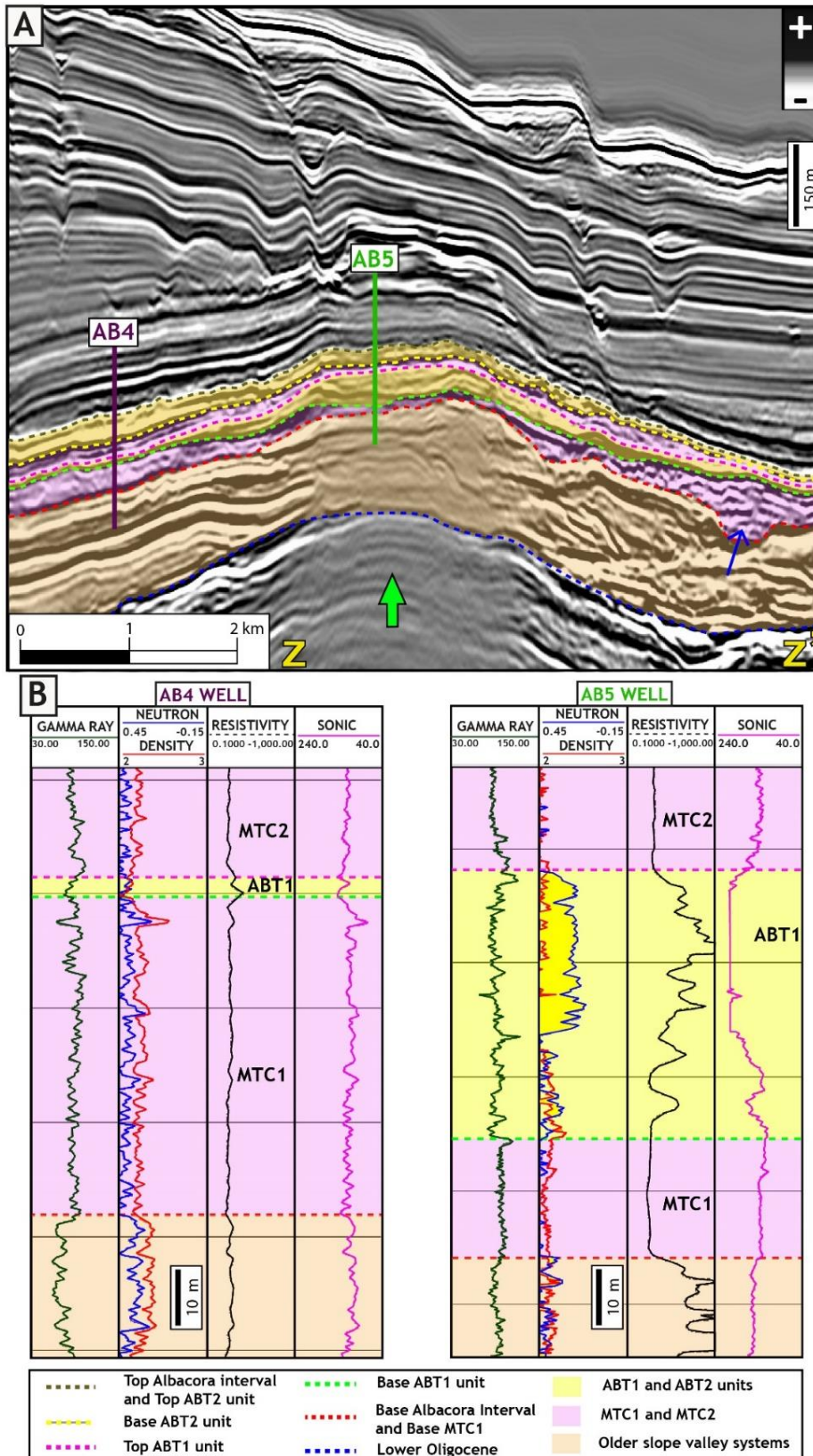
Figure 5.5: Thicknesses variations above the inverted graben in the middle of the Albacora depocentre. A- Strike seismic profile (depth domain, 5x vertical exaggeration, higher resolution seismic volume, see location in Figure 5.6). Note how MTC1, MTC2 and ABT2 thin above the uplifted structure (green arrow). In contrast, the ABT1 unit thickens. Thicknesses of the

Paleogene section, with detail on the Oligocene slope valley systems, seem unchanged above this structure, although thinning is observed above salt-cored structures at the edges of the depocentre. Discontinuous and contorted seismic reflections are seen in MTC1 seismic facies. Blue arrow indicates the interaction of MTC1 with an older channel. B – Wells confirm the thicknesses variations in the MTC1 and ABT1 (see text for explanation).
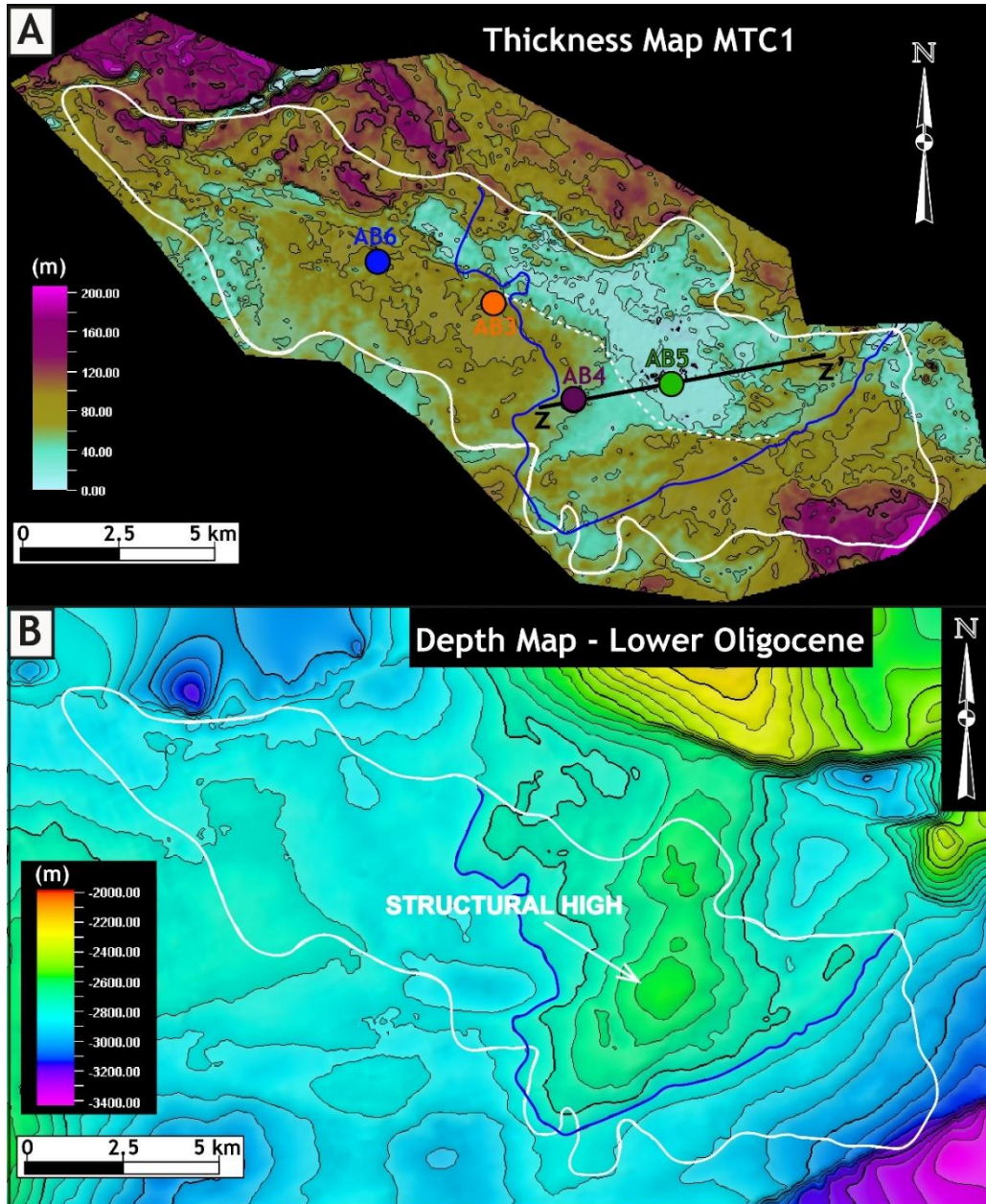
Figure 5.6: A – Thickness map (m) of MTC1 (in the area around ABT1 where mapping of the top MTC1 surface is reliable). The white solid polygon marks the contour of ABT1, and the white dashed line marks an area with very low thicknesses (see this polygon in Figure 5.11, above the thickness map of the ABT1 unit). The blue line marks the limit of the structural high

of the inverted graben in the Lower Oligocene horizon, showing correspondence between the present-day influence radius of this structure and the thinner area of MTC1 (see text for explanation). B- Depth map (m) of the Lower Oligocene.
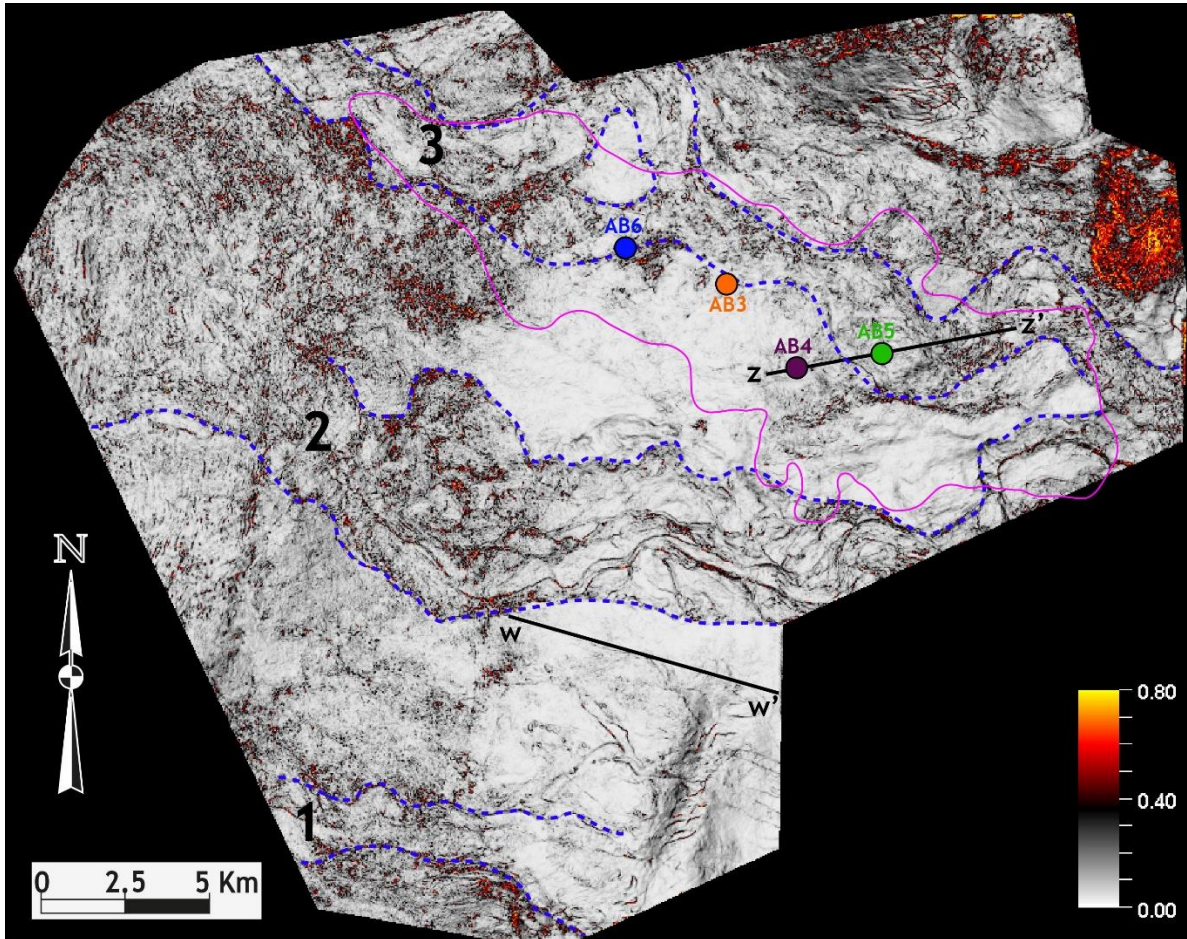
Figure 5.7: Variance attribute map (edge method) extracted from the base of MTC1 (higher resolution seismic volume). Outlined in dashed blue lines are the older slope valley systems below MTC1. The pink polygon is the limit of the ABT1 turbidite unit.

5.5.3.2 Seismic character

Description: MTC1 comprises packages with chaotic to partially continuous, semi-parallel and contorted reflections with variable amplitude strength consistent with seismic facies observed in mass wasting deposits (Figs. 5.3 and 5.5). These facies show lateral changes from dim to transparent reflections (Fig. 5.3). At the southwestern edge of the Albacora depocentre, where the ABT1 unit is absent, the MTC package (MTC1 and MTC2) displays semi-continuous reflections that are disrupted and bounded by faults verging towards the E. The rotated reflections

produce protuberances at the MTC2 surface, resulting in an undulating top surface (hummocky surface; Posamentier and Martinsen, 2011; Fig. 5.8).
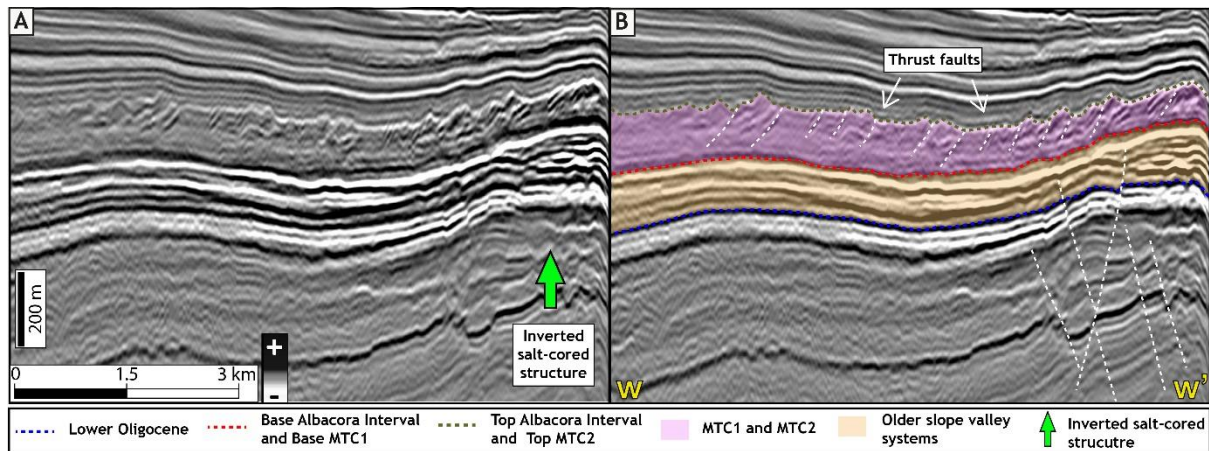
Figure 5.8: Thrust fault system in the mass transport complexes at the SE edge of the Albacora depocentre, where inverted salt-cored structures are documented. A and B uninterpreted and interpreted dip seismic profiles, respectively (depth domain, 5x vertical exaggeration, higher resolution seismic volume, see profile location in Figures 5.2 and 5.7). Note the generation of a hummocky surface at the top of MTC2. Eastward thrust fault vergence indicates the movement direction. MTCs are thinner above the inverted structure.

Interpretation: Chaotic reflections have been associated with debrites (Posamentier and Martinsen, 2011; Ortiz-Karpf et al., 2015, 2018) and with highly deformed slump deposits (Steventon et al., 2019; Wu et al., 2021). Partially continuous contorted reflections (i.e., folded) are here interpreted to represent less deformed strata that could be classified as slumps or slides. Seismically transparent facies have been associated with the poorly organised macrofabric of debrites (Posamentier and Martinsen, 2011; Steventon et al., 2019). The westward dipping fault planes are interpreted as an expression of a thrust system and are here used as a kinematic indicator of mass flows towards the east, which is largely concordant with the routeing direction of the underlying slope valley systems. Thrust faults are usually documented in the contractional domain at the toe of MTCs (e.g., Steventon et al., 2019); however, they can also develop in association with topographic highs (e.g., Bull et al., 2009; Doughty-Jones et al., 2019). The proximity of this facies to an inverted salt-cored structure at the southeastern border of the depocentre (Fig. 5.8) suggests that the syn-depositional topography might have influenced the formation of the thrusts, as well as the thinning of the MTC. However, as the mass transport complexes cover a larger

area than the study area, it is not possible to conclude in which part of the MTCs the thrust system formed.

5.5.3.3 Well calibration and sedimentology

Description: Well logs intersecting the whole MTC1 package show high gamma-ray values and a lack of effective porosity interpreted from the crossover pattern of density and neutron logs (Figs. 5.3 and 5.5). A distinctive zig-zag well log motif is observed in several wells, being particularly characteristic in the neutron/density logs but also identified in the gamma-ray and sonic logs (Fig. 5.9). The resistivity image log of well AB6 shows that the zig-zag log value variations correspond to packages with different composition and texture, like massive or speckled (Fig. 5.9). In other wells, MTC1 log values are less variable and characterised by a serrated motif, which has similar average values for the logs when compared to the zig-zag pattern (Fig. 5.5B). Core data was obtained in the uppermost part of MTC1 in 4 wells. Facies vary from mud-prone packages with preserved and deformed bedding (Fig. 5.9) to a debritic fabric with mudstone clasts in a mud-prone matrix (Fig. 5.10).

The image patterns in the interval with zig-zag logs are quite different from the layered mud-prone deposits below the MTC1, which are here interpreted as overbanks to the underlying slope valley systems (Fig. 5.9). In addition, MTC1 has higher gamma-ray values and lower density, which results in a log break when in contact with these channel-related mud deposits.

Interpretation: The zig-zag log patterns in the MTC1 interval suggest facies variability, which is supported by the different patterns observed in the image logs. The speckled pattern might be related to a more heterogeneous composition, such as a clast-rich debrite. In contrast, the massive parts can represent a more homogeneous composition, like a large mudstone block or mud-prone debrites. These different deposits suggest multi-phase depositional events, i.e., a complex. The serrated well logs suggest less lithological / facies variability than the zig-zag logs. The diversity of facies is also supported by the cores, which reflect different sedimentary and deformational processes within the range of mass transport deposits, such as slumping and folding (deformed mudstones) and cohesive debris flow (mud-rich debrites, Talling et al., 2012). Regarding the source of the MTC1, its high mud content

is compatible with mass flows originating from gravitational instabilities in the mid-to-upper slope (Posamentier and Martinsen, 2011).

Although some sedimentological interpretations are made here, it is noted that mass transport deposits have a marked spatial facies variability. Consequently, the one-dimensional analysis provided by well data only provides a snapshot and may not be fully reflective of the whole MTC. In addition, despite the comprehensive dataset available for the MTC1 analysis, there is no clear association between the cored facies, log motifs and seismic facies.

Figure 5.9: MTC1 well log motifs, image log and core. A distinctive zig-zag motif is observed in the well logs, which coincides with different patterns of the image log, suggesting lithological variability (see text for explanation). The zoomed image log shows a speckled pattern that suggests a clast-rich interval of what could be a debritic facies within the MTC1. The core image suggests deformed bedding in mud-prone facies in contact with horizontal bedding (contact is the yellow line). See well location in Figure 5.6.
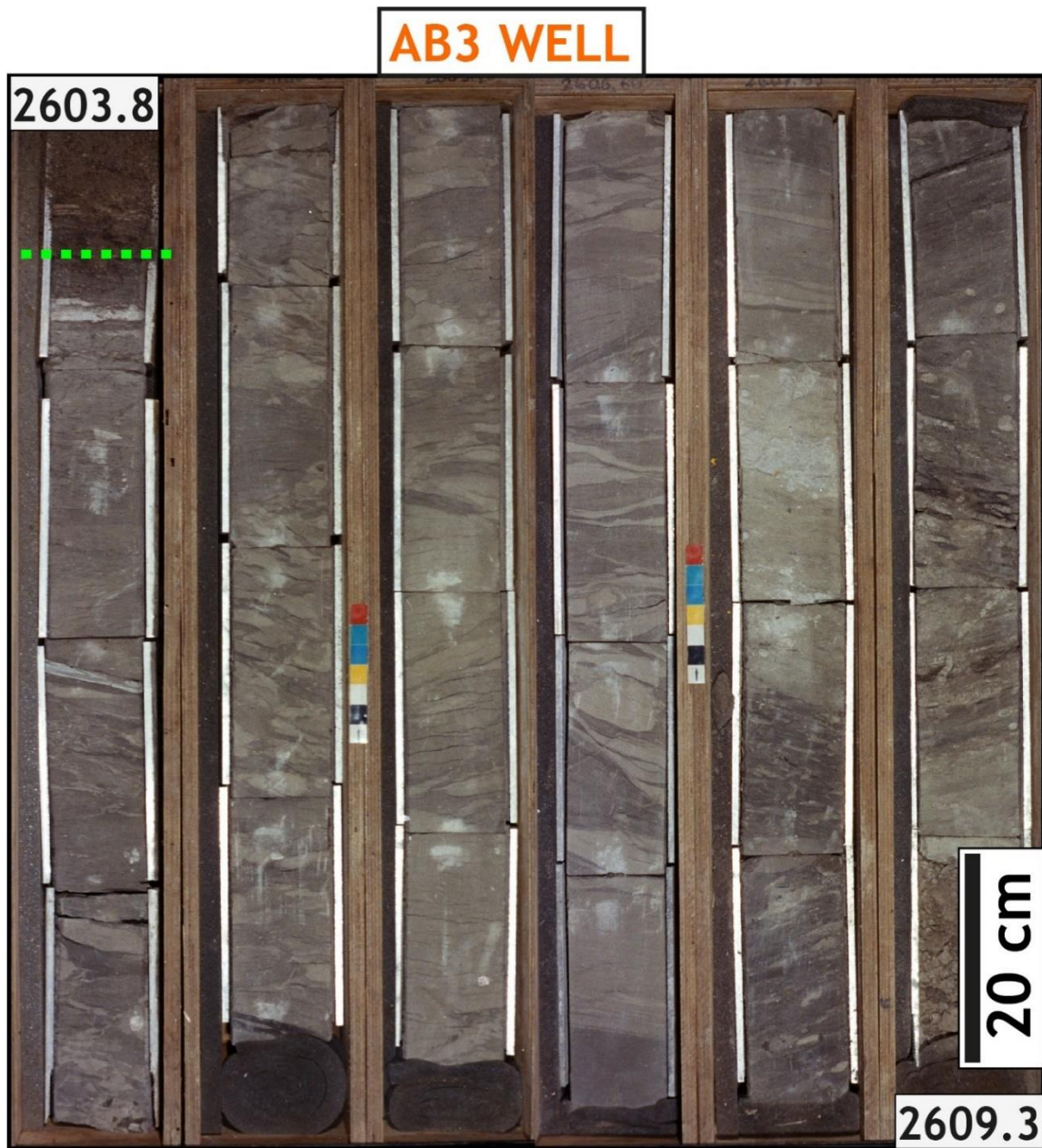
Figure 5.10: Mud-prone (matrix and clasts) debritic facies cored in MTC1. See well location in Figure 5.6 and well log patterns at the limit with the ABT1 unit in Figure 5.3.

.

5.5.4 Albacora Turbidite Unit 1 (ABT1) – general aspects

The ABT1 unit is intersected by 27 wells. Different stratigraphic phases are supported by seismic mapping to define two sand-prone subunits, separated by a mud-prone subunit, that are cut by an incisional surface.

5.5.4.1 Geometry and thickness patterns

Description: The ABT1 unit covers an area of 128 km^2, adjacent to and aligned with the salt wall at the northern edge of the Albacora depocentre. Seismic geomorphology and thickness patterns reveal an elongate NW-SE oriented geometry (Fig. 5.11). The average seismic thickness (well calibrated) is 22 m. However, higher thicknesses (25 to 70 m) are concentrated along a main NW-SE oriented axis that widens down-dip, whereas lower thicknesses (<15 m) are in marginal positions where the unit pinches out (Fig. 5.11A and seismic profile of Fig. 5.12). The ABT1 unit displays increased thicknesses above the N-S high (inverted graben above the salt wall) internal to the Albacora depocentre (see well AB5 in Fig. 5.5), in contrast to MTC1, which is thinner (Fig. 5.11A). Strata thinning above the inverted graben are also observed in MTC2 and ABT2 unit (Fig. 5.5A).

Interpretation: The NW-SE alignment of ABT1 parallels the orientation of the salt wall to the north. Together with the thickness changes above the N-S high suggest these structural elements were a control on the topography of the palaeo-slope. The thickness patterns suggest decreased down-dip confinement with a marked depositional axis up-dip.
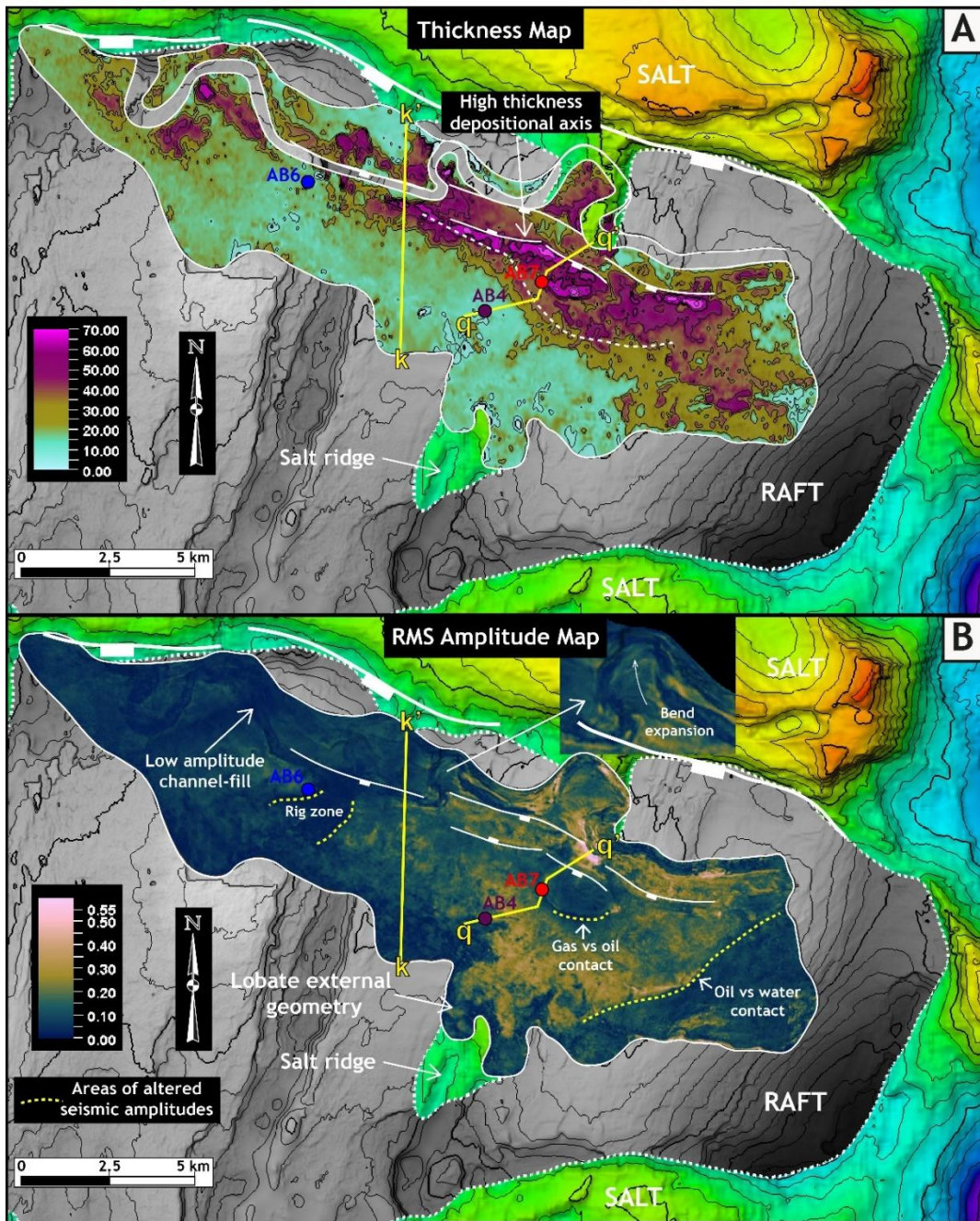
Figure 5.11: Maps for the ABT1 unit within the context of the Albacora depocentre. A- ABT1 unit thickness map. Note higher thicknesses along a main depositional axis and considerable thinning off this axis. Thickness patterns widen down-dip. Increased thicknesses are observed in the same area where the MTC1 thins (white dotted line marks this area, also in Figure 5.6A) (see text for explanation). B- RMS amplitude map of ABT1 (between top and base surfaces). The ABT1 is an elongate turbidite system with lobe-shaped geomorphology at the distal part, truncated by a low amplitude channel-fill. Note the lobate architectural pattern above the area of the salt ridge. The overall increase in amplitudes down-dip is due to reducing overburden, however fluid contacts and subsurface facilities also alter amplitudes (see yellow dotted lines). Section k-k' is shown in Figure 5.12 and section q-q' in Figure 5.14.

5.5.4.2 Seismic character

Description: The ABT1 unit comprises moderate to high-amplitude anomalies that form an elongate turbidite body that widens down-dip and displays an external lobate geometry (Fig. 5.11B). Typical lobate architecture is observed directly above the salt ridge (see the upper sand subunit in the next section). The ABT1 top surface is interpreted in a trough and the base in a peak (Fig. 5.12A). A through-going low amplitude channel-fill is observed in the amplitude map at the northern edge of the ABT1 unit (Fig. 5.11). Seismic profiles support that this channel truncates the ABT1 deposits (Fig. 5.12).

Interpretation: The lobate geometry in the down-dip part suggests unconfined deposits, such as lobes. This coincides with the change in thickness pattern described above the inverted graben, therefore, supporting that the seismic geomorphology by structural elements that were present on the seabed.
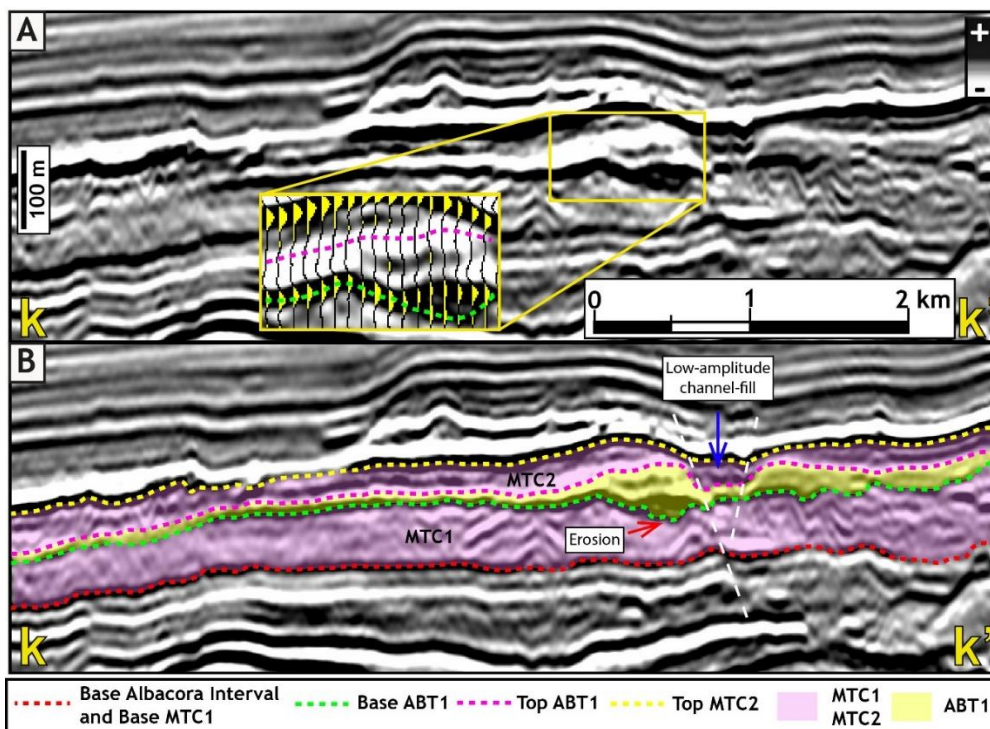
Figure 5.12: Seismic character of ABT1 unit. A and B – Uninterpreted and interpreted seismic profiles, respectively (depth domain, 5x vertical exaggeration, higher resolution seismic volume, see location in Figure 5.11). A- Inset of seismic profile showing top trough and base peak of the ABT1 unit. B – ABT1 unit above MTC1. Note the thickening of ABT1 reflections towards the main depositional axis, where basal erosion is interpreted (red arrow). The blue

arrow points to the low amplitude channel-fill cutting into the top of the sand-prone deposits of ABT1. In this position, channel edges coincide with faults (white dashed lines).

5.5.4.3 Well calibration and sedimentology

Description: Well calibration supports a high sandstone percentage in the NW-SE axial position of the ABT1 and a moderate to low sandstone percentage in the thinning to pinch-out areas. More details about well log calibration are presented in section 5.5.5 (ABT1 subunits). Cores reveal that a high proportion of sand-prone facies were sampled within the main depositional axis of the system (wells AB5 and AB6), in a position where the ABT1 unit is not very thick (~20 m) and there is not enough seismic resolution to differentiate stratigraphic subunits. Sandstones are dominantly fine-grained, well sorted and planar laminated, although locally structureless or normally graded coarser facies are present (medium- to coarse-grained sandstones) (Fig. 5.13). The cores of AB6 show amalgamated sandstone beds with a large amount of mud rip-up clasts (Fig. 5.13). The mud clasts have a tabular shape (not rounded) and considerable size (up to the diameter of the core, Fig. 5.13). Towards marginal positions, the few metre-long cores recovered in the upper stratigraphic phase record intercalation of thinly bedded fine-grained sandstones and mudstones.

Interpretation: Sandstones with planar lamination are deposited by tractional processes once the suspended load of turbidity currents decelerate, while the structureless sandstones record rapid deposition from turbulent high-density flows (Lowe, 1982). Vertical grading within sandstones is interpreted to record the decay of initial turbulence and decreasing competency in the tail of the turbidity current (Middleton and Hampton, 1973). The large amount of rip-up clasts indicates erosive power within the current, and the size and shape of the mud clasts suggest local entrainment of a mud-prone substrate and a short transport distance.
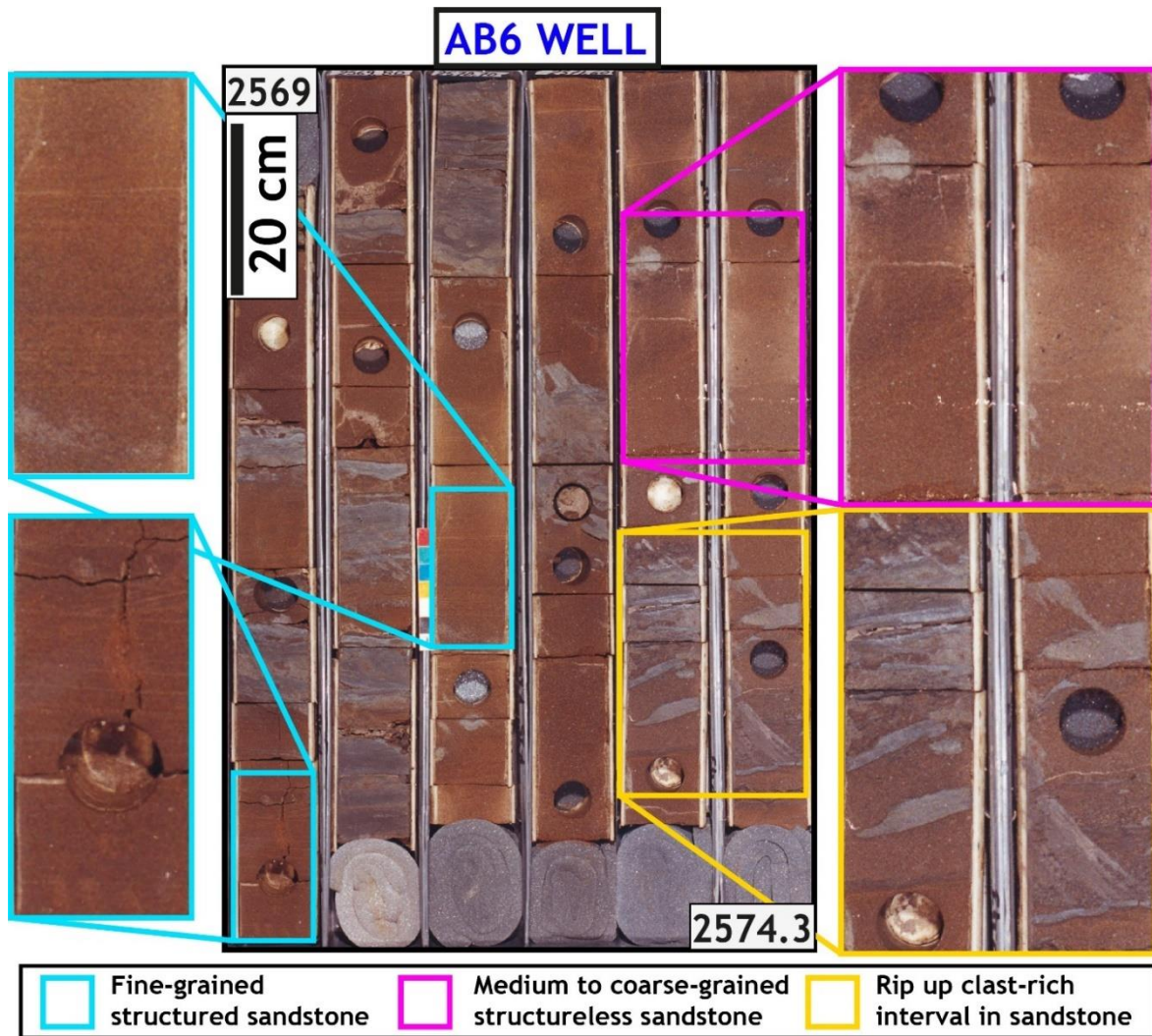
Figure 5.13: Core from the AB6 well located in the main deposition axis of the ABT1 unit (see location in Fig. 5.11). Core insets show the main sedimentary facies. Rip-up clast-rich intervals with tabular shaped clasts are evidence for erosive flows and minor clast transportation (see text for explanation).

5.5.5 ABT1 subunits

5.5.5.1 Lower sand-prone subunit

Description: A moderate-to-high amplitude internal trough restricted to the central part of the ABT1 unit is interpreted as the top of a basal stratigraphic subunit (from the peak base to the internal trough, Fig. 5.14), which from well calibration is sand-prone (Fig. 5.14C, well AB7). This subunit locally thickens to form a lens-shaped feature with moderate amplitudes that coincides with the high-thickness depositional axis (up to 60 m, Figs. 5.11A and 5.14A). Basal reflection patterns suggest localised erosion into

MTC1 (Fig. 5.12) and a tendency for passive infill of negative topography (Figs. 5.14 and 5.16). Well intersection in the marginal position of the lower sand-prone subunit suggests a moderate sandstone percentage, and the image log suggests a finning upward trend (Fig. 5.14, see well AB7).

Interpretation: The elongate thickness patterns and restricted occurrence suggest confined intraslope lobe deposits with a higher energy depositional axis (Fig. 5.17-1). Evidence for a final phase of channel incision, as documented in intraslope lobes in areas with transient accommodation (e.g., Adeogba et al., 2005; Spychala et al., 2015), is not identified.
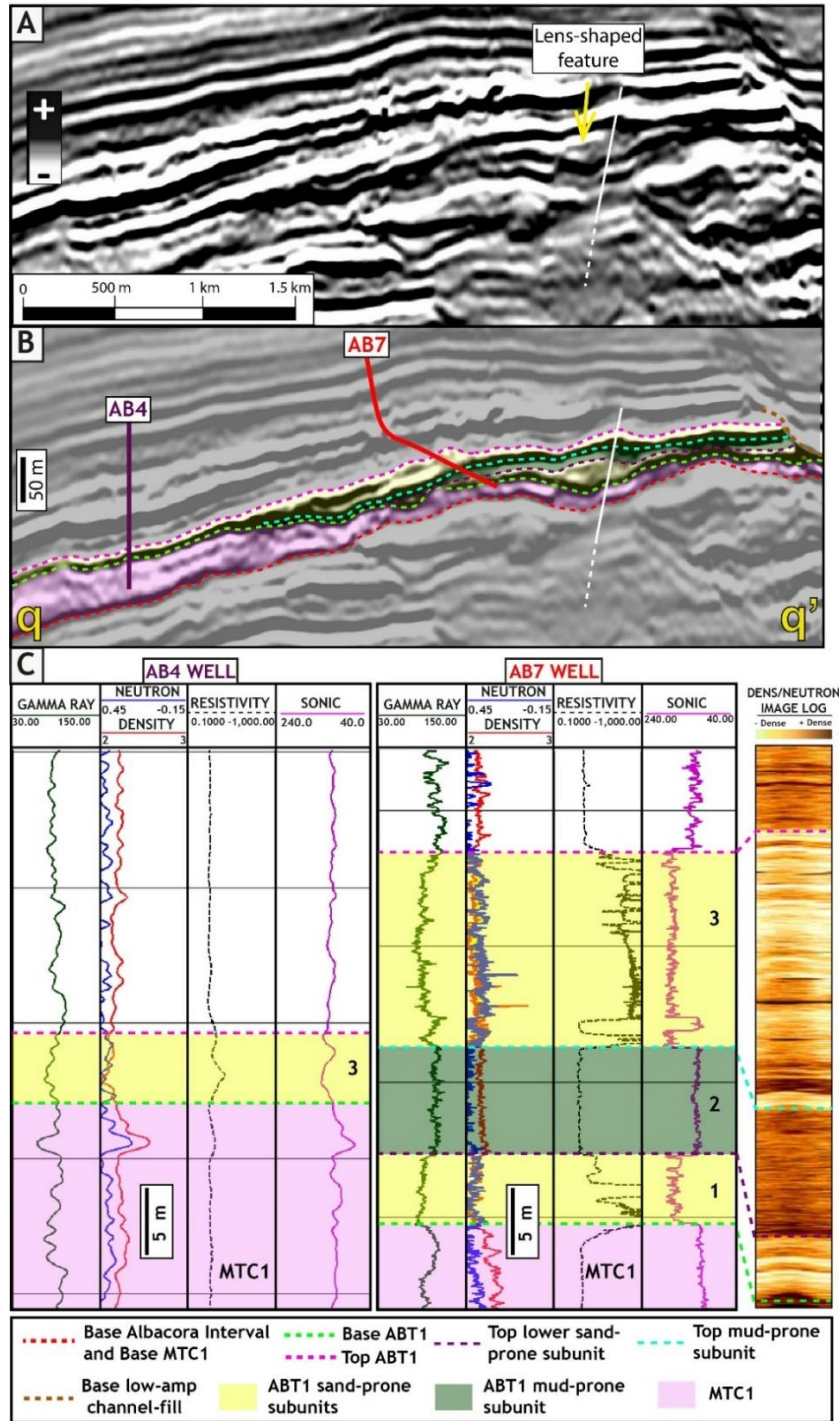
Figure 5.14: Stratigraphic subunits of ABT1 unit (lower sand, intervening mud and upper sand). A and B uninterpreted and interpreted seismic profiles, respectively (depth domain, 5x vertical exaggeration, higher resolution seismic volume, see location in Figure 5.11). A – Note the lens-shaped feature that coincides with the high thickness depositional axis. B- Seismic mapping of the internal stratigraphy of ABT1. C- Well log calibration of ABT1. The AB4 well intersects thin and mud-rich deposits at the pinch out zone of the upper sand subunit. The AB7 well intersects the edges of the main depositional axis. Note the finning upward trend suggested by the image log from the lower sand towards the mud-prone subunit.

5.5.5.2 Intervening mud-prone subunit

Description: Above the lower sand subunit (internal trough), there is an internal peak that varies in amplitude strength and continuity. Well calibration indicates this interval (from the trough to the peak) as mud-prone with thicknesses around a few metres (up to 8 m in well AB7, Fig. 5.14). The constant values in the well logs suggest a uniform lithology. This is supported by the image log, which shows a single lithological pattern that resembles fine-grained laminated facies (Fig. 5.14, see well AB7), differing from the lithological variability interpreted from the image log of MTC1 (Fig. 5.9). The extension of these fine-grained deposits is clear above the lower sand where the peak can be mapped more confidently. However, there is uncertainty of its occurrence in a larger area due to limitations on seismic resolution (Fig. 5.17-2).

Interpretation: The lithological character (i.e., laminated) of the mud-prone stratigraphic subunit suggests the deposition of fine-grained sediments by low-density turbidity currents, possibly combined with hemipelagics and, therefore, a phase of sand starvation.

5.5.5.3 Upper sand-prone subunit

Description: The last sand-prone subunit covers the whole ABT1 area and is mapped between the internal or basal peak (where the internal stratigraphic phases are absent) and the top ABT1 trough (Fig. 5.14). The thickness map displays a high thickness axis that widens down-dip. Increased thicknesses of the unconfined deposits are laterally offset towards the south (Figs. 5.14, 5.15B and 5.16B, see blue arrow) and extend basinward when compared to the lower sand subunit. Lateral to the main depositional axis up-dip, thicknesses are considerably reduced (Fig. 5.15B). Seismic reflections are mostly parallel but locally show some irregularities, which are attributed to the interactions of flows with the rugose top of the underlying MTC1. Well, log calibration shows a high sandstone percentage with blocky to bell log motifs in the axis, whereas serrated well logs reflect sand/mud intercalation towards the pinch-out zone (Fig. 5.14C).

Interpretation: The thick axis that widens down-dip suggests a weakly confined architecture, which is supported by lobate seismic geomorphology patterns at the distal part of the ABT1 unit (Fig. 5.11B), compatible with intraslope lobe deposits. The

location of the cores, with evidence for erosional flows (i.e., abundance of mud rip-up clasts), is consistent with thickness patterns that support a high-energy axis in the system. Isopach patterns that widen down-dip suggest a broad area of channel flaring in areas with minor to no gradient changes, similar to the channel-mouth expansion zones of Hodgson et al. (2022). Well calibration in the reflections that laterally pinch out from the thick depositional axis (Fig. 5.14 C) suggests interbedded facies that could represent the fringes of older lobes and/or external levees (Prélat et al., 2009; Hodgson et al., 2011; Hansen et al., 2015; Morris et al., 2016; Brooks et al., 2018a).
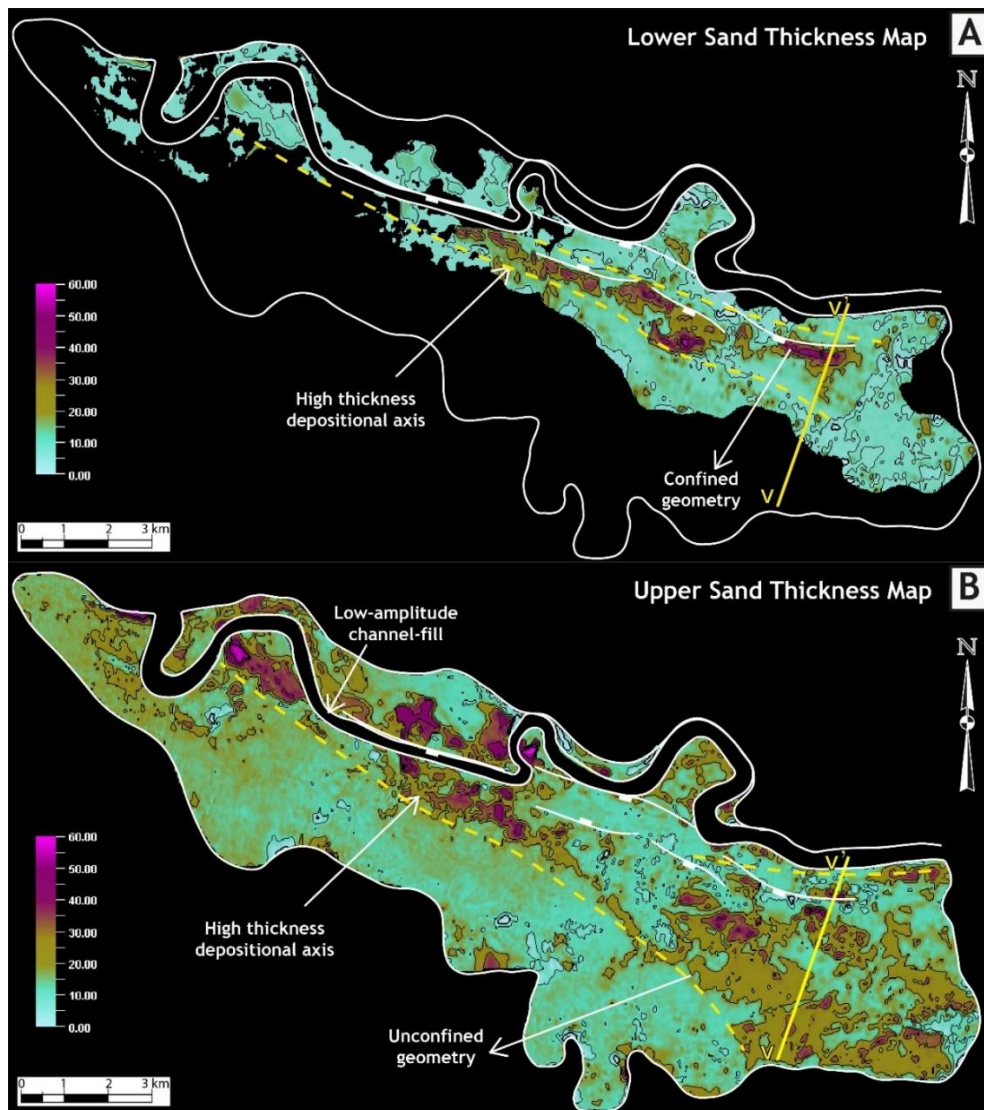
Figure 5.15: A- Thickness map of the lower sand subunit showing its restricted occurrence and elongate higher thicknesses suggesting confinement (marked by dashed yellow lines). B - Thickness map of the upper sand subunit showing elongate high thicknesses up-dip that pass down-dip to wide isopachs suggesting loss of confinement, marked between yellow dashed lines (see text for explanation).

5.5.5.4 Channelised phase and Incisional surface

Description: A low-amplitude channel-fill (Fig. 5.11B) represents the last stratigraphic phase of the ABT1 unit, which incises the older stratigraphic subunits. It is a through-going channel with sinuous and linear segments. Locally, the linear segments are bounded by faults (Figs. 5.11B, 5.12 and 5.17-4) that have the same orientation as the faults that edge the salt wall at the northern edge of the depocentre, to which the channel-fill is aligned (Fig. 5.11B). High-to-moderate amplitude features that resemble bend expansion deposits are laterally associated with sinuous segments of the low-amplitude channel-fill (Fig. 5.11B).

Interpretation: The large number of well intersections in the study area (Fig. 5.3C) and other Oligocene-Miocene turbidite units in the basin (Casagrande et al., 2022) support that low seismic amplitudes relate to high-mud content. Therefore, I interpret the channel to be filled with mud-prone deposits. Seismic mapping suggests the channel is filled with the deposits from the overlying MTC2; however, there are no well intersections within the channel-fill to confirm this interpretation. Seismic amplitudes in the sinuous segments suggest inner-bend sand-prone channel deposits (Peakall and Sumner, 2015) and, therefore, a phase of channel migration before the final incision. However, due to a lack of seismic resolution, the inferred channel deposits cannot be mapped separately from the deposits of the upper sand-prone phase.
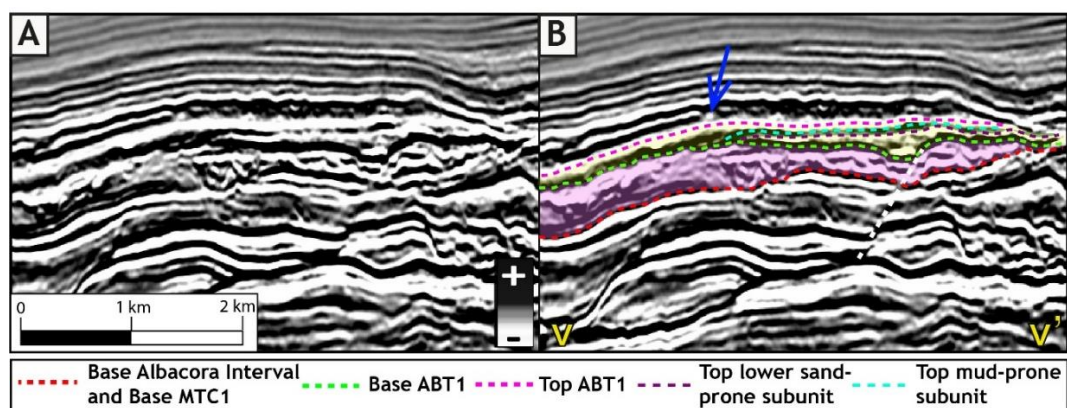
Figure 5.16: Stratigraphic subunits of ABT1. A and B uninterpreted and interpreted seismic profiles, respectively (depth domain, 5x vertical exaggeration, higher resolution seismic volume, see location in Figure 5.15). Seismic reflections of the lower sand support passive infill of negative topography, with no significant erosion. Note in B higher thicknesses of the upper sand towards the south (blue arrow, see text for explanation).
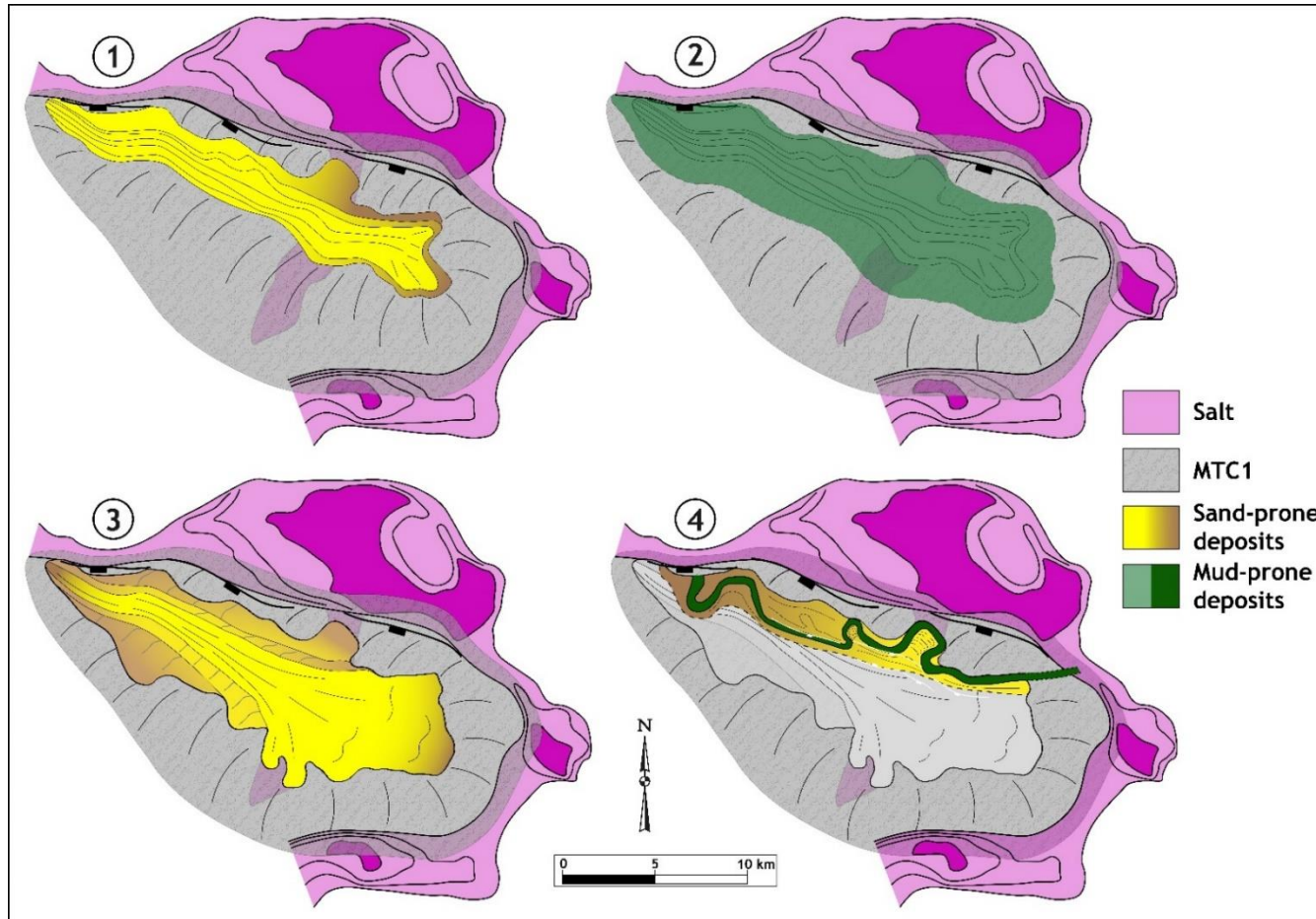
Figure 5.17: Stratigraphic evolution of the ABT1 unit. 1- Intraslope lobes of lower sand subunit deposited in elongate trough. 2 – Mud-prone subunit deposited above the lower sand and possibly in a wider area. 3- Upper sand subunit with high energy depositional axis that flares down-dip into lobate geometries. The upper sand extends towards the south and basinward. 4 – Channelised and incisional phase, marked by deposits cut by the low-amplitude channel-fill.

5.6 Discussion

5.6.1 Intraslope depocentres in the extensional salt domain – an overlooked type of depocentre

The Albacora depocentre is flanked by salt-cored structures that are primarily a product of extension during raft tectonics. These structures were buried since the Cretaceous but formed preferential areas for deformation during the Oligocene-Miocene, when complex slope topography was created by the contraction and normal faulting at the border of the prominent salt structure at the northern edge of the depocentre. A thick pre-kinematic stratigraphic section is recorded between the salt layer and the depocentre (Albian to Lower Oligocene strata). The subtle wedge-shaped stratal pattern towards the normal fault system (Fig. 5.2C) and thinning of strata above the inverted salt-cored structures at the eastern and southern edges of the depocentre suggest the evolution of an asymmetric (35 km long, 20 km wide) shallow depression, that deepened northwards, with relatively low deformation rates, similar to stepped slope profiles (e.g., Prather, 2003; Deptuck et al., 2012; Casagrande et al., 2022). This depression became more evident during the Miocene when the Albacora Interval turbidites were deposited. In contrast, minibasins are flanked by near seabed salt stocks or walls during their evolution, and are floored by thick salt (with eventually thin pre-kinematic strata and the salt can be welded with time, e.g., Prather et al., 1998, 2012b; Prather, 2003; Smith, 2004; Oluboyo et al., 2014; Jackson et al., 2020, do Amarante et al., 2021). Minibasins are characterised by high rates of subsidence, leading to ponded accommodation and bowl-shaped strata that eventually evolved into marked wedge-shaped strata (Rowan and Weimer, 1998; Jackson et al., 2020). In addition, they are generally smaller than the Albacora depocentre, varying from 5 km to 15 km in their axes (Prather et al., 1998, 2012; Wu et al., 2020; Rodriguez et al., 2021), and sometimes longer (more than 40 km) in elongate salt walled minibasins (e.g., Ge et al., 2020; Howlett et al., 2021; Oluboyo et al., 2014). Therefore, despite the similar elliptical shape compared to the classic minibasin and its association with salt flanking structures, there are substantial differences between the Albacora depocentre and minibasin-type depocentres.

The filling of the Albacora depocentre comprises mass transport deposits intercalated with sand-prone turbidite units, resembling the stratigraphic cyclicity described in salt-withdrawal minibasins (Prather, 1998; Doughty-Jones et al., 2019; Wu et al., 2020). MTCs in minibasins have been largely associated with sediment remobilisation from the active flanks (e.g., Prather et al., 1998; Madof et al., 2009, 2017; Doughty-Jones et al., 2017; Howlett et al., 2021), therefore, reflecting tectono-stratigraphic cyclicity. However, no evidence for this process is seen in the study area. MTC1 extends above the paleo-highs at the depocentre edges, albeit with some thinning. This observation, combined with the fact that in the extensional salt domain and during a mature phase of basin development it is unlikely that significant salt-related palaeo-highs form to trigger large mass failure events, support an external source for the MTC1 (e.g., regional MTDs of Doughty-Jones et al., 2019). In addition, the study area is located on the palaeo-slope, an area prone to recording externally sourced mass transport deposits. The repeated intercalation of mass transport complexes with turbidites within the Albacora Interval could indicate an allocyclic stratigraphic control, where the emplacement of MTCs is associated with the initial period of relative sea-level change (e.g., Posamentier and Kolla, 2003), and re-sculpting of the seabed topography to capture up dip sand supply. Although this is a possible interpretation, MTCs are triggered by many mechanisms, and more data would be needed to favour a particular hypothesis.

In summary, extensional intraslope depocentres, such as the Albacora depocentre, present several characteristics regarding basin configuration, stratal patterns and filling that differ from intraslope depocentres formed in transitional or contractional salt domains, such as the classic minibasin types. They directly reflect their position and evolutionary stage in the basin, recording modest deformation rates but a complicated deformational history that can involve the interaction of contrasting deformational styles.

5.6.2 Controls on accommodation within the Albacora depocentre

5.6.2.1 The role of salt-related slope deformation

The salt structures at the edges of the carbonate raft have a clear control on regional accommodation patterns, and the Oligocene-Miocene strata deposited in the Albacora

depocentre (Fig. 5.2). MTC1 was deposited over a larger area, despite the magnitude of the underlying salt-cored structures and preferential deep-water sand-prone deposition towards the North. The thinning of MTC1 above these structures suggests that it largely smoothed the salt-related seabed relief and that the top of MTC1 had a broadly flat upper surface immediately after deposition. However, by the time the overlying sand-prone turbidite system of the ABT1 unit developed, a trough-shaped intraslope depocentre within the Albacora depocentre had developed parallel to the large WNW-ESE oriented salt structure at the northern edge. Assuming an initially flat top to the MTC1, the subsequent depocentre was 24 km long and 10 km wide, and formed surface relief of at least 70 m, with deepening towards this structure.

Within the Albacora depocentre, the thinning of MTC1 above the inverted graben suggests that this structure formed a seabed high. Uplift of the high after emplacement could have led to erosion to explain the thickness variations. However, the apparent low variability of seismic facies at the flanks of the inverted graben does not suggest subsequent remobilisation, which could be seismically detected considering the 40 m difference between thick and thin areas of the MTC1 (Fig. 5.5). Therefore, during the MTC1 emplacement the inverted graben had a positive seabed expression (Fig. 5.18). In contrast, the ABT1 deposits thicken where the mass transport deposits thin (Fig. 5.11A). The pattern of reflections does not support thickening due to incision but rather passive infill of negative topography (Fig. 5.16). Therefore, I interpret that this structure controlled accommodation during the ABT1 unit (Fig. 5.11A, see white dotted line and Fig. 5.18). From these observations, it is here proposed that the area of the inverted graben underwent a transient phase of subsidence after the emplacement of MTC1. The subsequent thinning of the MTC2, the ABT2 unit and younger strata above the inverted graben suggests renewed uplift after unit ABT1 (Fig. 5.5A). Consequently, this structure had a predominant uplifting trend during the deposition of the Albacora Interval, which was temporarily reversed after MTC1 emplacement. Below MTC1, constant thicknesses of the Paleogene section in the area of the inverted graben suggest that the structure had not yet inverted (Fig. 5.18-0), and the development of slope valley systems suggests an intraslope depocentre had not developed. Considering that the large-scale salt-related topographic controls on sedimentary routeing and accommodation during the slope valley systems were the same as those operating during ABT1 deposition (i.e., northward lateral tilting towards fault system),

I interpret that deformation was enhanced in the area of the salt ridge underlying the present-day N-S inverted graben following MTC1 deposition, which had a key role on differential subsidence within the Albacora depocentre during ABT1 (Fig. 5.18-3).

The generation of the trough could be explained by a transient phase of salt-related extension after MTC1 emplacement during a longer-term contractional period (Fig. 5.18) that led to the inversion of structures. Evidence for these co-existing, yet contrasting, deformational styles can be observed in the prominent salt wall at the northern edge of the Albacora depocentre, which is bounded by normal faults, a product of extension or transtension. In the Campos Basin, both deformational styles are documented to alternate through time in the multi-phase (transitional) domain, where salt structures can develop through hybrid extensional-contractional evolution (do Amarante et al., 2021). Although the study area is interpreted to sit at the distal end of the extensional salt domain, local complexities associated with relief on the base of the salt surface and tectonic reactivation of the basement fabric can alter the salt flow and impact patterns of salt-related deformation (e.g., Fetter, 2009; Evans and Jackson, 2020; do Amarante et al., 2021). Folding and inversion of extensional structures above basement highs are documented during the Neogene in the Campos Basin, and interpreted to reflect transpression (Fetter, 2009). Therefore, the boundaries where deformational regimes can occur are not fixed. Regionally, the contraction could also reflect landward migration of the contractional front that propagated from the distal domain where the salt thickens (e.g., Brun and Fort, 2004). This applies also for the inverted salt-cored structures at the edges of the Albacora depocentre. Lateral shortening has been documented to concentrate on previous salt structures (Jackson and Hudec, 2017), as observed here. Transient extension could be associated with a period of reduced contraction, which was focused on existing salt-cored structures, like the salt ridge in the area of the inverted graben. Given the observations and previous work, I interpret that alternating contraction and extension deformation was in operation across the study area, affecting preferentially existent salt structures, like the inverted graben that acted as a weak zone within the rigid carbonate raft, prone to concentrate strain under a variable remote stress field controlled by salt tectonics. The mechanisms controlling deformation can be explained by different processes that are not addressed here since a regional structural analysis

is needed in order to understand all the variables involved in the deformation history of the Albacora depocentre.

5.6.2.2 The role of MTC1

MTC1 is a large instantaneous event that re-configured slope topography prior to the deposition of the ABT1 unit. There is a clear control of the present-day inverted graben structure on the deeper parts of the trough, where the lower sand of ABT1 was deposited. However, increased thicknesses of the upper sand are recorded at the distal part of the trough (Fig. 5.15B), where the inverted graben structure had a minor influence, and the MTC1 is thicker (Fig. 5.6A). In this area, I propose that the MTC could have enhanced compaction of the underlying, still soft and water-saturated sediments, inducing differential subsidence (Fig. 5.18-4,5). Furthermore, the instantaneous weight of the large MTC1 above salt-cored structures could have accelerated salt tectonic deformation rates, and impacted large-scale accommodation patterns, aiding in the development of the ABT1 depocentre. This contrasts with flank-derived MTCs recorded in minibasins, which are a consequence of slope deformation, and not the cause. The change in geomorphological patterns of the turbidite systems from Paleocene slope valley systems to the intraslope depocentre of ABT1 suggests that the amount of relief on the seabed and the rate of deformation increased dramatically immediately after the MTC1 emplacement, supporting the hypothesis that MTC1 contributed to accommodation patterns.

Load-driven subsidence has been proposed as an important mechanism in the formation of minibasins (Prather et al., 1998; Prather, 2003), especially in their mature evolutionary phase, when the average density of the basin fill becomes higher than the salt (Hudec et al., 2009). Minibasins form above thick salt layers. In the Albacora Depocentre, the salt is thin and at depth during ABT1 deposition, therefore, I do not envisage a density-driven subsidence mechanism similar to minibasins. Nevertheless, there is active salt tectonics during the evolution of the Albacora Interval meaning that the salt is still mobile, with reactivation of salt-rooted faults up to shallower levels. Therefore, I interpret that MTC emplacement enhanced fault reactivation and drove a transient and local increase in subsidence rate. Accommodation generation associated with relief and rugosity of the top surface of mass transport deposits has been reported in the literature (Kneller et al., 2016; Brooks et al., 2017; Ward et al.,

2018; Martínez-Doñate et al., 2021). However, this is the first time load-driven accommodation related to MTC emplacement is proposed.
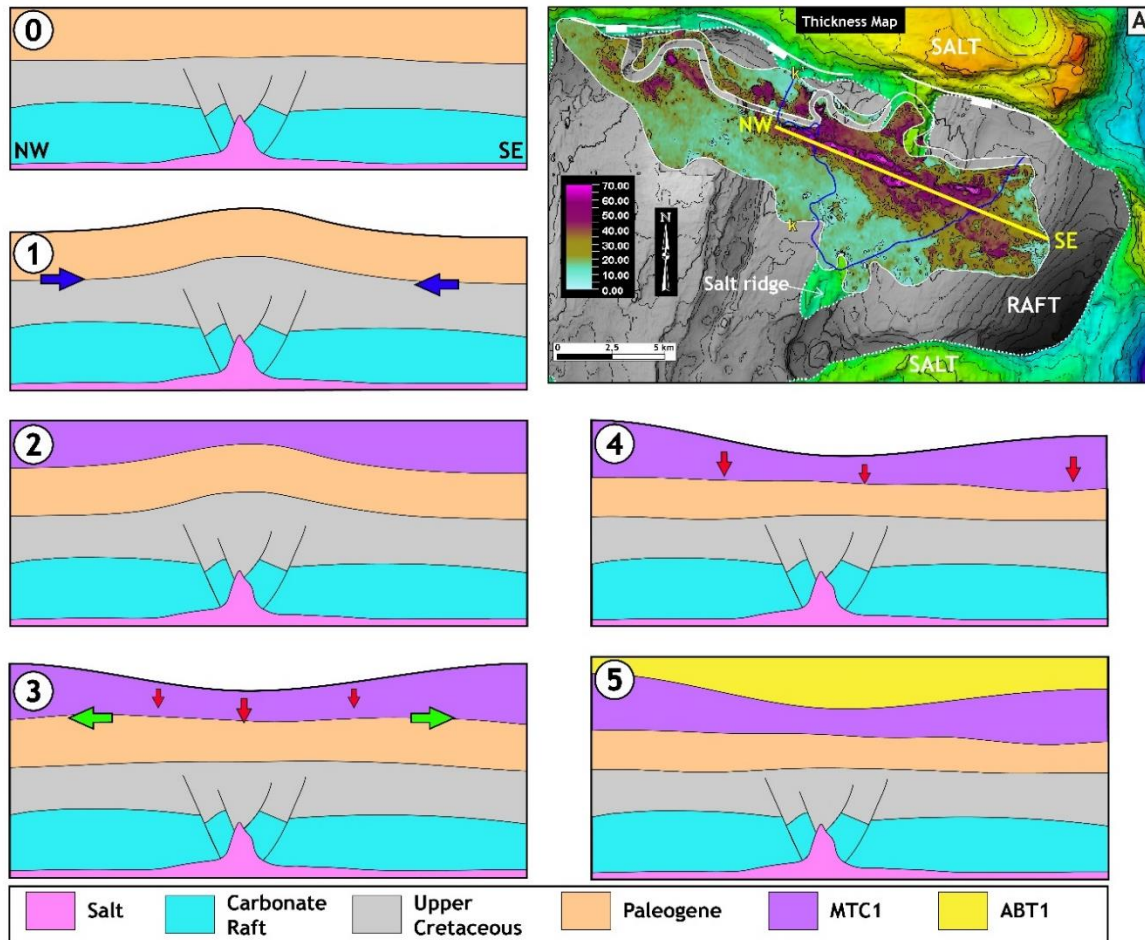
Figure 5.18: Alternating contraction and extension within the Albacora depocentre shown in dip geological sections crossing the area of the present-day inverted graben. See location of geological section in the thickness map (blue polygon indicates influence radius of the present-day inverted graben). 0 – Contraction not yet active during the Paleogene. 1 – Onset of contraction (blue arrows) and generation of positive relief on the seafloor. 2 – MTC1 emplacement and healing of long-wavelength topographic irregularities. 3 – Phase of transient extension (green arrows) affecting the area of the inverted graben and leading to increased subsidence above this structure (red arrows). Initial configuration of the trough. 4 – The MTC1 weight induces differential compaction and subsidence and alters accommodation patterns (red arrows), especially in areas where MTC1 is thicker. The final configuration of the trough is formed. 5 – Deposition of ABT1 turbidites (see text for explanation). Figure not at scale. The salt structure remains static in the geological sections, however differential deformation might have occurred.

5.6.3 Evolution of ABT1 unit

The ABT1 unit comprises the previously described stratigraphic subunits (Figs. 5.17 and 5.19). The restricted occurrence of the lower sand-prone subunit suggests that the volume of sediments brought in by the initial flows was not enough to infill the broader depocentre, and flows were concentrated to the lower parts of the trough (Fig. 5.19-1), which is here interpreted to be mainly controlled by differential subsidence in the area of the inverted graben. The fact that there is no clear evidence of significant sediment bypass and channel incision at the distal end of the lower sand-rich subunit supports the interpretation that accommodation was not healed; therefore an incomplete fill-and-spill cycle is inferred. The reduction of coarse sediment supply is supported by the overlying mud-prone subunit (Fig. 5.19-2). Therefore, the lower sand and the mud subunit reflect either an externally driven waxing and waning sediment supply cycle controlled by allogenic forcing (rising relative sea level, climate, e.g., Deptuck et al., 2003; Covault and Graham, 2010) or, alternatively, could record an up-dip avulsion (e.g., Prather et al., 1998; Sinclair and Tomasso, 2002). As the same sedimentary route is re-occupied during the deposition of the upper sand, and the well logs suggest a finning upwards trend from the lower sand to the mud subunit, therefore, not an abrupt facies transition as expected in avulsions, the hypothesis of allogenic control is here favoured.

The upper sand subunit records a renewed supply of coarse sediment deposited in a broader area than the lower sand subunit (Fig. 5.19-3). Higher thicknesses in the distal area that are laterally offset and extend further down-dip from the elongate depositional axis of the lower sand subunit suggest a down-dip lateral shift and progradation of the system. This lateral offset is attributed to uneven accommodation distribution, recording the interplay of different controls on accommodation generation (the MTC1 control and salt-related, see Fig. 5.18-4,5).

The lateral migration and deep incision observed in the low-amplitude channel-fill support that accommodation was healed in the depocentre, and that sediment gravity flows could spill basinward. Although the stratigraphic trend of the upper sand points to the southward migration of the system, this younger channel supports a northward shift in sediment dispersal patterns, aligned with the depocentre margin (Fig. 5.19-4). The deposits with bend expansion features suggest a phase of sand-prone channel

migration prior to the low-amplitude channel-fill, which might be plugged by the overlying MTC2. Channel deposits in the healing phase of intraslope depocentres, and prior to incision, have been related to a relative increase in the slope gradient within the depocentre, as entering flows are able to remain channelised (e.g., Barton et al., 2012). The lateral extent of these deposits is uncertain, although their location points to increased accommodation in the north. It is not clear whether the final channel propagated basinward or evolved through headward erosion after the depocentre was filled. Due to the lateral migration, sinuous sections, and consistent cross-sectional dimensions, a scenario where the channel propagated basinward as a slope channel is favoured rather than propagation through headward erosion.

In all stratigraphic phases, I interpret that the sand-rich flows used a similar entry point to the trough (Fig. 5.19). While pre-existing variation in accommodation explains the divergence in sediment dispersal patterns between the two sand-prone subunits, the position of the low-amplitude channel-fill could be explained by lateral tilting towards the fault system in the north. Alternatively, this could be through later differential subsidence along the inverted graben area, which acted as a zone of weakness where the salt structure underneath is connected with the main salt wall at the northern edge of the depocentre. The high sinuosity bend that the channel forms just above this area is additional support for this model (Fig. 5.19).
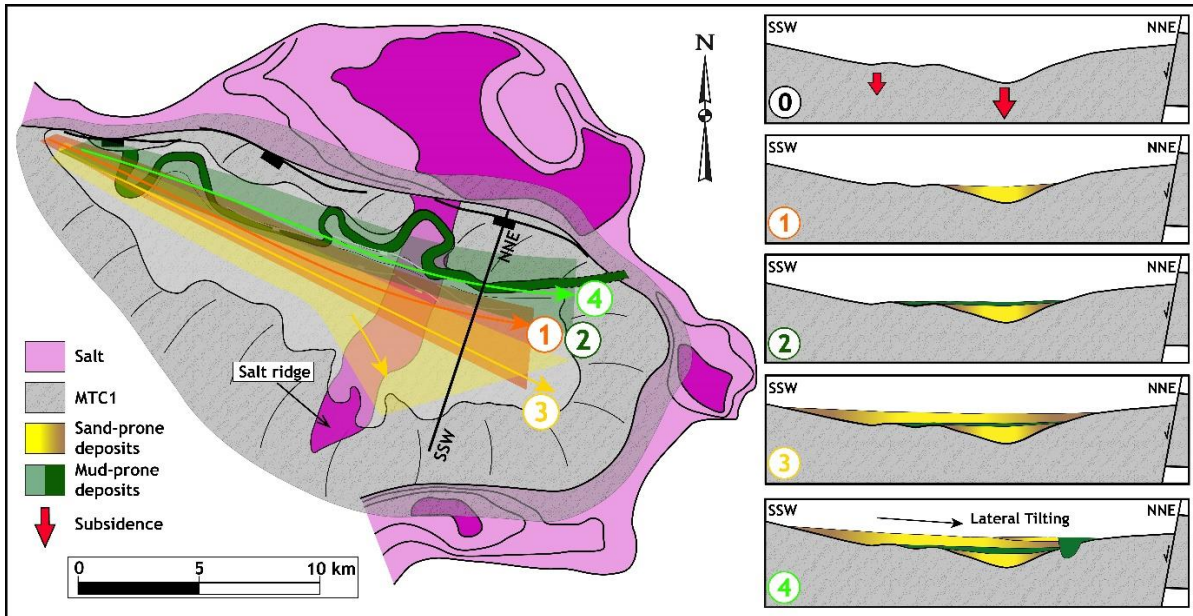
Figure 5.19: Map to show the reconstructed sediment dispersal patterns in each stratigraphic phase of ABT1. The cross sections show the ABT1 trough filling overtime. 0 – Differential subsidence in the area of the inverted graben generates uneven accommodation in a zone above and surrounding this structure, MTC1 also has an impact. 1 – The deeper parts of the trough are filled by the lower sand subunit. 2 – Deposition of fine-grained deposits of the mud-prone subunit. 3 – Deposition of the upper-sand subunit, healing accommodation space. Shift of sediment dispersal patterns towards the SSW is recorded in high thicknesses in that direction. 4 - Lateral tilting towards NNE shifts sediment dispersal patterns. A phase of channel deposition is followed by a final incision and bypass. The bypass channel is later filled by mud-prone deposits (see text for explanation).

5.7 Conclusions

This study uses 3D high-resolution seismic reflection data calibrated by wells to investigate the fill of an intraslope depocentre (Albacora depocentre) with tectonic-stratigraphic evidence for contemporaneous and alternating extensional and contractional displacement in the extensional salt domain of Campos Basin. The main findings of this study are:

- The Albacora depocentre evolved during a mature passive margin stage, and its external configuration was controlled by syn-depositional reactivation of salt-cored structures at depth, at the edges of a carbonate raft. This reactivation was by extension/transtension and contraction, which formed positive seabed topography at the flanks of the depocentre.

- Large-scale stratal patterns within the Albacora depocentre reflect increased subsidence towards the North during the Oligocene and Miocene, controlled by a major salt wall bounded by normal faults. A subtle wedge-shaped stratal pattern suggests modest rates of slope deformation, forming a large, shallow, and asymmetric depocentre.

- The characteristics of the Albacora depocentre differ from salt-withdrawal minibasins, reflecting its position, evolutionary stage in the basin and configuration and activity of salt structures.

- Alternating salt-related contraction and extension is interpreted to control accommodation patterns within the Albacora depocentre. The change in thickness patterns, from uniform thicknesses of the slope valley systems to the thinning of mass transport complexes above a N-S oriented graben, supports inversion of this structure. The formation of a through with intraslope lobes deposition above the MTC1 supports subsequent transient extension in the same site, inducing subsidence.

- The instantaneous weight of the MTC1 is interpreted to have increased subsidence rates by compaction and amplification of ongoing salt-related slope deformation, which impacted accommodation patterns during the deposition of ABT1 unit by forming a pronounced trough.

- The stratigraphic cyclicity within the ABT1 unit, with a sand-prone turbidite phase followed by a mud-prone phase, is interpreted to reflect a sediment supply cycle with an allogenic control, preserved within the trough.

- The abrupt shift in dispersal patterns in the last phase of ABT1 evolution, which is marked by channel incision, is interpreted to reflect fill-and-spill of the trough and lateral tilt of the slope towards the North controlled by salt-related deformation.

Chapter 6 - Synthesis and recommendations for future research

In this chapter, the research questions presented in Chapter 1 are addressed, referencing the results presented in Chapters 3-5 to provide discussion and synthesis to the research outcomes. Recommendations for future research are addressed at the end of this chapter.

6.1 How can the interplay of different stratigraphic controls on the record of deep-water systems deposited above mobile slopes be deciphered?

The stratigraphic record of all depositional systems, from continental to deep marine, reflects a complex interaction of controls. Large-scale changes in environmental conditions will produce distinctive stratigraphic signatures (e.g., Hajek and Straub, 2017), which are typically associated with extra-basinal controls, for instance, global scale sea-level variations (see Chapter 1). However, high-resolution stratigraphic analysis, makes disentangling extra- and intra-basinal controls difficult. Extra-basinal allogenic forcing is usually translated in sediment supply cycles (e.g., Kneller, 2003; Hodgson et al., 2011). However, recognising their stratigraphic expression is particularly challenging in areas with topographic control, such as in intraslope depocentres, where gradient variations affect the behaviour of sediment gravity flows, triggering erosion or deposition, and modifying the style of deposition (Kneller et al., 1999).

6.1.1 Extra-basinal allogenic forcing – study area context

This thesis investigates strata deposited in a passive margin setting in a tropical Southern Atlantic Ocean during the Oligocene-Miocene. This interval is part of a global long-term cooling trend that initiated in the Eocene-Oligocene transition, when the Antarctic ice sheet was established, which marked a significant climatic change from greenhouse to icehouse conditions (e.g., Miller et al., 1991; Lear et al., 2008). Within this cooling trend, the Oligocene-Miocene transition is interpreted as a transient global cooling event associated with a large-scale expansion of the Antarctic ice sheet (e.g.,

Lear et al., 2004; Beddow et al., 2015). Therefore, the study interval of this thesis coincides with an important climatic oscillation in a broader icehouse period.

Icehouse periods are marked by the growth and decay of ice sheets, which induce glacio-eustatic fluctuations with the potential to control sediment supply cycles (e.g., Mitchum and Vail, 1977; Haq et al., 1987; Miller et al., 1991). Oxygen isotopes suggest fluctuations in the Oligocene ice sheet in short (<0.5 Myr) and long (2-3 Myr) timescales, and in short periods (200-300 Kyr) during the transient expansion of the Antarctic ice sheet in the Oligocene-Miocene transition (Lear et al., 2004). The glacio-eustatic variation at the beginning of the Oligocene icehouse is interpreted to represent a more than 50 m sea-level fall, and the Oligocene-Miocene transition a larger fall of approximately 130 m (Miller et al., 2020). Therefore, the magnitude and time-scale of these glacio-static fluctuations support significant high-frequency climatically driven sea-level oscillations during the study interval in the Campos Basin. In addition, sedimentary environments in passive margins with broad shelves are particularly responsive to sea level variations (Covault and Graham, 2010). The mineralogical and textural maturity of the Oligocene-Miocene turbidites of Campos Basin presented in Chapters 3-5 support long distances between the source area and the sink (e.g., Fetter et al., 2009). Together with the physiography at the time (broad shelves), this means that the glacio-eustatic variations could control sediment supply cycles, resulting in pronounced changes in sedimentation patterns during this time of the basin's history. Therefore, the study area and stratigraphic interval presented in Chapters 3-5 are prone to record high-frequency climatic stratigraphic cyclicity.

6.1.2 Extra and intra-basinal allogenic forcing expression in intraslope depocentres

The fill-and-spill model has been used to explain the stratigraphic evolution of intraslope depocentres with different levels of confinement worldwide, including minibasins (Winker, 1996; Prather et al., 1998; Beauboueff and Friedmann, 2000; Sinclair and Tomasso, 2002; Smith, 2004) and stepped-slopes (Adeogba et al., 2005; Barton, 2012; Jobe et al., 2017). The model predicts that stratigraphic evolution in complex topography will reflect the filling of accommodation (i.e., ponded to bypass facies assemblage of Prather et al., 1998) and, therefore, a progressive slope grading.

Nevertheless, this widely applied model does not capture varying rates of deformation and sedimentation during the evolution of intraslope depocentres. The final stratigraphic signature in these sites will reflect not just changing accommodation but also sediment supply cycles and autocyclic changes. Therefore, intraslope depocentres on mobile slopes are ideal sites to investigate the interaction between extra and intrabasinal allogenic controls and local sedimentary dynamics.

In Chapter 3, the Marlim Unit comprises several fill-and-spill cycles that evolved above a stepped-slope profile. Each cycle comprises a sand-prone turbidite phase, with remnant lobe deposits followed by erosionally confined channel-fills in step 1, and distributary channels or lobe complexes on step 2 (Figs. 3.5, 3.8, Chapter 3). Both steps are incised by throughgoing bypass-dominated channels. Slope deformation with salt-related lateral tilting controls three-dimensional accommodation patterns that result in cycles that are laterally associated and not vertically stacked (Fig. 3.13, Chapter 3). The filling/bypass/abandonment trend could purely reflect gradient healing and down-dip migration of the system in each cycle, as recognised by the classic fill-and-spill model. Nevertheless, the repetition of these cycles in the Marlim Unit suggests an allogenic cyclical external control. In addition, the late filling of the bypass-dominated channels, partially by sandstone down dip, and laminated mudstones up-dip, supports decreasing flow magnitude as the channels backfilled (Fig. 3.14, Chapter 3; excluding the Marlim Sul Channel, which has a more complex story, see Chapter 4 and the next section). This filling pattern is compatible with a strong control on the stratigraphic record by externally-driven sediment supply cycles, with the filling of the channel representing the waning phase of the cycle, while the filling of the step could record the waxing phase. Nevertheless, a bypass-dominated phase precedes the filling of the channel, suggesting that the whole expression of the sediment supply cycle is not preserved in the area; therefore, there is a bypass gap in the stratigraphic record. Most of the sediment bypass occurred when sedimentation rates outpaced deformation rates, and this ideally coincides with the end of the waxing phase and the beginning of the waning phase (Fig. 3.14, Chapter 3). Therefore, this bypass gap might represent this phase in the sediment supply cycle and is explained by erosional processes coupled with sediment bypass acting towards a graded profile, as predicted by the fill and spill model (e.g., Pirmez et al., 2000, Fig. 6.1).

In Chapter 5, the Albacora Turbdite 1 unit (ABT1) has a similar scale in terms of thickness, area and seismic expression (a few seismic reflections) to the Marlim Unit (Figs. 5.3, 5.11, 5.12, Chapter 5). The ABT1 unit comprises a basal sand-prone turbidite subunit that passively infills the deepest part of an elongate depocentre and is overlain by a relatively thick and seismically mappable laminated fine-grained interval interpreted as low-density turbidites and hemipelagics (Fig. 5.14, Chapter 5). The lack of evidence for bypass-dominated channels in this basal interval supports the notion that accommodation was not healed after sand deposition, and no spillover phase started. The sand- and mud-prone facies are interpreted to record a waxing-to-waning sediment supply cycle. Therefore, facies stacking primarily records extra-basinal allogenic controls, although the shape of the turbidite unit is controlled by the pre-existent depocentre geometry (intrinsic control). A second cycle in the ABT1 unit refers to a larger sand-prone subunit, comprising submarine channels that flare into lobate features, followed by a phase of channelisation that culminates with a deep channel incision that exits the depocentre (Fig. 5.17D, Chapter 5). This channel is interpreted to represent a bypass-dominated phase after the depocentre was healed, suggesting that accommodation evolution in a complex topography controlled the stratigraphic signature, as predicted by the fill-and-spill model. In summary, the basal cycle of the ABT1 unit records a high-frequency sediment supply fluctuation that was externally controlled, whereas the top cycle is a fill-and-spill cycle that records topographic grading.

A lower frequency, stratigraphic cyclicity can also be interpreted in the Albacora Interval (Chapter 5), which comprises two packages of MTCs overlain by turbidite units (MTC1+ABT1, MTC2+ABT2, Fig. 5.3, Chapter 5). At the onset of a relative sea-level fall, a reduction of the water column causes upper slope instabilities due to increased pore pressure within the sediments, increasing the risk of mass failure (e.g., Posamentier and Kolla, 2003; Catuneanu, 2006). The rapid progradation of deltas to the shelf edge during continued relative sea level fall induces increased siliciclastic input to deep-water and the establishment of turbidite systems (Posamentier and Kolla, 2003). The mud-prone composition of the basal MTC1 suggests an upper slope source, and its considerable dimensions support a trigger that acted across a large area of the slope, such as glacio-eustatic sea-level fluctuations, present during the Oligocene-Miocene. The repeated succession of MTCs and turbidites suggests

stratigraphic cyclicity, with each pair of MTC and turbidite recording the falling relative sea-level and concomitant increase in sediment supply (Fig. 6.1, forced regression of Catuneanu, 2006 and Catuneanu et al., 2009). Nevertheless, the second MTC2 is thinner and smaller and controls other than sea level fluctuations cannot be discarded (Wu et al., 2020). Despite the likelihood of an evolutionary link between MTC1 and ABT1 and the sea-level variation curve and, therefore, an extra-basinal allogenic control, the external geometry and evolution of the ABT1 turbidite unit are clearly influenced by a topographic configuration within the Albacora Depocentre. Salt tectonics and differential compaction associated with the MTC1, both intra-basinal allogenic factors, controlled accommodation creation and depositional architecture within an elongate trough.

The findings of this thesis support the propensity of stepped-slopes to preserve stratigraphic cyclicity controlled by the evolution of accommodation (fill-and-spill cycles), which has been proposed in the literature (Meckel et al., 2002; Prather et al., 2003; Barton, 2012; Deptuck et al., 2012; Hay, 2012; Brooks et al., 2018a). However, the expression of waxing-to-waning sediment supply cycles is also recognised, although with a gap in the sediment supply curve. The interplay of sediment supply cycles and rates and style of slope deformation in stepped slopes has only been shown in high-resolution studies based on outcrops (e.g., Brooks et al., 2018a), and this thesis shows this for the first time in a subsurface dataset.

The comparative analysis between stepped-slopes and minibasin stratigraphic patterns suggests that waxing-to-waning sediment supply cycles will have distinctive expressions in different types of intraslope depocentres depending on the confinement level and deformation rates in relation to sedimentation rates. High deformation rates in minibasins inhibit sedimentary bypass, at least during the ponded phase. For this reason, high-frequency cycles in minibasins tend to preserve better facies transitions and sedimentary trends attributed to extra-basinal allogenic signal, like fining upward trends and changes in facies and architectural style (e.g., Rowan and Weimer, 1998; Beaubouef and Friedmann, 2000, Fig. 6.1).

At a depocentre scale, steps will record evidence for sedimentary bypass during multiple evolutionary phases (Chapter 3, Deptuck et al., 2012; Hay, 2012), while minibasins will record higher frequency of sedimentary bypass at the healing phase (bypass facies assemblage of Prather et al., 1998, healed slope accommodation of

Prather, 2003). Therefore, in general, identifying the extra-basinal allogenic signals will be more challenging in weakly-confined depocentres with reduced accommodation, factors that favour sediment bypass. However, the high rates of deformation and steep flanks of minibasins favour mass failure, inducing widespread deposition of locally sourced mass transport complexes (e.g., Madof et al., 2009, 2017; Wu et al., 2020), which will also make "signal reading" difficult.
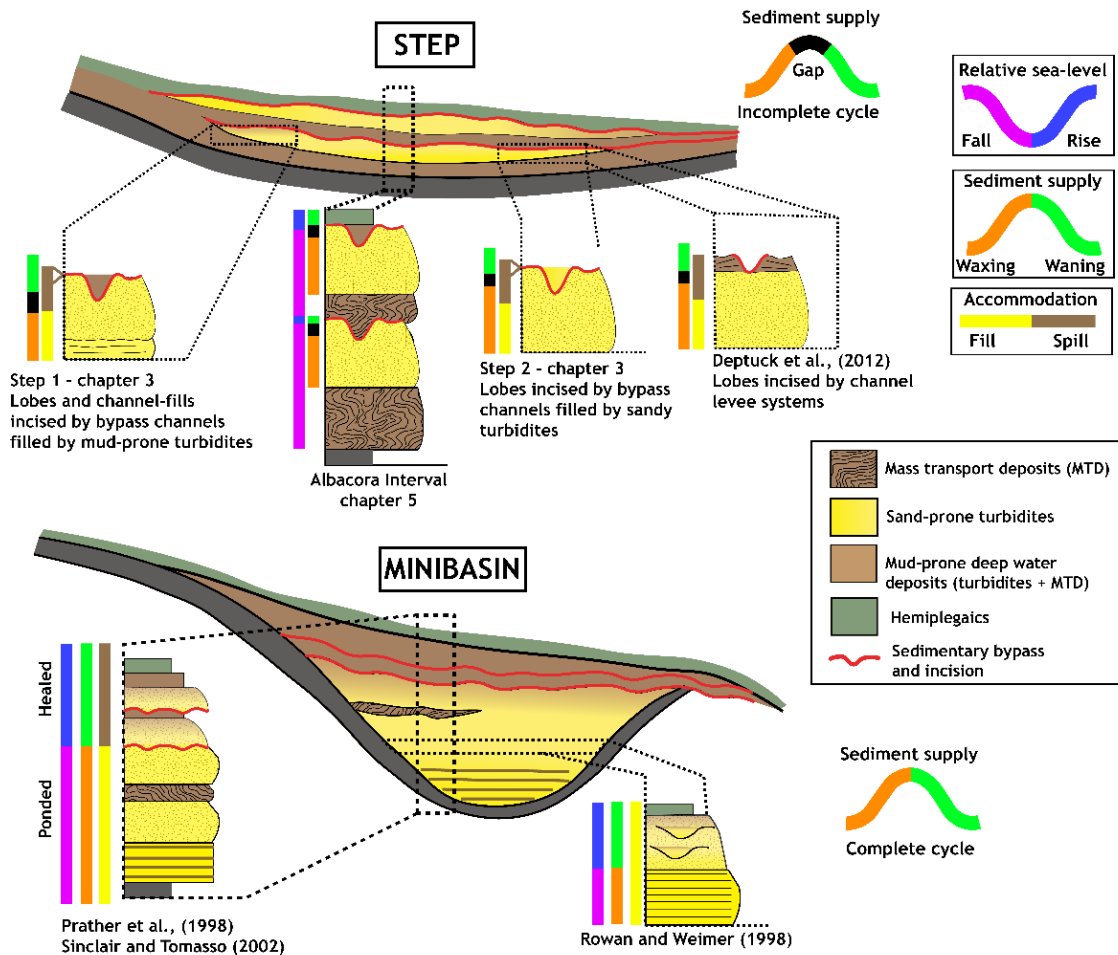
Figure 6.1: Stratigraphic cyclicity in steps and minibasins at the depocentre scale and high frequency cycles. In the step, sediment bypass is common at the end of the high-frequency fill-and-spill cycles, which reflects the evolution of accommodation. Sediment supply cycles are also identified concomitant to fill-and-spill dynamics, however, these will not be totally preserved due to a bypass gap (see text for explanation, note black area in the sediment supply curve and bars). On the contrary, ponded high frequency cycles/sequences in minibasins do not show evidence for bypass and can preserve most of the sediment supply curve. For more details on literature examples check section 2.1.3.2 in Chapter 2.

6.1.3 Extra and intra-basinal allogenic forcing expression in submarine channels

The evolution of submarine channels reflects an evolving equilibrium profile, which controls accommodation, and is affected by extra- and intra-basinal allogenic forcing (e.g., Pirmez et al., 2000; Kneller, 2003; Kane et al., 2010; 2012; Jobe et al., 2015). The Marlim Sul Channel (MSC, chapter 4) is a deeply incised channel, with patterns of incision and abrupt longitudinal thickness changes that do not conform to the stepped-slope configuration active during the deposition of the lobe deposits cut by the channel (Fig. 4.2, Chapter 4). This discrepancy is explained by a basinward tilting that altered the slope gradient, uplifting the proximal slope area prior to, or during, the inception and evolution of the Marlim Sul Channel (MSC). High levels of incision indicate that the flows had enough erosive power to respond to the topographic changes. The erosive power of a turbidity current is influenced by flow magnitude (volume), grain size distribution (density) and velocity (Hansen et al., 2015), which is highly impacted by slope gradient (e.g., Komar et al., 1971; Garcia and Parker, 1993). Higher magnitude flows with a higher concentration of coarse grain-size fractions would be expected in the waxing phase of a sediment supply cycle (e.g., Kneller, 2003; McHargue et al., 2011). Therefore, although incision patterns were controlled by the slope deformation style that increased the slope gradient, it is likely that channel incision itself was possible because the flows had enough volume, density and velocity to cut through the uplifting slope. Therefore, a possible interpretation is that the incisional phase of the MSC records the interplay of extra and intra-basinal allogenic controls (waxing phase of sediment supply with slope basinward tilting).

A unique characteristic of the MSC channel is its highly rugose longitudinal basal surface with scours and knickpoints associated with structural control (Figs. 4.4, 4.6, Chapter 4). The depositional phase of the MSC is marked by passive vertical aggradation of homogenous structureless sand-prone packages formed by rapid deposition of high-density flows with low erosive power (Figs. 4.5, 4.6, Chapter 4), intercalated with highly preserved fine-grained packages, with a main mud-prone interval that calibration with well data shows longitudinal continuity (Upper Mudstone Package, Chapter 4, Fig. 4.6). The preservation of the rugose basal surface and the filling style are unusual for submarine channels, which are typically marked by longitudinally smooth basal surfaces with lag deposits that represent long-term erosion

and sediment bypass during a waxing sediment supply, with filling characterised by scouring, several cut and fill phases, longitudinal backfilling pattern and a finning upwards trend related to gradual channel abandonment in a waning sediment supply (e.g., Mutti and Normark, 1987; Posamentier and Kolla, 2003; McHargue et al., 2011; Hubbard et al., 2014; Fig. 6.2). Due to the fact that most of the deposition occurs during the waning phase of the cycle compared to erosion during much of the waxing phase, in a typical submarine channel, a waxing to waning cycle will appear highly asymmetrical (McHargue et al., 2011) (Fig. 6.2).

The preserved rugose basal surface and the stratigraphic pattern of the MSC fill indicate a rapid switch from erosional to depositional processes, which prevented channel base smoothing and could be caused by changes in flow properties or slope deformation, the latter preferred in the active salt-tectonics scenario interpreted in the area (see discussion in Chapter 4). Channel deposition could have been occurred during the whole sediment supply cycle, and not necessarily preferentially during the waning phase, as in a typical channel (Fig. 6.2). Therefore, it is uncertain to link the channel filling phase with a stage of the sediment supply curve. Nevertheless, the internal fine-grained longitudinally continuous intervals might represent the waning phase of high-frequency sediment supply variations within a lower frequency cycle (Fig. 6.2). Typically, the identification of high-frequency extrinsic cyclicity, which is preserved in the fill of the MSC, is extremally challenging due to the cut and fill dynamics of submarine channel complexes.

The distinctive characteristics of the MSC reflect the interaction of the different stratigraphic controls during channel inception and filling, shedding light on evolutionary processes of submarine channels not commonly observed in modern and buried systems (see discussion in Chapter 4).
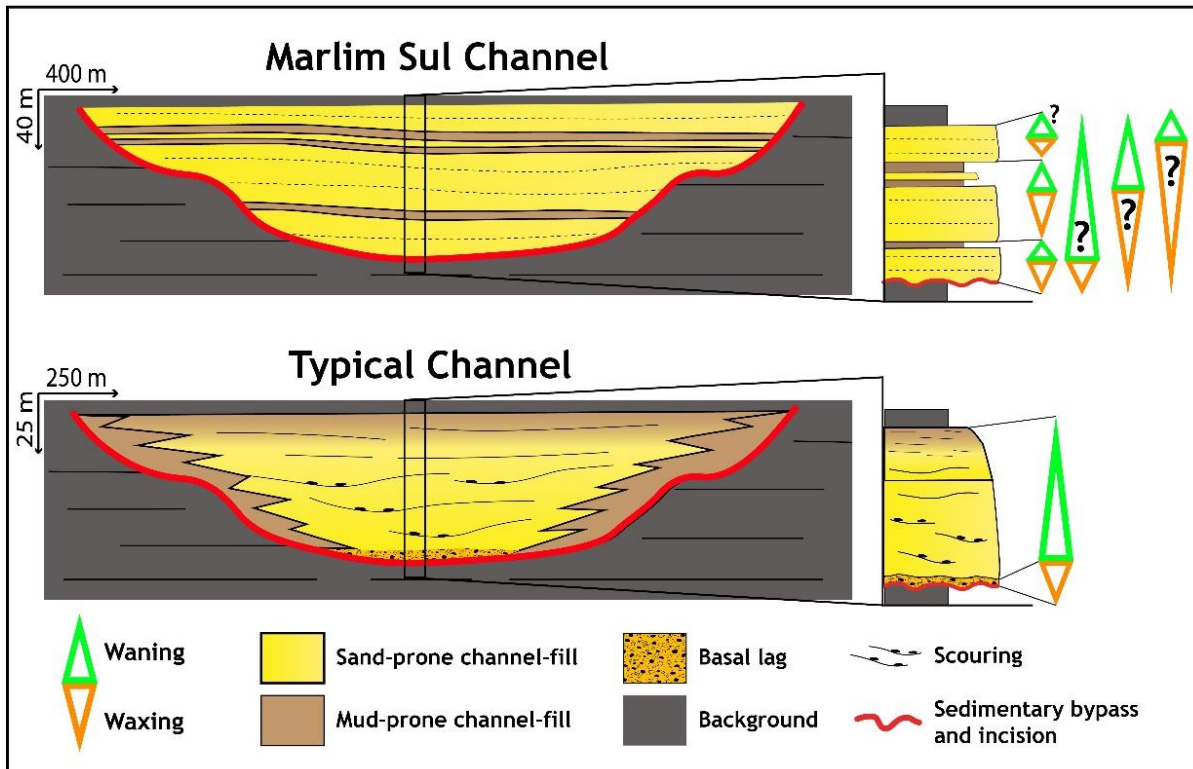
Figure 6.2: Comparison between the Marlim Sul Channel (with average dimensions) and a typical submarine channel (dimensions from Hubbard et al., 2014). In typical submarine channels, the waxing sediment supply phase is mainly represented by the basal incisional surface and lag deposits, whereas the waning sediment supply phase is recorded in channel-filling and is reflected in a fining upward trend. The cycle is asymmetrical. However, in the MSC, the abrupt shift from incision to deposition, with flows that lack erosive power during filling, resulted in an aggradational channel-fill with preservation of mud intervals. Channel-fill deposits could have been deposited during waxing and/or waning phases of the sediment supply curve, not being possible to know cycle geometry. Nevertheless, the preserved mud-prone packages suggest high frequency sediment supply cycles.

6.2 How do the stratigraphic record and configuration of topographically complex depocentres vary across different domains and under variable deformation rates in salt-bearing passive margins?

Chapters 3 and 5 address depocentres in the extensional salt-domain during a mature stage of Campos Basin passive margin evolution (Marlim Unit stepped-slope system in Chapter 3 and the Albacora depocentre in Chapter 5, Oligocene-Miocene, see Figs. 3.1, 3.4, 5.2, Chapters 3 and 5), when the horizontal extension was reduced compared

to initial stages (e.g., Demercian et al., 1993; Rouby et al., 1993; Quirk et al., 2012). This tectonic template induced a complicated seabed relief, and the creation of weakly confined and relatively shallow depocentres. These contrast with depocentres formed under high rates of salt deformation due to horizontal extension in the extensional salt domain and with minibasins or tortuous corridors formed in areas of thick salt in the transitional or contractional salt domains of salt-bearing passive margins. Below, the main characteristics of the depocentres investigated in this thesis are summarised and compared to literature examples of different types of depocentres formed in areas of complex salt-related topography. The comparison is focused on depocentres where submarine fans were documented.

6.2.1 Weakly confined depocentres in the extensional salt domain

6.2.1.1 External configuration and large-scale accommodation control

The results of this thesis show that salt tectonics played a key role in the accommodation of the Marlim Unit stepped slope system (Chapters 3 and 4) and the Albacora depocentre (Chapter 5). The salt structures underneath the study intervals (i.e., salt diapirs, salt-rollers) were formed during the raft tectonics phase that started during the Albian, which generated major seabed topographic irregularities such as troughs between rafts that were healed by the Upper Cretaceous. Although there is convincing evidence for salt tectonic activity during the evolution of these areas, slope deformation consists of fault activity associated with previously formed salt structures. There was no contact of the salt with Oligocene-Miocene strata because the salt was buried during this time. While extensional reactivation is observed in the Marlim Unit stepped slope system, extension and contraction occur in the Albacora depocentre (Figs. 3.4, 5.2, Chapters 3 and 5). Both areas are interpreted to be positioned in the distal part of the extensional domain of Campos Basin, where extension progressed to growth-fault rollover systems and complete separation of rafts. Tilted blocks of Albian strata (pre-rafts and raft-like), therefore, not totally fragmented, are more common in the proximal extensional domain (e.g., Quirk et al., 2012; do Amarante et al., 2021). This would be equivalent to the subdomain E2 of do Amarante et al. (2021). In the Campos Basin extensional domain, salt-related deformation concentrates at the

edges, and in between, the Albian-Cenomanian carbonate rafts and pre-rafts (e.g., Quirk et al., 2012; do Amarante et al., 2021). The Albacora depocentre (35 km long and 20 km wide) evolved above a large partially fragmented carbonate raft surrounded by salt structures (Fig. 5.2, Chapter 5). The semi-elliptical external configuration and large-scale accommodation patterns were controlled by structural relief generated by extensional/transtensional and contractional reactivation of these flanking salt structures. On the other hand, the Marlim stepped slope system is elongate (40 km long and 15 km wide) and evolved above a series of minor rafts separated by salt rollers and grabens (Fig. 3.4, Chapter 3). Large-scale accommodation patterns on the stepped profile were controlled by differential compaction across the more rigid carbonate rafts and less rigid mud-prone inter-raft zones, resulting in a slope configuration comprising two steps bounded by ramps and connected by a corridor (Fig. 3.11, Chapter 3).

6.2.1.2 Thickness, sedimentary filling and stratal patterns

The Marlim stepped slope system comprises the Marlim Unit, a relatively thin turbidite unit with average thicknesses of 25 m (up to 80 m, Fig. 3.10, Chapter 3). Seismically, it is mainly seen as a pair of reflections. Therefore, it represents a very thin stratigraphic interval in Campos Basin history. Low-amplitude reflections calibrated by wells support fine-grained deposits encasing the unit. These are interpreted as low-density turbidites and hemipelagics. Partially continuous high-amplitude reflections are also observed in the Oligocene section above and below the Marlim Unit (Fig. 3.9, Chapter 3). Although only the Marlim Unit was the focus of Chapter 3, the dataset available supports that these high-amplitude reflections are also sand-prone turbidites. Therefore, the Oligocene section (~200 m thick) comprises the intercalation of turbidites (sand- and mud-prone) and hemipelagic sediments. The physiographic configuration of the slope above and below the Marlim Unit was not investigated. However, considering that the large-scale topographic control relates to differential compaction associated with the underlying configuration of rafts and, that evidence for syn-depositional salt-related tectonic activity covers the whole Oligocene section, it is possible that stepped slope topography was present for a long period. Having this understanding is important for comparison with the Albacora depocentre in a similar time and thickness scale. Topographic control is observed during the Oligocene up to

the Lower Miocene in the Albacora depocentre, which records a section of approximately 300 m (Fig. 5.2, Chapter 5). The filling of the depocentre comprises a succession of slope valley systems that do not change morphology, indicating minimal topographic change downslope (Figs. 5.2, 5.3, 5.7, Chapter 5), followed by laterally extensive mass transport complexes (MTC1 and MTC2, Fig. 5.3, Chapter 5) intercalated with turbidite units composed of sand-prone submarine channel-fills and lobes (ABT1 and ABT2, Fig. 5.3, Chapter 5). The size of the large and thick basal MTC1 suggests an external source and possibly an allogenic control related to sea-level variations. In both areas, seismic packages related to Oligocene-Miocene strata are continuous over large areas, crossing depocentre boundaries, with thinning or thickening according to the structural configuration of the depocentre at the time. The thin turbidite systems of the Marlim Unit and Albacora turbidites (ABT1 and ABT2) (average 25 m thick), which show evidence for a final phase of sediment bypass with channel incision and mud-filling (Fig. 5.11, Chapter 5), support weakly confined and relatively shallow depressions controlled by low to moderate deformation rates and structural relief.

Local-scale accommodation control: The Marlim Unit stepped slope system and the Albacora depocentre show evidence of a dynamic slope during deposition. The laterally associated fill-and-spill cycles of the Marlim Unit are explained by salt-driven lateral slope tilting. Likewise, the reactivation of salt structures internal to the Albacora depocentre is interpreted to induce changes in accommodation patterns prior to and after MTC1 emplacement and, during the ABT1 unit evolution, with lateral slope tilting shifting the late-phase channel systems towards the North (Figs. 5.17 and 5.19, Chapter 5).

6.2.2 Depocentres as a function of deformation styles and rates

In salt-bearing passive margins, gravity-driven deformation above salt creates kinematically-linked domains of salt-detached deformation (extensional, transitional/intermediate/translational/multi-phase and contractional; Fig. 1.3, Chapter 1), which largely control salt deformation style (e.g., Cobbold and Szatmari, 1991; Demercian et al., 1993; Fort et al., 2004; do Amarante et al., 2021). Deformation rates can be highly variable in time and space. Nevertheless, in the extensional salt domain

of passive margins, the largest magnitudes of extension accumulate at the deepest levels (Rouby et al., 1993); therefore, there is a tendency for the reduction of deformation rates as the basin is filled and the salt thins over time. On the other hand, in the contractional domain, salt inflation and salt-sediment interaction are evidence for high deformation rates in recent times in many basins (e.g., Fort et al., 2004; Brun and Fort, 2011; Demercian et al., 2013; Quirk et al., 2012; do Amarante et al., 2021). This supports the formation of depocentres associated with low to moderate deformation rates in the extensional domain in a mature phase of salt-bearing passive margins but not in the contractional domain.

The table below (Table 6.1) summarises the characteristics of the main types of depocentres with reported sand-prone deep-water systems across salt-bearing passive margins (see Chapter 2, section 2.1.3 for references), including the weakly confined depocentres (steps) documented in this thesis. Figure 6.3 represents these graphically, located in a dip section of a salt-bearing passive margin. The subsidence mechanisms, external configuration, and stratal patterns of topographically complex depocentres largely reflect deformation style and deformation rates. The sedimentary filling may also be related to the depocentre type. For instance, minibasins record considerable amounts of locally sourced mass transport deposits remobilised from their flanks, which is not expected in stepped slopes with shallow depocentres. Also, ponding in minibasins favours sheet-like deposits and preservation of mud caps, which are not expected in connected depocentres.

*Table 6.1: Characteristics of the main types of depocentres in the salt domains of passive margins. The steps/shallow depressions in the salt extensional domain are documented for the first time in this thesis, being the context of the Marlim Unit (Chapter 3) and the Albacora depocentre (Chapter 5). *Not documented in the literature.*

Salt domain	EXTENSIONAL DOMAIN		TRANSITIONAL/COMPRESSIONAL	
Depocentre type	Steps/Shallow depressions	Elongate troughs between rafts	Tortuous corridors	Minibasins
Deformation rates	Low to moderate	High	Moderate	High
Shape	Semi-circular to elongate	Elongate troughs	Elongate tortuous corridors	Elliptical to elongate
Size	15-20 km wide; 35-40 km long	5-10 km wide; dozens of Km long	A few to several km wide - dozens km long	5-20 km diameter
Thickness	Hundreds of metres	Hundreds of metres to km	n/a*	A few to several Km
Confinement	Weakly confined	High lateral confinement	Laterally confined	3-dimensionally confined
Controls on subsidence	Differential compaction/reactivation of buried salt structures	Active horizontal extension	Density-driven salt-withdrwal, salt inflation by contraction	Density-driven salt-withdrwal; salt inflation by contraction
Stratal patterns	Layered - continuous	Divergent (growth faults)	Convergent and onlapping towards lateral flanks, layered/continuous in dip direction	Bowl or/and wedge with onlap, layered at the top
Dominant acommodation patterns during deposition	Lateral and vertical	Vertical	Vertical	Vertical
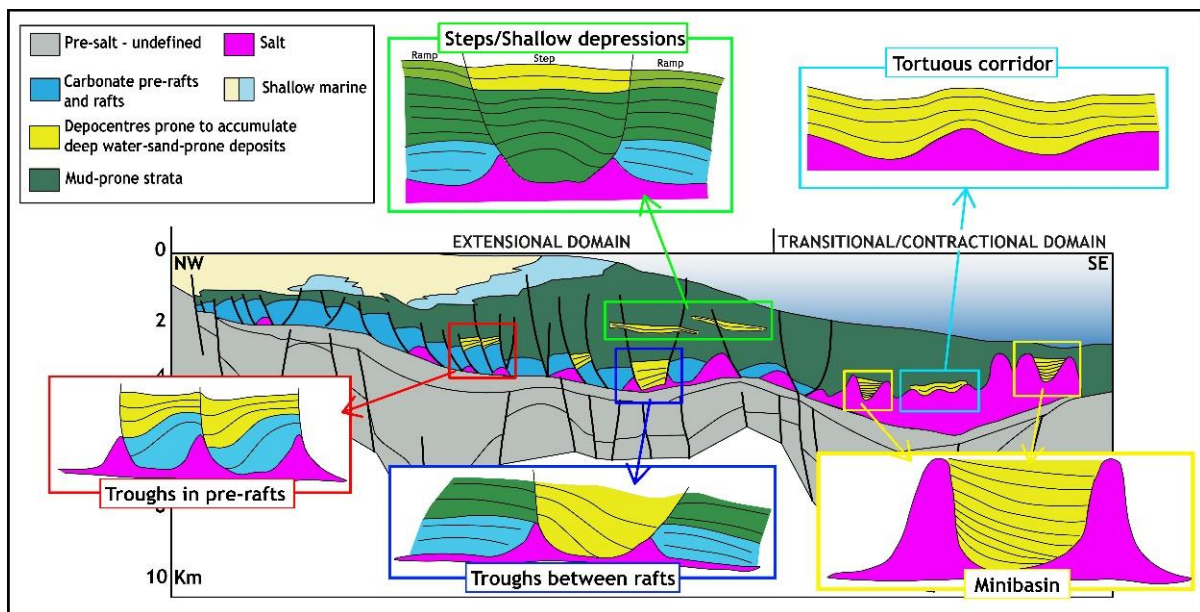
Figure 6.3: Types of depocentres distributed along a dip geological section of a salt-bearing passive margin (Campos Basin used as a model, section modified after Guardado et al., 2000 and Rangel and Martins, 1998). The depocentres of chapters 3 and 5 are steps/shallow depressions formed in the distal position of the extensional salt domain in a mature phase of Campos Basin.

6.2.3 An overlooked type of depocentre in salt basins?

The steps of the Marlim Unit (Fig. 3.11, Chapter 3) and the Albacora depocentre (Fig. 5.2, Chapter 5) represent weakly confined shallow depocentres in a stepped slope setting with subtle to moderate topographic variations and deformation rates related to salt tectonics in the extensional salt domain, and in a mature stage of basin development. This configuration is in marked contrast to the previously documented salt-controlled depocentres (Table 6.1), including tortuous corridors, considered a type of stepped slope in salt basins but more frequent in areas of thick salt (e.g., Meckel, 2002; Prather, 2003; Smith, 2004; Hay, 2012). The depocentres here investigated have a similar large-scale configuration to steps documented in slopes affected by mud diapirism, which usually show modest deformation rates and weak confinement (e.g., Adeogba et al., 2005; Barton, 2012; Jobe et al., 2017). Nevertheless, in salt basins, topography might be more dynamic and with potential for rapid changes in the rate and direction of tilting, even in a setting dominated by low deformation rates (see discussion in section 6.3). This characteristic makes weakly confined depocentres in salt basins unique because of their potential for variable accommodation patterns in three dimensions during the evolution of deep-water systems. This is demonstrated by the FaSTaR model in Chapter 3, which reflects the progressive lateral creation of accommodation in a tilting slope concomitant to sediment supply cycles, producing multiple fill-and-spill cycles and exit points at the edges of the step. This stratigraphic pattern is not observed in minibasins, tortuous corridors or shallow steps controlled by mud diapirism. The stratigraphic signature of the Marlim Unit cannot be explained by the classic fill-and-spill model, which is more adequate for static depocentres or with pure vertical subsidence. These are less likely to present lateral variations in accommodation patterns that will significantly impact depositional architecture and stratigraphic evolution. Regarding rapid slope adjustments, these are interpreted to cause the shift in sedimentary routeing in the channel system of ABT1 (Chapter 5) and in the Marlim Sul Channel incision patterns (see Chapter 4) above the Marlim Unit.

The repetition of large-extent mass transport complexes in the Albacora depocentre suggests that these deposits might be common in weakly confined depocentres in a mature stage of salt basins. This interpretation is supported by the relatively proximal position of these depocentres in the basin, still in the extensional domains and in the slope/base of slope setting, and by the passive margin evolutionary phase with a well-

established platform/slope/basin configuration. These conditions support large mass failure events from the shelf/slope settings.

The turbidites of the Marlim Unit and the Albacora depocentre comprise a variety of deep-water systems, including sand-prone submarine channel-fills and lobes that host significant energy resources (e.g., Bruhn et al., 2003). The stratigraphic and sedimentological characteristics of the sand-prone Cenozoic turbidites of Campos Basin have been documented in the past (e.g., Bruhn et al., 1998; Fetter et al., 2009). However, this is the first time that the controls on the configuration of the depocentres that contain some of these accumulations have been investigated and understood within a basin-scale framework. Considering that passive margins with thin-skinned salt tectonics show similar large-scale structural configuration and evolutionary patterns worldwide, it is likely that shallow depocentres in a similar context of the Marlim Unit and the Albacora depocentre occur in other basins, with potential for recording sand-prone deposition in slope settings.

6.3 What is the impact of dynamic slopes on sedimentation, in three dimensions?

Dynamic slope topography during the evolution of submarine channels and lobe systems has been interpreted in the three core chapters of this thesis (Chapters 3-5). The impact of a deforming seabed is identified across different scales, from architectural elements and their stacking patterns to depocentre evolution. The study areas here investigated show evidence for strike and dip changes on accommodation patterns, and therefore three-dimensional variations, due to slope deformation. This dynamic slope is proposed to be a characteristic of the shallow salt-controlled depocentres addressed in this thesis (see section 6.2), and similar depocentre settings globally. In addition, the impact of local syn-sedimentary faulting on the stratigraphic evolution of submarine channels and the control of mass transport complexes on the accommodation of turbidite systems are also addressed in this thesis.

6.3.1 The impact of lateral slope tilting

The FaSTaR (Fill-and-spill, tilt-and-repeat) model in Chapter 3 synthesised the stratigraphic evolution of the Marlim Unit stepped slope system affected by lateral

tilting, driven by salt tectonics, coupled with fluctuations in sediment supply (see discussion in section 6.1.2).

Accommodation on the steps was progressively created and filled, resulting in several laterally associated fill-and-spill cycles comprising a phase of sand-prone deposition followed by a phase of bypass, and the formation of a channel (Fig. 3.13, Chapter 3). The result is that each cycle exhibits a separate entry and exit point (Fig. 3.16, Chapter 3), contrasting with vertically stacked cycles that exhibit fixed positions for entry and exit points in salt-controlled depocentres with static topography or vertical increments in subsidence (e.g., Winker, 1996; Prather et al., 1998; Prather, 2000, 2003; Beauboueff and Friedmann, 2000; Pirmez et al., 2000; Sinclair and Tomasso, 2002; Smith, 2004). Gradual lateral tilting created spatially limited accommodation during each FaSTaR cycle on the upstream step. This factor, combined with a mild up-dip slope break, is interpreted to induce the development of low-sinuosity erosionally confined channel systems that contrast to the distributary channel and lobe complexes commonly documented above shallow and broad steps (e.g., Adeogba et al., 2005; Deptuck et al., 2012, Fig. 3.16).

The lateral tilting in the Marlim Unit is supported by thicknesses and seismic geomorphology patterns, and stratigraphic truncation relationships between step deposits and feeder channels (see details in Chapter 3). The channel systems responded to tilting with a unidirectional lateral migration, preserving laterally stepping channel-fills (Fig. 3.12, Chapter 3). Stratigraphic continuity of the channel-fills forming a sand-prone composite body is interpreted to result from gradual channel migration associated with relatively low rates of tilting and/or short periods between flows. The contrary would result in pronounced stepping (avulsion) and/or isolated channel ribbons (e.g., Peakall et al., 2000c; Kane et al., 2010, 2012). Therefore, considering a regular period between flows but a variable rate of tilting (punctuated deformation), lateral slope tilting can determine not just the stacking patterns (unidirectional migration) but also the overall architectural style and connectivity of sand-prone channel deposits.

The impact of lateral tilting on unconfined architecture is observed above the distal step, in this case with less accommodation restriction than in the proximal step. Lobate features comprising distributary channel and lobe systems display a progradational but oblique trend towards the tilting direction, being laterally offset (Fig. 3.8, Chapter

3). This supports lateral tilting as a control on stacking patterns of the lobate features at the lobe complex scale (*sensu* Prélat et al., 2009), considering thicknesses. This contrasts with lobe complexes in static or vertically deforming instraslope depocentres, or on the basin floor, which are interpreted to laterally compensate or aggrade according to previous depositional topography or topographic confinement (e.g., Hodgson et al., 2006; Prélat et al., 2010; Spychala, 2016; Jobe et al., 2017; Brooks et al., 2018a).

In Chapter 5, seismic mapping and thicknesses of internal stratigraphic subunits of the ABT1 turbidite unit suggest an initially uneven accommodation distribution in the distal part of the ABT1 trough. As the deeper parts of the trough were filled, a shift in the sediment dispersal patterns is suggested by the position of mud-prone channel-fill that represents incision and bypass at the end of the ABT1 unit (Fig. 5.19, Chapter 5). The position of this channel is explained by lateral slope tilting due to differential subsidence controlled by extension of a salt structure (i.e., the area of the inverted graben), or differential reactivation of a salt-rooted normal fault at the edges of the Albacora depocentre. This shift is observed at the distal part of the trough (the sediment entry point in the proximal part seems to remain fixed through time). Therefore, there is a divergent pattern on the sediment dispersal route controlled by initial uneven accommodation and late lateral tilting.

The identification of lateral tilting operating in a relatively restricted area (just the distal part of the ABT1 trough) and in a specific evolutionary phase of the ABT1 unit, reveals that spatially and temporally limited salt-related lateral slope adjustments induce changes in sedimentary routeing that can be preserved in the stratigraphic record. The shift of sedimentary routes by gradual or abrupt re-positioning of channels through avulsions has been interpreted to reflect laterally tilting slopes in other locations (e.g., Gee and Gawthorpe, 2006; Kane et al., 2010, 2012; Clark and Cartwright, 2009).

6.3.2 The impact of basinward tilting and local faulting

The Marlim Sul channel (MSC, Chapter 3) records extreme basal erosion preserved above the corridor/step segments of the Marlim unit (Figs. 4.1, 4.2, Chapter 4). Usually, higher levels of incision are expected at the edges of intraslope depocentres as flows respond to the base level of the next basinward depocentre (e.g., Pirmez et

al., 2000; Sinclair and Tomasso, 2000; Ferry et al., 2005; Deptuck et al., 2012). However, the MSC presents a deep incision in the proximal part of the corridor/step, where sand-prone deposits are thick, and progressively shallower incision towards the edges of the step and ramp (Fig. 4.2, Chapter 4). This atypical trend suggests an uplift caused by a basinward tilting of the slope traversed by the MSC, with increased uplift at the proximal corridor-step area and reduced uplift down dip (see Chapter 4). Basinward slope tilting is interpreted to be due to far-field effects of salt tectonics, having a longer length-scale than the corridor/step/ramp topography, and likely common to other systems. For example, tectonically-driven basinward titling has been documented as a large-scale process in continental margins, inducing margin progradation and degradation of the slope by the action of channelised turbidity currents and mass-wasting processes (Georgiopoulou et al., 2021; Jackson et al., 2021). The MSC is a few dozens of kilometres long; therefore, its incision patterns are interpreted to reflect a local expression of slope degradation related to the basinward tilting. Nevertheless, the reducing thicknesses and incision levels along the longitudinal profile are compatible with the expected trend in large-scale basinward tilting, which shows a downslope reduction in the potential for degradation (e.g., Jackson et al., 2021).

The MSC channel has a low aspect-ratio with locally very deep incision below the sand-prone step deposits, cutting a mud-prone and cohesive substrate. In this sense, localised uplift associated with basinward tilting promotes deep incision, controlled by the propensity for degradation of uplifted above grade slopes. Heavily incised channel systems have been documented in areas undergoing large-scale slope adjustments (e.g., Allen et al., 2022), and deep incision across slope convexities is common in above grade complex slopes (e.g., Hay, 2012, Huyghe et al., 2004).

The MSC presents three areas of preserved increased incision and thickness that coincide with local salt-related syn-sedimentary faulting of different orientations with respect to the channel course (Figs. 4.3 and 4.4, Chapter 4). Faulting along a submarine channel profile leads to gradient changes, inducing knickpoints (Heiniö and Davies, 2004; Adeogba et al., 2005; Jolly et al., 2017). Gradient changes can also induce channel base scouring and the formation of plunge pools (Mitchell, 2006; Gardner et al., 2020; Guiastrennec-Faugas et al., 2020, 2021). In the case of the MSC, the faults created accommodation and induced gradient changes, which led to the

formation of knickpoints that increased the potential for channel base scouring, including the formation of plunge pools, further increasing channel accommodation. Therefore, active faulting during the evolution of submarine channels has the potential to create complex 3D accommodation patterns due to the interaction of channelised sediment gravity flows with structurally complex topography. Local faulting combined with ongoing basinward tilting produced areas of deep incision, resulting in large-scale scouring of a cohesive substrate, forming larger and deeper scours than the features previously documented in submarine channels (Snedden, 2013).

The marked phase of incision of the MSC is followed by a phase of passive aggradation of the channel floor (Fig. 4.6, Chapter 5). In a basin margin affected by longitudinal tilting, aggradation above an erosional surface is explained by landward migration of the fulcrum, the point at which the slope rotates, resulting in an onlap configuration (Jackson et al., 2021). In the case of the MSC, the preservation of a rugose basal surface and the channel filling character indicate a sudden loss of erosive power and capacity of the flows to transport their load, supporting an abrupt change in the channel operating mode, from erosion to deposition (Fig. 4.8, Chapter 4). This change is explained by the return to subsidence after the transient uplift due to basinward tilting or changes in flow properties (Fig. 4.9, Chapter 4). Active salt tectonics in the area suggests the likelihood of the subsidence hypothesis, which would imply a countereffect on the basinward tilting. Therefore, the MSC history might reflect phases of slope adjustment that acted in opposite directions during channel incision and filling. This resulted in the premature filling of the up-dip reaches of the MSC while the distal reaches were filled later. This contrasts with the expected depositional pattern of slopes subject to basinward tilting, which is the prior filling of the down dip reaches of sediment dispersal routes such as canyons or channels (e.g., Jackson et al., 2021). The filling of the up-dip reaches of slope systems takes place as the fulcrum point progressively advances landward; however, in the case of the MSC, it seems that the fulcrum point had an abrupt advance, and the depositional patterns were inverted.

6.3.3 Summary

In summary, the work presented in Chapters 3-5 suggests that combined lateral and basinward components of slope deformation, with different rates and magnitudes, are

essential factors to consider across a range of different settings, as they control submarine accommodation through time. In addition, large-scale regionally sourced mass transport complexes are here shown to impact accommodation patterns in shallow depocentres by amplifying slope deformation and inducing subsidence by (differential) compaction. These findings suggest that many mobile slopes will be atypical of the classical fill-and-spill models that assume there is no transverse deformation and emphasise simple vertical subsidence patterns in depocentres with high rates of deformation that favour local mass wasting processes from steep depocentres flanks.

An important variable to consider when applying these models is the ratio of the rate of sedimentation, and the rate and geometry of 3D deformation, which will drive a wide range of responses that cannot be addressed in a single model. Nonetheless, the models developed here that capture the impact of lateral and basinward tilt on sediment dispersal patterns on resulting sedimentary architectures, are more representative of shallow salt-controlled depocentres than fill-and-spill models, and can be readily applied to similar situations globally.

6.4 Recommendations for future research

The main contribution of this thesis is to improve the understanding of deep-water deposition above dynamic slopes subject to mild salt-related deformation in a mature phase of passive margin development. The research investigates the controls on the configuration of intraslope depocentres and proposes new models for the stratigraphic evolution of dynamic slopes considering three-dimensionally variable accommodation patterns over time. Despite the novelties presented, three-dimensionally complex patterns of slope deformation and, consequently, submarine accommodation, should be expected in other areas in the extensional domain of salt-bearing passive margins. In addition, this research presents the possibility of large-scale subsidence generation due to the emplacement of large mass transport deposits, a topic to be further investigated. In summary, there are exciting research opportunities brought to light by this thesis that are summarised below.

6.4.1 Extending the knowledge regarding shallow depocentres above the extensional salt domain and in a mature phase of salt-bearing passive margins

The two areas here investigated (Barracuda + Marlim Sul and Albacora +Albacora Leste) are part of a series of intraslope depocentres that hold oil accumulations in turbidite reservoirs, evolving during the mature phase of the Campos Basin (Oligocene/Miocene, e.g., Bruhn et al., 1998; 2003) above the extensional salt domain. Despite having the same age and being in the same tectonic setting within the basin, the configuration of these depocentres has different controls related to salt deformation style and the configuration of the underlying structural elements, such as the carbonate rafts. This encourages the investigation of accommodation control on the other depocentres of Campos Basin and in depocentres in a similar context in the neighbouring basins, such as the Santos and Espírito Santo Basins (Contreras et al., 2010; Davison et al., 2012; Quirk et al., 2012, Gamboa and Alves, 2015) and, in the African salt-bearing passive margin, which share the same evolutionary history of the basins of the Brazilian Margin (i.e., Gondwana break-up, Mohriak et al., 2008; Quirk et al., 2012). Spatiotemporal variability in accommodation patterns has been defined here as a critical factor in the stratigraphic evolution of shallow depocentres in the context of the study areas. Therefore, extending this research topic to these other areas will validate and/or test the applicability of the models here proposed. In addition, the reactivation of basement structures and basement topography have been considered important factors in salt deformation patterns and overall basin structure, even affecting strata much younger than the salt (e.g., Fetter, 2009, Evans and Jackson, 2020; do Amarante et al., 2021). Therefore, the investigation of the deformation history that leads to the formation of shallow depocentres should contemplate large and local-scale basement features and basement tectonic reactivations.

6.4.2 Investigation of sedimentation rates in salt-controlled shallow depocentres and numerical stratigraphic modelling in dynamic slopes

Shallow depocentres, such as stepped slopes, are characterised by having relatively low deformation rates, with sedimentation rates outpacing deformation rates as the depocentres are healed (e.g., Deptuck et al., 2012; Hay et al., 2012). Nevertheless, sedimentation and deformation rates have a much closer balance when compared to minibasins, which subside very fast (e.g., Prather, 2000; 2003). As the interplay of rates controls the resultant stratigraphic patterns, it would be beneficial to acquire high-resolution chrono and biostratigraphic data in modern/shallow stepped-slopes in salt basins in order to interpret high frequency cyclicity and quantify sedimentation rates. A similar approach has been undertaken in minibasins in the Gulf of Mexico (e.g., Booth et al., 2003; Prather et al., 2012b), and in intraslope fans in the Niger Delta slope (e.g., Jobe et al., 2017). This would provide greater sensitivity to how sedimentation rates impact stratigraphic patterns and also help to constrain deformation rates.

This thesis demonstrates that shallow and dynamic depocentres produce complex stratigraphic patterns and high-frequency cyclicity prone to record sedimentary bypass. Stratigraphic numerical modelling simulating the filling of salt-controlled depocentres has been concentrated on representing stratal or stacking patterns in minibasins with static topography (e.g., Wang et al., 2017), with vertical increment in subsidence (e.g., Prather, 2000; Sylvester et al., 2015) or with three-dimensionally variable subsidence, although vertical subsidence is dominant (e.g., Christie et al., 2021). Therefore there is an opportunity for modelling the filling of dynamic depocentres with low deformation rates and spatially variable accommodation creation. Numerical modelling simulations could contemplate multiple scenarios of slope deformation styles (lateral or basinward tilting, abrupt or progressive) combined with variable sedimentation rates, therefore, predicting stratigraphic patterns in hypothetical, but possibly real, contour conditions and validating the models proposed in this thesis.

6.4.3 Numerical modelling of subsidence generated by the weight of large-scale mass transport deposits in salt basins

It has been demonstrated that sedimentary loading can induce subsidence in areas sinking above thick salt, such as minibasins in the transitional and contractional domain of salt passive margins (e.g., Prather et al., 1998; Hudec et al., 2009). What is less clear, however, is the effect of sedimentary load on subsidence in areas where the salt is thinner, such as the distal reaches of the extensional domain of salt basins. In particular, the impact of the instantaneous emplacement of large-scale mass transport deposits could induce subsidence generation in a mobile deforming slope where the salt is relatively thin, but there is a complex array of pre-existing salt structures, as interpreted in Chapter 5. Quantifying the impacts of mass transport deposits above complex structural elements would be useful to understand how subsidence rates vary spatially and, in which scale load-driven subsidence operates and, therefore, where overlying sands might be deposited.

References

Adeogba, A.A., Mchargue, T.R. and Graham, S.A. (2005). Transient fan architecture and depositional controls from near-surface 3-D seismic data, Niger Delta continental slope. AAPG Bulletin, 89, 627–643. https:// doi.org /10 .1306 /11200404025

Albertão, G.A., Mulder, T. and Eschard, R. (2011). Impact of salt-related palaeotopography on the distribution of turbidite reservoirs: evidence from well-seismic analyses and structural restorations in the Brazilian offshore. Marine and Petroleum Geology, 28, 1023–1046. https://doi.org/10.1016/j.marpetgeo. 2010.09.009

Alexander, J. and Morris, S. (1994). Observations on experimental, nonchannelized, high-concentration turbidity currents and variations in deposits around obstacles. Journal of Sedimentary Research, 64, 899-909.

Allen, C., Gomis Cartesio, L.E., Hodgson, D.M., Peakall, J. and Milana, J-P. (2022). Channel incision into a submarine landslide on a Carboniferous basin margin, San Juan, Argentina: Evidence for the role of knickpoints. The Depositional Record, 8, 628-655. https://doi.org/10.1002/dep2.178

Anderson, J. E., Cartwright, J., Drysdall, S. J. and Vivian, N. (2000). Controls on turbidite sand deposition during gravity-driven extension of a passive margin: Examples from Miocene sediments in block 4, Angola. Marine and Petroleum Geology, 17, 1165– 1203.

Armitage, D.A., McHargue, T., Fildani, A. and Graham, S.A. (2012). Postavulsion channel evolution: Niger Delta continental slope. AAPG Bulletin, 96, 823-843. http://dx.doi.org/10.1306/09131110189.

Barton, M.D. (2012). Evolution of an intra-slope apron, offshore Niger Delta Slope: Impact of step geometry on apron architecture. In Prather, B. E., Deptuck, M. E., Mohrig, D. C., van Hoorn B. and Wynn, R. B. (Eds.), Application of the Principles of Seismic Geomorphology to Continental-Slope and Base-of-Slope Systems: Case studies from seafloor and near-seafloor analogue. SEPM Special Publication, 99, 181-197.

Baudouy, L., Haughton, P.D. and Walsh, J.J. (2021). Evolution of a fault-controlled, deep-water sub-basin, Tabernas, SE Spain. Frontiers in Earth Science, 9, 767286. https://doi.org/10.3389/feart.2021.767286

Beaubouef, R.T. and Friedmann, S.J. (2000). High resolution seismic/sequence stratigraphic framework for the evolution of Pleistocene intra slope basins, western Gulf of Mexico: depositional models and reservoir analogs. In Weimer, P., Slatt, R.M., Coleman, J., Rosen, N.C., Nelson, H., Bouma, A.H., Styzen, M.J., and Lawrence, D.T (Eds.), Deep-Water Reservoirs of the World: 20th Annual Gulf Coast Section, SEPM Foundation, Bob F. Perkins Research Conference, 40–60.

Beddow, H.M., Liebrand, D., Sluijs, A., Wade, B.S. and Lourens, L.J. (2016). Global change across the Oligocene-Miocene transition: High-resolution stable isotope records from IODP Site U1334 (equatorial Pacific Ocean). Paleoceanography, 31, 81–97. https://doi.org/10.1002/2015PA002820

Booth, J. R., Dean, M. C., DuVernay, A. E. III and Styzen, M. J. (2003). Paleo-bathymetric controls on the stratigraphic architecture and reservoir development of confined fans in the Auger Basin: Central Gulf of Mexico slope. Marine and Petroleum Geology, 20, 563–586. https://doi.org/10.1016/j.marpetgeo.2003.03.008

Bouma, A.H. (2005). Key controls on the characteristics of turbidite systems. In: Lomas, S.A., Joseph, P. (Eds.), Confined Turbidite Systems. Geological Society Special Publication 222, 9–22.

Bourget, J., Zaragosi, S., Ellouz-Zimmermann, N., Mouchot, N., Garlan, T., Schneider, J.L., Lanfumey, V. and Lallemant, S. (2011). Turbidite system architecture and sedimentary processes along topographically complex slopes: the Makran convergent margin. Sedimentology, 58, 376–406, https://doi.org/10.1111/j.1365-3091.2010.01168.x

Brooks, H.L., Hodgson, D.M., Brunt, R.L., Peakall, J., and Flint, S.S. (2017). Exhumed lateral margins and increasing flow confinement of a submarine landslide complex: Sedimentology, 65(4), 1067-1096.

Brooks, H.L., Hodgson, D.M., Brunt, R.L., Peakall, J., Poyatos-Moré, M. and Flint, S.S. (2018a). Disconnected submarine lobes as a record of stepped slope evolution

over multiple sea-level cycles. Geosphere, 14, 4, 1753–1779. https://doi .org /10 .1130 /GES01618.1

Brooks, H.L., Hodgson, D.M., Brunt, R.L., Peakall, J., Hofstra M., And Flint, S.S. (2018b). Deep-water channel-lobe transition zone dynamics: Processes and depositional architecture, an example from the Karoo Basin, South Africa. GSA Bulletin, 130 (9-10)- 1723–1746. https://doi.org/10.1130/B31714.1

Broucke, O., Temple, F., Rouby, D., Robin, C., Calassou, S., Nalpas, T., Guillocheau, F. (2004). The role of deformation processes on the geometry of mud-dominated turbiditic systems, Oligocene and Lower–Middle Miocene of the Lower Congo basin (West African Margin). Marine and Petroleum Geology 21, 327–348. https://doi.org/10.1016/j. marpetgeo.2003.11.013.

Brown, A. R. (2011). Interpretation of three-dimensional seismic data, Society of Exploration Geophysicists and American Association of Petroleum Geologists, 560p.

Bruhn, C.H.L. (1998). Deep-Water Reservoirs from the Eastern Brazilian Rift and Passive Margin Basins. AAPG International Conference and Exhibition, Rio de Janeiro, Brazil, AAPG Short Course Notes, Part 2, 191p.

Bruhn, C. H. L., Gomes, J. A. T., Del Lucchese, C., Jr. and Johann, P. R. S. (2003). Campos Basin: Reservoir characterization and management - Historical overview and future challenges. In Offshore Technology Conference 15220-MS, Houston, Texas. https://doi.org/10.4043/15220-ms

Brun, J.-P. and Fort, X. (2004). Compressional salt tectonics (Angolan margin). Tectonophysics 382, 129-150.

Brun, J.-P. and Fort, X. (2011). Salt tectonics at passive margins: Geology versus models. Marine and Petroleum Geology, 28, 1123–1145. https://doi.org/10.1016/j.marpe tgeo.2011.03.004

Bull, S., Cartwright, J. and Huuse, M. (2009). A review of kinematic indicators from mass-transport complexes using 3D seismic data. Marine and Petroleum Geology, 26, 1132–1151. https://doi. org/10.1016/j.marpetgeo.2008.09.011

Burgess, P.M. and Hovius, N. (1998). Rates of delta progradation during highstands; consequences for timing of deposition in deep-marine systems. Journal of the

Geological Society of London, 15, 217–222. https://doi.org/10.1144/gsjgs.155.2.0217

Cainelli, C. and Mohriak, W. U. (1999). Some remarks on the evolution of sedimentary basins along the Eastern Brazilian continental margin. Episodes, 22, 206–216.

Carter, R.M. (1988). The nature and evolution of deep-sea channel systems. Basin Research, 1, 41-54.

Casagrande, J., Hodgson, D.M., Peakall, J. and Benac, P.M. (2022). Fill-and- Spill, Tilt-and-Repeat (FaSTaR) cycles: Stratigraphic evolution above a dynamic submarine stepped slope. Basin Research, 34, 2162-2188. https://doi.org/10.1111/bre.12700

Castro, R.D. and Picolini, J.P. (2015). Main features of the Campos Basin regional geology. In: Kowsmann, R.O. (Ed.), Geology and Geomorphology. Habitats, 1, 1-12.

Catuneanu, O. (2006). Principles of sequence stratigraphy: Amsterdam, Netherlands, Elsevier, 375 p.

Catuneanu, O., Abreu, V., Bhattacharya, J., Blum, M.D., Dalrymple, R.W., Eriksson, G., Fielding, C.R., Fisher, W.L., Galloway, W.E., Gibling, M.R., Giles, K.R., Holbrook, J.M., Jordan, R., Kendall, C.G.St.C., Macurda, B., Martinsen, O.J., Miall, A.D., Neal, J.E., Nummedal, D., Pomar, L., Posamentier, H.W., Pratt, B.R., Sarg, J.F., Shanley, K.W., Steel, R.J., Strasser, A., Tucker, M.E. and Winker, C. (2009). Towards the standardization of sequence stratigraphy. Earth-Science Reviews 92, 1–33.

Chang, H.K., Kowsmann, R.O., Figueiredo, A.M.F. and Bender, A. (1992). Tectonics and stratigraphy of the East Brazil rift system: An overview. Tectonophysics, 213, 97–138.

Chen, Y., Parsons, D.R., Simmons, S.M., Williams, R., Cartigny, M.J., Hughes Clarke, J.E., Stacey, C.D., Hage, S., Talling, P.J., Azpiroz-Zabala, M. and Clare, M.A. (2021). Knickpoints and crescentic bedform interactions in submarine channels. Sedimentology, 68(4), 1358-1377.

Chima, K.I., Do Couto, D., Leroux, E., Gardin, S., Hoggmascall, N., Rabineau, M., Granjeon, D. and Gorini, C. (2019). Seismic stratigraphy and depositional

architecture of Neogene intraslope basins, offshore western Niger Delta. Marine and Petroleum Geology, 109, 449-468. https://doi.org/10.1016/j.marpetgeo.2019.06.030

Christie, D.N., Peel, F.J., Apps, G.M. and Stanbrook, D.S. (2021). Forward Modelling for Structural Stratigraphic Analysis, Offshore Sureste Basin, Mexico. Frontiers in Earth Science, 9:767329. https://doi.org/10.3389/feart.2021.767329

Clark, I. R., and Cartwright, J. A. (2009). Interaction between submarine channel systems and deformation in deepwater fold belts: Examples from the Levant Basin, eastern Mediterranean Sea: Marine and Petroleum Geology, 26, 1465–1482. https://doi:10.1016/j.marpetgeo.2009.05.004

Cobbold, P.R. and Szatmari, P. (1991). Radial gravitational gliding on passive margins. Tectonophysics, 188, 249–289. https://doi.org/10.1016/0040-1951(91)90459-6

Collier, R.E.L. (1991). The Lower Carboniferous Stainmore Basin, N. England: extensional basin tectonics and sedimentation. Journal of the Geological Society of London, 148, 379-390.

Contreras, J., Zuhlke, R., Bowman, S. and Bechstadt, T. (2010). Seismic stratigraphy and subsidence analysis of the southern Brazilian margin (Campos, Santos and Pelotas basins). Marine and Petroleum Geology, 27(9), 1952–1980, https://doi:10.1016/j.marpetgeo.2010.06.007.

Covault, J.A and Graham, S.A. (2010). Submarine fans at all sea-level stands: Tectono-morphologic and climatic controls on terrigenous sediment delivery to the deep sea. Geology, 38(10), 939-942. https://doi: 10.1130/G31081

Covault, J.A., Fildani, A., Romans, B.W. and McHargue, T. (2011). The natural range of submarine canyon-and-channel longitudinal profiles. Geosphere, 7, 313-332. http://dx.doi.org/10.1130/GES00610.1

Cumberpatch, Z.A., Kane, I.A., Soutter, E.L., Hodgson, D.M., Jackson, C.A.-L., Kilhams, B.A. and Poprawski, Y. (2021). Interactions of deep-water gravity flows and active salt tectonics. Journal of Sedimentary Research, 91, 34-65. https://doi.org/10.2110/jsr.2020.047

Dalla Valle, G. and Gamberi, F. (2011). Slope channel formation, evolution and backfilling in a wide shelf, passive continental margin (northeastern Sardinia slope, central Tyrrhenian Sea). Marine Geology, 286, 95–105, https://doi.org/10.1016/j.margeo.2011.06.005

Davison, I., Anderson, L. and Nuttall, P. (2012). Salt deposition, loading and gravity drainage in the Campos and Santos salt basins. In Alsop, G. I., Archer, S. G., Hartley, A. J., Grant, N. T. and Hodgkinson, R. (Eds.), Salt Tectonics, Sediments and Prospectivity. Geological Society, London, Special Publications, 363, 159–174. https://doi.org/10.1144/sp363.8

De Gasperi, A. and Catuneanu, O. (2014). Sequence stratigraphy of the Eocene turbidite reservoirs in Albacora field, Campos Basin, offshore Brazil. AAPG Bulletin, 98 (2), 279-313.

Demercian, S., Szatmari, P., and Cobbold, P. R. (1993). Style and pattern of salt diapirs due to thin-skinned gravitational gliding, Campos and Santos basins, offshore Brazil. Tectonophysics, 228(3–4), 393–433. https://doi.org/10.1016/0040-1951(93)90351-J

Deptuck, M.E., Steffens, G.S., Barton, M. and Pirmez, C. (2003). Architecture and evolution of upper fan channel-belts on the Niger Delta slope and in the Arabian Sea. Marine and Petroleum Geology, 20(6), 649-676, https://doi.org/10.1016/j.marpetgeo.2003.01.004

Deptuck, M.E., Sylvester, Z., Pirmez, C. and O'Byrne, C. (2007). Migration–aggradation history and 3D seismic geomorphology of submarine channels in the Pleistocene Benin-major Canyon, western Niger Delta slope. Marine and Petroleum Geology, 24, 406–433, https://doi.org/10.1016/j.marpetgeo.2007.01.005

Deptuck, M. E., Sylvester, Z. and O'Byrne, C. (2012). Pleistocene seascape evolution above a "simple" stepped slope–Western Niger Delta. In Prather, B. E., Deptuck, M. E., Mohrig, D. C., van Hoorn B. and Wynn, R. B. (Eds.), Application of the Principles of Seismic Geomorphology to Continental-Slope and Base-of-Slope Systems: Case studies from seafloor and near-seafloor analogue. SEPM Special Publication, 99, 199–222. https://doi. org/10.2110/pec.12.99

Di Celma, C.N., Brunt, R.L., Hodgson, D.M., Flint, S.S. and Kavanagh, J.P. (2011). Spatial and temporal evolution of a Permian submarine slope channel–levee system, Karoo Basin, South Africa. Journal of Sedimentary Research, 81(8), 579-599. https://doi. org/10.2110/jsr.2011.49

Dorrell, R.M., Darby, S.E., Peakall, J., Sumner, E.J., Parsons, D.R. and Wynn, R.B. (2013). Superelevation and overspill control secondary flow dynamics in submarine channels. Journal of Geophysical Research – Oceans, 118, 3895-3915, doi:10.1002/jgrc.20277

Dorrell, R.M., Peakall, J., Sumner, E.J., Parsons, D.R., Darby, S.E., Wynn, R.B., Özsoy, E. and Tezcan, D. (2016). Flow dynamics and mixing processes in hydraulic jump arrays: implications for channel-lobe transition zones. Marine Geology 381, 181–193. http://dx.doi.org/10.1016/j.margeo.2016.09.009

Doughty-Jones, G., Mayall, M. and Lonergan, L. (2017). Stratigraphy, facies, and evolution of deep-water lobe complexes within a salt-controlled intraslope minibasin. AAPG Bulletin, 101, 1879–1904. https://doi.org/10.1306/01111716046

Doughty-Jones, G., Lonergan, L., Mayall, M. and Dee, S. (2019). The role of structural growth in controlling the facies and distribution of mass transport deposits in a deep-water salt minibasin. Marine and Petroleum Geology, 104, 106–124. https://doi.org/10.1016/j.marpetgeo.2019.03.015

do Amarante, F. B., Jackson, C. A.-L., Pichel, L. M., Scherer, C. M. S. and Kuchle, J. (2021). Pre-salt rift morphology controls salt tectonics in the Campos Basin, offshore SE Brazil. Basin Research, 33, 2837–2861. https://doi.org/10.1111/bre.12588

Duffy, O.B., Dooley, T.P., Hudec, M.R., Fernandez, N., Jackson, C.A.L. and Soto, J.I. (2021). Principles of shortening in salt basins containing isolated minibasins. Basin Research, 33, 2089-2117. https://doi.org/10.1111/bre.12550

Duval, B., Cramez, C. and Jackson, M. P. A. (1992). Raft tectonics in the Kwanza Basin, Angola. Marine and Petroleum Geology, 9, 389–404. https://doi.org/10.1016/0264-8172(92)90050-O

Evans, S. L. and Jackson, C. A. L. (2020). Base-salt relief controls salt-related deformation in the Outer Kwanza Basin, offshore Angola. Basin Research, 32,668–687. https://doi.org/10.1111/bre.12390

Ferguson, R.A., Kane, I.A., Eggenhuisen, J.T., Pohl, F., Tilston, M., Spychala, Y.T. and Brunt, R.L. (2020). Entangled external and internal controls on submarine fan evolution: an experimental perspective. The Depositional Record, 6(3), 605-624.

Ferry, J-N., Mulder, T., Parize, O. and Raillard, S. (2005). Concept of equilibrium profile in deep-water turbidite systems: effects of local physiographic changes on the nature of sedimentary process and the geometries of deposits. In Hodgson, D.M., and Flint, S.S. (Eds.), Submarine Slope Systems: Processes and Products: Geological Society of London, Special Publications 244,181–193.

Fetter, M. (2009). The role of basement tectonic reactivation on the structural evolution of Campos Basin, offshore Brazil: Evidence from 3D seismic analysis and section restoration. Marine and Petroleum Geology, 26, 873–886. https://doi.org/10.1016/j.marpe tgeo.2008.06.005

Fetter, M., De Ros, L.F. and Bruhn, C.H.L. (2009). Petrographic and seismic evidence for the depositional setting of giant turbidite reservoirs and the palaeogeographic evolution of Campos Basin, offshore Brazil. Marine and Petroleum Geology, 26 (6), 824-853.

Fildani, A., Hubbard, S.M., Covault, J.A., Maier, K.L., Romans, B.W., Traer, M. and Rowland, J.C. (2013). Erosion at inception of deep-sea channels. Marine and Petroleum Geology, 41, 48–61. https://doi:10.1016 /j.marpetgeo .2012.03.006

Flint, S.S., Hodgson, D.M., Sprague, A., Brunt, R.L., Box, D., Van Der Merwe, W.C., Figueiredo, J., Di Celma, C., Prelat, A. and Kavanagh, J.P. (2011). Depositional architecture and sequence stratigraphy of the Karoo basin floor to shelf edge succession, Laingsburg depocentre, South Africa. Marine and Petroleum Geology, 28, 658-674.

Fort, X., Brun, J.-P., & Chauvel, F. (2004). Salt tectonics on the Angolan margin, synsedimentary deformation processes. AAPG Bulletin, 88, 1523–1544. https://doi.org/10.1306/06010 403012

Galloway, W.E. (1998). Siliciclastic slope and base-of-slope depositional systems: component facies, stratigraphic architecture and classification. AAPG Bulletin 82, 569–595.

Gamberi, F. and Marani, M. (2007). Downstream evolution of the Stromboli slope valley (southeastern Tyrrhenian Sea). Marine Geology, 243, 180-189. https://doi.org/10.1016/j.margeo.2007.05.006

Gamboa, D., and Alves, T. M. (2015). Spatial and dimensional relationships of submarine slope architectural elements: A seismic scale analysis from the Espírito Santo Basin (SE Brazil). Marine and Petroleum Geology, 64, 43–57. https://doi.org/10.1016/j.marpetgeo.2015.02.035

Garcia, M. H. (1993). Hydraulic jumps in sediment-driven bottom currents. Journal Of Hydraulic Engineering, 119, 1094–1117.

Garcia, M. and Parker, G. (1989). Experiments on hydraulic jumps in turbidity currents near a canyon-fan transition, Science, 245, 393–396.

Gardner, T.W (1983). Experimental study of knickpoint and longitudinal profile evolution in cohesive, homogeneous material. Geological Society of America Bulletin, 94(5), 664–672. https://doi.org/10.1130/0016-7606(1983)94<664:ESOKAL>2.0.CO;2

Gardner, J.V., Peakall, J., Armstrong, A.A. and Calder, B.R. (2020). The Geomorphology of Submarine Channel Systems of the Northern Line Islands Ridge, Central Equatorial Pacific Ocean. Frontiers in Earth Science, 8:87, https://doi.org/10.3389/feart.2020.00087

Ge, Z., Gawthorpe, R. L., Rotevatn, A., Zijerveld, L., Jackson, C. A. L. and Oluboyo, A. (2020). Minibasin depocentre migration during diachronous salt welding, Offshore Angola. Basin Research, 32, 875–903.

Ge, Z., Gawthorpe, R. L., Zijerveld, L. and Oluboyo, A. P. (2021). Spatial and temporal variations in minibasin geometry and evolution in salt tectonic provinces: Lower Congo Basin, Offshore Angola. Basin Research, 33, 594–611.

Gee, M.J.R. and Gawthorpe, R.L. (2006). Submarine channels controlled by salt tectonics: examples from 3D seismic data offshore Angola. Marine and Petroleum Geology, 23, 443–458.

Georgiopoulou, A. and Cartwright, J.A. (2013). A critical test of the concept of submarine equilibrium profile. Marine and Petroleum Geology, 41, 35–47, https://doi.org/10.1016/j.marpetgeo.2012.03.003

Georgiopoulou, A., Owens, M. and Haughton, P.D.W. (2021). Channel and inter-channel morphology resulting from the long-term interplay of along slope and downslope processes, NE Rockall Trough, NE Atlantic. Marine Geology 441, 106624. https://doi.org/ 10.1016/j.margeo.2021.106624

Gerber, T.P., Amblas, D., Wolinsky, M.A., Pratson, L.F. and Canals, M. (2009). A model for the long-profile shape of submarine canyons. Journal of Geophysical Research: Earth Surface, 114, F03002, doi:10.1029/2008JF001190.

Giorgio Serchi, F., Peakall, J., Ingham, D.B. and Burns, A.D. (2011). A unifying computational fluid dynamics investigation on the river-like to river-reversed secondary circulation in submarine channel bends. Journal of Geophysical Research – Oceans, 116, C06012. doi:10.1029/2010JC006361

Guardado, L. R., Spadini, A. R., Brandão, J. S. L. and Mello, M. R. (2000). Petroleum system of the Campos Basin. In Mello, M. R. and Katz B. J. (Eds.), Petroleum systems of South Atlantic margins. AAPG Memoir, 73, 317–324.

Guiastrennec-Faugas, L., Gillet, H., Jacinto, R.S., Dennielou, B., Hanquiez, V., Schmidt, S., Simplet, L. and Rousset, A. (2020). Upstream migrating knickpoints and related sedimentary processes in a submarine canyon from a rare 20-year morphobathymetric time-lapse (Capbreton submarine canyon, Bay of Biscay, France). Marine Geology, 423, 106143, https://doi.org/10.1016/j.margeo.2020.106143

Guiastrennec-Faugas, L., Gillet, H., Peakall, J., Silva Jacinto, R. and Dennielou, B. (2021). Initiation and evolution of knickpoints and their role in cut and fill processes in active submarine channels. Geology, 49, 314-319. https://doi.org/10.1130/G48369.1

Hage, S., Cartigny, M.J., Clare, M.A., Sumner, E.J., Vendettuoli, D., Clarke, J.E.H., Hubbard, S.M., Talling, P.J., Lintern, D.G., Stacey, C.D. and Englert, R.G. (2018). How to recognize crescentic bedforms formed by supercritical turbidity currents in

the geologic record: Insights from active submarine channels. Geology, 46, 563-566.

Hajek, E.A. Straub, K.M. (2017). Autogenic sedimentation in clastic stratigraphy. Annual Review of Earth and Planetary Sciences., 45, 981-709.

Hansen, L. A., R. H. Callow, I. A. Kane, F. Gamberi, M. Rovere, B. T.Cronin, and B. C. Kneller. (2015). Genesis and character of thin-bedded turbidites associated with submarine channels: Marine and Petroleum Geology, 67, 852–879. doi:10.1016/j.marpetgeo.2015.06.007

Hansen, L., Janocko, M., Kane, I. and Kneller, B. (2017). Submarine channel evolution, terrace development, and preservation of intra-channel thin-bedded turbidites: Mahin and Avon channels, offshore Nigeria. Marine Geology, 383, 146–167. https://doi.org/10.1016/j.margeo.2016.11.011.

Haq, B. U., Hardenbol, J. and Vail, P. R. (1987). The chronology of fluctuating sea level since the Triassic. Science, 235, 1156-1167.

Haughton, P., Davis, C., McCaffrey, W. and Barker, S. (2009). Hybrid sediment gravity flow deposits – Classification, origin and significance. Marine and Petroleum Geology, 26, 1900–1918.

Hay, D. C. (2012). Stratigraphic evolution of a tortuous corridor from the stepped slope of Angola. In Prather, B. E., Deptuck, M. E., Mohrig, D. C., van Hoorn B. and Wynn, R. B. (Eds.), Application of the Principles of Seismic Geomorphology to Continental-Slope and Base-of-Slope Systems: Case studies from seafloor and near-seafloor analogue. SEPM Special Publication, 99, 163–180.

Heijnen, M.S., Clare, M.A., Cartigny, M.J.B., Talling, P.J., Hage, S., Lintern, D.G., Stacey, C., Parsons, D.R., Simmons, S.M., Chen, Y., Sumner, E.J., Dix, J.K. and Hughes Clarke, J.E. (2020). Rapidly-migrating and internally-generated knickpoints can control submarine channel evolution. Nature Communications, 11:3129. https://doi.org/10.1038/s41467-020-16861-x

Heiniö, P. and Davies, R.J. (2007). Knickpoint migration in submarine channels in response to fold growth, western Niger Delta. Marine and Petroleum Geology, 24, 434–449, https://doi.org/10.1016/j.marpetgeo.2006.09.002

Heiniö, P., Davies, R.J. (2009). Trails of depressions and sediment waves along submarine channels on the continental margin of Espirito Santo Basin, Brazil. Geological Society of America Bulletin 121, 698-711.

Hodgson, D.M. and Haughton, P.D. (2004). Impact of syndepositional faulting on gravity current behaviour and deep-water stratigraphy: Tabernas-Sorbas Basin, SE Spain. In: Lomas, S.A. and Joseph, J. (eds) Confined Turbidite Systems. Geological Society, London, Special Publications, 222, 135-158.

Hodgson, D.M. (2009). Distribution and origin of hybrid beds in sand-rich submarine fans of the Tanqua depocentre, Karoo Basin, South Africa. Marine and Petroleum Geology, 26, 1940–1956.

Hodgson, D. M., Di Celma, C. N., Brunt, R. L. and Flint, S. S. (2011). Submarine slope degradation and aggradation and the stratigraphic evolution of channel–levee systems. Journal of the Geological Society, 168(3), 625-628. https://doi.org/10.1144/0016-76492010-177

Hodgson, D.M., Kane, I.A., Flint, S.S., Brunt, R.L. and Ortiz-Karpf, A. (2016) Time-transgressive confinement on the slope and the progradation of basin-floor fans: implications for the sequence stratigraphy of deep-water deposits. Journal of Sedimentary Research, 86(2), 73–86.

Hodgson, D. M., Peakall, J. and Maier, K.L. (2022). Submarine Channel Mouth Settings: Processes, Geomorphology, and Deposits. Frontiers in Earth Science 10:790320. http://doi:10.3389/feart.2022.790320

Hofstra, M., Hodgson, D.M., Peakall, J. and Flint, S.S. (2015). Giant scour-fills in ancient channel-lobe transition zones: Formative processes and depositional architecture: Sedimentary Geology, 329, 98–114. https://doi.org /10 .1016/j.sedgeo .2015.09.004

Holbrook, J. and Schumm, S.A. (1999). Geomorphic and sedimentary response of rivers to tectonic deformation: a brief review and critique of a tool for recognizing subtle epeirogenic deformation in modern and ancient settings. Tectonophysics, 305, 287-306

Howlett D.M., Gawthorpe R.L., Ge Z., Rotevatn A. and Jackson CA-L. (2021). Turbidites, topography and tectonics: Evolution of submarine channel-lobe

systems in the salt-influenced Kwanza Basin, offshore Angola. Basin Research, 33, 1076–1110. https://doi.org/10.1111/bre.12506

Hubbard, S.M., Covault, J.A., Fildani, A. and Romans, B.W. (2014). Sediment transfer and deposition in slope channels: deciphering the record of enigmatic deep-sea processes from outcrop. Geological Society of America Bulletin, 126(5-6), 857-871, https://doi.org/10.1130/B30996.1

Hudec, M. R., Jackson, M. P. A. and Schultz-Ela, D. D. (2009). The paradox of minibasin subsidence into salt: Clues to the evolution of crustal basins. Geological Society of America Bulletin, 121(1–2), 201–221.

Huyghe, P., Foata, M., Deville, E. and Mascle, G. (2004). Channel profiles through the active thrust front of the southern Barbados prism: Geological Society of America Bulletin, 32, 429–432.

Jackson, C.A-L, Barber, G.P. and Martinsen, O.J. (2008). Submarine slope morphology as a control on the development of sand-rich turbidite depositional systems: 3D seismic analysis of the Kyrre Fm (Upper Cretaceous), Maloy Slope, offshore Norway. Marine and Petroleum Geology, 25, 663-680. https://doi:10.1016/j.marpetgeo.2007.12.007

Jackson, C. A. L., Duffy, O. B., Fernandez, N., Dooley, T. P., Hudec, M. R., Jackson, M. P. and Burg, G. (2020). The stratigraphic record of minibasin subsidence, Precaspian Basin, Kazakhstan. Basin Research, 32(4), 739–763. https://doi.org/10.1111/bre.12393

Jackson, C.A.L., McAndrew, A.E., Hodgson, D.M. and Dreyer, T. (2021). Repeated degradation and progradation of a submarine slope over geological time scales. Journal of Sedimentary Research, 91, 116-145. https:// doi:10.2110/jsr.2020.77

Jackson, M.P.A. and Hudec, M.R. (2017). Salt Tectonics: Principles and Practise: Cambridge University Press, 515 p.

Jervey, M.T., 1988. Quantitative geological modeling of siliciclastic rock sequences and their seismic expression. In: Wilgus, C.K., Hastings, B.S., Kendall, C.G.St.C., Posamentier, H.W., Ross, C.A., Van Wagoner, J.C. (Eds.), Sea Level Changes — An Integrated Approach. SEPM Special Publication, 42, 47–69.

Jobe, Z.R., Howes, N.C. and Auchter, N.C. (2016). Comparing submarine and fluvial channel kinematics: implications for stratigraphic architecture. Geology, 44, 931–934, https://doi.org/10.1130/G38158.1

Jobe, Z.R., Sylvester, Z., Howes, N., Pirmez, C., Parker, A., Cantelli, A., Smith, R., Wolinsky, M.A., O'Byrne, C., Slowey, N. and Prather, B. (2017). High-resolution, millennial-scale patterns of bed compensation on a sand-rich intraslope submarine fan, western Niger Delta slope. Geological Society of America Bulletin, 129, 23-37.

Johnson, S.D., Flint, S.S., Hinds, D. and Wickens, H.D.V. (2001) Anatomy of Basin Floor to Slope Turbidite Systems, Tanqua Karoo, South Africa: Sedimentology, Sequence Stratigraphy and Implications For Subsurface Prediction. Sedimentology, 48, 987–1023.

Jolly, B.A., Whittaker, A.C., and Lonergan, L. (2017). Quantifying the geomorphic response of modern submarine channels to actively growing folds and thrusts, deep-water Niger Delta: Geological Society of America Bulletin, 129, 1123–1139, https://doi.org/10.1130/B31544.1

Kane, I.A., Catterall, V., McCaffrey, W. D. and Martinsen, O. J. (2010). Submarine channel response to intra-basinal tectonics. AAPG Bulletin, 94, 189– 219.

Kane, I.A., McGee, D.T. and Jobe, Z.R. (2012). Halokinetic effects on submarine channel equilibrium profiles and implications for facies architecture: conceptual model illustrated with a case study from Magnolia Field, Gulf of Mexico. In Alsop, G. I., Archer, S. G., Hartley, A. J., Grant, N. T. and Hodgkinson, R. (Eds.), Salt Tectonics, Sediments and Prospectivity. Geological Society, London, Special Publications, 363, 289–302.

Kane, I.A. and Clare, M.A. (2019). Dispersion, accumulation, and the ultimate fate of microplastics in deep-marine environments: A review and future directions. Frontiers in Earth Science, 7:80, https://doi.org/10.3389/feart.2019.00080

Kane, I.A., Ponten, A.S.M., Vangdal, B., Eggenhuisen, J.T., Hodgson, D.M. and Spychala, Y.T. (2017). The stratigraphic record and processes of turbidity current transformation across deep-marine lobes. Sedimentology, 64, 1236–1273.

Kneller, B.C. and McCaffrey, W.D. (1999). Depositional effects of flow non-uniformity and stratification within turbidity currents approaching a bounding slope: deflection, reflection and facies variation. Journal of Sedimentary Research, 69, 980-991.

Kneller, B. C., Bennett, S. J. and McCaffrey, W. D. (1999). Velocity structure, turbulence and fluid stresses in experimental gravity currents. Journal of Geophysical Research, Oceans, 104, 5281–5291.

Kneller, B. (2003). The influence of flow parameters on turbidite slope channel architecture. Marine and Petroleum Geology, 20, 901–910.

Kneller, B., Dykstra, M., Fairweather, L., and Milana, J. P. (2016). Mass-transport and Slope Accommodation: Implications for Turbidite sandstone Reservoirs. AAPG Bulletin 100, 213–235. doi:10.1306/09011514210

Komar, P.D. (1971). Hydraulic jumps in turbidity currents. Geological Society of America Bulletin, 82 (6), 1477–1487.

Konsoer, K., Zinger, J. and Parker, G. (2013). Bankfull hydraulic geometry of submarine channels created by turbidity currents: relations between bankfull channel characteristics and formative flow discharge. J. Geophys. Res. Earth Surf., 118, 216–228, https://doi.org/10.1029/2012JF002422.

Kostic, S. and Parker, G. (2006). The response of turbidity currents to a canyon-fan transition: Internal hydraulic jumps and depositional signatures, Journal of Hydraulic Research, 44, 631–653.

Kubo, Y.S. (2004). Experimental and numerical study of topographic effects on deposition from two-dimensional, particle-driven density currents. Sedimentary Geology, 164, 311-326.

Lear, C.H., Rosenthal, Y., Coxall, H.K., and Wilson, P.A. (2004). Late Eocene to early Miocene ice-sheet dynamics and the global carbon cycle. Paleoceanography, 19, PA4015. https://doi.org/10.1029/2004PA001039.

Lear, C. H., Bailey, T. R., Pearson, P. N., Coxall, H. K., and Rosenthal, Y. (2008). Cooling and ice growth across the Eocene-Oligocene transition, Geology, 36, 251-254, https://doi.org/10.1130/G24584A.1

Lee, S.E., Talling, P.J., Ernst, G.G.J. and Hogg, A.J. (2002). The occurrence and origin of submarine plunge pools at the base of the US continental slope. Marine Geology, 85, 363–377, https://doi.org/10.1016/S0025-3227(01)00298-5

Li, P., Kneller, B. and Hansen, L. (2021). Anatomy of a gas-bearing submarine channel-lobe system on a topographically complex slope (offshore Nile Delta, Egypt). Marine Geology, 437, 106496.

Lowe, D.R. (1982). Sediment gravity flows II, depositional models with special reference to the deposits of high-density turbidity currents. Journal of Sedimentary Petrology, 52, 279–297.

Macauley, R.V. and Hubbard, S.M. (2013). Slope channel sedimentary processes and stratigraphic stacking, Cretaceous Tres Pasos Formation slope system, Chilean Patagonia. Marine and Petroleum Geology, 41, 146-162, https://doi.org/10.1016/j.marpetgeo.2012.02.004

Madof, A. S., Christie-Blick, N. and Anders, M. H. (2009). Stratigraphic controls on a salt-withdrawal intraslope minibasin, north-central Green Canyon, Gulf of Mexico: Implications for misinterpreting sea level change. AAPG Bulletin, 93(4), 535–561. https://doi. org/10.1306/12220 808082

Madof, A. S., Christie-Blick, N., Anders, M. H. and Febo, L. A. (2017). Unreciprocated sedimentation along a mud-dominated continental margin, Gulf of Mexico, USA: Implications for sequence stratigraphy in muddy settings devoid of depositional sequences. Marine and Petroleum Geology, 80, 492–516. https://doi.org/10.1016/j.marpetgeo.2016.12.022

Marini, M., Milli, S., Ravnås, R., And Moscatelli, M. (2015). A comparative study of confined vs. semi-confined turbidite lobes from the Lower Messinian Laga Basin (Central Apennines, Italy): Implications for assessment of reservoir architecture: Marine and Petroleum Geology, 63, 142–165. https:// doi .org /10 .1016 /j.marpetgeo.2015.02.015.

Martínez-Doñate, A., Privat, A.M.L.J., Hodgson, D.M., Jackson, C.A.L., Kane, I.A., Spychala, T., Duller, R.A., Stevenson, C., Keavney, E., Schwarz, E. and Flint, S.S. (2021). Substrate Entrainment, Depositional Relief, and Sediment Capture: Impact of a Submarine Landslide on Flow Process and Sediment Supply. Frontiers in Earth Science, 9, 1–23.

Mayall, M., Lonergan, L., Bowman, A., James, S., Mills, K., Primmer, T., Pope, D., Rogers, L. and Skeene, R. (2010). The response of turbidite slope channels to growth-induced seabed topography. AAPG Bulletin, 94, 1011–1030. https://doi.org/10.1306/01051009117

Mayall, M. and O'Byrne, C. (2002). Reservoir prediction and development challenges in turbidite slope channels. In Offshore Technology Conference, 14029, Houston, Texas.

Mayall, M., Lonergan, L., Bowman, A., James, S., Mills, K., Primmer, T., Pope, D., Rogers, L. and Skeene, R. 2010. The response of turbidite slope channels to growth-induced seabed topography. American Association of Petroleum Geologists Bulletin, 94, 1011–1030, https://doi.org/10.1306/01051009117

Mchargue, T., Pyrcz, M. J., Sullivan, M. D., Clark, J. D., Fildani, A., Romans, B. W. and Drinkwater, N. J. (2011). Architecture of turbidite channel systems on the continental slope: patterns and predictions. Marine and Petroleum Geology, 28(3), 728-743.

Meckel, L.D. III, Ugueto, G.A., Lynch, H.D., Cummings, E.W., Hewett, B.M., Bogage, E.J., Winker, C.D. and O'Neil, B.J. (2002). Genetic stratigraphy, stratigraphic architecture, and reservoir stacking patterns of the Upper Miocene-Lower Pliocene greater Mars-Ursa intraslope basin, Mississippi Canyon, Gulf of Mexico. In Armentrout, J.M., and Rosen, N.C. (Eds.), Sequence Stratigraphic Models for Exploration and Production: Evolving Methodology, Emerging Models, and Application Histories: 22nd Annual Gulf Coast Section, SEPM Foundation, Bob F. Perkins Research Conference, 113-147.

Micallef, A., Mountjoy, J., Barnes, P.M., Canals, M. and Lastras, G. (2014). Geomorphic response of submarine canyons to tectonic activity: insights from the Cook Strait canyon system, New Zealand. Geosphere, 10 (5), 905–929, https://doi.org/10.1130/GES01040.1

Mignard, S., Mulder, T., Martinez, P. and Garlan, T. (2019). The Ogooue Fan (offshore Gabon): a modern example of deep-sea fan on a complex slope profile. Solid Earth, 10(3), 851-869.

Miller, K. G., J. Wright, and Fairbanks, R. (1991). Unlocking the icehouse: Oligocene-Miocene oxygen isotopes, eustacy and margin erosion, Journal of Geophysical Research, 96, 6829–6848. https://doi:10.1029/90JB02015.

Miller, K. G., Browning, J. V., Schmelz, W. J., Kopp, R. E., Mountain, G. S. and Wright, J. D. (2020). Cenozoic sea-level and cryospheric evolution from deep-sea geochemical and continental margin records. Science Advances. 6, eaaz1346.

Mitchell, N.C. (2006). Morphologies of knickpoints in submarine canyons. Geological Society of America Bulletin, 118(5-6), 589–605, https://doi.org/10.1130/B25772.1

Mitchell, H.W., Whittaker, A.C., Mayall, M., Lonergan, L. and Pizzi, M. (2021). Quantifying the relationship between structural deformation and the morphology of submarine channels on the Niger Delta continental slope. Basin Research, 33, 186–209. https:// doi.org/10.1111/bre.12460

Mitchum Jr., R.M., Vail, P.R., Thompson III, S. (1977). Seismic stratigraphy and global changes of sea-level, part 2: the depositional sequence as a basic unit for stratigraphic analysis. In: Payton, C.E. (Ed.), Seismic Stratigraphy — Applications to Hydrocarbon Exploration. AAPG Memoir, 26, 53–62.

Mohriak, W. U., Basseto, M. and Vieira, I. S. (1998). Crustal architecture and tectonic evolution of the Sergipe-Alagoas and Jacuípe basins, offshore northeastern Brazil. Tectonophysics, 288, 199–220.

Mohriak, W., Nemčok, M. and Enciso, G. (2008). South Atlantic divergent margin evolution: Rift-border uplift and salt tectonics in the basins of SE Brazil. In: Pankhurst, R.J., Trouw, R.A.J., Brito Neves, B.B. and de Wit, M.J. (Eds.), Geological Society, London, Special Publications, 294, 365–398. https://doi.org/10.1144/sp294.19

Mohriak, W. U., Szatmari, P. and Anjos, S. (2012). Salt: Geology and tectonics of selected Brazilian basins in their global context. Geological Society, London, Special Publications, 363, 131–158. https://doi.org/10.1144/sp363.7

Morris, S.A. and Alexander, J. (2003). Changes in flow direction at a point caused by obstacles during passage of a density current. Journal of Sedimentary Research, 73, 621-629.

Morris, E.A., Hodgson, D.M., Flint, S.S., Brunt, R.L., Butterworth, P.L. and Verhaeghe, J. (2014). Sedimentology, stratigraphic architecture and depositional context of submarine frontal lobe complexes. Journal of Sedimentary Research, 84, 763–780.

Morris, E.A., Hodgson, D.M., Flint, S., Brunt, R.L., Luthi, S.M., and Kolenberg, Y.(2016). Integrating outcrop and subsurface data to assess the temporal evolution of a submarine channel–levee system. AAPG Bulletin, 100, 1663–1691. https:// doi .org /10 .1306 /04271615056.

Morris, P.D., Sylvester, Z., Covault, J.A. and Mohrig, D. (2022). Channel trajectories control deep-water stratigraphic architecture. The Depositional Record, 8, 880-894, https:// doi.org/10.1002/dep2.189

Mulder, T., Alexander, J. (2001). Abrupt change in slope causes variation in the deposit thickness of concentrated particle-driven density currents. Marine Geology 175, 221– 235.

Normark, W.R. and Piper, D.J.W. (1991). Initiation processes and flow evolution of turbidity currents: implications for the depositional record. In Osborne, R.H. (Ed.), From Shoreline to Abyss: Contributions in Marine Geology in Honor of Francis Parker Shepard, SEPM Special publication, 46, 207-230.

Mutti, E. and Normark, W.R. (1987). Comparing examples of modern and ancient turbidite systems: problems and concepts. In: Leggett, J.K. and Zuffa, G.G. (Eds.), Marine Clastic Sedimentology: Concepts and Case Studies. Graham and Trotman, London, 1–38.

Oluboyo, A. P., Gawthorpe, R. L., Bakke, K. and Hadler-Jacobsen, F. (2014). Salt tectonic controls on deep-water turbidite depositional systems: Miocene, southwestern lower Congo basin, offshore Angola. Basin Research, 26, 597–620. https://doi.org/10.1111/bre.12051

Omosanya, K.O. and Alves, T.M. (2013). A 3-dimensional seismic method to assess the provenance of mass-transport deposits (MTDs) on salt-rich continental slopes (Espírito Santo Basin, SE Brazil). Marine and Petroleum Geology, 44, 223–239.

Ortiz-Karpf, A., Hodgson, D.M. and Mccaffrey, W.D. (2015). The role of mass-transport complexes in controlling channel avulsion and the subsequent sediment dispersal

patterns on an active margin: the Magdalena Fan, offshore Colombia. Marine and Petroleum Geology, 64, 58–75.

Ortiz-Karpf, A., Hodgson, D. M., Jackson, C. A. L., and McCaffrey, W. D. (2018). Mass-transport complexes as markers of deep-water fold and-thrust belt evolution: Insights from the southern Magdalena fan, offshore Colombia. Basin Research, 30, 65–88.

Palm, F.A., Peakall, J., Hodgson, D.M., Marsset, T., Silva Jacinto, R., Dennielou, B., Babonneau, N. and Wright, T.J. (2021). Width variation around submarine channel bends: Implications for sedimentation and channel evolution. Marine Geology, 437, 106504, https://doi.org/10.1016/j.margeo .2021.106504.

Peakall, J., McCaffrey, W. D., Kneller, B. C., Stelting, C. E., McHargue, T. R., and Schweller, W. J. (2000a). A process model for the evolution of submarine fan channels; implications for sedimentary architecture. In Bouma, A. and Stone, C. (Eds.), Fine-grained turbidite systems. AAPG Memoir 72, 73-89.

Peakall, J., McCaffrey, W.D. and Kneller, B.C. (2000b). A process model for the evolution, morphology and architecture of sinuous submarine channels. Journal of Sedimentary Research, 70, 434-448.

Peakall, J., Leeder, M.R., Best, J.L. and Ashworth, P.J. (2000c). River response to lateral ground tilting: a synthesis and some implications for the modelling of alluvial architecture in extensional basins. Basin Research, 12, 413-424.

Peakall, J., Amos, K.J., Keevil, G.M., Bradbury, P.W. and Gupta, S. (2007). Flow processes and sedimentation in submarine channel bends. Marine and Petroleum Geology, 24, 470-486.

Peakall, J. and Sumner, E.J., (2015). Submarine channel flow processes and deposits: A process-product perspective. Geomorphology, 244, 95-120.

Pettinga, L.A. and Jobe, Z.R. (2020). How submarine channels (re)shape continental margins. Journal of Sedimentary Research, 90(11), 1581-1600.

Picot, M., Droz, L., Marsset, T., Dennielou, B. and Bez, M. (2016). Controls on turbidite sedimentation: Insights from a quantitative approach of submarine channel and lobe architecture (Late Quaternary Congo Fan). Marine and Petroleum Geology, 72, 423-446.

Pirmez, C., Beaubouef, R.T., Friedmann, S.J. and Mohrig, D.C. (2000). Equilibrium profile and base level in submarine channels: examples from Late Pleistocene systems and implications for the architecture of deep-water reservoirs. In Weimer, P., Slatt, R.M., Coleman, J., Rosen, N.C., Nelson, H., Bouma, A.H., Styzen, M.J., and Lawrence, D.T (Eds.), Deep-Water Reservoirs of the World: 20th Annual Gulf Coast Section, SEPM Foundation, Bob F. Perkins Research Conference, 782–805.

Piper, D.J.W., Normark, W.R., 2001. Sandy fans—from Amazon to Hueneme and beyond. AAPG Bulletin, 85, 1407– 1438.

Pitman, W. C. (1979). The effect of eustatic sea level changes on stratigraphic sequences at Atlantic margins. AAPG Memoir 29, 453-460.

Pizzi, M., Whittaker, A.C., Mayall, M. and Lonergan, L. (2023). Structural controls on the pathways and sedimentary architecture of submarine channels: New constraints from the Niger Delta. Basin Research, 35, 141–171. https://doi.org/10.1111/bre.12707

Posamentier, H.W. and Vail, P.R. (1988). Eustatic controls on clastic deposition; II, Sequence and systems tract models. In: Wilgus, C.K. (Ed.), Sea-level Changes; An Integrated Approach, SEPM Special Publication 42, 125–154.

Posamentier, H.W., Erskine, R.D., and Mitchum, R.M., Jr. (1991), Submarine fan deposition within a sequence stratigraphic framework. In Weimer, P., and Link, M.H., (Eds.), Seismic facies and sedimentary processes of submarine fans and turbidite systems: New York, Springer-Verlag, 127–136.

Posamentier, H.W., Kolla, V. (2003). Seismic geomorphology and stratigraphy of depositional elements in deep-water settings. Journal of Sedimentary Research 73, 367-388.

Posamentier, H. W. and Martinsen, O. J. (2011). The character and genesis of submarine mass transport deposits: Insights from outcrop and 3D seismic data. In Shipp, R.G., Weimer, P. and Posamentier, H.W. (Eds.), Mass-transport Deposits in Deepwater Settings: SEPM Special Publication, 96, 7–38.

Prather, B. E., Booth, J. R., Steffens, G. S. and Craig, P. A. (1998). Classification, lithologic calibration and stratigraphic succession of seismic facies from intraslope basins, deep water Gulf of Mexico, USA. AAPG Bulletin, 82, 701–728.

Prather, B. E. (2000). Calibration and visualization of depositional process models for above-grade slopes: a case study from the Gulf of Mexico. Marine and Petroleum Geology, 17(5), 619–638.

Prather, B. E. (2003). Controls on reservoir distribution, architecture and stratigraphic trapping in slope settings. Marine and Petroleum Geology, 20, 529–545. https://doi.org/10.1016/j.marpe tgeo.2003.03.009

Prather, B.E., O'Byrne, C.J., Pirmez, C. and Sylvester, Z. (2009). Sediment partitioning across tertiary continental slopes (abstract): AAPG Annual Convention, Denver, Colorado, Abstracts, CD.

Prather, B. E., Pirmez, C., Sylvester, Z., and Prather, D. S. (2012a). Stratigraphic response to evolving geomorphology in a submarine apron perched on the upper Niger delta slope. In B. E. Prather, M. E. Deptuck, D. C. Mohrig, van Hoorn B. and R. B. Wynn (Eds.), Application of the Principles of Seismic Geomorphology to Continental-Slope and Base-of-Slope Systems: case studies from seafloor and near-seafloor analogue. SEPM Special Publication, 99, 145–161.

Prather, B.E., Pirmez, C. and Winker, C.D. (2012b). Stratigraphy of Linked Intraslope Basins: Brazos–Trinity System Western Gulf of Mexico. In B. E. Prather, M. E. Deptuck, D. C. Mohrig, van Hoorn B. and R. B. Wynn (Eds.), Application of the Principles of Seismic Geomorphology to Continental-Slope and Base-of-Slope Systems: case studies from seafloor and near-seafloor analogue. SEPM Special Publication, 99, 83–109.

Prather, B.E., O'Byrne, C., Pirmez, C. and Sylvester, Z. (2017). Sediment partitioning, continental slopes and base-of-slope systems. Basin Research, 29, 394– 416. https:// doi.org /10 .1111 /bre.12190

Prélat, A., Hodgson, D.M. and Flint, S.S. (2009). Evolution, architecture and hierarchy of distributary deep-water deposits: a high-resolution outcrop investigation from the Permian Karoo Basin, South Africa. Sedimentology, 56, 2132-2154.

Prélat, A., Covault, J.A., Hodgson, D.M., Fildani, A. and Flint, S. S. (2010). Intrinsic controls on the range of volumes, morphologies, and dimensions of submarine lobes. Sedimentary Geology 232, 66-76.

Privat, A.M-L., Hodgson, D.M., Jackson, C.A-L., Schwarz, E. and Peakall, J. (2021). Evolution from syn-rift carbonates to early post-rift deep-marine intraslope lobes: the role of rift basin physiography on sedimentation patterns. Sedimentology, 68, 2563-2605. https://doi.org/ 10.1111/sed.12864

Quirk, D.G., Schødt, N., Lassen, B., Ings, S.J., Hsu, D., Hirsch, K.K., and Von Nicolai, C. (2012). Salt tectonics on passive margins: Examples from Santos, Campos and Kwanza basins. In Alsop, G. I., Archer, S. G., Hartley, A. J., Grant, N. T. and Hodgkinson, R. (Eds.), Tectonics, sediment and Prospectivity. Geological Society, London, Special Publications, 363, 207–244. https://doi.org/10.1144/sp363.10

Rangel, H.D. and Martins, C.C. (1998). Principais compartimentos exploratórios, Bacia de Campos. In Taha, M. (Ed.), Cenário Geológico nas Bacias Sedimentares no Brasil. The Search-Searching for oil and gas in the land of giants, Special Publication, 2, 32-40.

Reading, H. G. and Richards, M. (1994). Turbidite systems in deepwater basin margins classified by grain size and feeder system. AAPG Bulletin, 78, 192-822.

Rodriguez, C.R., Jackson, C.A-L., Bell, R.E., Rotevatn, A. and Francis, M. (2021). Deep-water reservoir distribution on a salt-influenced slope, Santos Basin, offshore Brazil. AAPG Bulletin, 105 (8), 1679-1720. doi:10.1306/11182017340.

Rouby. D.. Cobbold, P.R., Szatmari, P., Demercian. S., Coelho. D. and Rici. J.A. (1993). Restoration in plan view of faulted Cretaceous and Oligocene horizons and its bearing on the history of salt tectonics in the Campos basin (Brazil). In: P.R. Cobbold (Ed.), New Insights to Salt Tectonics. Tectonophysics, 228: 435-445.

Rouby, D., Raillard, S., Guillocheau, F., Bouroullec, R. and Nalpas, T. (2002). Kinematics of a growth fault/raft system from restoration in 3D (West African Margin). Journal of Structural. Geology, 24, 783-796.

Rowan, M. G., and Weimer, P. (1998). Salt-sediment interaction, northern Green Canyon and Ewing bank (offshore Louisiana), northern Gulf of Mexico. AAPG Bulletin, 82(5), 1055–1082.

Rowan, M. G., Peel, F. J. and Vendeville, B. C. (2004). Gravity-driven fold belts on passive margins. In McClay, K. R. (Ed.), Thrust tectonics and hydrocarbon systems. AAPG Memoir 82, 157– 182.

Shumaker, L.E., Jobe, Z.R., Johnstone, S.A., Pettinga, L.A., Cai, D. and Moody, J.D. (2018). Controls on submarine channel-modifying processes identified through morphometric scaling relationships. Geosphere, 14 (5), 2171–2187. doi:10.1130/ges01674.1

Sinclair, H.D. and Tomasso, M. (2002). Depositional evolution of confined turbidite basins. Journal of Sedimentary Research, 72, 451–456. http://dx.doi.org/10.1306/111501720451

Snedden, J.W. (2013). Channel-body basal scours: Observations from 3D seismic and importance for subsurface reservoir connectivity. Marine and Petroleum Geology, 39, 150–163, https://doi.org/10.1016/j.marpetgeo.2012.08.013

Smith, R. (2004). Silled sub-basins to connected tortuous corridors: sediment distribution system on topographically complex sub-aqueous slopes. In Lomas, S.A. and Joseph, P. (Eds.), Confined Turbidite Systems. Geological Society of London, Special Publication, 222, 23– 43.

Southern, S.J., Kane, I.A., Warchol, M.J., Porten, K.W. and McCaffrey, W.D. (2017). Hybrid event beds dominated by transitional-flow facies: character, distribution and significance in the Maastrichtian Springar Formation, north-west Vøring Basin, Norwegian Sea. Sedimentology, 64, 747–776.

Sprague, A. R. G., Garfield, T. R., Goulding, F. J., Beaubouef, R. T., Sullivan, M. D., Rossen, C., Campion, K. M., Sickafoose, D. K., Abreu, V., Schellpeper, M. E., Jensen, G. N., Jennette, D. C., Pirmez, C., Dixon, B. T., Ying, D., Ardill, J., Mohrig, D. C., Porter, M. L., Farrell, M. E. and Mellere, D. (2005). Integrated Slope Channel Depositional Models: The Key to Successful Prediction of Reservoir Presence and Quality in Offshore West Africa. In: CIPM - E-Exitep 2005, Feb 20-23, 2005, Veracruz, México. 1-13.

Spychala, Y.T., Hodgson, D.M., Flint, S.S. and Mountney, N.P. (2015). Constraining the sedimentology and stratigraphy of submarine intraslope lobe deposits using

exhumed examples from the Karoo Basin, South Africa. Sedimentary Geology, 322, 67–81. https://doi.org/10.1016/j.sedgeo.2015.03.013.

Spychala, Y.T. (2016). Are all lobes made equal? Comparing the sedimentological processes and depositional architecture of submarine lobes in different palaeogeographic and sequence stratigraphic positions. Ph.D. thesis, University of Leeds, Leeds.

Spychala, Y.T., Eggenhuisen, J.T., Tilston, M. and Pohl, F. (2020). The influence of basin setting and turbidity current properties on the dimensions of submarine lobe elements. Sedimentology, 67, 3471-3491.

Steffens, G.S., Biegert, E.K., Sumner, H.S. and Bird, D. (2003). Quantitative bathymetric analyses of selected deepwater siliciclastic margins: receiving basin configurations for deepwater fan systems. Marine and Petroleum Geology, 20, 547–561.

Stevenson, C.J., Talling, P.J., Wynn, R.B., Masson, D.G., Hunt, J.E., Frenz, M., Akhmetzhanhov, A. and Cronin, B.T. (2013). The flows that left no trace: very large volume turbidity currents that bypassed sediment through submarine channels without eroding the sea floor. Marine and Petroleum Geology, 41, 186–205.

Stevenson, C.J., Jackson, C.A-L., Hodgson, D.M., Hubbard, S.M. and Eggenhuisen, J. (2015). Deep-water sediment bypass. Journal of Sedimentary Research, 85, 1058-1081.

Steventon, M.J., Jackson, C.A.-L., Hodgson, D.M. and Johnson, H.D. (2019). Strain analysis of a seismically imaged mass-transport complex, offshore Uruguay. Basin Research, 31, 600–620. https://doi.org/10.1111/bre.12337

Steventon, M.J., Jackson, C.A.L., Johnson, H.D., Hodgson, D.M., Kelly, S., Omma, J., Gopon, C., Stevenson, C. and Fitch, P. (2021). Evolution of a sand-rich submarine channel–lobe system, and the impact of mass-transport and transitional-flow deposits on reservoir heterogeneity: Magnus Field, northern North Sea. Petroleum Geoscience, 2, 2020-2095. http://doi:10.1016/j.marpetgeo.2006.01.002

Stow, D., Howell, D. and Nelson, C. (1984). Sedimentary, tectonic, and sea-level controls on submarine fan and slope-apron turbidite systems. Geo-Marine Letters, 3, 57–64.

Straub, K.M., Paola, C., Mohrig, D., Wolinsky, M.A. and George, T. (2009). Compensational stacking of channelized sedimentary deposits. Journal of Sedimentary Research, 79(9), 673-688.

Stright, L., Jobe, Z., Fosdick, J.C. and Bernhardt, A. (2017). Modeling uncertainty in the three-dimensional structural deformation and stratigraphic evolution from outcrop data: Implications for submarine channel knickpoint recognition. Marine and Petroleum Geology, 86, 79–94.

Sumner, E.J., Peakall, J., Parsons, D.R., Wynn, R.B., Darby, S.E., Dorrell, R.M., Mcphail, S.D., Perrett, J., Webb, A. and White, D. (2013). First direct measurements of hydraulic jump sin an active submarine density current. Geophysical Research Letters, 40, 5904-5908. http://dx.doi.org/10.1002/2013GL057862.

Sumner, E.J., Peakall, J., Dorrell, R.M., Parsons, D.R., Darby, S.E., Wynn, R.B., McPhail, S.D., Perrett, J., Webb, A. and White D. (2014). Driven around the bend: spatial evolution and controls on the orientation of helical bend flow in a natural submarine gravity current. Journal of Geophysical Research – Oceans, 119, 898-913. doi: 10.1002/2013JC009008

Sylvester, Z., Pirmez, C. and Cantelli, A. (2011). A model of submarine channel-levee evolution based on channel trajectories: Implications for stratigraphic architecture. Marine and Petroleum Geology, 28, 716–727, https://doi.org/10.1016/j.marpetgeo.2010.05.012

Sylvester, Z., Deptuck, M.E., Prather, B.E., Pirmez, C. and O'byrne, C.J. (2012) Seismic stratigraphy of a shelf-edge delta and linked submarine channels in the Northeastern Gulf of Mexico. In Prather, B. E., Deptuck, M. E., Mohrig, D. C., van Hoorn B. and Wynn, R. B. (Eds.), Application of the Principles of Seismic Geomorphology to Continental-Slope and Base-of-Slope Systems: Case studies from seafloor and near-seafloor analogue. SEPM Special Publication, 99, 31–59.

Sylvester, Z., Cantelli, A. and Pirmez, C. (2015). Stratigraphic evolution of intraslope minibasins: Insights from surface-based model. AAPG Bulletin, 99, 1099-1129.

Sylvester, Z. and Covault, J.A. (2016). Development of cutoff-related knickpoints during early evolution of submarine channels. Geology, 44, 835–838, https://doi.org/10.1130/G38397.1.

Talling, P.J., Masson, D.G., Sumner, E.J. and Malgesini, G. (2012). Subaqueous sediment density flows: Depositional processes and deposit types. Sedimentology, 59, 1937-2003, https://doi.org/10.1111/j.1365-3091.2012.01353.x

Tek, D.E., McArthur, A.D., Poyatos-Moré, M., Colombera, L., Patacci, M., Craven, B. and McCaffrey, W.D. (2021). Relating seafloor geomorphology to subsurface architecture: how mass-transport deposits and knickpoint-zones build the stratigraphy of the deep-water Hikurangi Channel. Sedimentology, 68, 3141–3190.

Varnes, D.J. (1978). Slope movement types and processes. In: Schuster RL, Krizek R.J. (Eds.), Landslides, analysis and control, special report 176: Transportation research board, National Academy of Sciences, Washington, DC., 11–33

Wang, X., Luthi, S.M., Hodgson, D.M., Sokoutis, D., Willingshofer, E. and Groenenberg, R.M. (2017). Turbidite stacking patterns in salt-controlled minibasins: insights from integrated analogue models and numerical fluid flow simulations. Sedimentology, 64, 530–552.

Ward, N.I.P., Alves, T.M., and Blenkinsop, T.G. (2018). Submarine sediment routing over a blocky mass transport deposit in the Espírito Santo Basin, SE Brazil: Basin Research, 30(4), 816–834.

Winker, C.D. (1996). High resolution seismic stratigraphy of a late Pleistocene submarine fan ponded by salt-withdrawal mini-basins on the Gulf of Mexico continental slope. In Offshore Technology Conference, 8024, Houston, Texas, 619–628.

Winter, W. R., Jahnert, R. J. and França, A. B. (2007). Bacia de Campos. Boletim de Geociências da Petrobras, 15(2), 511–529.

Wu, N., Jackson, C. A. L., Johnson, H. D., Hodgson, D. M., and Nugraha, H. D. (2020). Mass-transport complexes (MTCs) document subsidence patterns in a northern Gulf of Mexico salt minibasin. Basin Research, 32, 1300-1327. https://doi.org/10.1111/bre.12429

Wu, N., Jackson, C.A.-L., Johnson, H. and Hodgson, D.M. (2021). Lithological, petrophysical and seal properties of mass-transport complexes (MTCs), northern Gulf of Mexico. AAPG Bulletin,105, 1461–1489.

Wynn, R.B., Talling, P.J., Masson, D.G., Le Bas, T.P., Cronin, B.T. And Stevenson, C.J. (2012). The influence of subtle gradient changes on deep-water gravity flows: a case study from the Moroccan turbidite system. In Prather, B. E., Deptuck, M. E., Mohrig, D. C., van Hoorn B. and Wynn, R. B. (Eds.), Application of the Principles of Seismic Geomorphology to Continental-Slope and Base-of-Slope Systems: Case studies from seafloor and near-seafloor analogue. SEPM Special Publication, 99, 347–369.